Energy Efficient Control of Heating, Ventilation and Air Conditioning Systems with use of Adaptive and Predictive Control Techniques

Oświecińska, Aleksandra

Award date:
2021

Awarding institution:
Coventry University

Energy Efficient Control of Heating, Ventilation and Air Conditioning Systems with use of Adaptive and Predictive Control Techniques

Author:

Aleksandra Oświecińska

A thesis submitted in partial fulfilment of the University's requirements for the Degree of Doctor of Philosophy

June 2020

Faculty of Engineering, Environment and Computing

Coventry University

Acknowledgements

I would like to express my gratitude to Dr. Ivan Zajic for his consistent support and guidance during the running of this project. Ivan introduced me to HVAC systems and let me contribute to this complex field under his supervision. Ivan's commitment, patience, knowledge and enthusiasm has been encouraging and has pushed me to the accomplishment of this research project. I would also like to thank Dr. Mathias Foo and Dr. Hafiz Ahmed for supporting me in the final stage of the project.

I would like to appreciate Prof. Keith Burnham for providing me with the opportunity to be part of Coventry University, engaging me with this project and his extraordinary support throughout this journey. Keith's attitude, role and influence was priceless.

I would like to acknowledge my industrial partner Jet Environmental Systems Ltd for giving me the opportunity to work together and sharing their expertise on HVAC systems with me. I've deeply enjoyed the collaboration, which made this research project exceptionally interesting. I appreciate the time I had with my colleagues at Jet Environmental Systems and the time they gave me. I wish to extend my special thanks to Jason Hibbs for overseeing me and supporting me.

Finally, I am grateful for my family and friends - my dear parents and brother Ewa, Marek and Michal Oswiecinski, and all others who always believed in me and supported me in various ways. I would also like to thank my partner Aaron Thomas for cheering me on throughout this journey and making it special.

Thank you all, you have been amazing!

Abstract

A large building with an open space is exposed to substantial influence of the outdoor conditions on the exterior side of the walls and roof, which in return affects the indoor temperature conditions. This thermal process within the building is characterised by highly nonlinear behaviour and slow dynamics, presenting additional challenges of indoor climate control mechanism that the small to mid size constructions do not encounter. Many existing commercial and industrial buildings require these indoor climate control solutions to ensure that the indoor temperature remains within the specified boundaries. Currently it is often achieved through the use of heating, ventilation and air conditioning (HVAC) systems, which tend to be energy intensive and contribute to the peak demand for gas and electricity. Many of the existing solutions, which are based on Proportional-Integral (PI) controller method, despite achieving some energy-saving, it is still inefficient particularly when operating to satisfy several indoor climate requirements concurrently. The research presented in this thesis has been conducted to develop an innovative approach for indoor climate control. The proposed reliable and energy efficient control solution adopts Model Predictive Control (MPC) architecture, which optimises the energy consumption by altering the air entering the Air Handling Unit (AHU) between the recirculated indoor air and the fresh outdoor air. The proposed control strategy is able to utilise only the mechanical ventilation (i.e. damper blades position) to pre-cool and pre-heat the indoor space, at the same time contributing to the indoor climate requirements satisfaction. The model derived for this purpose is a State-Dependent Parameter (SDP) model that is capable of responding to the changes in the model parameters caused by the variation in the supply air mass flow rate and alteration of the source air, which are nonlinear. The prediction of the indoor conditions is made with prior knowledge of the weather forecast. This prediction is used by the Genetic Algorithm (GA) to find the optimal control action for the position of damper blades on the AHU entrance. The results of using optimisation with the MPC via simulation approach indicate the ability of the proposed method to lower the HVAC system energy consumption achieved through redesign of the control strategy. In the summer time it is possible to decrease energy consumption and save around 8%, whereas in other season it varies between 0% and 3%. This approach benefits from the fact that it doesn't require additional mechanical equipment to the existing solutions other than a controller that can handle the algorithm locally or remotely, offering a reliable and robust energy efficient indoor air temperature control system.

Contents

List of Abbreviations

AHU	Air Handling Unit
CT	Continuous-time domain
DT	Discrete-time domain
GA	Genetic Algorithm
HVAC	Heating, Ventilation and Air Conditioning
IAE	Integral Absolute Error
IV	Instrumental Variables
LS	Least Squares
MIMO	Multi-input multi-output
MPC	Model Predictive Control
MSE	Mean Squared Error
NMSS	Non-minimal State Space
PID	Proportional-Integral-Derivative
PIP	Proportional-Integral-Plus
R_T^2	Coefficient of determination
SDP	State-Dependent Parameter
SID	System Identification
SISO	Single-input single-output
TF	Transfer Function

Chapter 1

Introduction

Temperature control of an indoor air is a common practice in residential, industrial and commercial buildings to provide the desired environmental conditions for human activities or stored goods using heating, ventilation and air conditioning (HVAC) systems. Solutions vary from widely used Proportional-Integral-Derivative (PID) controllers to PID-based controllers to adaptive and predictive control schemes to optimisation algorithms to Artificial Intelligence (AI) and offer diverse applications within the HVAC system, its control strategy and components. New control approaches are being developed to decrease the energy consumption as the building sector in the European Union accounts for up to 40% of the overall energy consumption, with indoor space heating and cooling accounting for 74% of energy consumption within residential sector and 56% in tertiary sector as outlined by Foucquier et al. (2013). Paris et al. (2010) discusses three heating control schemes aiming at reducing energy consumption and promoting the use of renewable energy, namely PID, PID-FLC (Proportional-Integral-Derivative Fuzzy Logic Control) and PID-MPC (Proportional-Integral-Derivative Model Predictive Control). The findings obtained through simulation show that the PID-MPC provided the best results, but is the most challenging to develop, whereas PID-FLC was found to be good compromise in terms of results and development difficulty, setting out PID as not very efficient, but easy to develop. An application focused on controlling the vapor compression cycle (VCC) in an air-conditioning system to optimise the energy consumption using Model Predictive Control (MPC) is proposed by Wallace et al. (2012). The results of using this approach to control the air temperature within the building demonstrated better disturbance rejection ability in the zone air temperature and higher energy efficiency than a PI-based control. Further, Mayer et al. (2017) discusses application of Hierarchical Model Predictive Controller (HMPC) in support of a flexible and sustainable building automation in comparison to conventional PID controller. The proposed HMPC algorithm demonstrated a significant increase in energy

efficiency with additional benefits coming from flexible pricing incorporation and capability to integrate with smart grid while meeting users' thermal comfort requirements in smart building. Recognising potential of the MPC strategies in the building control sector, Valenzuela et al. (2020) discusses MPC-based HVAC system control that incorporates the closed-loop dynamics of the heating and ventilation subsystems to control performance and the building energy efficiency. This data-based study addresses the problem of adjusting multiple set points (both temperature and flow rates) based on weather conditions, occupancy, and actual thermal comfort. Chen & Chang (2016) and Kampelis et al. (2019) propose optimisation of the HVAC system energy consumption with use of Genetic Algorithm (GA). The first paper combines Support Vector Machine (SVM) and GA to find the optimal combination of operating parameters of the HVAC systems, achieving 22% on average in comparison to operation under fixed parameters. The considered parameters of the Air Handling Unit (AHU) thermal balance equation used in this paper include chiller, AHU, and pump operating parameters. In the second paper the user thermal comfort is achieved by minimising the daily cost of energy and finding optimum temperature set-points while integrating Predicted Mean Vote (PMV) in the objective function. In this approach the energy savings are dependent on the trade-off between the energy cost and the thermal comfort, reducing the amount of the energy consumed by 10-25%. Moon et al. (2014) provided numerical comparative performance tests for an Artificial Neural Network (ANN)-based temperature control algorithm and conventional non-ANN-based counterpart in an indoor air temperature control. The ANN-based temperature controller utilised the predictive and adaptive features of ANN models. While ANN control strategy didn't exhibit significant superiority in energy efficiency over the conventional control method, it showed an improvement in the indoor temperature environment with an increased comfortable temperature period and decreased overshoot and undershoot of temperatures outside of the operating range. Another application of ANN is discussed by Demirezen et al. (2020), where AI is used to predict the ambient temperature for a location-specific building. This can improve the operation of the HVAC system as the outdoor temperature data is critical for energy efficient temperature control.

In thermal modelling, an application of State-Dependent Parameter (SDP) method is considered by Tsitsimpelis & Taylor (2014), who formulate an SDP model for heating and ventilation control of conceptual thermal zones in a closed-environment growing system to obtain the dynamic thermal response. This follows an observation that the airflow, or the supply fan input, is state variable and affect both ventilation rate and temperature. Taylor et al. (2011b) discussed preliminary results of implementation of a gain scheduled PIP controller for the regulation of ventilation rate in agricultural buildings in comparison to equivalent PID design. The study shows that PIP controller can

help stabilise the airflow and provide robust control, ultimately leading to minimisation of the operating cost. Similarly, a PIP controller is designed and used for temperature control of multi-thermal zones in a ventilated space by Youssef et al. (2011a). The paper reports that the controller is robust to the unexpected noise that might be associated with the estimated data-based model parameters. Another approach combines PIP control system design with SDP models to regulate ventilation rate in mechanically ventilated agricultural buildings (Stables & Taylor, 2006). Assessed on a forced ventilation test chamber, the proposed SDP-PIP control systems show an improved performance in comparison to both linear and conventional scheduled PIP control, for no increase in the implementational complexity.

In this thesis the attention is dedicated to providing desirable temperature control for large single space commercial and industrial buildings such as warehouses, aircraft hangars or retail park stores. These type of building constructs require insight into the thermal process dynamics to understand how it operates and be able to develop strategies minimising the operational cost of the HVAC system as well as its energy consumption. This application is currently under-researched and strategies leading to considerable savings are still lacking. The challenges characterising large single space buildings, as compared to e.g. commercial office buildings are: the large volume of conditioned space, the small rate of change in the indoor air temperature, occurrences of thermal stratification, thermal mass within the building changing over time, and the large impact of the outdoor conditions through the walls and roof. Additionally, some commercial sectors are imposed with legislative requirements creating a demand for accurate temperature regulation within the building, e.g. storage of temperature-sensitive products such as food and medications. The case studied in this thesis is based on an existing warehouse storing pharmaceutical products located in Midlands, UK described in Section 2.2 of Chapter 2. Having studied numerous methods for indoor thermal control outlined above, it is concluded that more advanced control algorithms demonstrate numerous benefits for the HVAC system and indoor temperature control over conventional approaches, including lower energy consumption, increased temperature stability, thermal comfort assurance and optimisation of specific HVAC system parameters. To balance computation and structural complexity and the potential of the method to handle predictive control with constraints to reduce the cost of the energy consumed, the solution proposed in this thesis is a model based approach, where a custom-design MPC introduced in Chapter 5 uses GA to achieve energy efficient control of the HVAC system. The MPC and GA employing a custom objective function are used to find the optimal control values for the mixing damper, which alters the air intake between recirculating the indoor air and drawing ambient air from the outside. The use of the outdoor air temperature forecast supports simulation of the indoor conditions. It is

found that the method proposed in this thesis has potential to lower the HVAC system energy consumption achieved through redesign of the control strategy. The results show that during summer months it is possible to decrease the energy consumption by 8%, whereas in other season it varies between 0% and 3%.

The complexity of the indoor air temperature is high when modelling is considered. The dynamics of the thermal process within the building differ from one to another due to size, volume, design of the indoor space, building envelope and air supply strategy. To capture the indoor air temperature for simulation and control as a part of the GA MPC approach (Chapter 5), a State-Dependent Parameter (SDP) model structure is proposed in Chapter 3. This unique solution is motivated by varying parameter values subject to the supply fan operation and the position of damper blades. The thermal model which forms a basis for SDP is introduced in Chapter 2. This thermal model is derived from first principles and relies on the energy balance equations, similar to a thermal-electrical analogy model of a building for heating system control described by Tate et al. (2019). It contains sub-models of the HVAC system components, including supply fan, heating and cooling units with parameters estimated from the data. Further, a Proportional-Integral-Plus (PIP) controller is designed and introduced in Chapter 4. PIP is implemented internally as a part of GA MPC to calculate the heating and cooling controls. This formulation is derived explicitly for the proposed SDP indoor temperature model from Chapter 5.

The research presented in this thesis is a result of a collaborative work between Jet Environmental Systems Ltd. and Coventry University and a continuation of the project summarised in the author's Master thesis (Oswiecinska, 2014). Jet Environmental Systems Ltd. specialises in design, installation and maintenance of the HVAC systems in some of the largest logistics and pharmaceutical warehouses, retail stores, museums, leisure facilities and production sites for many of the UK's leading businesses (Jet Environmental Systems, n.d.). Their aim is to provide their clients with cost and energy efficient solutions while contributing to low carbon emission goals. Therefore, the research presented in this thesis is a response to an existing problem brought by the industry partner to be solved. Two strategies are proposed in the Master thesis to improve the energy efficiency of the indoor air temperature control system: (1) Model Predictive Control (MPC) was used for the damper blades position control to select between recirculating the indoor and outdoor air intake and (2) adaptive set-point management, where the dead-band is temporary expanded within safe limits. The work summarised in this thesis is built on the ideas from the Master thesis and expands it by proposing state-dependent model of the indoor air temperature, re-implementation of the MPC and more comprehensive simulation study. An overview of the approach motivated by a potential real world application has been published as a paper *Towards energy efficient*

operation of Heating, Ventilation and Air Conditioning systems via advanced supervisory control design (Oswiecinska et al., 2015), where a two-level control approach is proposed. The two-level control approach is offered to extend the capabilities of already existing control systems with some level of energy efficient strategies, which performance could be improved making use of the advanced control strategy utilising the predictive methods initially proposed in the MSc thesis and then continued in this thesis. The author of the thesis also had an opportunity through collaboration with Jet Environmental Systems to work with the real controllers operating on the existing buildings, maintain them and then design and implement similar strategy in MATLAB and on a TREND controller, while gaining valuable insight into control systems operations through these experiences.

1.1 Environmental impact

Environmental concerns, including climate change and depletion of resources have been growing significantly over the last years (Fitzpatrick, 2013). Global trends around environmental risks have led to focus on sustainability among governments, industry, businesses and investors following the Great Acceleration, which relates to dramatic acceleration in human enterprise and the impacts on the Earth system over the last two centuries, starting with the Industrial Revolution at around 1800 and reveals synchronous acceleration of trends from the 1950s to the present day (Future Earth, 2015; Steffen et al., 2015). In light of that, the agreements made by the United Nations General Assembly in 2015 set goals to be achieved by 2030 called Sustainable Development Goals (SDG) that have targets and are measured with indicators, see (United Nations Sustainable Development, n.d.; United Nations Development Programme, n.d.; GOV.UK, n.d., e.g.). These goals are:

- No Poverty
- Zero Hunger
- Good Health and Well-being
- Quality Education
- Gender Equality
- Clean Water and Sanitation
- Affordable and Clean Energy
- Decent Work and Economic Growth
- Industry, Innovation, and Infrastructure
- Reducing Inequality
- Sustainable Cities and Communities
- Responsible Consumption and Production
- Climate Action
- Life Below Water
- Life On Land
- Peace, Justice, and Strong Institutions
- Partnerships for the Goals

There are mutual relationships between the environment, society and economy, which includes finance, business and government, indicating that imbalance in one of the areas causes imbalance in the others. This caused practices to change over the past few years in support of SDGs. For the environment, the efforts are visible in shift toward reducing plastic usage, carbon offsetting and carbon footprint reduction, turning into renewable energy and many more. Larry Fink, Chairman and Chief Executive Officer at BlackRock, an American global investment management corporation, stated in his letter published in 2020 *Larry Fink's Letter to CEOs* (Fink, 2020) that *Climate change has become a defining factor in companies' long-term prospects* and *Every government, company, and shareholder must confront climate change*. Nowadays investors look far beyond company's good financial score, predicting the company's future based on sustainability ratings, e.g. using Environment, Social and Government (ESG) criteria.

Climate change leading to global warming to some degree is caused by the greenhouse gas emissions following the Industrial Revolution. As the average global temperature rises, there is a threshold of 2°C that is extremely dangerous to the ecosystem if exceeded. Therefore, there is a limit on greenhouse gases that can be emitted before temperature rises by 2°C compared to pre-industrial era. The carbon emissions make a significant contribution in reaching of the 2°C threshold and the governments have taken steps in attempt to slow it down. A visual presentation of the problem as of 2011 is depicted in Figure 1.1, where it is shown that a half of the carbon emission allowance has already been used since the start of the industrial era until 2011. The history of the climate change and the 2°C threshold is described by Carbon Brief in (2014).

The growing interests and actions toward helping environment is not just a temporary trend, but a way of working towards the future of the planet and forthcoming generations with understanding that investment goes beyond pure financial interest. UK, and many other countries worldwide, is committed to the delivery of the SDGs, therefore the goals are fully embedded in planned activity of each Government department. By doing so, the Government ensures that the message is distributed across all sectors. Sustainability is everyone's business and everyone's effort is needed to meet the targets and balance social, economic and environmental sectors. While rapid growth in the technology and industry over the past few decades contributed significantly to the carbon emissions and pollution of the Earth, it also enabled access to tremendous number of opportunities in engineering applied to various fields such as science, medicine and biology, biochemistry, aerospace, economy, sustainability and others. The research presented in this thesis is a way of recognition for the technology advancement and people behind it, without which the world would not be what it is now. Most importantly, it is a way of contribution to act upon sustainability concerns. The research described in this thesis encourages methods aiming to reduce the carbon footprint and support the environment

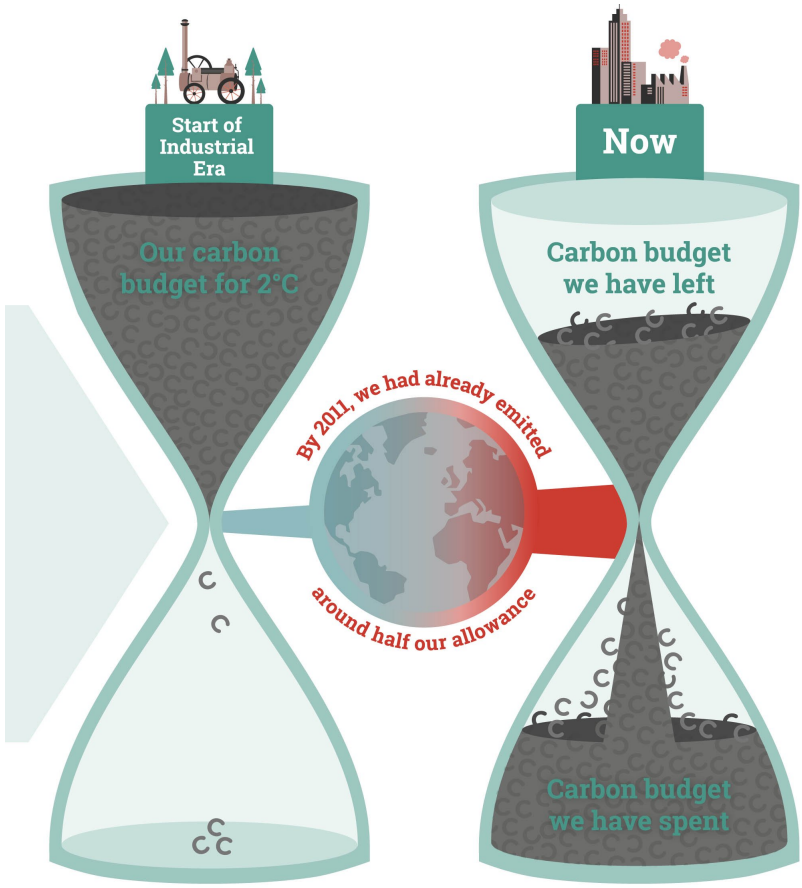

FIGURE 1.1: Estimated carbon budgets as of 2011. (Fitzpatrick, 2013)

through energy efficient control strategies achieved by advanced control strategies and without the need for additional mechanical equipment for the HVAC system.

1.2 Research aim and objectives

The aim of the research work reported in this thesis is to provide a reliable and energy efficient operation of indoor air temperature control system targeting large volume open plan buildings with particular focus on the warehouse facility studied as a part of the research. The outcome of this project is to offer a solution that minimises operational costs of a heating, ventilation and air conditioning (HVAC) systems while ensuring the required temperature conditions are met. These are the objectives:

- To investigate linear and nonlinear model structures for building temperature, including linear transfer function models and nonlinear SDP models.
- To develop a control oriented mathematical model of the indoor air temperature derived from first principles.

- To propose a control method calculating heating and cooling demands and their respective control inputs.
- To propose a new control framework that optimises the damper position in order to minimise the energy consumption through design of an advanced, high-level, control system based on Model Predictive Control (MPC) architecture.
- To incorporate potential future controls and input data such as weather forecast and the position of damper blades into predictive controller.
- To take advantage of the outdoor air temperature for ventilation and free cooling of the indoor space, see Section 5.2, regulated through the damper position.
- To formulate a cost function representing the energy consumption resulting from the HVAC system operation.
- To propose a optimisation method that minimises the cost function by finding a set of consecutive mixing damper controls. Whereas the damper position itself is not a part of the cost function, it has an impact on the temperature of the air supplied to the building, which translates to heating and cooling demand.
- To evaluate the performance of the new controller via simulation using outdoor temperature data representing various seasons of the UK climate.

1.3 Academic contributions

The main contributions identified during development of the novel approach to energy efficient indoor air temperature control proposed in this thesis are:

- Identification of the state-dependent character of an indoor air thermal process and the sub-models of the heating and cooling units in Chapter 2.
- State-dependent model formulation for indoor air temperature and the use of damper position and air mass flow rate for model parameter estimation in Chapter 3.
- Non-minimal state space (NMSS) design of a State-Dependent Parameter (SDP) model of the indoor air temperature and respective Proportional-Integral-Plus (PIP) controller design using State-Variable Feedback (SVF) in Chapter 4. The PIP controller is utilised to calculate heating and cooling control inputs.
- Optimisation problem formulation for a state-dependent indoor air temperature model, cost function and application-specific MPC design utilising Genetic Algorithm (GA) in Chapter 5.

1.4 Thesis outline

The thesis is organised in the following manner:

- **Chapter 2** Starting with first principles consideration, an indoor thermal process is formulated and studied. The simulation study incorporated sub-models of heating and cooling units based on the real system and analysis of the model indoor air temperature, which is observed to be state-dependent.
- **Chapter 3** Reflecting on the conclusions in Chapter 2 with regard to model parameters, a general SDP model structure is introduced as well as reduced order SDP model of an indoor air temperature. Demonstration of the SDP model is shown through simulation study by covering system identification of state-dependent parameters, comparison study of linear and SDP model performance and full SDP model simulation scenario.
- **Chapter 4** In this chapter, control approach for SDP models is proposed. Starting from general NMSS form to SVF and PIP, the next section provides NMSS model and PIP control design for the indoor air temperature. Then, it culminates at formulation of SDP-PIP controller for an indoor air temperature control. This controller utilised SDP model introduced in Chapter 3. The simulation study demonstrates operation of SDP-PIP controller under different outdoor air temperature scenarios and pole placements.
- **Chapter 5** MPC method proposed in this chapter utilises SDP model and SDP-PIP controller introduced in previous chapters as an internal part of MPC. The sections elaborate on the control setup for MPC and optimisation problem formulation, with the most important parts being presentation of the cost function and introduction to GA setup. The simulation study demonstrates the MPC algorithm operation and contains a brief study on the cost associated with running the HVAC system.
- **Chapter 6** This chapter serves as a summary of the previous chapters, focusing on the main outcomes and conclusions on each subject. It also reflects on possible improvements and offers suggestions regarding further development.

Chapter 2

Thermal modelling of an open air-conditioned indoor space

2.1 Introduction

Mathematical model is often used to describe, study and understand phenomena occurring in the real world and also for theoretical considerations. As an indivisible part of science, models allow simulations and demonstrations of complex interactions that are not feasible to be investigated using physical experimentation. They are also used to gain greater insight into phenomena or process by conceptualisation and decomposing them into parts that are used for its reconstruction. Models are an approximation of a real system and can be formulated in multiple ways, allowing for various classification approaches. On the basis of mechanistic or physical insight into studied system, there are three model types that can be distinguished: white-box, grey-box and black-box (Larkowski & Burnham, 2011, p. 9-12). Overview of each type is summarised in Table 2.1. Alternative method is the data-based mechanistic approach well described by Peter Young in (Young, 2002) and (Young, 2011, p. 357) that allows to obtain the model structure parameters via system identification and parameter estimation methods while, as oppose to black box concept, the parameters explain the data well and in the same time have physical meaning. Once the modelling approach is determined, modellers have a choice between different types of model, i.e. static or dynamic models (Ljung & Glad, 1994, p. 19). In brief, the link between variables in the static models is instantaneous. These models are described by algebraic equations only where the outputs are a function of the inputs only and depend only on the present values. On the contrary, dynamic models can be described by algebraic and differential equations, where the outputs are a function of the inputs, system states and previous outputs with the variables change

with time. In this thesis, the dynamic models are used to describe the thermal process using different mechanistic insight approaches.

TABLE 2.1: Model types classification according to the level of mechanistic insight.

White-box	**Black-box**	**Grey-box**
• Physical laws-based or user-defined • *A priori* knowledge of the process required • Defined by differential and/or integral equations • Direct reflection of the modelled phenomena • Physical meaning of parameters • Can be complex and of high order, especially for non-trivial systems • Obtainable without system identification tools	• Empirical or experimental models with unknown underlying dynamics • No physical meaning of the parameters • No prior engineering knowledge required • All parameters require identification • Parametric model structure must be assumed • Relatively simple modelling procedure • Model reliability fully dependent on system identification data and results	• Semi-physical models • Some underlying dynamics known, some not (hybrid of white-box and black-box) • Knowledge of all physical parameters not necessary • Parameter estimation required for unknown aspect • Potential for simplification of certain dynamics • Medium model complexity • Model reliability partially dependent on system identification data and results

After determining whether a static or dynamic model to be used, the modellers will have to decide on the purpose of the model, the choice of model structure and the inputs and outputs of interest. The importance lays in the fact that a wrong setup of a modelling approach may result in the model that does not suit the application, producing results with intolerable inaccuracies and inability to be tuned or being overcomplicated. Once all those aforementioned characteristics of the model are determined, one can progress to find model parameters.

The quality of the model, according to Ljung & Glad (1994, p. 244), is predominantly determined based on three basic facts: its adequacy of use for intended purpose, ability to reproduce the behaviour of the system and its stability. If the model is able to fulfill all of these aspects, the model is considered to be good. Therefore, modelling is a vital part of developing reliable and energy efficient model-based control techniques for heating, ventilation and air conditioning (HVAC) systems (Chartered Institution of Building Services Engineers, 2005, e.g.). This chapter is dedicated to comprehensive

description of the thermal system model development characterising an indoor air temperature behaviour. The model is derived using physical modelling approach (Ljung & Glad, 1994, p. 16), i.e. based on first principles, where energy balance, physical properties of the building and heat transfer are of main interest. The main contributions of this chapter are (1) an indoor air temperature model formulation, (2) the sub-models of the heating and cooling units, (3) the use of damper position and air mass flow rate for model parameter estimation and (4) observations regarding nonlinearity and state-dependence of the model structure. Note that the term *thermal* used in the thesis is referring to heat, whereas the term *thermodynamic* possesses a broader reference, including heat, pressure and state. The research presented in the thesis is focused solely on the temperature aspect which is the manifestation of the thermal energy and signifies the presence of heat in all of the matters.

2.1.1 Literature review

The mathematical modelling of the thermal behaviour dates back to the 1800s owing to physicist Jean Baptiste Joseph Fourier. He contributed to the science of heat by developing mathematical theory of heat induction. The work of the analytic theory of heat was published in 1822 and is considered to be a classical literature in this domain. The Fourier's transient heat conduction equation in modern notation is expressed as

$$\nabla \cdot K \nabla T = c \frac{\delta T}{\delta t} \tag{2.1.1}$$

where K denotes thermal conductivity, T denotes temperature, c denotes specific heat capacity of the solid per unit volume, and t is time (Narasimhan, 1999). The heat balance approaches introduced in the 1970s improved the heat transfer model, leading to further developments and more complex methods of the HVAC systems modelling in the 1980s (Homod, 2013; Kusuda, 1976). The modelling of the indoor air temperature using energy balance equations used in the thesis is proposed by Underwood (1999), who discussed comprehensively concerns regarding modelling for control of the HVAC systems along with various control technologies including Proportional-Integral-Derivative (PID) control, adaptive control and artificial intelligence. This demonstrates a variety of ways in which indoor air temperature control could be approached. Therefore, the approach proposed in the further chapters of this thesis represents one of the possible solutions to the problem.

Challenges associated with the modelling of an indoor thermal process for temperature control have been recognised in research body. From a statistical point of view, a thermal process is classified as stochastic, therefore changing over time in an unpredicted

manner. From the control engineering point of view, these indoor thermal models represent a highly nonlinear process, where current parameter values are dependent on the past and present values, leading to complex model structures and dependencies. Atam & Helsen (2016) have illustrated in every aspect the issues related to control oriented thermal modelling of the multi-zone building, providing list of concepts, methods and aspects of related modelling approaches. The challenges described in the paper have been found familiar to the author of the thesis who encountered similar difficulties and tendencies during the studies on the energy efficiency of the HVAC systems serving large single space buildings. These structures are characterised by slow dynamics, nonlinear behaviour, thermal mass stored in shelving units, goods and machinery, air stratification, additional heat gains and losses on every wall and roof from the solar irradiation and high speed winds and other disturbances introduced by opening the warehouse door for HGVs when no vehicle is parked on the entry for example. Another examples of work providing thermal model development methodologies for the HVAC systems with analysis of difficulties, advantages and drawbacks of modelling approaches, e.g. resistance or computational fluid dynamics (CFD) models, and simulation tools are review papers by Homod (2013) and Harish & Kumar (2016b), where research gaps have also been identified. Simulation tools vary for multi-purpose computation and simulation software, such as MATLAB, Scilab or Maple, to software dedicated specifically to building thermal behaviour simulation, e.g. SIMEDIF developed at INENCO (Non Conventional Energy Research Institute) used by Larsen et al. (2009) to analyse thermal behaviour of the building walls in summer in Argentina. Modelling based on first principles and differential equations proposed in this chapter is not new methodology, however authors explore different ways to prepare the model tailored for needs of their research. The advantage of first principle modelling is its flexibility to model every construction and thermal process, provided the physical quantities are known or can be well estimated. It should be noted, however, that every model is only an approximation of the real system. The examples of thermal modelling based on first principles and differential equations are works by Faizollahzadeh Ardabili et al. (2016) and Harish & Kumar (2016a). In the first work, the model is used for HVAC system control with use of fuzzy and predictive control, while authors of the second paper use the first principles method to model building energy systems and energy transfer processes; both use MATLAB as a simulation software. The alternative strategy is proposed by Zajíc (2013), where Hammerstein-bilinear approach is considered for nonlinear modelling, analysis and control design of HVAC, where the results shown demonstrate that knowledge of the system's nonlinearities combined with ability to handle them brings improvement in an overall control performance.

Data-based mechanistic modelling (DBM) of the indoor air temperature distributions based on energy input is proposed by Youssef et al. (2011b). This approach acknowledges that better understanding and management of energy distribution in heating, ventilating and air conditioning of the indoor spaces is essential for the improvement of process quality and efficiency of energy use. The paper states that the proposed study is intended to be used with advanced multivariable Proportional-Integral-Plus (PIP) control algorithms based on the Non-minimal State Space (NMSS) methods, which are introduced in Chapter 4 of the thesis.

Variety of modelling approaches for thermal control shows the importance of obtaining reliable model to facilitate good control design to optimal thermal control. Nevertheless, a thermal control of the large single space buildings is an underresearched area. Exadaktylos (2007) considers state-dependent parameter (SDP) model structure to account for the nonlinearity in an indoor thermal process when designing Model Predictive Control (MPC). This approach allows to predict the output and find optimal control values while preserving nonlinear (SDP) model structure. The author of this thesis believes that the use of SDP model interpretation can contribute to cost reduction in the model-based indoor temperature control systems applications.

2.1.2 Chapter overview

The purpose of this chapter is to introduce a model of an indoor air temperature derived from first principles. This model is based on an existing building, where an HVAC system is in operation. Recommended reading for thermal systems, HVAC systems and indoor temperature control include, but is not limited to, (Bell Jr., 2000; Chartered Institution of Building Services Engineers, 2005; Montgomery & McDowall, 2008; Underwood, 1999), which were also used for consultation during research and writing up of this chapter.

The chapter is structured in the following manner. Firstly, Section 2.2 introduces the case study facility, a warehouse storing pharmaceutical products, then Section 2.3 provides details of the plant (i.e. the system to be controlled) and a thermal system setup for a large single space building based on the pharmaceutical warehouse; then, Section 2.4 introduces mathematical formulation of the indoor thermal process based on first principles; next, Section 2.5 discusses on the system identification approach for modelling heating and cooling units using the data collected from the studied warehouse; further, the simulation study in Section 2.6 provides insight into first principles-based model; finally, the chapter is summarised in Section 2.7.

2.2 Case study facility

During the run of the project, the author of this thesis was privileged through collaboration with Jet Environmental Systems Ltd. to study one of the facilities served by their HVAC control system. This facility was chosen as it represents a typical warehouse setup with heating and cooling capabilities. The temperature control is in operation to meet the indoor air temperature requirements for safe storage of pharmaceutical products. The warehouse is located in Midlands, UK and has the following dimensions: $100 \times 96 \times 15.5$ [m] (length $\times$ width $\times$ height) as found in Design Technical Submission provided by Jet Environmental Systems. There is also a three-floor open mezzanine area within the warehouse, i.e. ground floor, then first and second floor, each measuring 32×60 [m] (length $\times$ width). Mezzanine area is neglected in modelling and considerations in further chapters.

2.2.1 Heating, ventilation and air conditioning system

The warehouse is served by two identical air handling units focused on two main temperature zones, each having its own Air Handling Unit (AHU), cooling unit, heating unit, supply air ductwork, return air ductwork, supply fan and inlet dampers section. One AHU distributes the air in the main warehouse area, whereas the other distributes the air across the mezzanine area. An image showing the considered AHUs is provided in Figure 2.1, where elements for one of them have been marked and described. An image showing the inside of the warehouse is given in Figure 2.2.

A set of dampers for each AHU allows to switch between recirculating the indoor air or drawing the fresh air from the outside. If the damper blades are open, fresh air is drawn into AHU. Alternatively, if the damper blades are closed, the air entering the AHU via the return air duct is passed through the AHU and then back into the conditioned space (provided the supply air fan is operating). The temperature of the air passing through the AHU can be decreased by using cooling unit, increased by using heating unit, or the air can be passed as it is to stir the air and reduce stratification for example.

2.2.1.1 Controller and temperature sensors

Each AHU has its dedicated TREND IQ3 series controller with continuous space temperature control and two indoor temperature sensors. That is, there are four indoor sensors in total, two per zone. Each zone has one sensor located around 3m above the

FIGURE 2.1: The warehouse facility - outdoor HVAC system elements of two identical air handling units. The elements of the AHU serving the main warehouse area are: 1 - condenser unit (for cooling), 2 - fresh air inlet damper, 3 - return air duct, 4 - air handling unit, 5 - supply air duct, 6 - heating unit.

floor (low sensor) and one located close to the roof (high sensor). The temperature difference between two sensors from the same zone can be used to monitor air temperature stratification within the conditioned area. There is no return air temperature sensor, therefore the average air temperature is used for control.

The IQ3 controllers are networked together to share common information (e.g. the outdoor air temperature) and each controller is addressed separately. Both controllers are accessed via one IQView network display panel used by both units. The IQ3 control logic operates in 15 min intervals, which means that the air temperature measurements from sensors are read every 15 min to update the controls accordingly for heating, cooling, supply fan and mixing dampers. The algorithm implemented on the controllers calculates heating and cooling demand using proportion control of the PID module, which is then used to determine stage, i.e. 0, low (1) or high (2) of heating or cooling. To avoid competitive heating or cooling between the two AHUs, the indoor air temperature sensor readings are shared by both controllers to calculate the average indoor air temperature. To do that, each zone has calculated a mean value of its high and low sensor readings. Then, the mean values for each zone are used to calculate the

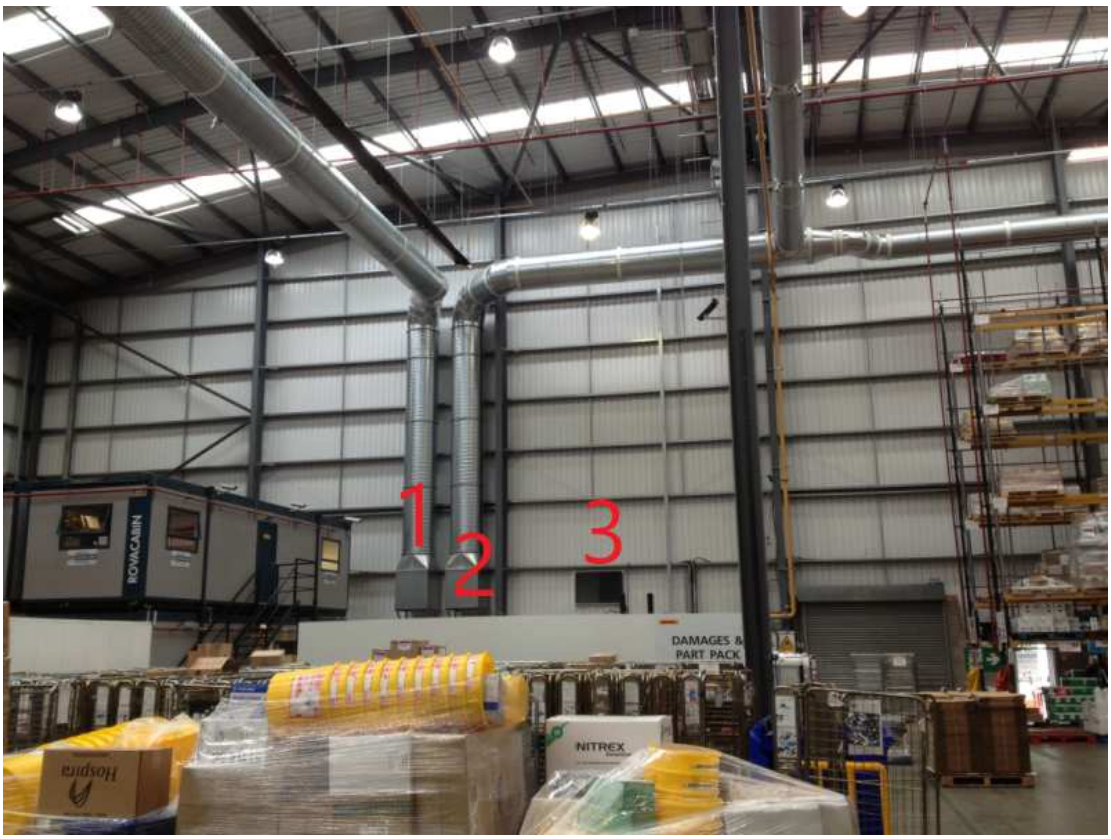

FIGURE 2.2: The warehouse facility - inside view. Legend: 1 - supply air duct (mezzanine area), 2 - supply air duct (main warehouse area), 3 - return air duct (main warehouse area)

average indoor air temperature. The average indoor temperature then is calculated as a weighted average taking 0.75 of the mean air temperature of the area the AHU is serving and 0.25 of the mean air temperature of the other area.

There is an outdoor air temperature sensor measuring the ambient air temperature, located behind one of the AHUs and shaded from sun and wind. The outdoor air temperature readings are passed to both controllers and used to determine free cooling capabilities described in Chapter 5, Section 5.2. Moreover, there is a supply air temperature sensor located in the supply air duct, but is not directly used for control, although it can be used to monitor temperature difference between the air entering the AHU (the outdoor air temperature or the average indoor air temperature) and the air leaving the AHU.

2.2.1.2 Technical details

Bespoke design of the HVAC system components for the considered warehouse facility assumes the following setup for each AHU:

- Airflow generated by supply fan: 9.25 m^3/s.
- Supply fan electric motor power: 18.5 kW.
- Two stage direct expansion (DX) cooling unit connected to an external, air cooled, condenser unit Climavenata HCAT 0512. Each condenser uses two compressors and provide two step cooling. Overall cooling capacity: 160 kW.
- Two stage gas fired burner unit: Reznor indirect gas burner RHC 8200 containing 200 kW heat exchanger with two stage burner control (low and high), although four stage is also possible.
- A set of mixing dampers.
- Panel filter section.

Each fan operates at 50-100 % of total fan speed or is switched off. The air is distributed through ductwork comprising of high velocity jet nozzle system for efficient blowing of the air at considerable distance from the ductwork to minimise air temperature stratification within the zone. If both supply fan units are operating at 100% of maximum speed, the air leaves the AHUs at rate of 18.5 m^3/s in total. Similarly, both cooling units can provide up to 320 kW cooling capacity.

2.2.2 Data acquisition

The IQ3 controller can be approached in multiple ways to access data and maintain settings such as heating and cooling set-points or manually set the damper position to closed. This can be done in multiple ways:

1. Use IQView panel on site to access the IQ3 controllers connected to the same network.
2. Connect PC to the local network on site (to which IQView panel and IQ3 controllers are connected) and use TREND-dedicated software to maintain the control strategy and settings.
3. Dial into the controller remotely using TREND-dedicated software or IP address (separate for each controller) in web browser. This requires local control system to be equipped with an active sim card with mobile data allowance.

2.2.2.1 Method of data collection

The data collection performed by the author of the thesis was achieved by accessing the controller remotely through IP address, where access is restricted and requires signing in as an administrator or other users with an appropriate level of rights. After signing in, the data can be viewed as a graph or as a list as depicted in Figures 2.3 and 2.4.

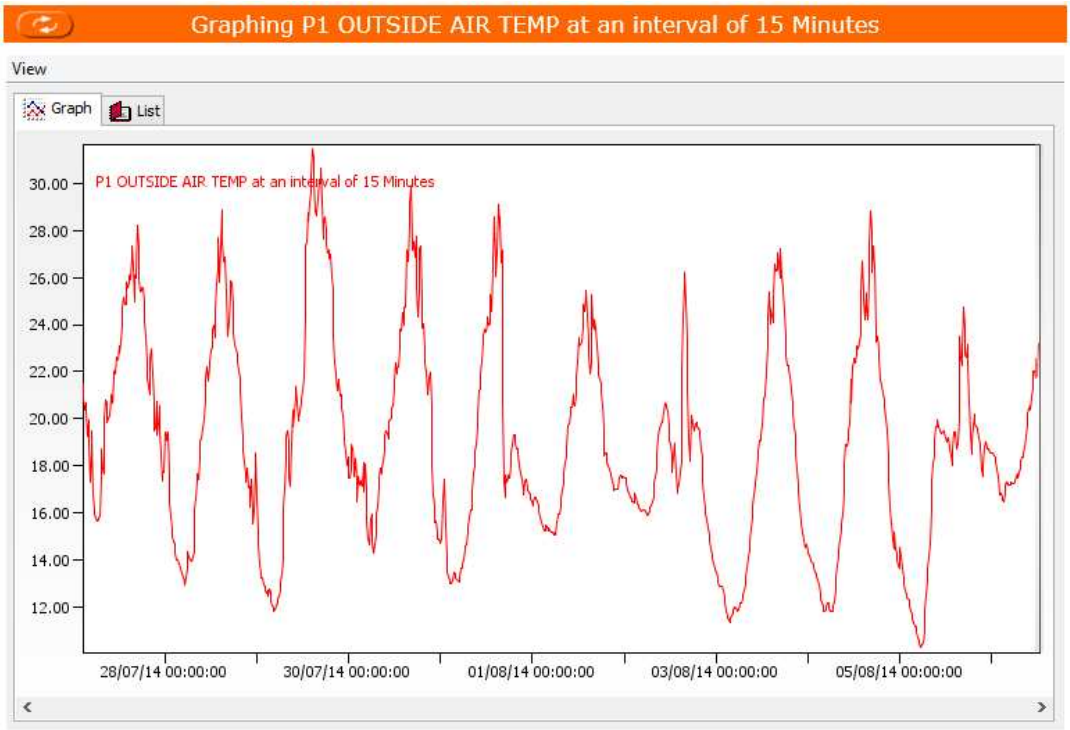

FIGURE 2.3: Graph representation of data recorded on the controller. Data is accessed remotely.

The controller is capable of storing the last 1000 records of each module (e.g. outdoor air temperature or damper position), therefore it is important to backup the data on regular basis. Having data saved every 15 min, the log holds the data of the past 10.4 days and the oldest sample is overridden with the newest value. In order to create a data backup the data must be collected manually as there is no easy way to set up automatic data recording. To do so, each data of interest (such as sensor readings, average indoor air temperature, heating and cooling operation, fan operation, damper position) has to be opened separately and displayed as a list, then the rows of the list have to be selected manually, then copied and pasted into previously prepared spreadsheet. The data from spreadsheet can be imported to MATLAB and processed as required. By default it is not possible to select rows in the list and copy them. To unlock this feature, user must make changes in Oracle Java policy on the machine used to collect the data. Recording data for a specific module has to be explicitly set within the control strategy or on the controller and no data is recorded on its own.

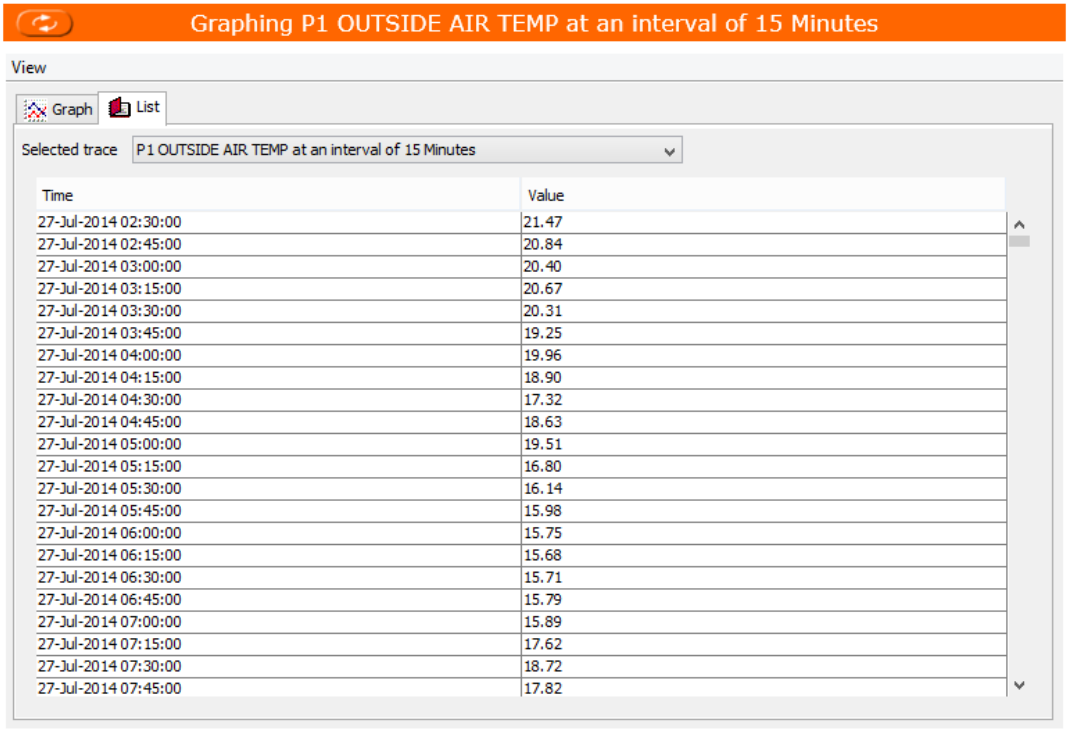

Time	Value
27-Jul-2014 02:30:00	21.47
27-Jul-2014 02:45:00	20.84
27-Jul-2014 03:00:00	20.40
27-Jul-2014 03:15:00	20.67
27-Jul-2014 03:30:00	20.31
27-Jul-2014 03:45:00	19.25
27-Jul-2014 04:00:00	19.96
27-Jul-2014 04:15:00	18.90
27-Jul-2014 04:30:00	17.32
27-Jul-2014 04:45:00	18.63
27-Jul-2014 05:00:00	19.51
27-Jul-2014 05:15:00	16.80
27-Jul-2014 05:30:00	16.14
27-Jul-2014 05:45:00	15.98
27-Jul-2014 06:00:00	15.75
27-Jul-2014 06:15:00	15.68
27-Jul-2014 06:30:00	15.71
27-Jul-2014 06:45:00	15.79
27-Jul-2014 07:00:00	15.89
27-Jul-2014 07:15:00	17.62
27-Jul-2014 07:30:00	18.72
27-Jul-2014 07:45:00	17.82

FIGURE 2.4: List representation of data recorded on the controller. Data is accessed remotely.

The choice of the data collected was made based on how informative and useful it is. While some data might be found not important at first, they could be used to cross check controller operation and identify inaccuracies and unexpected outputs. Examples of the data points collected and stored include:

- outside air temperature,
- supply air temperature,
- minimum space temperature,
- maximum space temperature,
- supply fan heating mode usage,
- supply fan free cooling mode usage,
- supply fan mechanical cooling mode usage,
- damper blades usage,
- cooling stage 1 usage,
- cooling stage 2 usage,
- combined average space temperature (weighted average specific to controller).

2.2.2.2 Data reliability and sensors

The temperature sensors have been placed by TREND-trained engineers in the most representative place and free of disturbance, e.g. not directly under the nozzle, and tuned to provide the most representative air temperature reading for the area it is placed in, removing possible biases. The sensors are provided by TREND and are a part of T-Px series. The outdoor air temperature is measured using internal wall sensor and the outdoor air temperature is measured using wall outside sensor. The accuracy of the sensing element of the outdoor and duct sensors is $dt = \pm(0.15 + 0.002|t|)°\text{C}$. The accuracy of the indoor sensor is $\pm 0.3°\text{C}$ at $+20°\text{C}$. The author of the thesis didn't have an option to add or remove temperature sensor or manually change the operation of heating or cooling units.

2.3 Thermal system setup

The considered system is based on an existing pharmaceutical warehouse facility located in Midlands, United Kingdom introduced in Section 2.2. This represents a typical arrangement for an indoor air temperature control solution providing thermal comfort in large volume open plan buildings (Goodfellow & Tahti, 2001). The developed system model will be subsequently used for control design purposes and simulation studies provided in this thesis. The system set-up is depicted schematically in Figure 2.5. The total volume of the conditioned space is $185\,472\,\text{m}^3$ and is served by the AHU adjacent to the warehouse.

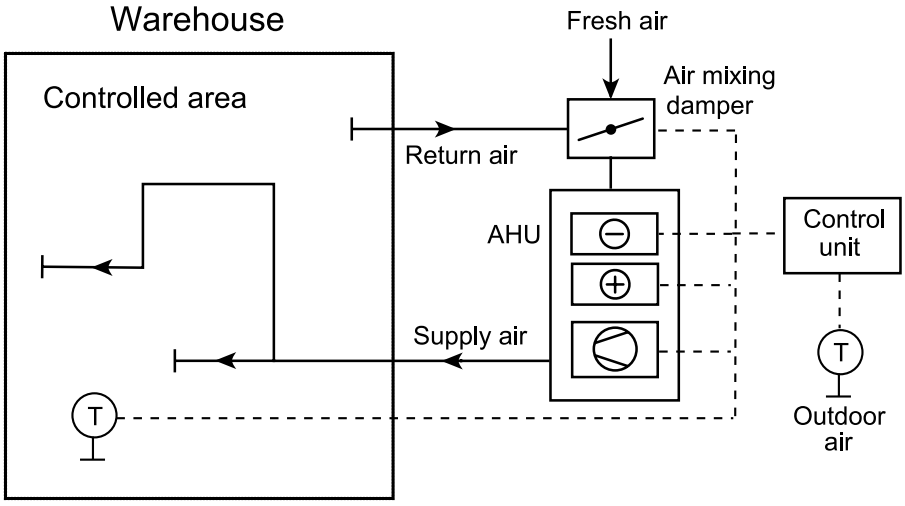

FIGURE 2.5: Indoor air temperature control system of a large space building.

The following components can be distinguished in the thermal system depicted in Figure 2.5:

- **Controlled area** The indoor space of a large volume building where the temperature is controlled to a given temperature set-point.
- **Air mixing damper** An air damper which regulates the mixing ratio between the outdoor air intake and indoor air re-circulation. In other words, the damper is used to control the airflow analogous to a valve that controls water flow. The damper uses a set of blades which allows for full fresh outdoor air entry when fully open or allows for full indoor air re-circulation when fully closed.
- **Air handling unit** Central air conditioning system comprising of heating unit, cooling unit and supply air fan unit to condition the air passing through and distribute it via the ductwork within the controlled area.
- **Control unit** The main micro-controller which contains the implemented control strategy to maintain the indoor environmental conditions by manipulating the actuators of the AHU together with an air mixing damper. The unit also uses multiple indoor and outdoor temperature sensor readings (denoted T) and is capable of remote internet communication with a master server. The master server commonly runs the building management system used by a building facility management.
- **Ductwork** The necessary duct system allowing for the conditioned air to be equally distributed within the conditioned area.

Considering the system depicted in Figure 2.5, the air temperature control is achieved through the distribution of conditioned supply air from the AHU. Subsequently, the air is returned back from the controlled area to the AHU via a network of return air ducts. The air recirculation is achieved via the choice of the damper blade position within the air mixing damper. The damper blade position allows to choose between a fresh outside air intake or to recirculate the indoor (return) air. The indoor and outdoor air temperatures are constantly monitored by the control unit which then calculates the demand for heating or cooling at every sampling time instance based on the area's temperature set-points. Subsequently, the control unit decides on how this demand is going to be met. This can be achieved in two ways: (1) either via passive conditioning by using directly the outdoor air or (2) to actively condition the return air by means of mechanical heating or cooling. The control unit also must decide on whether to switch on or off the supply fan. By default, the air mixing damper is closed, i.e. full air re-circulation is assumed. Note that there is enough of fresh air for human personnel within the building due to air leakage (infiltration) and its volume.

For mathematical modelling and subsequent control design purposes it is beneficial to re-draw the system schematic diagram from Figure 2.5 into a control block diagram

as shown in Figure 2.6. Four system inputs are considered: (1) The internal heat gain within the conditioned zone denoted $q(t)$ [W]. (2) Measured outdoor air temperature $T_a(t)$ [K], which is perceived as a load disturbance together with the heat gain $q(t)$. Note that $T_a(t)$ is entering the system directly at the inlet of the mixing box and also introduces heat gain within the conditioned zone indirectly via a heat transfer through the building's envelope. (3) The differential temperature of the air passing through the AHU introduced by active heating or cooling denoted $\Delta T(t)$ [K]. (4) A final manipulated input is the position of damper blades, denoted $u_d(t)$, defined as

$$T_d(t) = \begin{cases} T_a(t), & u_d(t) = 1 \\ T_r(t), & u_d(t) = 0 \end{cases} \tag{2.3.1}$$

where $T_d(t)$ denotes the temperature of the air leaving the air mixing damper (before it enters the AHU). Alternatively, $T_d(t)$ can be also expressed as

$$T_d(t) = u_d(t)T_a(t) + (1 - u_d(t))T_r(t) = u_d(t)T_a(t) + T_r(t) - u_d(t)T_r(t) \tag{2.3.2}$$

The supply air temperature, denoted $T_s(t)$ [K], is defined as a sum of $T_d(t)$ and $\Delta T(t)$, i.e. $T_s(t) = T_d(t) + \Delta T(t)$. The measured return air temperature is denoted $T_r(t)$ [K] and is chosen to be the single output of the thermal system. Air flow rate is denoted $m_a(t)$ [m^3/s].

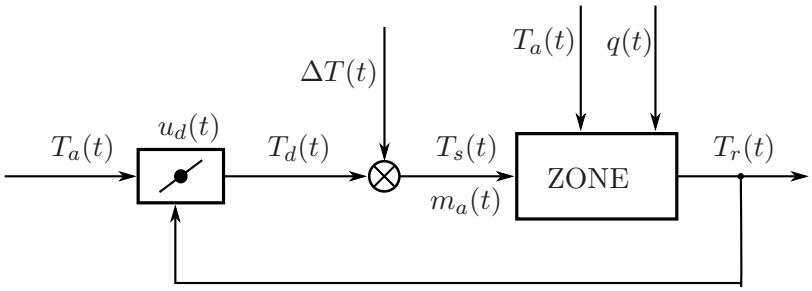

FIGURE 2.6: Control block diagram representation of the large space building (system) represented by ZONE.

Note that the indoor air can be passed back into AHU and then back to ZONE, creating a loop. While it is desirable under certain conditions to reuse the indoor air, it is worth to consider that the model represented by the block diagram shown in Figure 2.6 contains a positive feedback loop, which tends to cause system to become unstable.

2.4 Mathematical modelling of the indoor thermal process

Mathematical modelling of the real world thermal process based on first principles presented in this thesis allowed to grasp the main characteristics of the large space building in accordance with a heat flow concept (see e.g. Bell Jr., 2000; Çengel & Boles, 2006; Chartered Institution of Building Services Engineers, 2005; Underwood, 1999). A simple model of the indoor air temperature is settled on energy balance where the temperature of the indoor air is a dynamic thermal process compounding three essential thermal energy exchanges. That is, the indoor air temperature in single space building is shaped by (1) an internal heat gain, (2) the temperature of the air supplied and (3) a heat transfer accompanying the building envelope, i.e. the temperature of the walls surrounding the controlled area. A simplified diagram representing thermal energy exchange for a single space building as a multiple input single output (MISO) system is shown in Figure 2.7. Time index t has been chosen to emphasise a continuous-time nature of the process. The supply air entering the conditioned space is dispensed at temperature $T_s(t)$ [K] and air volume flow rate $m_a(t)$ [m^3/s]. The indoor air temperature is altered by thermal energy generated within the building, e.g. lights, personnel or operating machines, denoted $q(t)$. Further, the heat transfer through conduction is used to describe the heat transfer through the walls, where the ambient (outdoor) air temperature, denoted $T_a(t)$ [K] and the wall temperature denoted $T_w(t)$ [K] are of main interest. Note the mean temperature of the walls is shaped by the exterior conditions on the outer side and the indoor conditions on the inner side; the term walls is used to describe a building envelope enclosing the controlled area, where the structure consists of external walls of the building supporting the roof and the roof (or ceiling on the inner side). Carrying three main contributions, $\{T_a(t),\, T_s(t),\, q(t)\}$, the return air leaves the building at the temperature $T_r(t)$ [K] which is equivalent to the mean temperature of the air within the controlled area. It is assumed that thermal stratification is not present and the supply air temperature is evenly distributed across the whole space in no time.

The selection of inputs and outputs of the thermal system shown in Figure 2.7 is taken directly from the literature (Underwood, 1999) and is also based on the actual control strategies implemented on the controllers. It is worth noting that the overall thermal process is more complicated and the accuracy of the model can be further improved if the following are considered. For instance, the heating effects originating from building's outside can be further refined by incorporating the more weather conditions beyond the outdoor air temperature only, such as solar irradiation and wind speed. Accordingly, the heat transfer through walls could be refined by taking into account the solar energy affecting the walls and roof of the building. Furthermore, the model can be further improved by considering the effect of wind speed prominence by means of

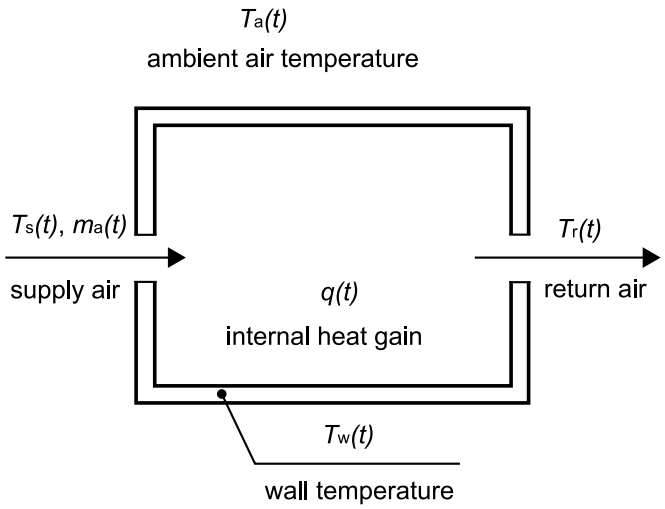

FIGURE 2.7: Basic model of a thermal process for an open space building.

infiltration through change in rate of air leakage and chilling effect on the walls and roof areas. While all these variables can further improve the accuracy of the model, their inclusion to the model depend vastly on whether they can be measured or not. On the other hand, including too many variables may tend to complicate the model and compromise the use of the model for our purpose of control design. In this case, we can treat those variables as variable disturbance or offset term while keeping the main dynamics of the model simple.

While the internal heat gain and the supply air temperature together with the air flow can be relatively easy to estimate or known in value, it should be noted, however, that the temperature of the wall is a total of heat exchange between the wall and the outdoor air on the outer side plus the wall and the indoor air on the inner side of the wall. To account for the two part heat exchange of the thermal process describing the temperature of the walls (i.e. outdoor air-outer wall and indoor air-inner wall), we consider each part of the heat exchange as a state variable and the resulting two state variables is modelled with a second order linear differential equation. Representation of two individual energy elements is expected to be reflected in two individual rates of change, with one being faster than the other. The set of two differential equations is detailed in Section 2.4.1. It is considered that rate of change related to building envelope is lower in comparison to the indoor air temperature process, however, the first one is explicitly dependable on the wall thermal attributes resting on material properties it is built of and its thickness. Assuming the rate of change in the wall temperature is equal to 0, a reduced order model can be obtained and the details of this is given in Section 3.4.

2.4.1 First principles conceptual model of the indoor thermal process

The model of the thermal system shown in Figure 2.7 has been established as a core of further considerations to define a model of the system with respect to mathematics. Additional simplifying assumptions has been adopted such that the lumped parameter modelling approach is considered, meaning that some contributions, difficult for modelling, are neglected and model accuracy is biased (Ramallo-González et al., 2013; Touretzky & Baldea, 2014). For simplicity, it is assumed that the air is evenly distributed across the space with no delay and the air is within the building is perfectly mixed with all points across the space having the equal temperature; similarly, no time delay for the heat transfer through walls is assumed. With that the final equations representing the thermal system are reduced into ordinary differential equations (Atkinson, 2009; Jackiewicz, 2009) with a finite number of parameters. The two states of the model are the return air temperature $T_r(t)$ [K] and the temperature of the wall $T_w(t)$ [K] (Underwood, 1999; Çengel & Boles, 2006; Zajíc, 2013). Predominant contributions have been encapsulated in the energy balance statement given in Equations (2.4.1a) and (2.4.1b) forming conceptual mathematical model of the indoor thermal process as a continuous dynamical system of two differential equations

$$\begin{aligned} C_r \frac{\mathrm{d}T_r(t)}{\mathrm{d}t} =& m_a(t)\rho_a c_a \left[T_s(t) - T_r(t)\right] - (UA)_{int}\left[T_r(t) - T_w(t)\right] \\ &+ q(t) - n_v \frac{\rho_a V_r c_a}{3600}\left[T_r(t) - T_a(t)\right] \end{aligned} \tag{2.4.1a}$$

$$\begin{aligned} C_w \frac{\mathrm{d}T_w(t)}{\mathrm{d}t} =& (UA)_{int}\left[T_r(t) - T_w(t)\right] - (UA)_{ext}\left[T_w(t) - T_a(t)\right] \\ &+ q_i(t) \end{aligned} \tag{2.4.1b}$$

where

- C_r/C_w [J/K] - thermal capacity of the air/wall,
- $m_a(t)$ [m^3/s] - air volume flow rate,
- ρ_a [kg/m^{u}3] - density of the air,
- c_a [J/(kg · K)] - specific heat capacity of the air,
- U_{int}/U_{ext} [W/(m^2 · K)] - heat transfer coefficient on the inner/outer side of the walls,
- A_{int}/A_{ext} [m^2] - effective surface area of the inner/outer walls,
- $q(t)$ [W] - heat load disturbance within the indoor space,
- V_r [m^3] - volume of the air within the indoor space,

- $T_a(t)$ [K] - outdoor air temperature,
- $T_w(t)$ [K] - mean temperature of the walls,
- $T_s(t)$ [K] - supply air temperature,
- $T_r(t)$ [K] - mean temperature of the air within the indoor space,
- n_v [1/h] - air change rate,
- $q_i(t)$ [W] - solar irradiation heat load on the outer side of the walls.

The calculation of the units for the variables given in Equations (2.4.1a) and (2.4.1b), respectively, are

$$\begin{aligned}\frac{\mathrm{J}}{\mathrm{K}}\cdot\frac{\mathrm{K}}{\mathrm{s}} =& \frac{\mathrm{m}^3}{\mathrm{s}}\frac{\mathrm{kg}}{\mathrm{m}^3}\frac{\mathrm{J}}{\mathrm{kg}\cdot\mathrm{K}}\cdot[\mathrm{K}-\mathrm{K}]-\left(\frac{\mathrm{W}}{\mathrm{m}^2\cdot\mathrm{K}}\cdot\mathrm{m}^2\right)\cdot[\mathrm{K}-\mathrm{K}]\\ &+\mathrm{W}-\frac{1}{\mathrm{h}}\cdot\frac{\frac{\mathrm{kg}}{\mathrm{m}^3}\cdot\mathrm{m}^3\cdot\frac{\mathrm{J}}{\mathrm{kg}\cdot\mathrm{K}}}{3600}\cdot[\mathrm{K}-\mathrm{K}]\\ \frac{\mathrm{J}}{\mathrm{K}}\cdot\frac{\mathrm{K}}{\mathrm{s}} =& \left(\frac{\mathrm{W}}{\mathrm{m}^2\cdot\mathrm{K}}\cdot\mathrm{m}^2\right)\cdot[\mathrm{K}-\mathrm{K}]-\left(\frac{\mathrm{W}}{\mathrm{m}^2\cdot\mathrm{K}}\cdot\mathrm{m}^2\right)\cdot[\mathrm{K}-\mathrm{K}]\\ &+\mathrm{W}\end{aligned}$$

which reduces to

$$\begin{aligned}\frac{\mathrm{J}}{\mathrm{s}} =& \frac{\mathrm{J}}{\mathrm{s}}-\mathrm{W}+\mathrm{W}-\frac{1}{\mathrm{h}}\cdot\frac{\mathrm{J}}{3600}\\ \frac{\mathrm{J}}{\mathrm{s}} =& \mathrm{W}-\mathrm{W}+\mathrm{W}\end{aligned}$$

Since $\frac{\mathrm{J}}{\mathrm{s}}=\mathrm{W}$ and $\frac{1}{\mathrm{h}}\cdot\frac{1}{3600}=\frac{1}{\mathrm{s}}$, it is confirmed that the units are consistent.

Note that while the unit for temperature considered in Equations (2.4.1a) and (2.4.1b) is Kelvin, the final unit (J/s) is independent of the temperature unit. Moreover, the dynamics of Equations (2.4.1a) and (2.4.1b) are described by the difference of temperature. Thus, the choice of temperature unit will not affect the dynamics of the thermal process.

The thermal capacities C_r and C_w are calculated with the following formula

$$C_r = \rho_a V_r c_a \tag{2.4.4}$$

$$C_w = \rho_w V_w c_w \tag{2.4.5}$$

where ρ_w [kg/m^3], V_w [m^3] and c_w [J/(kg $\cdot$ K)] are wall material density, volume of the walls and specific heat capacity of the wall material, respectively. The units on the

right-hand side of both above equations are

$$\frac{\text{kg}}{\text{m}^3} \cdot \text{m}^3 \cdot \frac{\text{J}}{\text{kg} \cdot \text{K}} = \frac{\text{J}}{\text{K}}$$

which is equal to the units on the left-hand side.

The area-integrated fabric surface U-value, denoted (UA), is the overall heat transfer calculated as a sum of the heat flows through the individual areas such as walls, ceiling and floor. The heat transfer through the inner wall side, $(UA)_{int}$, and outer wall side, $(UA)_{ext}$, respectively, are computed as

$$(UA)_{int} = \sum U_i A_i = U_{wall} A_{wall} + U_{ceil} A_{ceil} + U_{floor} A_{floor} \tag{2.4.6a}$$

$$(UA)_{ext} = \sum U_i A_i = U_{wall} A_{wall} + U_{ceil} A_{ceil} \tag{2.4.6b}$$

The internal heat transfer is calculated using the areas of walls, denoted A_{wall}, ceiling, denoted A_{ceil}, and floor, denoted, A_{floor}, and its respective heat transfer coefficients, namely U_{wall}, U_{ceil} and U_{floor}. The external heat transfer is calculated using the areas of walls, denoted A_{wall} and ceiling, denoted A_{ceil}, and its respective heat transfer coefficients, namely U_{wall} and U_{ceil}.

The conceptual model of the system is made up by two separate energy balance equations (2.4.1a) and (2.4.1b), each referring to one of two possible states. Equation (2.4.1a) refers to changes in the indoor air temperature, specified on the left-hand side of the equation. Equation (2.4.1b) refers to changes in the mean temperature of the wall, which is not directly measured. The components on the right-hand side of Equation (2.4.1a) contributing toward the indoor air temperature are energy received from the AHU, heat transfer on an inner side of the wall, the internal heat gain and the outdoor air leakage into the building. The mean temperature of the walls on the left-hand side of Equation (2.4.1b) is shaped by the exterior conditions on the outer side and the indoor conditions on the inner side. The components on the right-hand side of Equation (2.4.1b) contributing to the mean temperature of the walls are the heat transfer on the inner side of the wall, the heat transfer on the outer side of the wall, the heat gain due to sun irradiation on the outer side of the wall and the heat gain due to wind blowing on the outer side of the wall.

For the thermal systems described using Equations (2.4.1a) and (2.4.1b) to be representative of the thermal system, the physical quantities in the equations have to be known or estimated. Alternatively, the unknown terms should be substituted with black box components. Investigating the consequences of assuming some parameters of the first principles model to be constant, i.e. the thermal capacity of the air, the density

of the air and the air specific heat capacity, it has been recognised that the discrepancies between extreme values are negligible when modelling for control is considered. These parameters are altered by meteorological variables such as atmospheric pressure and water vapour in the air. The studies have been carried out by direct calculation of the thermal capacity of the air, the density of the air and the air specific heat capacity for range of possible values of the atmospheric pressure and the air humidity. Therefore, these parameters are set to constant at the most representative value within the considered range.

2.4.2 Laplace transform interpretation of the indoor thermal process differential equations

The indoor thermal process model proposed in previous subsection has two states, $T_r(t)$ and $T_w(t)$. Since the main interest lies in obtaining a dynamic model describing the relationship between the system inputs $\{T_s(t),\, m_a(t),\, T_a(t),\, q(t)\}$ and the output $T_r(t)$ and the knowledge of the wall temperature $T_w(t)$ is not of direct interest here, the wall temperature $T_w(t)$ has been substituted with its energy balance equivalent. The model of the indoor thermal process in Equation (2.4.7) has been obtained as a continuous time second order model by solving a coupled system of first order differential Equations (2.4.1). Assuming no changes in $m_a(t)$ and $q(t)$, the first derivative terms $\dot{m_a}(t) = 0$ and $\dot{q}(t) = 0$. The solution leads to the indoor thermal process represented as

$$a_0\ddot{T_r}(t)+a_1\dot{T_r}(t)+a_2T_r(t) = b_0\dot{T_s}(t)+b_1T_s(t)+\bar{b_0}\dot{T_a}(t)+\bar{b_1}T_a(t)+c_0q(t)+\bar{c_0}q_i(t) \quad (2.4.7)$$

Applying Laplace transform to Equation (2.4.7), assuming zero initial conditions, and using C_r dependencies given in Equation (2.4.4), the indoor thermal process is represented in s-domain as

$$\big(a_0s^2 + a_1s + a_2\big)T_r(s) = \big(b_0s + b_1\big)T_s(s) + \big(\bar{b_0}s + \bar{b_1}\big)T_a(s) + c_0q(s) + \bar{c_0}q_i(s) \quad (2.4.8)$$

where

$$
\begin{aligned}
a_0 &= 1 \\
a_1 &= \frac{(UA)_{int}}{C_r} + \frac{n_v}{3600} + \frac{m_a}{V_r} + \frac{(UA)_{int} + (UA)_{ext}}{C_w} \\
a_2 &= \frac{(UA)_{int} + (UA)_{ext}}{C_w} \cdot \left[\frac{m_a}{V_r} + \frac{n_v}{3600}\right] + \frac{(UA)_{int}(UA)_{ext}}{C_w C_r} \\
b_0 &= \frac{m_a}{V_r} \\
b_1 &= \frac{(UA)_{int} + (UA)_{ext}}{C_w} \cdot \frac{m_a}{V_r} \\
\bar{b_0} &= \frac{n_v}{3600} \\
\bar{b_1} &= \frac{(UA)_{int} + (UA)_{ext}}{C_w} \cdot \frac{n_v}{3600} + \frac{(UA)_{int}(UA)_{ext}}{C_w C_r} \\
c_0 &= \frac{(UA)_{int} + (UA)_{ext}}{C_w C_r} \\
\bar{c_0} &= \frac{(UA)_{int}}{C_w C_r}
\end{aligned}
$$

and term $m_a(t)$ is denoted m_a. Such representation of the indoor thermal process may be used to create a discrete time domain model for simulation purposes in a mathematical software and analysis of the model characteristics.

2.5 Black-box temperature model of Air Handling Unit

The main components of the AHU are the air mixing box with damper, the heating unit, the cooling unit and the supply fan unit, see Section 2.3. The air mixing damper acts as a switch, but the other units can be approximated with simple first order models and used to simulate the AHU operation. This section is focused on extracting parameters for the heating and cooling units sub-models using system identification. Since the dynamics of the indoor air temperature is slow and the data used for parameter estimation is recorded at 15 min sampling time, the parameter estimation is performed in discrete time domain. The data have been recorded in the existing warehouse facility operating the HVAC system, therefore the data represents the actual control system operation without prior experimental setup.

2.5.1 Heat loads within the Air Handling Unit

The heat load $\Delta T(t) = T_s(t) - T_d(t)$ generated in the AHU (Section 2.3) can be rewritten as

$$\Delta T(s) = \Delta T_h(s) + \Delta T_c(s) + \Delta T_f(s) + G_a(s) \cdot T_a(s) \tag{2.5.1}$$

with

$$\Delta T_h(s) = G_h(s) \cdot u_h(s) \tag{2.5.2}$$

$$\Delta T_c(s) = G_c(s) \cdot u_c(s) \tag{2.5.3}$$

$$\Delta T_f(s) = G_f(s) \cdot u_f(s) \tag{2.5.4}$$

where $\Delta T_h(s)$, $\Delta T_c(s)$ and $\Delta T_f(s)$ reflect the temperature changes caused by the heating unit, cooling unit and the supply fan unit, respectively, and $G_h(s)$, $G_c(s)$, $G_f(s)$ and $G_a(s)$ are the continuous-time transfer functions corresponding to three manipulated control inputs $u_h(s)$, $u_c(s)$, $u_f(s)$, and one uncontrollable input $T_a(s)$, respectively. The inputs $u_h(s)$, $u_c(s)$ and $u_f(s)$ control the heating unit, cooling unit and supply fan unit, respectively, taking values between 0 and 1, where 0 corresponds to 0% and 1 corresponds to 100% of total potential of a controlled unit. Note that $\Delta T_h(s)$ and $\Delta T_f(s)$ take non-negative values because heat is generated while the heating unit or the supply fan unit is in operation. Note also that $\Delta T_c(s)$ takes non-positive values since the heat is removed to decrease the temperature of the air whenever the cooling unit is in operation. The impact of the outdoor conditions acting through the AHU walls $G_a(s) \cdot T_a(s)$ can be modelled in a similar manner as done for the building if the thermal properties of the AHU walls are known or can be estimated to improve the accuracy of the $\Delta T(s)$. Ideally, the AHU should be insulated well enough to avoid outdoor conditions influence the air passing through AHU in any manner other than known, measurable and controlled via the position of damper blades. In further considerations this disturbance in neglected due to its insignificant impact compared to the overall system and inability to measure it. It has been confirmed that all effort has been taken to insulate the AHUs of the studied warehouse and the outdoor conditions should have minimal impact on the air within AHU.

Equations (2.5.2), (2.5.3) and (2.5.4) allow to model separately each of the components within the AHU. Here, $G_h(s)$, $G_c(s)$ and $G_f(s)$ are modelled as first order systems. The achievable temperature change caused the operation of the heating unit, the cooling unit and the supply fan unit is calculated as

$$\Delta T_{h/c/f}(t) = \frac{q_{max}}{m_a(t) c_a \rho_a} \tag{2.5.5}$$

where q_{max} [W] is the total maximum power output generated by the units, which is translated into the heating load. The right-hand side units calculation is

$$\frac{\mathrm{W}}{\frac{\mathrm{m}^3}{\mathrm{s}} \cdot \frac{\mathrm{J}}{\mathrm{kg \cdot K}} \cdot \frac{\mathrm{kg}}{\mathrm{m}^3}} = \frac{\mathrm{W}}{\frac{\mathrm{J}}{\mathrm{s \cdot K}}} = \frac{\mathrm{W}}{\mathrm{W}} \cdot \mathrm{K} = \mathrm{K}$$

which is consistent with the unit of the left-hand side referring to the temperature change. Since a change of one unit of Kelvin is equal to a change of one unit of degree Celsius, Equation (2.5.5) can also be used for calculations involving the latter unit. In further calculations of temperature change using Equation (2.5.5) it is assumed, based on specification of the studied warehouse, that $m_a = 18.5\,\mathrm{m}^3/\mathrm{s}$, $c_a = 1005\,\mathrm{J}/(\mathrm{kg}\cdot\mathrm{K})$ and $\rho_a = 1.183\,\mathrm{kg}/\mathrm{m}^3$. Note that q_{max} in the numerator of Equation (2.5.5) can be written as $q_{h/c} + q_f$, i.e. as a sum of the heat load coming from heating or cooling unit and supply fan. The physical meaning of this relationship is that the higher air flow rate, the smaller change in the air temperature. It is explained by the fact that the same amount of heat is distributed among bigger amount of the air. Similarly, the same heating load used to warm up (or cool down) smaller amount of air results in increased value of change in the temperature of the air. Note that the value of the air temperature change calculated using Equation (2.5.5) should be equal to the process gain of the respective function $G_h(s)$, $G_c(s)$ or $G_f(s)$.

2.5.2 Heating unit sub-model

It has been observed that the supply air temperature T_s depends on the input ΔT_O, the temperature of the air entering the AHU T_d and the outdoor air temperature T_a acting on the walls of the AHU. Any additional heat gains, e.g. accounting for a heat generated by fan motor, can be captured in an offset term denoted O. Assuming with regard to Equation (2.5.1) that there is no cooling element and the supply fan term is neglected on account of the offset term, the following equation can be formulated:

$$\Delta T_O(s) = G_h(s)\cdot u_h(s) + G_a(s)\cdot T_a(s) + O \tag{2.5.6}$$

The term $G_a(s)$ corresponds to the outdoor air temperature effect on the heating unit through the AHU envelope. Since the AHU is well insulated, according to the system specialists from Jet Environmental, the outdoor conditions should have negligible influence on the temperature within the AHU. The following first order discrete time transfer function is proposed with respect to the heating process based on Equation 2.5.6:

$$\Delta T_O(k) = \frac{b_h z^{-1}}{1 + a_h z^{-1}}\cdot u_h(k) + \frac{b_{hOAT} z^{-1}}{1 + a_h z^{-1}}\cdot T_a(k) + O \tag{2.5.7}$$

where the z operator denotes the forward shift operation, i.e. $z^i y(k) = y(k+i)$. The first term on the right-hand side refers to heating unit control input component, the second term refers to the outdoor air temperature component and the last is the offset term, which is a scalar. The left-hand side term $\Delta T_O(k)$, which is an output signal, equals to $T_s(k) - T_r(k)$, assuming the damper position is closed. The index k has been used to

emphasise discrete-time domain of the equation. The coefficients b_h and b_{hOAT} refer to two respective inputs u_h and T_a. Note that both terms have common denominator.

2.5.2.1 Dataset

The heating in the AHU of the real system as described in Section 2.2 is generated using gas burner. The heating unit model is characterised by the following features based on the real system:

- There are two AHUs operating with the same control strategy, but having different average indoor air temperature input T_r; one is biased toward open warehouse area (W), other toward mezzanine area (M). The data collected from both AHUs have been merged into one, i.e. it is assumed both AHUs work combined together. The system inputs and outputs used for the system identification are an average of the supply air temperature values coming from both AHUs, e.g. $T_s = (T_{sW} + T_{sM})/2$.
- Each AHU operates with 0 %, 50 % (stage 1) and 100 % (stage 2) of total heating capabilities, switching ON and OFF as dictated by the control system.
- The gas burner output for stage 1 based on the data provided is observed to be slightly different for both AHUs. It is concluded from the values of the supply air temperature readings as if for one of the units had 40% or 60% for stage 1 instead of 50%. To simplify, this discrepancy is neglected in further considerations.

The data presented in Figure 2.8 have been used as estimation dataset for system identification and hold the following criteria:

- The overall length of data used is 78 samples recorded uninterrupted with 15 min sampling time starting at 22/02/2017 15:15; the data has been recorded in the pharmaceutical warehouse in Midlands, UK supported by use of four indoor sensors and one outdoor sensor as described in Section 2.2.1.1.
- The position of damper blades is closed across all data points and the indoor air is recirculated.
- The supply fans are ON at all times, meaning that the air is supplied through the ductwork. The fan operates at 72.5% of its maximum speed when the heating unit is ON and 62% when the heating unit is OFF. For simplicity, the fan speed is neglected and assumed constant.

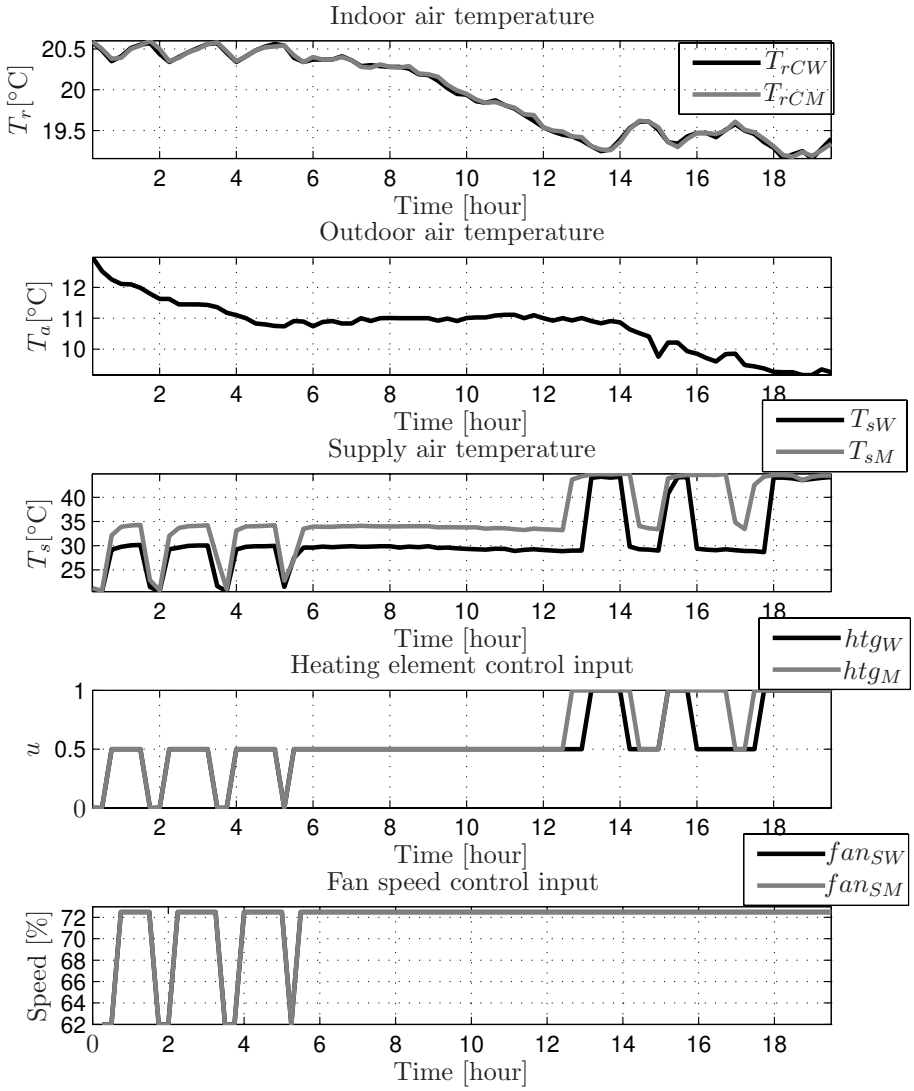

FIGURE 2.8: The heating unit sub-model estimation dataset.

The data presented in Figure 2.9 have been used as validation dataset and hold the following criteria:

- The overall length of data used is 150 samples recorded uninterrupted with 15 min sampling time starting at 05/04/2018 21:30; the data has been recorded in the pharmaceutical warehouse in Midlands, UK.
- The position of damper blades is closed across all data points and the indoor air is recirculated.
- The warehouse area supply fan is ON across all data points and operates at 100% of its maximum speed. The mezzanine area supply fan operates at 100% of its maximum speed when the heating is ON and 0% (air not supplied) when the

heating is OFF and the average mezzanine area air temperature T_{rM} is above switching differential level defined within the AHU control strategy. For simplicity, the fan speed is neglected in calculations.

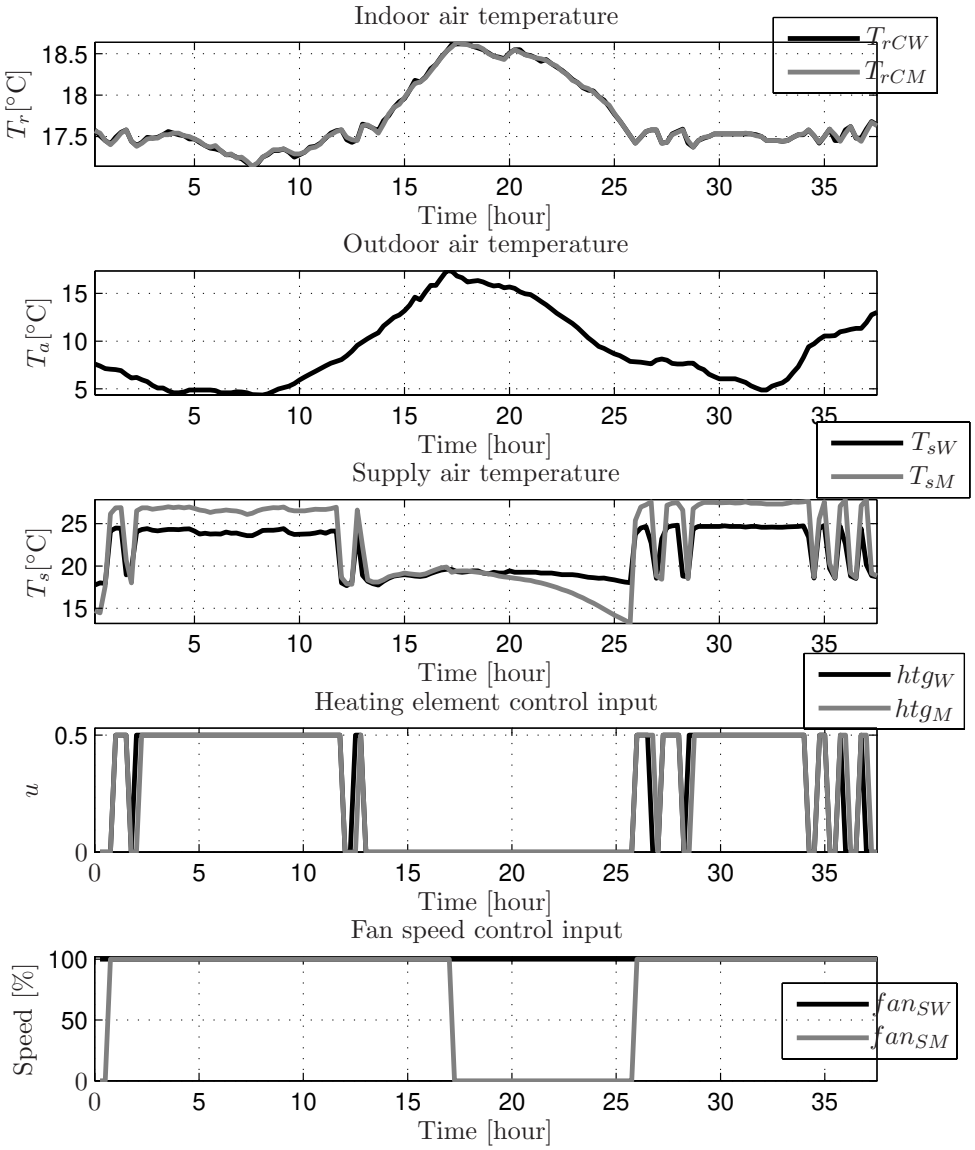

FIGURE 2.9: The heating unit sub-model validation dataset.

The fan speed control input shown in Figures 2.8 and 2.9 is not taken into consideration in system identification, but is provided for information purposes only to show coherence of data and analysis. Note that the use of heating unit (stage 1 or 2) means constant, non-variable, speed at which the supply fan operates, hence the data provided is not informative enough to identify meaningful parameters of the supply fan unit. The supply fan operation is well enough correlated with the heating unit operation, therefore the system identification methods might not be able to distinguish well between the head

loads of the heating unit and the supply fan unit. It is concluded that taking into consideration the supply fan as a separate term would not bring valuable improvement in the parameter estimation as the supply fan unit sub-model parameters would be poorly estimated.

The heating element control input has been normalised to vary between 0 and 1 corresponding to 0 and 100% of heating capabilities, respectively. Note that the control inputs, in this instance for heating unit and fan unit, may at times differ between AHUs as a consequence of correlated yet independent operation. Though the average is taken into consideration for the model parameters estimation, the values recorded by both AHUs separately are shown in Figures 2.8 and 2.9 to offer the reader deeper insight into the data. Analysing stage operation of the heating unit with constant interval between stages and visually inspecting the data provided, it is deemed that with the data provided a linear model is good assumption for system identification and control purposes, regardless of the expected nonlinear characteristics of the gas burner (typically found in the gas burner documentation). However, the estimated model of the heating unit could be improved in accuracy if nonlinear or bilinear model would be used and more informative data provided.

In all calculations and simulations, the disturbances such as warehouse loading door open, sun irradiation on the roof and the walls, heat generated by people and machines and effects due to storage mass are captured by the offset term O. Also, although the indoor air temperature sensors (four in total) have been tested and calibrated, all of them are used for control purposes and might have been calibrated to reflect the most accurate environmental conditions within the indoor space according to the engineer performing the calibration instead of actual reading for that particular space where the temperature sensor is placed. Similarly, the some of the sensor might be not calibrated properly. Another concern for the sensor readings is its accuracy of ± 0.3°C at +20°C as found in data sheet. These observations apply to both heating and cooling units.

2.5.2.2 System identification and validation and estimated model analysis

The parameter estimation method used to obtain the model parameters characterising the heating element using Equation (2.5.7) is Least Squares (LS) (see e.g. Bobál et al., 2005; Larkowski & Burnham, 2011). Although it has tendency to suffer from parameter bias in noisy data, LS is an elemental tool for parameter estimation in control engineering and regression analysis. It has been assumed that a first order system is enough to capture the main behaviour of the system and higher order model will not provide much improvement in model fit based on the current knowledge of the real system and quality

of the data available. The model parameters of Equation (2.5.7) obtained using the LS method are $b_h = 20.6858$, $a_h = -0.2093$, $b_{hOAT} = 0.3501$ and $O = -0.7582$ and the overall model fit for the estimation dataset is shown in Figure 2.10. The estimated model has been validated on different dataset and the results are shown in Figure 2.11.

The first term on the right-hand side of Equation (2.5.7) relates to the temperature increase caused by the heating unit operation. By not considering the other two terms of Equation (2.5.7) the heating unit sub-model is formulated as

$$\Delta T_h(k) = \frac{b_h z^{-1}}{1 + a_h z^{-1}} \cdot u_h(k) \tag{2.5.8}$$

and can be directly used in a simulation using discrete time model of the indoor air temperature to represent the heating unit operation.

The performance of the estimator was subjected to the following metrics calculation:

- R_T^2 - coefficient of determination, the percentage amount of variance calculated with respect to the output simulated by the estimated model,
- IAE - normalised integral of absolute error, a measure of the mean absolute error between the actual output and the estimated values,
- MSE - mean squared error, the average squared deviation of the estimated values from the actual output,

calculated, respectively, as

$$R_T^2 = 100(1 - \frac{||y - \hat{y}||_2^2}{||y - \bar{y}||_2^2}) \tag{2.5.9}$$

$$IAE = \frac{1}{N} \sum_{i=1}^{n} y(k) - \hat{y}(k) \tag{2.5.10}$$

$$MSE = \frac{1}{N} \sum_{i=1}^{n} y(k) - \hat{y}(k) \tag{2.5.11}$$

where y is a vector of actual output values, $\hat{y}$ is a vector of outputs generated (simulated) by a model and $\bar{y}$ is a mean value of y. These metric values produced for the estimated model for estimation and validation datasets are given in Table 2.2. The model fit on validation dataset demonstrates less accuracy than on estimation dataset, however the peaks and general behaviour are well reflected. The possible reasons for discrepancy include not informative enough indoor air temperature sensor readings, different level of internal heat loads, disturbances and weather conditions, e.g. sunny day on one dataset and overcast on the other.

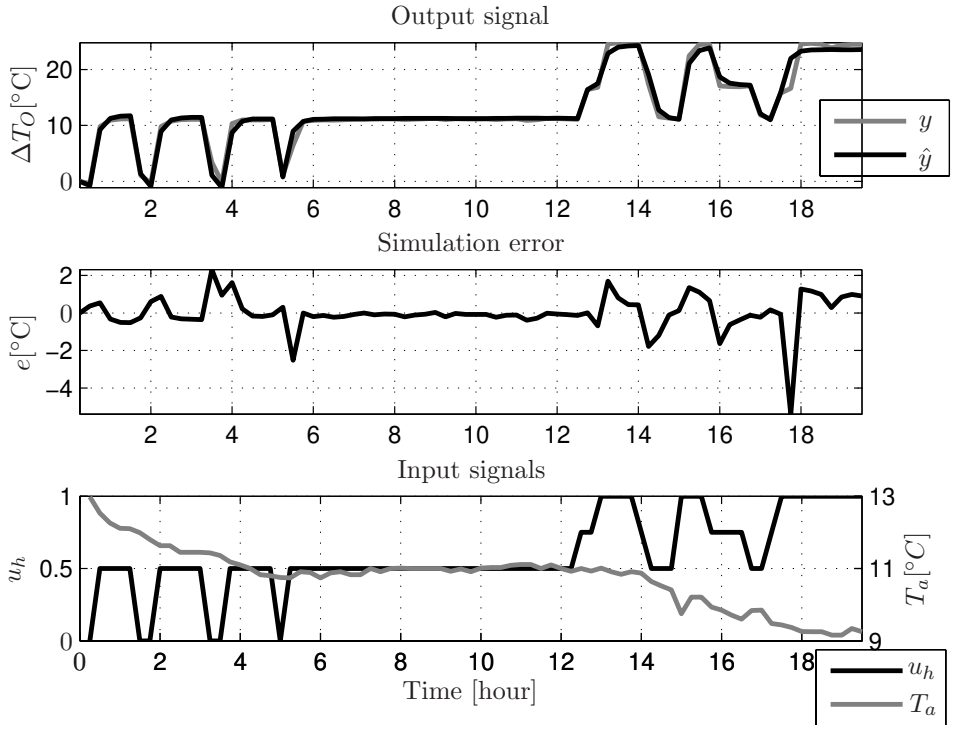

FIGURE 2.10: The heating unit sub-model (Equation (2.5.8)) using estimation dataset with ΔT_O (Equation (2.5.7)), error and input signals as a function of time.

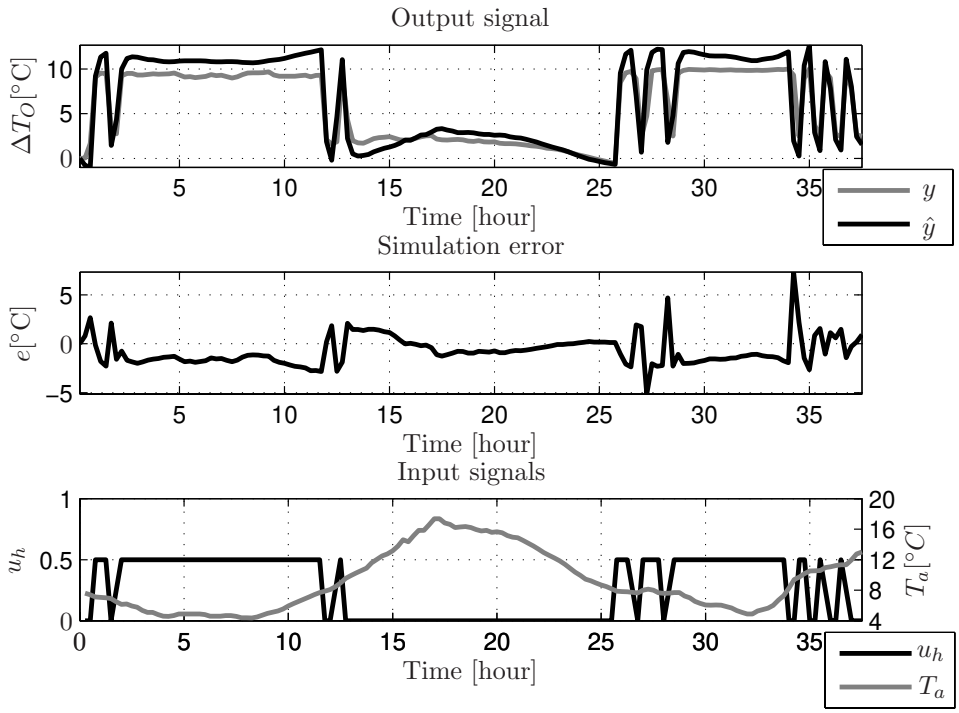

FIGURE 2.11: The heating unit sub-model (Equation (2.5.8)) using validation dataset with ΔT_O (Equation (2.5.7)), error and input signals as a function of time.

The discrete-time step response of the estimated model given in Equation (2.5.8) is shown in Figure 2.12; a hold between samples is assumed. Note that exciting the system

TABLE 2.2: Measures of the performance criteria for the estimated parameters of the heating unit sub-model (Equation (2.5.8)).

Criteria	**Estimation**	**Validation**
R^2_T [%]	97.8367	81.7624
IAE	0.5433	1.3605
MSE	0.8996	2.7733

with input signal $u_h = 1$ means that the heating unit is 100 % ON (stage 2) and this results in warming the air passing through the AHU. The temperature of the supply air leaving the AHU is changed by 26.16 °C from the temperature of the air entering the AHU and this is the process gain of sub-system provided in Equation (2.5.8). Note also that the steady state is approached in relatively short time, with settling time of 45 min, which is three times of the sampling interval. There is no overshoot or undershoot observed. The calculated time constant is $\tau_h = 9.59$ min which is a shorter time period than the sampling interval. This observation is consistent with the expected heating unit time constant. The step response leads to an overall temperature rise caused mainly by the heating unit and the heat gain coming from the supply fan motor. By knowing the maximum heating unit output 400 kW and the maximum supply fan output is 37 kW, the expected maximum temperature rise is be calculated using Equation (2.5.5) as

$$\Delta T_h = \frac{400 \cdot 10^3 + 37 \cdot 10^3 \cdot 0.725}{18.5 \cdot 0.725 \cdot 1005 \cdot 1.183} = 26.77\,^{\circ}\text{C} \tag{2.5.12}$$

assuming the fan speed is 72.5%. Note that this value is less than 1 °C different from the results obtained using system identification methods, where the step response settles at 26.16 °C.

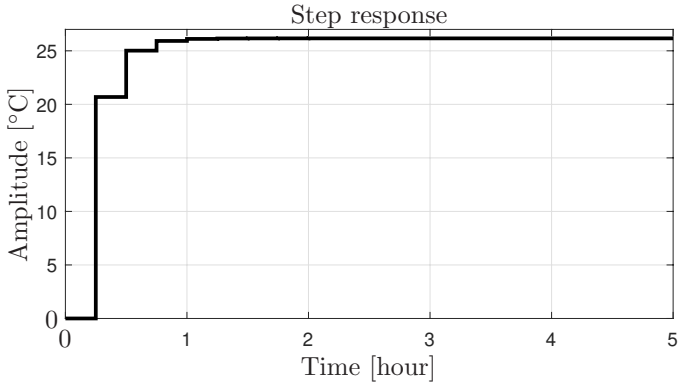

FIGURE 2.12: The heating unit sub-model step response - ΔT_h settling at 26.16 °C.

2.5.2.3 Second order model system identification of the heating unit

The data provided in Section 2.5.2.1 was used to estimate the heating unit sub-model assuming second order model structure provided in Equation 2.5.14, extracted from Equation 2.5.13, a respective second order model form of Equation 2.5.7.

$$\Delta T_O(k) = \frac{b_{h1}z^{-1} + b_{h2}z^{-2}}{1 + a_{h1}z^{-1} + a_{h2}z^{-2}} \cdot u_h(k) + \frac{b_{h1OAT}z^{-1} + b_{h2OAT}z^{-2}}{1 + a_{h1}z^{-1} + a_{h2}z^{-2}} \cdot T_a(k) + O \quad (2.5.13)$$

$$\Delta T_h(k) = \frac{b_{h1}z^{-1} + b_{h2}z^{-2}}{1 + a_{h1}z^{-1} + a_{h1}z^{-2}} \cdot u_h(k) \quad (2.5.14)$$

The model parameters of Equation (2.5.13) obtained using the LS method are $b_{h1} = 20.6344$, $b_{h2} = 2.1840$, $a_{h1} = -0.1157$, $a_{h2} = 0.0136$, $b_{h1OAT} = 0.2573$, $b_{h2OAT} = 0.1186$ and $O = -0.8904$.

The results represented through performance criteria are provided in Table 2.3. The improvement is negligible compared to first order system results in Table 2.2, offering less than 1% increase in R_T^2 and decrease in IAE and MSE observed at second and third decimal places. The settling point of ΔT_h is 26.21 °C. It is concluded that the higher order model does not allow to capture the heating unit behaviour better than a first order model with the given dataset. The explanation for that is the 15 min interval of the data sampled, which is not informative enough to provide more insight into the heating unit dynamics. The presence of a second or higher order dynamics is indistinguishable, hinting the data could be undersampled it terms of heating unit sub-model parameters estimation. While 15 min is suitable for control of a large space building, the heating unit is characterised by much faster thermal response given heating the passing air up by around 26 °C. In order to obtain tangible improvement in the model parameter estimations for the heating unit it is recommended for the sampling time to be at least 10 min. The suggested optimal sampling time to gather more informative data for heating unit identification is 5-10 min, bearing in mind overall controller performance and thermal response of the building. Furthermore, the improvement in both estimation and validation results could be observed if another dataset was available. Ideally, the dataset would come from an experiment where the heating unit operation is determined manually and/or pre-planned and is not relevant to the heating set-point, changing freely between 0, 50% and 100% output or additional stages if possible.

TABLE 2.3: Measures of the performance criteria for the estimated parameters of the heating unit sub-model using second order model structure (Equation (2.5.14)).

Criteria	**Estimation**	**Validation**
R^2_T [%]	97.8429	81.9908
IAE	0.5337	1.341
MSE	0.897	2.7386

2.5.3 Cooling unit sub-model

Following the concept proposed in the beginning of Section 2.5 in Equation (2.5.1), where the heat gain characterising the heating unit is obtained from the real data, the following transfer function has been formulated with respect to cooling unit

$$\Delta T_O(s) = G_c(s) \cdot u_c(s) + G_a(s) \cdot T_a(s) + G_f(s) \cdot u_f(s) + O \tag{2.5.15}$$

assuming there is no heating unit. Therefore, a first order discrete time transfer function representing the cooling unit is formulated as

$$\Delta T_O(k) = \frac{b_c z^{-1}}{1 + a_c z^{-1}} \cdot u_c(k) + \frac{b_{cOAT} z^{-1}}{1 + a_c z^{-1}} \cdot T_a(k) + \frac{b_f z^{-1}}{1 + a_c z^{-1}} \cdot u_f(k) + O \tag{2.5.16}$$

where the first term on the right-hand side refers to cooling unit control input component, the second term refers to the outdoor air temperature, the third term refers to the supply fan unit and the last one is the offset term, which is a scalar. The left-hand side term $\Delta T_O(k)$, which is an output signal, equals to $T_s(k) - T_r(k)$, assuming the damper position is closed. The coefficients b_c, b_{cOAT} and b_f refer to three inputs $u_c(k)$, $T_a(k)$ and u_f, respectively, and all three terms share a common denominator of the corresponding transfer functions.

2.5.3.1 Dataset

The cooling in the AHU of the real system as described in Section 2.2 is achieved using direct expansion air conditioning unit (DX unit). The cooling unit model is characterised by the following features based on the real system:

- There are two AHUs operating with the same control strategy, but having different average indoor air temperature input T_r; one is biased toward open warehouse area (W), other toward mezzanine area (M). The data collected from both AHUs have been merged into one, i.e. it is assumed both AHUs work combined together. The

system inputs and outputs used for the system identification are an average of the supply air temperature values coming from both AHUs, e.g. $T_s = (T_{sW} + T_{sM})/2$.

- Each AHU operates with 0 %, 50 % (stage 1) and 100 % (stage 2) of total cooling capabilities, switching ON and OFF as dictated by the control system.
- The cooling output for stage 2 is twice as the cooling output for stage 1 as the cooling unit consists of two identical DX units running on their full capacity when enabled. Demand for stage 1 cooling enables one of the unit, while demand for stage 2 cooling enables both of them.

The data presented in Figure 2.13 have been used as estimation dataset for system identification and hold the following criteria:

- The overall length of data used is 343 samples recorded uninterrupted with 15 min sampling time starting at 24/05/2017 09:45; the data has been recorded in the pharmaceutical warehouse in Midlands, UK supported by use of four indoor sensors and one outdoor sensor as described in Section 2.2.1.1.
- The position of damper blades is closed across all data points and the indoor air is recirculated.
- The supply fans are ON at all times, meaning the air is supplied through the ductwork. The fan speed varies from 62.5% (nheating OFF) up to 100% (72.5%, 80% or 100%, cooling ON).

The data presented in Figure 2.14 have been used for validation and hold the following criteria:

- The overall length of data used is 370 samples recorded uninterrupted with 15 min sampling time starting at 30/05/2017 07:15; the data has been recorded in the pharmaceutical warehouse in Midlands, UK.
- The position of damper blades is closed across all data points and the indoor air is recirculated.
- The supply fans are ON at all times, meaning the air is supplied through the ductwork. The fan speed varies from 62.5% (cooling OFF) up to 100% of its maximum speed (72.5%, 80% or 100%, cooling ON).

For this sub-unit, the fan speed control input shown in Figures 2.13 and 2.14 is taken into calculations, unlike for the heating unit model in Section 2.5.2. It is believed

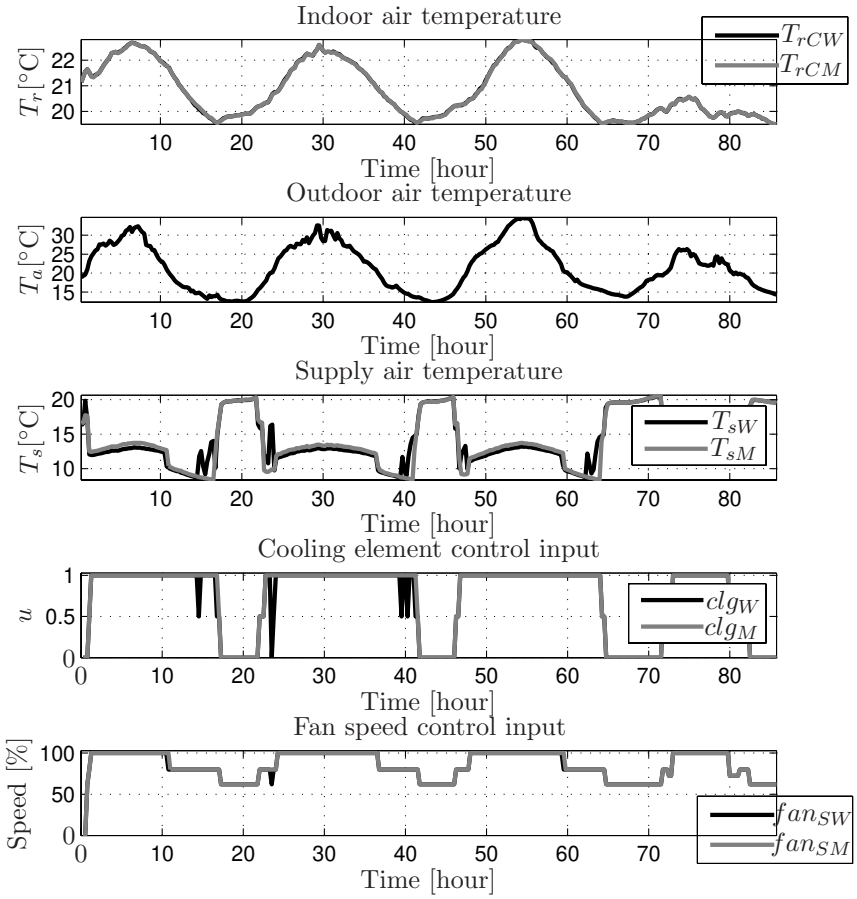

FIGURE 2.13: The cooling unit sub-model estimation dataset.

that the model parameters may be estimated more accurately when the fan speed is taken into account. This can be explained by the fact that there are two stages of cooling unit operation yet the fan speed is among one of three possible speed for active cooling unit, either 72.5%, 80% or 100%. The operation of the supply fan and cooling units are less correlated, hence the heat load generated due to the supply fan operation may be estimated and separated from the cooling load, as opposed to the heating unit model, where the heat loads of the heating and supply fan units blend. It has been also concluded that it is important to differentiate the supply fan heat load from the cooling unit heat load for two reasons: (1) they carry different signs when active and the cooling leads to a dip in the temperature, while the supply fan contributes to the temperature rise, and (2) the expected absolute value of the cooling unit heat load is much lower than from the heating unit, therefore the supply fan contribution has more significant weight. Ignoring this fact could lead to a decreased value of the estimated cooling unit gain and poor accuracy, since the expected gains are known based on the calculations and consultations with the subject expert.

The supply fan control input has been normalised to vary between 0 and 1 that

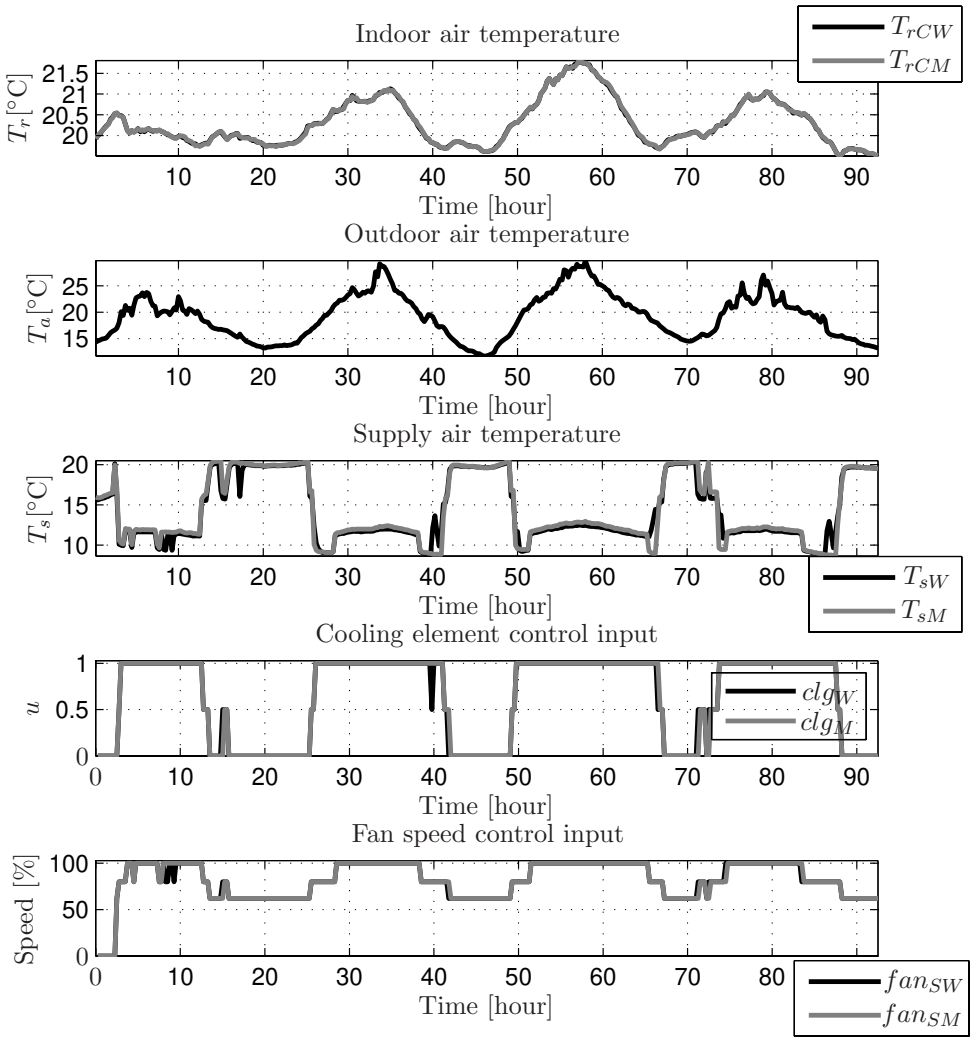

FIGURE 2.14: The cooling unit sub-model validation dataset.

correspond to 0 and 100% of the maximum speed, respectively. Similarly, the cooling unit control input has been normalised to vary between 0 and 1 corresponding to 0 and 100% of cooling capabilities, respectively. By analysing the stage operation of the cooling unit with constant interval between stages (each stage enables one of two identical DX cooling units running at their full cooling capacity) and visually inspecting the data provided, it is deemed that a linear model is a good approximation for system identification and control purpose. More informative data, however, would allow to challenge it.

2.5.3.2 System identification and validation

The parameter estimation method used to obtain model parameters characterising cooling unit in Equation (2.5.16) is the LS. It has been assumed that a first order system is enough to capture the main behaviour of the system and higher order will not provide

much improvement in model fit based on the current knowledge of the real system and quality of the data available. The model parameters obtained using the LS are $b_c = -6.6397$ and $a_c = -0.4509$, $b_f = 4.0331$, $b_{cOAT} = -0.0032$ and $O = 0.1913$ and the overall model fit for the SID dataset is shown in Figure 2.15. The estimated model has been validated on different dataset and the results are shown in Figure 2.16. Note that parameter b_c is negative, hence the output $\Delta T_c(k)$ is negative when the cooling unit is switched on, i.e. $u_c(k) > 0$.

The first term on the right-hand side of Equation (2.5.16) relates to the temperature drop caused by the cooling unit operation. By not considering the other two terms of Equation (2.5.16), the cooling unit sub-model is formulated as

$$\Delta T_c(k) = \frac{b_c z^{-1}}{1 + a_c z^{-1}} \cdot u_c(k) \tag{2.5.17}$$

and can be directly used in a simulation using discrete time model of the indoor air temperature to represent the cooling unit operation.

The performance of the estimator was subjected to the metrics calculation introduced and defined in Section 2.5.2 as R^2_T, IAE and MSE. The metric values calculated for the estimated model for both estimation and validation datasets are provided in Table 2.4. The results obtain present good model fit in estimation dataset in all metrics. Moreover, the validation trial demonstrated also good fit with R^2_T 0.5% lower than for estimation dataset and IAE and MSE higher by 40% and 26%, respectively, remaining below 0.625.

TABLE 2.4: Measures of the performance criteria for the estimated parameters for the cooling unit sub-model (Equation (2.5.17)).

Criteria	**SID**	**Validation**
R^2_T [%]	97.1652	96.6607
IAE	0.4422	0.6219
MSE	0.4798	0.6067

The discrete-time step response of the estimated model given in Equation (2.5.17) is shown in Figure 2.17; a hold between samples is assumed. Note that exciting the system with input signal $u_c = 1$, meaning the cooling unit is 100 % ON (stage 2), results in cooling of the air passing through the AHU. The temperature of the supply air leaving the AHU is changed by $-12.09\,^{\circ}\mathrm{C}$ from the temperature of the air entering the AHU and this is the process gain of the cooling sub-system provided in Equation (2.5.17). Note also that the steady state is approached in more than an hour while the settling time is 75 min, which is five times the sampling interval. There is no overshoot or undershoot

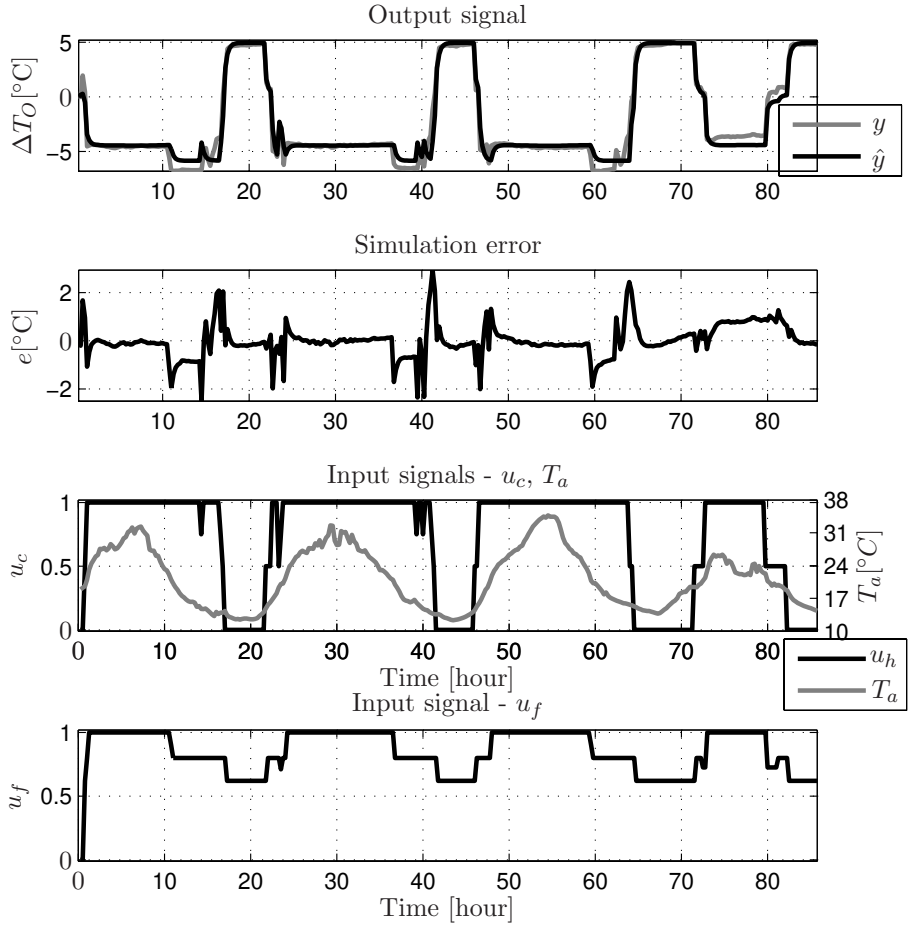

FIGURE 2.15: The cooling unit sub-model (Equation (2.5.17)) using estimation dataset with ΔT_O (Equation (2.5.16)), error and input signals as a function of time.

observed. The calculated time constant is $\tau_c = 18.83\,\text{min}$ and this period is close to the sampling interval. This observation is consistent with the expected cooling unit time constant. The overall air temperature change between the air entering and leaving the AHU is caused mainly by the cooling unit, but also includes the heat gain coming from the supply fan motor. By knowing the maximum cooling unit output is 314 kW and the maximum supply fan output is 37 kW, the expected maximum temperature change calculated using Equation (2.5.5) is

$$\Delta T_c = \frac{-314 \cdot 10^3 + 37 \cdot 10^3 \cdot 0.8}{18.5 \cdot 0.8 \cdot 1005 \cdot 1.183} = -16.16\,^{\circ}\text{C} \tag{2.5.18}$$

assuming the fan speed is 80% and

$$\Delta T_c = \frac{-314 \cdot 10^3 + 37 \cdot 10^3}{18.5 \cdot 1005 \cdot 1.183} = 12.59\,^{\circ}\text{C} \tag{2.5.19}$$

assuming the fan speed is 100%. The difference of the air temperature leaving AHU

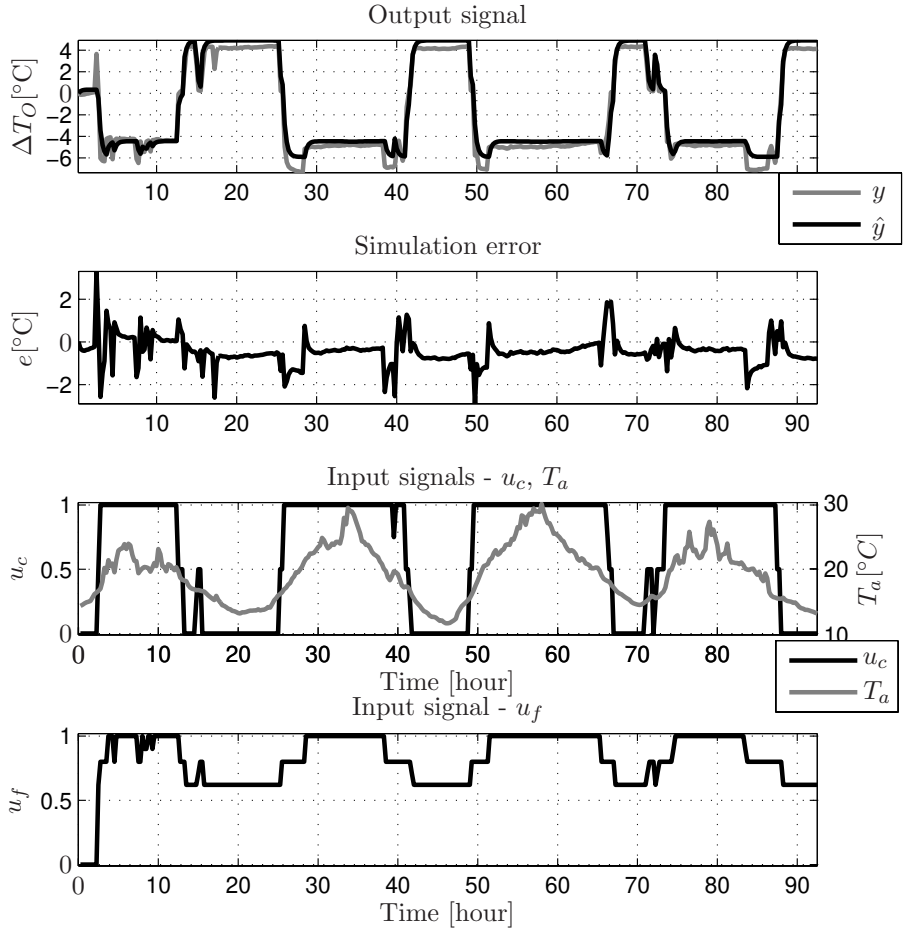

FIGURE 2.16: The cooling unit sub-model (Equation (2.5.17)) using validation dataset with ΔT_O (Equation (2.5.16)), error and input signals as a function of time.

with regard to the fan speed is expected as the lower fan speed indicates that the air moves slower through the AHU, hence the cooling power influences the air for a longer period of time. In other words, the higher fan speed is, the less time cooling unit has to cool the air down. As the cooling capacity is constant, a higher fan speed means that certain amount of cooling is distributed among bigger amount of air, while for a lower fan speed the same amount of cooling is distributed among bigger amount of air, providing more of cooling per unit of air.

2.6 Simulation study

The study presented in this section is to demonstrate and analyse a response of the second order indoor air temperature model derived from first principles. It is achieved through a number of simulations covering various supply fan, heating and cooling units operation scenarios combined with two possible positions of damper blades. The system

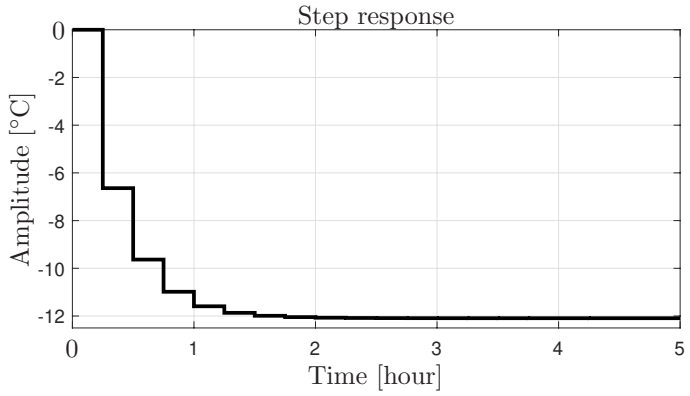

FIGURE 2.17: The cooling unit sub-model step response - ΔT_c settling at $-12.09\,^{\circ}\mathrm{C}$.

model is also analysed with regard to effect of the fan and the position of damper blades on the model. The measurement noise is not considered as the interest at this stage is in nominal value only (although it is good to consider it in the future by utilising Monte Carlo simulation study, for example). External disturbances are considered by means of the outdoor air temperature, which is a manipulated input through the damper position and in the same time has indirect impact on the indoor conditions through the walls.

2.6.1 First principles model equations for simulation

The two differential equations provided in Equation (2.4.1) are discretised using the forward (explicit) Euler method (Atkinson, 2009, p. 4) and implemented in MATLAB for simulation purposes. The discretised equations for the indoor air temperature and the wall temperature, respectively, are

$$\begin{aligned} T_r(k) = T_r(k-1) &+ \frac{ts}{V_r} \cdot m_a(k-1) \cdot \big(T_s(k-1) - T_r(k-1)\big) \\ &+ \frac{ts}{C_r} \cdot q(k-1) + \frac{ts}{C_r} \cdot (UA)_{int} \cdot \big(T_w(k-1) - T_r(k-1)\big) \\ &+ ts \cdot \frac{n_v}{3600} \cdot \big(T_a(k-1) - T_r(k-1)\big) \end{aligned} \tag{2.6.1}$$

$$\begin{aligned} T_w(k) = T_w(k-1) &+ \frac{ts}{C_w} \cdot (UA)_{ext} \cdot \big(T_a(k-1) - T_w(k-1)\big) \\ &+ \frac{ts}{C_w} \cdot (UA)_{int} \cdot \big(T_r(k-1) - T_w(k-1)\big); \end{aligned} \tag{2.6.2}$$

where ts is sampling interval. Equations (2.6.1) and (2.6.2) are used to simulate the indoor conditions, whereas Equations (2.6.5)-(2.6.8) are used to add the damper blades position and heating and cooling units directly into consideration. To be more specific, the temperature of the air supplied to the indoor space $T_s(k)$ in Equation (2.6.1) is calculated separately on each simulation step using Equations (2.6.3) and (2.6.4) and then the results are passed into Equation (2.6.1). The final value of $T_s(k)$ acts as the

input to the plant following the configuration in Figure 2.6 and Equation (2.3.2) and makes use of the AHU model parameters provided in Section 2.5. Consider now the following equations in Laplace domain

$$T_d(s) = u_d(s) \cdot T_a(s) + \big(1 - u_d(s)\big) \cdot T_r(s) \tag{2.6.3}$$

$$T_s(s) = T_d(s) + \Delta T_h(s) + \Delta T_c(s) \tag{2.6.4}$$

which can be rewritten as

$$T_d(s) = u_d(s) \cdot T_a(s) + \big(1 - u_d(s)\big) \cdot T_r(s)$$

$$T_s(s) = T_d(s) + \Delta T_h \cdot u_h(s) + \Delta T_c \cdot u_c(s)$$

to allow for the damper blades position control using term $u_d(s)$ and manipulation of the heating and cooling units operation following heating and cooling unit models from Equations (2.5.8) and (2.5.17) with control inputs $u_h(s)$ and $u_c(s)$, respectively. Then, Equations (2.6.3)-(2.6.4) are discretised resulting in the following equations

$$T_d(k) = u_d(k) \cdot T_a(k-1) + T_r(k-1) - u_d(k) \cdot T_r(k-1) \tag{2.6.5}$$

$$\Delta T_h(k) = -a_h \cdot \Delta T_h(k-1) + b_h \cdot u_h(k-1) \tag{2.6.6}$$

$$\Delta T_c(k) = -a_c \cdot \Delta T_c(k-1) + b_c \cdot u_c(k-1) \tag{2.6.7}$$

$$T_s(k) = T_d(k) + \Delta T_h(k) + \Delta T_c(k) \tag{2.6.8}$$

Equations (2.6.5)-(2.6.8) are implemented in MATLAB along with Equations (2.6.1) and (2.6.2) in a recursive manner for simulation of the indoor thermal conditions, recalculating inputs at each time step as required. The overall model of the system represented by these equations is of second order. Note that the model is obtained using grey box approach, linking together known parameters of first principles model with the black box models of the heating and cooling units. No internal heat gains are present.

2.6.1.1 Model parameters

The parameters of the first principles model used in simulation are provided in Table 2.5. The values chosen, where possible, have been motivated by the specification documents of the pharmaceutical warehouse located in Midlands, UK. The sampling interval used for simulation is ts=180 s and this value was chosen as an attempt to find deeper insight into the studied system than using the 15 min sampling interval from the previously used dataset.

TABLE 2.5: The first principles model parameters. The units of the parameters are provided in Section 2.4.1.

Coefficient	**Value**	**Coefficient**	**Value**
V_r	185472	V_w	784.1
m_a	$0 - 18.5$	n_v	0.35
c_a	1005	A_{floor}	11520
c_w	1000	A_{ceil}	11520
ρ_a	1.183	A_{wall}	7833.2
ρ_w	600	U_{floor}	0.13
U_{wall}	0.35	U_{ceil}	0.25

Note that the value of n_v indicates that 35% of the air within the indoor space is exchanged to fresh each hour. Normally this is not the case in the real conditions to prevent heat losses, nevertheless for the simulation purposes the value has been chosen to compensate for the overinsulation effect. The need for n_v manipulation arose from two reasons. Firstly, the exact components of the wall are not known, hence assumptions have been made to represent simple model of concrete brick wall. Secondly, the proposed model is intended to be simple and represent main behaviour, hence some potentially meaningful inputs, e.g. solar irradiation on a sunny day or wind on a windy day, have been neglected. As per specification of the studied building $n_v = 0.25$, however, $n_v = 0.35$ is used for simulation as empirically found value that represents the studied system.

Cooling and heating unit models have been upsampled from their original $ts = 15\,\text{min}$ to required $ts = 3\,\text{min} = 180\,\text{s}$ using zero-order hold method as a conversion method for approximation of a continuous time model and then discretised back using zero-order hold method with $ts = 180\,\text{s}$.

2.6.2 Results

The results of this study are divided into three scenarios depending on the supply fan and heating and cooling units operation, in which open and closed damper position situations are considered. The first scenario studies the tracking of the indoor air temperature in the absence of operating supply fan unit, where no air is distributed into the conditioned area using ductwork. The second scenario considers supply fan unit active with air distributed through the ductwork, however the heating and cooling units are disabled. The third scenario combines active supply fan with heating and cooling units operating at different levels of their maximum capacity. In each scenario the following steps were performed:

1. Load the first principles model parameters.

2. Represent the outdoor air temperature T_a as a square wave changing between 0 and 10 °C every 3 days.

3. Simulate the indoor air temperature using equations from Section 2.6.1.

4. Perform system identification with second order system model structure using Least Squares method.

5. Gather all the relevant coefficients and metrics representing the identified model.

6. Produce figures to visually represent identified system model.

The following second order model structure has been formulated for system identification:

$$T_r(s) = G_s(s) \cdot T_s(s) + G_a(s) \cdot T_a(s) \tag{2.6.9}$$

where $G_s(s)$ and $G_a(s)$ are the transfer functions corresponding to inputs $T_s(s)$ and $T_a(s)$, respectively. It is assumed that the internal heat gains are not present. Following the system model given in Equation (2.4.8), the functions $G_s(s)$ and $G_a(s)$ have a common denominator and are represented as

$$G_s(s) = \frac{b_0 s + b_1}{s^2 + a_1 s + a_2} \tag{2.6.10}$$

and

$$G_a(s) = \frac{\bar{b_0} s + \bar{b_1}}{s^2 + a_1 s + a_2} \tag{2.6.11}$$

The system model represented by Equation (2.6.9) is a second order MISO system having two inputs and one output. This second order system model will be used to evaluate how precise the model parameters can be obtained for the same order system model as the reference system model represented by white-box model from Equations (2.4.1) and (2.4.8).

The indoor air temperature generated by the model in the figures from subsection below showing the system identification results is denoted *data* and the indoor air temperature simulated using parameters obtained using system identification method is denoted SID. The error is calculated as $Error = data - SID$. The step response of a system function representing the relationship between input T_a and output T_r is denoted G_a. Similarly, the step response of a system function representing relationship between input T_s and output T_r denoted G_s. Note that only scenario involving heating and cooling will have G_s term present. The supply fan on its own is assumed to not introduce additional input to the system and the heat gains resulting from the supply fan operation are neglected.

2.6.2.1 Supply fan disabled scenario

In this scenario it is studied how the outdoor air temperature is able to influence the indoor air temperature by means of a heat transfer through the walls only and the supply fan is not in operation. The indoor air temperature simulation results including model fit and the input outdoor air temperature are presented in Figure 2.18. The step response of the system function G_a is presented in Figure 2.19.

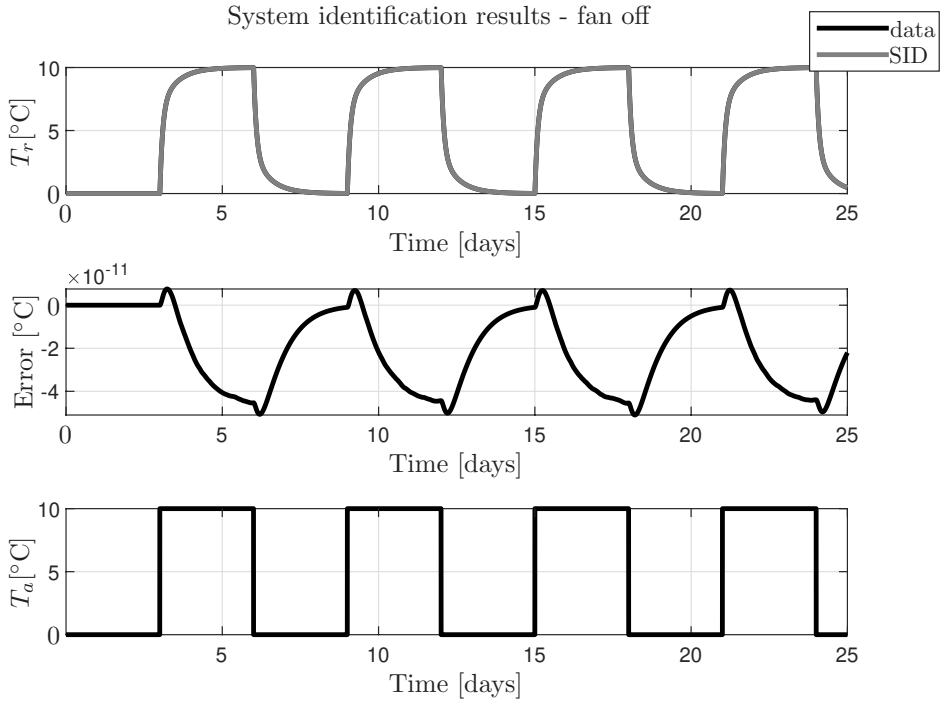

FIGURE 2.18: The indoor air temperature simulation with supply fan disabled (damper position not relevant).

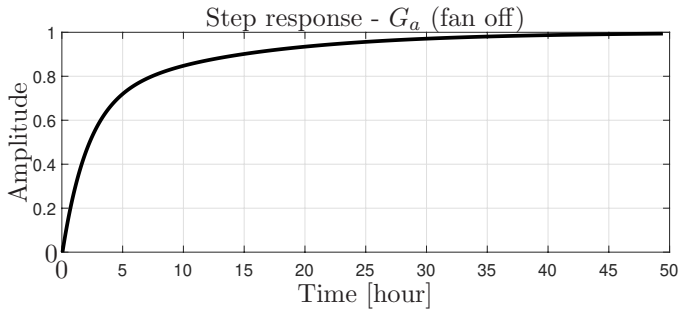

FIGURE 2.19: Outdoor temperature process (Equation (2.6.11)) step response for supply fan disabled (damper position not relevant).

2.6.2.2 Supply fan in operation scenario

In this scenario the operation of the supply fan is introduced to evaluate system model separately for an open ($u_d = 1$) and a closed ($u_d = 0$) loop system scenario. Consequently, the supply fan passes through the ductwork either the fresh air from the outside or the recirculated indoor air at 75% of its maximum speed. There is no heating and cooling present. The simulation results of the indoor air temperatures for the open and closed loop systems are presented in Figure 2.20. An indoor air temperature simulation using model parameters from system identification of the open loop system is presented in Figure 2.21, while the closed loop system is presented in Figure 2.23. The step response of a system function G_a for the open loop system is presented in Figure 2.22 and for the closed loop system in Figure 2.24.

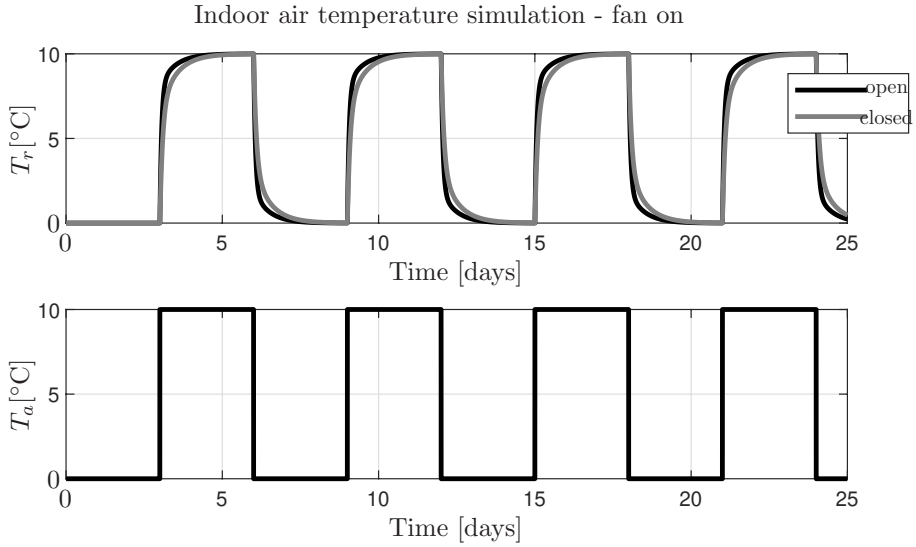

FIGURE 2.20: The indoor air temperature simulation with supply fan operating at 75% of its maximum speed.

2.6.2.3 Heating and cooling supply scenario

In this scenario the operation of heating and cooling units is introduced to evaluate system model with controlled heat gains. The open and closed loop system scenarios are differentiated and evaluated separately. Consequently, the supply fan passes the air through the ductwork, either the fresh air from the outside or the recirculated indoor air, that can be heated or cooled by heating and cooling units. The simulation results of the indoor air temperatures for the open and closed loop systems are presented in Figures 2.25 and 2.28, respectively. The indoor air temperature simulation using the model parameters from system identification of the open loop system is presented in Figure 2.26 and in Figure 2.29 for the closed loop system. The step responses of the

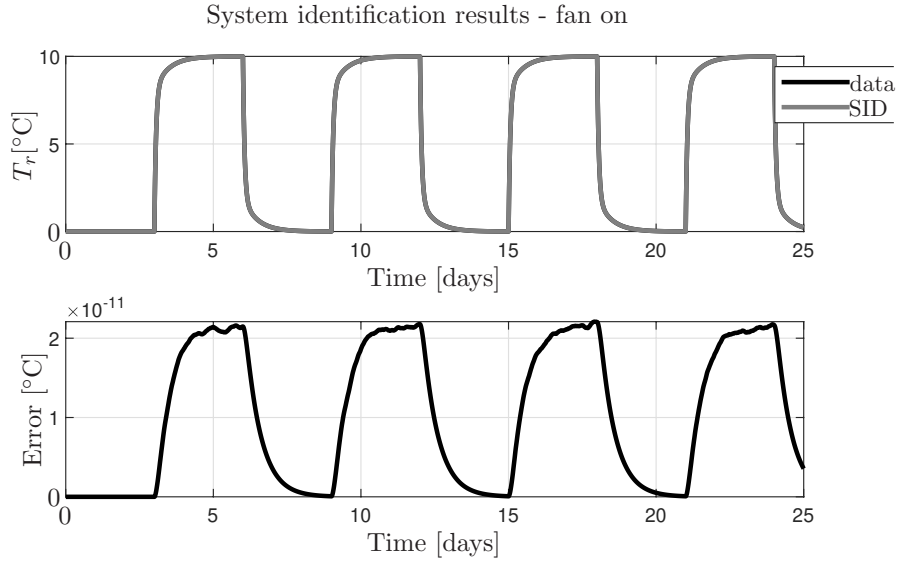

FIGURE 2.21: System identification of the indoor air temperature simulation (Equation (2.6.9)) with supply fan operating at 75% of its maximum speed and damper blades in an open position; $u_d = 1$.

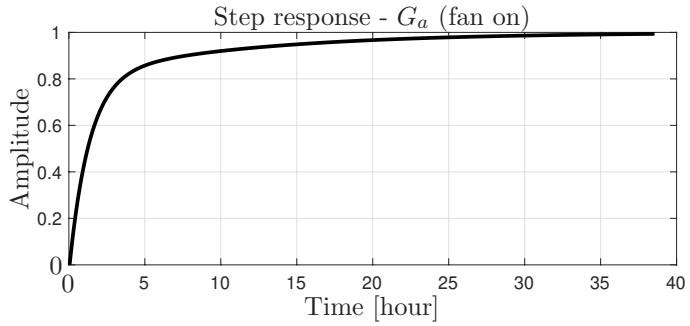

FIGURE 2.22: Outdoor temperature process (Equation (2.6.11)) step response for supply fan operating at 75% of its maximum speed and damper blades in an open position; $u_d = 1$.

system functions G_s and G_a for the open loop system are presented in Figure 2.27 and for the closed loop system in 2.30. It is assumed that the supply fan operates at 75% of its maximum speed.

2.6.2.4 Discussion

Numerical values gathered from the system identification for all scenarios and Figures 2.18 to 2.30 have been summarised in Tables 2.6 and 2.7. Additional simulation study has been done for 100% of maximum fan speed with numerical results briefly summarised in Tables 2.8 and 2.9.

Considering Equation (2.4.8) and its a and b coefficients definition from the first principles model, one could expect to get the same values for each simulation, regardless

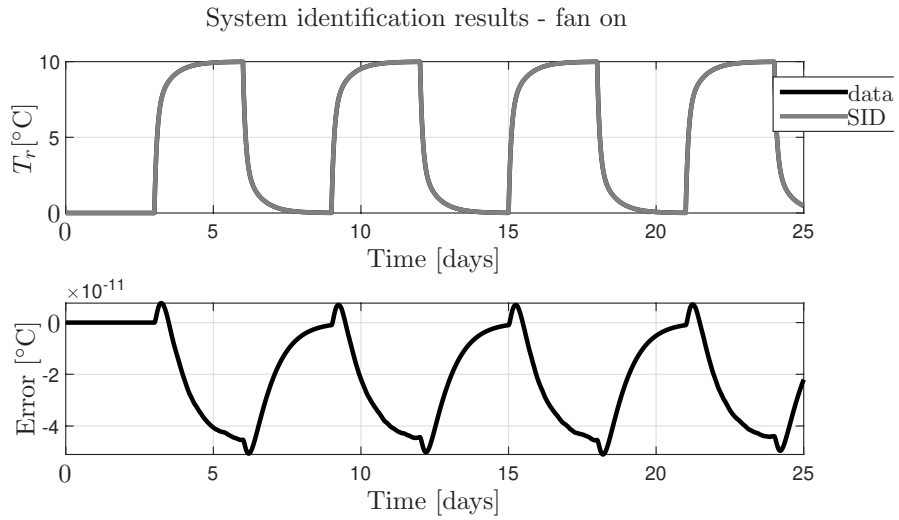

FIGURE 2.23: System identification of the indoor air temperature simulation (Equation (2.6.9)) with supply fan operating at 75% of its maximum speed and damper blades in a closed position; $u_d = 0$.

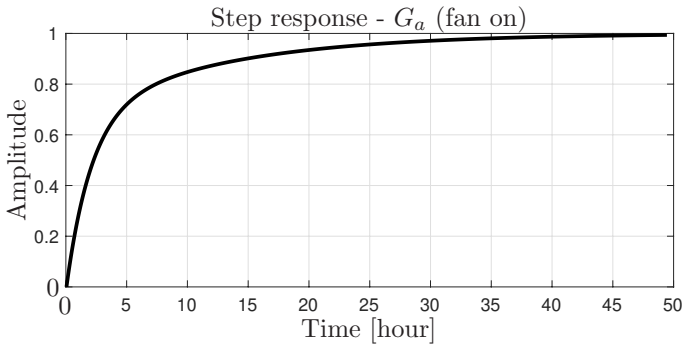

FIGURE 2.24: Outdoor temperature process (Equation (2.6.11)) step response for supply fan operating at 75% of its maximum speed and damper blades in a closed position; $u_d = 0$.

of scenario, provided the air mass flow rate is constant. Nonetheless, the coefficients a_1, a_2, b_0 and b_1 are dependent on the air mass flow rate and $\bar{b_0}$ and $\bar{b_1}$ are independent of it. The values shown in Tables 2.6 and 2.8, however, differ between scenarios even when the same fan speed is assumed. This difference is related to the position of damper blades. Therefore, it has been concluded that in these studied scenarios there are two parameters that have notable influence on the system function coefficients and the system dynamics - the air mass flow rate and the position of damper blades. It has been demonstrated that when the supply fan is in operation and the air is distributed though the ductwork, the open loop system dynamics is faster than the closed loop as the outdoor air is passed directly to the inside of the building through the ductwork. Also, recirculating the air when no heating and cooling is present is no different to keeping the supply fan disabled. Note that for a scenario with an open loop configuration, the supply fan is ON and no heating and cooling are present, the term G_a accounts not only

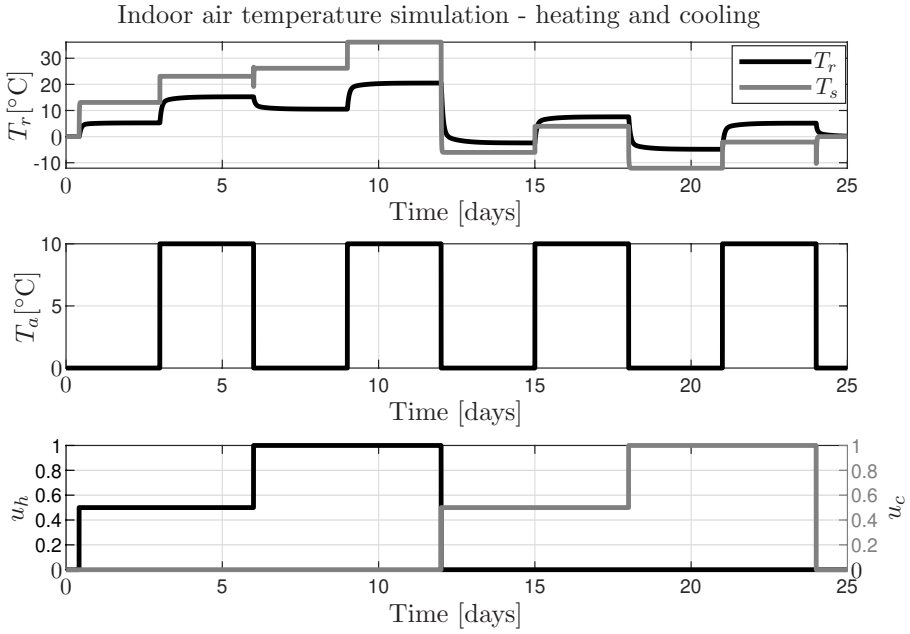

FIGURE 2.25: The indoor air temperature simulation with supply fan operating at 75% of its maximum speed and heating and cooling present. Damper blades in an open position; $u_d = 1$.

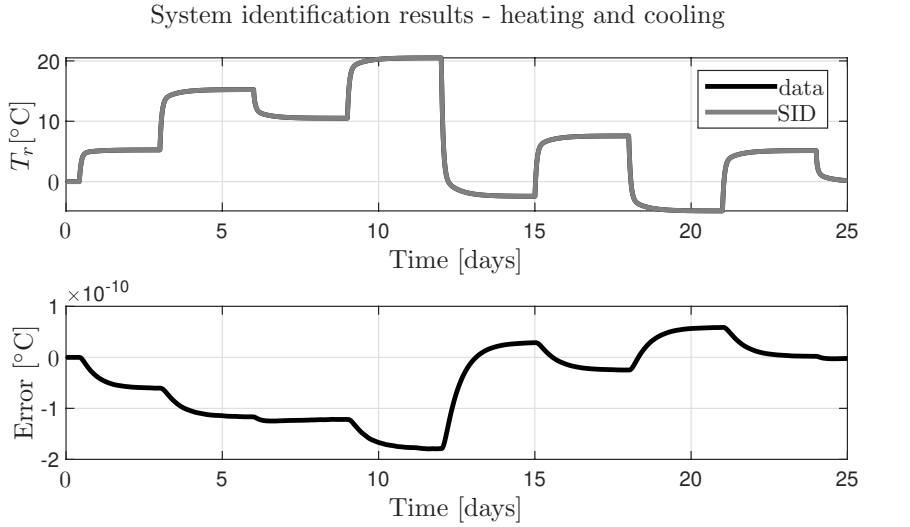

FIGURE 2.26: System identification of the indoor air temperature simulation (Equation (2.6.9)) with supply fan operating at 75% of its maximum speed, heating and cooling present and damper blades in an open position; $u_d = 1$.

for the heat transfer through walls and infiltration n_v, but also the air supplied directly through the ductwork. This results in its coefficients being different than the closed loop with the supply fan ON scenario.

Once the heating and cooling are introduced, the outdoor air process appears to be slower compared to the open loop with the supply fan on scenario. This matter, however, would need more investigation as the simulation study assumes variable position

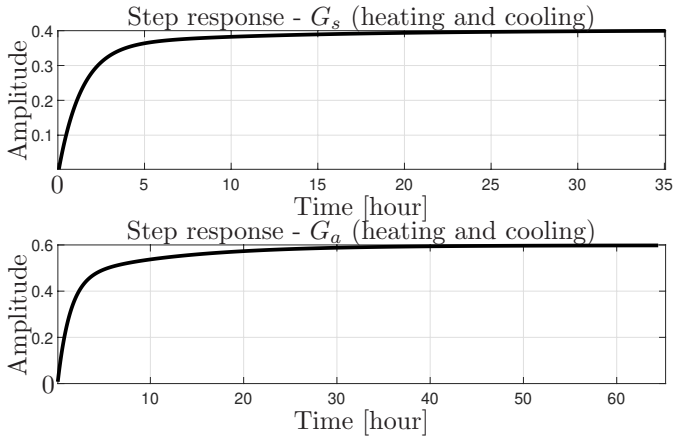

FIGURE 2.27: Supply air temperature (top) and outdoor temperature (bottom) process (Equation (2.6.10) and (2.6.11)) step response for supply fan operating at 75% of its maximum speed and damper blades in an open position; $u_d = 1$.

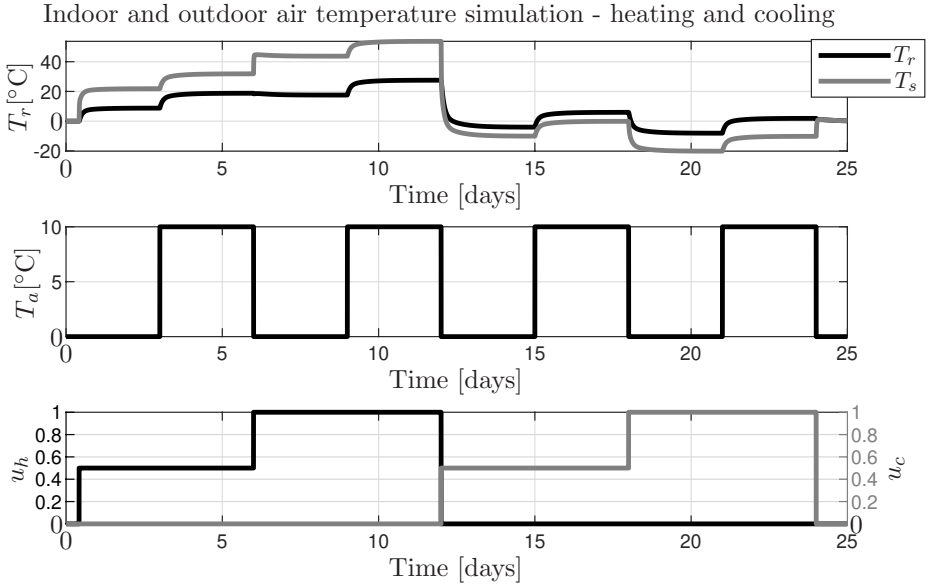

FIGURE 2.28: The indoor air temperature simulation with supply fan operating at 75% of its maximum speed and heating and cooling present. Damper blades in a closed position; $u_d = 0$.

of damper blades throughout the simulation. By keeping the damper blades position constant, the same coefficient of the system functions is obtained as the method cannot discern between the source of the incoming air in the presence of heating and cooling. Instead, G_s is perceived as a system function related to the overall supply air. Note also, that the rise time, settling time and peak time for G_a are somewhat between the values for the open and closed loop with fan ON scenarios, which may be due to the problem with discerning between the open and closed loop system in the presence of heating and cooling. Similarly, G_a has different coefficient values than in the other scenarios, yielding yet another model parameters.

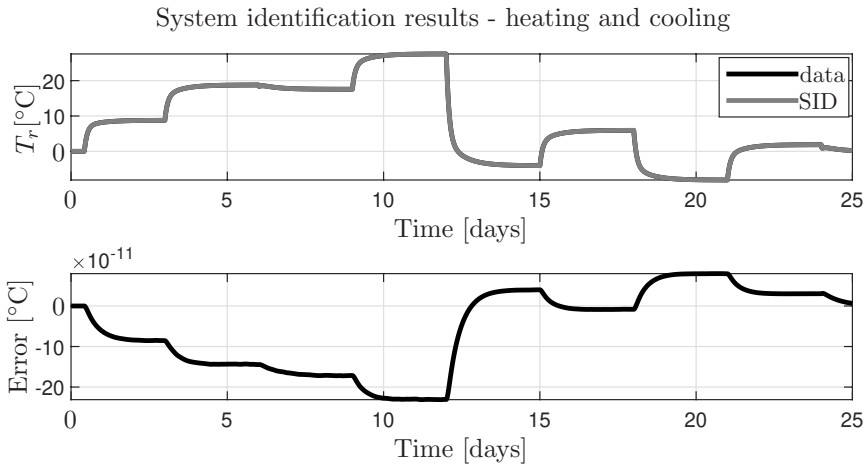

FIGURE 2.29: System identification of the indoor air temperature simulation (Equation (2.6.9)) with supply fan operating at 75% of its maximum speed, heating and cooling present and damper blades in a closed position; $u_d = 0$.

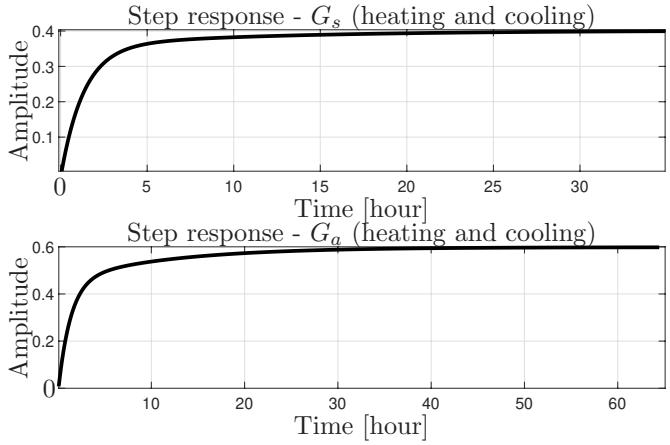

FIGURE 2.30: Supply air temperature (top) and outdoor temperature (bottom) process (Equation (2.6.10) and (2.6.11)) step responses for supply fan operating at 75% of its maximum speed and damper blades in a closed position; $u_d = 0$.

Comparing values obtained from simulation with 75% and 100% of maximum fan speed, it has been noticed that the trends are consistent, i.e. coefficients for the supply fan OFF or the closed loop with the supply fan ON scenarios are the same, while dynamics of the other scenarios increases together with speed. Also, Table 2.8 containing coefficients related to the simulation with the supply fan operating at 100% of its maximum speed presents the edge values. For example, it shows the maximum G_s gain possible with the current first principles model given maximum $m_a = 18.5\,\mathrm{m}^3/\mathrm{s}$ or the expected step response characteristics for the maximum control input.

Overall, the model obtained is of good fit with the estimated model and matches well the input model. It can be noticed in the high values of R_T^2 and close to zero values of IAE and MSE in Tables 2.7 and 2.9, where measures of performance criteria

TABLE 2.6: The second order continuous time system model parameters (Equation (2.6.9)) for operating supply fan open and closed position of damper blades and supply fan disabled. Fan operating at 75% of maximum speed for open and closed damper position.

Coefficient	**Heating and cooling**		**Fan on**		**Fan off**
	Open	**Closed**	**Open**	**Closed**	
$G_s(s)$ Gain	0.4016	0.4016	n/a	n/a	n/a
$G_a(s)$ Gain	0.5984	0.5984	1.0	1.0	1.0
b_0	7.622^{-5}	7.622^{-5}	n/a	n/a	n/a
b_1	2.069^{-9}	2.069^{-9}	n/a	n/a	n/a
$\bar{b_0}$	9.902^{-5}	9.902^{-5}	1.752^{-4}	9.834^{-5}	9.834^{-5}
$\bar{b_1}$	3.089^{-9}	3.089^{-9}	5.152^{-9}	3.062^{-9}	3.062^{-9}
a_1	2.354^{-4}	2.354^{-4}	2.354^{-4}	1.583^{-4}	1.583^{-4}
a_2	5.152^{-9}	5.152^{-9}	5.152^{-9}	3.062^{-9}	3.062^{-9}
$G_s(s)$ Rise time [h]	4.55	4.55	n/a	n/a	n/a
$G_s(s)$ Settling time [h]	19.8	19.8	n/a	n/a	n/a
$G_s(s)$ Peak time [h]	40.95	40.95	n/a	n/a	n/a
$G_a(s)$ Rise time [h]	10.0	10.0	7.5	14.45	14.45
$G_a(s)$ Settling time [h]	28.5	28.5	25.75	34.55	34.55
$G_a(s)$ Peak time [h]	74.95	74.95	66.95	85.95	85.95

TABLE 2.7: Measures of the performance criteria for the estimated parameters of a second order model of the system with open and closed position of damper blades (Equation (2.6.9)). Fan operating at 75% of maximum speed, unless stated differently.

Criteria	**Heating and cooling**		**Fan on**		**Fan off**
	Open	**Closed**	**Open**	**Closed**	
R^2_T [%]	100	100	100	100	100
IAE	6.6248^{-11}	9.0341^{-11}	1.0364^{-11}	2.1433^{-11}	2.1433^{-11}
MSE	7.535^{-21}	1.3442^{-20}	1.8772^{-22}	7.7094^{-22}	7.7094^{-22}

are listed. Lack of a visible difference between tracks of *data* and SID on plots from previous subsection also reflects this relationship.

2.6.2.5 Conclusions

By nothing the varying values of G_a between different scenarios, it is concluded that the model parameters are dependent on the air mass flow rate and the position of damper blades. Secondly, the nature of these two states, i.e. the air mass flow rate and the position of damper blades, prompts to observe the model as highly nonlinear. Therefore, it is suggested to formulate a bilinear or a state-dependent system model

TABLE 2.8: The second order continuous time system model parameters (Equation (2.6.9)) for operating supply fan open and closed position of damper blades and supply fan disabled. Fan operating at 100% of maximum speed for open and closed damper position.

Criteria	**Heating and cooling**		**Fan on**		**Fan off**
	Open	**Closed**	**Open**	**Closed**	
$G_s(s)$ Gain	0.4723	0.4723	n/a	n/a	n/a
$G_a(s)$ Gain	0.5277	0.5277	1.0	1.0	1.0
b_0	1.019^{-4}	1.019^{-4}	n/a	n/a	n/a
b_1	2.765^{-9}	2.765^{-9}	n/a	n/a	n/a
$\bar{b_0}$	9.925^{-5}	9.925^{-5}	2.011^{-4}	9.834^{-5}	9.834^{-5}
$\bar{b_1}$	3.09^{-9}	3.09^{-9}	5.855^{-9}	3.062^{-9}	3.062^{-9}
a_1	2.614^{-4}	2.614^{-4}	2.614^{-4}	1.583^{-4}	1.583^{-4}
a_2	5.855^{-9}	5.855^{-9}	5.855^{-9}	3.062^{-9}	3.062^{-9}
$G_s(s)$ Rise time [h]	3.85	3.85	n/a	n/a	n/a
$G_s(s)$ Settling time [h]	17.95	17.95	n/a	n/a	n/a
$G_s(s)$ Peak time [h]	53.95	53.95	n/a	n/a	n/a
$G_a(s)$ Rise time [h]	9.15	9.15	6.15	14.45	14.45
$G_a(s)$ Settling time [h]	27.4	27.4	23.9	34.55	34.55
$G_a(s)$ Peak time [h]	58.95	58.95	59.45	85.95	85.95

TABLE 2.9: Measures of the performance criteria for the estimated parameters of a second order model of the system with open and closed position of damper blades (Equation (2.6.9)). Fan operating at 100% of maximum speed, unless stated differently.

Criteria	**Heating and cooling**		**Fan on**		**Fan off**
	Open	**Closed**	**Open**	**Closed**	
R_T^2 [%]	100	100	100	100	100
IAE	6.6248^{-11}	4.7344^{-11}	8.6531^{-12}	2.1433^{-11}	2.1433^{-11}
MSE	1.2973^{-21}	3.7266^{-21}	1.2832^{-22}	7.7094^{-22}	7.7094^{-22}

to capture this phenomena, which could be used to simulate the indoor conditions and for control. A state-dependent system model is proposed in Chapter 3, where State-Dependent Parameter (SDP) model of an indoor air temperature is formulated and analysed in depth.

2.6.3 First principles model validation

A preliminary trial and simulation of the indoor air temperature using Equations (2.6.1)-(2.6.2), as derived from first principles differential equations provided in Equation (2.4.1),

have been performed using the real data gathered in the studied pharmaceutical warehouse. The first principles model parameters were chosen for simulation as per Table 2.5. Additionally, a heat gain $q = 120000$ has been considered to mimic the internal heat gains within the building. The choice was supported by technical documentation of the case study warehouse and manual tuning. The results are provided in Figure 2.31, where the simulated T_r (dashed line) is shown along the recorded indoor air temperature denoted $T_{r[ref]}$ (dark grey), which is an average of four sensors as explained in Section 2.2. The operation of heating and cooling units was simulated using the black box models estimated in Section 2.5 and was derived from the recorded heating and cooling units operation data for both AHUs combined together. This is shown in Figure 2.31 through ΔT, which indicates the amount of heat added or removed from the air supplied to the AHU. Similarly, the air mass flow rate m_a is an average of the values from the data recorded for both supply fans, where the recorded fan speed was translated into the air mass flow rate m_a.

While visually there is a considerable difference between the simulated T_r and the expected $T_{r[ref]}$ in Figure 2.31, it is also seen that the simulated T_r follows the expected value and oscillates around, reacting to the outdoor air temperature and the AHU operation. It is observed that the model appears to overreact to the outdoor air temperature in comparison to $T_{r[ref]}$, which can be related to the wall structure assumptions, a difference between the roof structure and the external walls structure (roof has been assumed to be the same as each external wall) and the weather conditions not captured by the recorded data, such as solar irradiation and wind speed. Moreover, the model doesn't take into consideration the heat stored in the goods and furniture within the building, which may contribute to the inaccuracies. It is possible to improve the accuracy of the predicted indoor air temperature by including the outdoor conditions data, obtaining more representative parameters for the building envelope and considering variable internal heat gain q, if such data was available. Further, distributed modelling approach and consideration of the thermal mass due to the objects stored inside could bring additional boost in the model's performance. For the needs of the research described in this thesis it is thought the model obtained is enough to perform preliminary studies and to design energy efficient temperature control system with understanding that further work is needed to improve the model. In real application the initial model would be assumed according to information available and then improved based on new data recorded by the controllers and/or additional equipment.

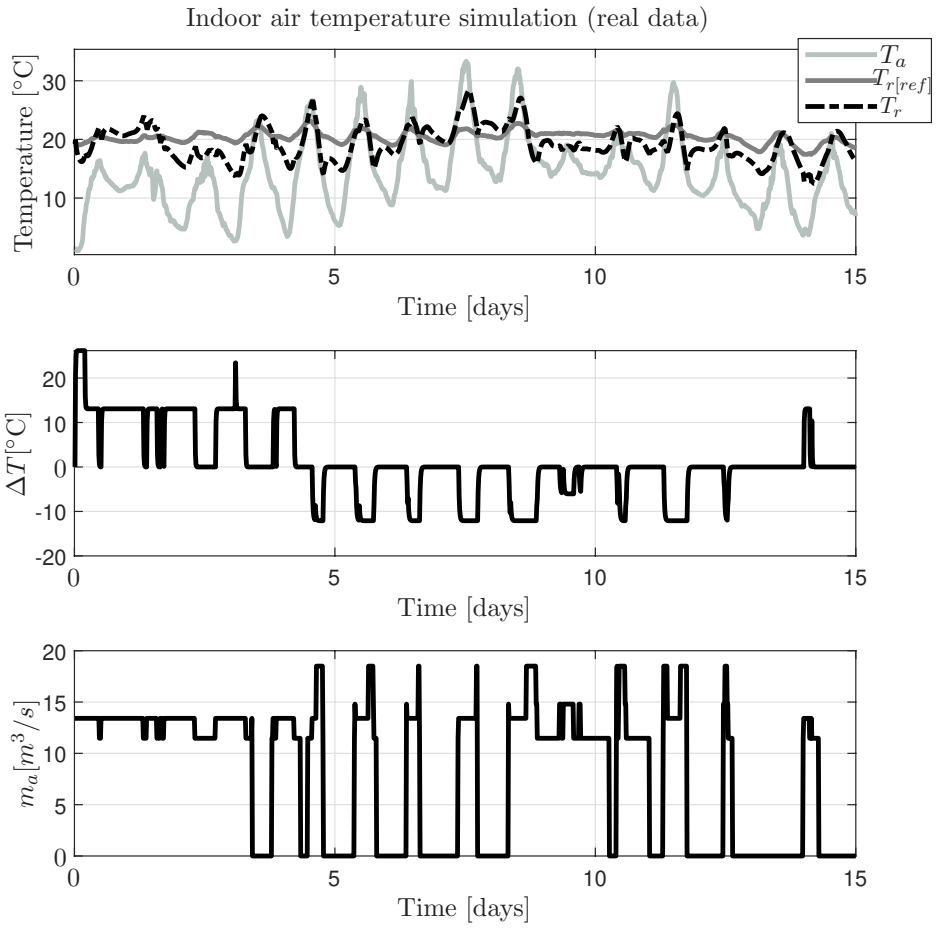

FIGURE 2.31: The indoor air temperature simulation based on the real data (Equations (2.6.1)-(2.6.2)). Damper position is closed. Performance criteria: R_T^2 = -578.5518, IAE = 2.2699, MSE = 6.9954.

2.7 Conclusions

In this chapter, the mathematical formulation of the thermal process describing the indoor air temperature within open plan building is presented. The model is derived from first principles and offer relevant insights to the understanding of the thermal characteristics. Based on the obtained results, the key points are summarised as follows.

Firstly, the proposition of the indoor air temperature model encapsulates the essence of thermal process, requiring variety of assumptions and simplifications, while assuring it is safe for the intended use. It is understood that uncertainties will be present in the system model and it can be dealt with in two approaches: obtain an accurate model as possible until no significant improvement in the considered metrics can be seen and determine the offset and error terms to improve model's prediction accuracy.

Secondly, whereas the indoor thermal process was introduced using white-box model approach, the simple model of the AHU has been obtained using black-box model

and system identification method from real data. This provided the model of the heating and cooling units located in the case study pharmaceutical warehouse from Midlands, UK, which is sufficient for simulations and control. It has been noted that recirculation of the indoor air creates a closed loop system with positive feedback, where the output becomes the input, while the use of the outdoor air in the AHU creates the open loop system. From system identification point of view, the parameter estimation of such a closed loop system needs to be handle differently since the indoor air temperature is input and output at the same time. Things get more complicated when the outdoor air temperate becomes another input to the system. The proposed solution to address this issue is the use of dedicated closed loop system identification methods. Alternatively, one could find correlation between open and closed loop system such that the model parameters obtained for the open loop would allow calculation of the closed loop system parameters.

Thirdly, it has been demonstrated in simulation how the second order system model can reproduce first principles model data used for system identification. The results obtained for relatively simple scenario provided promising results, encouraging development of the models with more controlled inputs and gains that cannot be controlled. Also, interpretation of the model parameters in physical terms relates the first principles model with estimated model and improvement of one from the other is an advantage as in data-based mechanistic approach (Young, 2002, 2011).

Finally, it has been observed that a linear model structure may not be sufficient to provide a credible model output. Special attention is given to the analysis of the indoor thermal process dynamics with regard to the position of damper blades, changing between recirculation of the indoor air and using the outside air in the AHU. The air, whether recirculated or indrawn, is a thermal energy carrier in the HVAC system distributed through the ductwork at specified supply air flow rate that is regulated by the fan speed control. The model provided shows capabilities to explain the building's thermal response and thermodynamics processes within the controlled area with a degree sufficient for research purposes and control development. By knowing the thermodynamics process is a nonlinear process, it is expected that a nonlinear model such as state-dependent, bilinear or Hammerstein structure should provide model fit of higher accuracy than the linear structure. Identifying the need for more complicated model than the simple linear model to capture main characteristics of the indoor thermal process, State-Dependent Parameter (SDP) modelling approach is addressed in Chapter 3. This allows to create a model that is able to simulate the indoor air temperature regardless of the changing air mass flow rate and the position of damper blades.

Chapter 3

State-Dependent Parameter modelling of an indoor air thermal process for energy optimisation

3.1 Introduction

It has been demonstrated in Chapter 2 that a simple yet representative model of a system characterising the indoor air temperature can be captured using second order system with two inputs: the supply air temperature and the outdoor air temperature. Observing the dynamic behaviour of the simulated system and the results of system identification, it has been noted that there are changes in the model parameters, demonstrating a nonlinearity within the studied system. When a real time system is considered, the parameters of the system will change as demanded by the Air Handling Unit (AHU) control system to satisfy the indoor air temperature requirements. These parameters will vary over time, yet it would be a mistake to consider such a system as a non-stationary with unpredictable time variable parameters as these parameters depend on the control logic. Therefore, the approach presented in this chapter comes from recognition of the fact that the changes in the model parameters are functions of the states and variables determined by the control strategy and immersed in the first principle model definition.

3.1.1 State-Dependent Parameter approach background and motivation

State-Dependent Parameter (SDP) modelling methods (Young, 2011, p. 327) are capable of dealing with highly nonlinear systems, whose parameters can be established from the state dependencies. While changes in the time variable parameters are typically slow and happen over time, a state-dependent parametric change is much more rapid and temporary, arising from the state dependency. The SDP methods can be perceived in a similar way as gain scheduling (Åström & Wittenmark, 2008, p. 390) or linearisation around working point (equilibrium) (Nise, 2011, p. 89, 141) for selected state. Although the extension of the time varying parameter estimation methods to allow for state dependency can be tracked down to a 1966 conference paper by Hoberock & Kohr (1966), one of the most significant contributors in developing the SDP modelling approach are Peter Young (Young, 1969, 1981) and Jerry Mendel (Mendel, 1969; Mendel & Fu, 1970). In both approaches it was assumed that the model parameters could vary because of their dependence on the variations in the other measured variables. More extensive history and evolvement of SDP has been described by Young (2011, p. 327).

The SDP approach has been chosen to model the indoor air temperature following observations in Chapter 2 that the model parameters vary with regard to the air flow rate and the position of damper blades. As damper blades position is a part of the energy efficient solution offered in this thesis and is an important part of the control strategy, there is a need to find a suitable model capturing the identified nonlinearities. The position of damper blades is a scheduling parameter for control design purposes, therefore the parameters will change as dictated by states such as the control input for the damper blades. In this instance temperature control with damper blades open and closed can be perceived as operating under different conditions as the system is changed from open to closed-loop. A state-dependent parameter model structure is a convenient method to approximate the indoor thermal process with known nonlinearities that cause rapid changes in the parameter values. This allows to determine online the response of the system at an operating point that is the most representative of the actual system. The SDP method is presented in this chapter understating how critical is the indoor air temperature model in the model-based control approaches Proportional-Integral-Plus (PIP) with Non-minimal State Space (NMSS) and Model Predictive Control (MPC) introduced in Chapters 4 and 5, respectively, contributing to robustness, efficiency and reliability of the dynamic model and the control system.

3.1.1.1 State-Dependent Parameter method applications

Studies, practical applications and utility of the SDP approach are found in the literature, academia and various industry sectors. An example of the SDP method in modelling is the multi-state dependent parameter model identification and estimation for nonlinear dynamic systems (Sadeghi et al., 2010), which is an extension of a univariate SDP estimation to handle multi-state dependency. Demonstration of how bilinear systems are a special case of a more general SDP model is proposed by Taylor et al. (2011a), where Proportional-Integral-Plus (PIP) controller is used along with SDP model. Identification and estimation of the SDP models are discussed by Young et al. (2002), where SDP Non-minimal State Space (NMSS) model structure is defined and utilised in SDP-PIP approach for the control of nonlinear systems.

Recognising the importance in industrial applications, the first application of SDP-PIP methods to practical nonlinear system is summarised by Shaban et al. (2004), where an SDP-PIP control system was developed for a 1/5th scale representation of the Lancaster University Computerised Intelligent Excavator (LUCIE), a nonlinear robot digger arm. In another project discussed by Li & Lu (2013) a state-dependent parameter estimation is applied to regional importance measures (RIMs), where failure probability is analysed. Another application considers a quasi-linear SDP model structure to model a wind turbine (Cross & Ma, 2013). This approach is less common as typically SDP models have been used as the basis for nonlinear controllers and this paper considers employing SDP for a model-based condition monitoring system. In agriculture, Stables & Taylor (2006) proposed nonlinear PIP control for regulating ventilation rate in mechanically ventilated agricultural building. This method uses SDP models to represent a livestock building or glasshouse. The SDP-PIP control systems where developed and evaluated for a forced ventilation test chamber and demonstrated improved performance and better disturbance response compared to linear and conventional scheduled PIP control. Propp et al. (2016) formulated state-of-charge-dependent model to develop a multi-temperature state-dependent equivalent circuit discharge model of a lithium-sulfur battery. In chemistry, the SDP models are used by Bidar et al. (2017) to improve product quality monitoring on a simulated continuous stirred tank reactor and an industrial debutaniser column.

Examples of the SDP methods use within academia are PhD theses by Exadaktylos (2007) and Hitzemann (2013). Exadaktylos utilises Model Predictive Control (MPC) methods together with a Non-minimal State Space (NMSS) model to handle a system with constraints and proposes MPC-SDP control approach to handle the nonlinear systems. Similar approach is taken by Hitzemann, who also focuses on model-based control

utilising linear NMSS and nonlinear SDP forms. The MPC method is used in conjunction with proportional-integral-plus (PIP) pole assignment control with the SDP model, forming SDP-PIP, presented on a practical example of a DC-DC boost converter. Both approaches promote an approach employing model-based control with state-dependent model structure and make use of PIP control scheme, which encouraged the use of these methods for the research presented in this thesis. In another PhD thesis the SDP approach is used for perturbation extremum seeking control, where UK patent *State dependent electricity controller* has been filed as a part of the research (Maganga, 2015).

3.1.2 Contributions

The literature review conducted didn't find many applications of SDP for the indoor air temperature control. Given state-dependent nature of the indoor air temperature process and various examples of the SDP methods applied to other nonlinear systems, it is believed that this research is valid and important to the body of knowledge. The contributions presented in this chapter include (1) a state-dependent-parameter formulation of a second order indoor air temperature model, (2) reliance of the SDP model parameters on the damper position and the amount of air supplied to the indoor space, (3) formulation of a reduced order model of an indoor air temperature and (4) parameter estimation for various damper position and air mass flow rate values to demonstrate state-dependent characteristics of the studied system. The SDP model proposed in this chapter is developed for the purpose of simulation and control used as a part of the MPC algorithm proposed in Chapter 5, where energy use of the heating, ventilation and air conditioning (HVAC) control system is optimised.

3.1.3 Chapter overview

This chapter is motivated by the properties of the indoor air temperature model introduced in Chapter 2, where it has been discussed how model parameters depend on two manipulated control variables, the air mass flow rate m_a and the position of damper blades u_d. Therefore, recognising the need to define model parameters as variables subject to the values of two states, the next Section 3.2 of this chapter introduced the general form of SDP model structure, which leads to a state-dependent form of the second order model of an indoor air temperature defined in Section 3.3. Then, the first principles model structure is reduced to first order and derived into state-dependent form in Section 3.4. Further, Section 3.5 presents simulation study results based on the model of the indoor air temperature with regard to state-dependent parameter structure, followed by overall chapter conclusions in Section 3.6.

3.2 General State-Dependent Parameter form

This section introduces general SDP model structure. The first subsection focuses on a SISO system, the second on a MISO system, and in the third one a first order SDP model is formulated for the indoor air temperature control application discussed in the thesis.

3.2.1 State-Dependent Parameter model structure for single input single output systems

The single input, single output discrete-time form of SDP model (Young, 2011) can be formulated as

$$y(k) = \mathbf{z}^T(k) \cdot \boldsymbol{\rho}(k) + e(k); \qquad e(k) = \mathcal{N}(0, \sigma^2) \tag{3.2.1}$$

where $\mathbf{z}^T(k)$ is a vector $1 \times (m+n+1)$ and $\boldsymbol{\rho}(k)$ a vector $(n+m+1) \times 1$ defined as

$$\mathbf{z}^T(k) = [-y(k-1) \quad -y(k-2) \ldots -y(k-n) \quad u(k-\delta) \ldots u(k-\delta-m)] \tag{3.2.2}$$

$$\boldsymbol{\rho}(k) = [a_1\{\chi(k)\} \quad a_2\{\chi(k)\} \ldots a_n\{\chi(k)\} \quad b_0\{\chi(k)\} \ldots b_m\{\chi(k)\}]^T \tag{3.2.3}$$

and $y(k)$ is the output signal, $\mathbf{z}^T(k)$ the regression vector of previous input and output signals and $\boldsymbol{\rho}(k)$ the state-dependent parameter vector of $a_i\{\chi(k)\}$, $i = 1, 2, \ldots, n$ and $b_j\{\chi(k)\}$, $j = 0, 1, \ldots, m$, which are assumed to be functions of one of the variables in a non-minimal state vector $\chi^T(k) = [\mathbf{z}^T\, \mathbf{U}^T(k)]$. Here $\mathbf{U}(k) = [U_1(k)\, U_2(k) \ldots U_r(k)]^T$ is a $r \times 1$ vector of other variables that may affect the relationship between these two primary variables, but are not variables that appear in $\mathbf{z}(k)$. Then, δ is a pure time delay on the input variable and $e(k)$ is a zero mean, white noise input with Gaussian normal amplitude distribution and variance σ^2 (although this assumption is not essential to the practical application of the resulting estimation algorithms). Finally, for convenience of notation, let $\boldsymbol{\rho}(k)$ be defined as a $(n+m+1) \times 1$ vector

$$\boldsymbol{\rho}(k) = [\rho_1\chi(k)\, \rho_2\chi(k) \ldots \rho_{n+m+1}\chi(k)]^T \tag{3.2.4}$$

with $\rho_i\{\chi(k)\}, i = 1, 2, \ldots, n+m+1$, relating to $a_i\{\chi(k)\}$ and $b_j\{\chi(k)\}$ through (3.2.2).

Transfer function form dedicated for the state-dependent models is also possible. SDP-TF (State-Dependent Parameters Transfer Function) is introduced by Taylor et al. (2013) as

$$y(k) = \frac{B\{\chi(k)\}}{A\{\chi(k)\}} u(k-\delta) + \xi(k) \tag{3.2.5}$$

in its general form, which can be perceived as a pseudo-TF form, where $\xi(k)$ is a general additive noise term and

$$B\{\chi(k)\} = \sum_{j=0}^{m} b_j\{\chi(k)\} \tag{3.2.6}$$

$$A\{\chi(k)\} = \sum_{i=1}^{n} a_i\{\chi(k)\} \tag{3.2.7}$$

where the model parameters are functions of other variables. This form enables to preserve TF representation while utilising highly nonlinear models.

3.2.2 State-Dependent Parameter model structure for multi input single output systems

Following SDP formulation in Section 3.2.1, multi input single output form for the second order system model has been derived to capture the thermal system model proposed in Chapter 2 and used as presented in Section 3.3. Then, first order SDP form has been derived to accommodate for reduced order model presented in Section 3.4. Both SDP forms are introduced below.

3.2.2.1 Second order State-Dependent Parameter model form

The multi input, single output discrete-time form of a second order SDP model having two input terms with common denominator can be formulated as

$$y(k) = \mathbf{z}_1^T(k) \cdot \boldsymbol{\rho}_1(k) + \mathbf{z}_2^T(k) \cdot \boldsymbol{\rho}_2(k) + e(k); \qquad e(k) = \mathcal{N}(0, \sigma^2) \tag{3.2.8}$$

where

$$\mathbf{z}_1^T(k) = [-y(k-1) \; -y(k-2) \, u_1(k-\delta) \, u_1(k-\delta-1)] \tag{3.2.9}$$

$$\boldsymbol{\rho}_1(k) = [a_1\{\chi_1(k)\} \, a_2\{\chi_1(k)\} \, b_0\{\chi_1(k)\} \, b_1\{\chi_1(k)\}]^T \tag{3.2.10}$$

and

$$\mathbf{z}_2^T(k) = [-y(k-1) \; -y(k-2) \, u_2(k-\delta) \, u_2(k-\delta-1)] \tag{3.2.11}$$

$$\boldsymbol{\rho}_2(k) = [a_1\{\chi_1(k)\} \, a_2\{\chi_1(k)\} \, \bar{b_0}\{\chi_2(k)\} \, \bar{b_1}\{\chi_2(k)\}]^T \tag{3.2.12}$$

and $y(k)$ is an output variable, $\mathbf{z}_1^T(k)$ and $\mathbf{z}_2^T(k)$ are 1×4 regression vectors of previous input and output signals for the first and second input u_1 and u_2, respectively, and $\boldsymbol{\rho_1}(k)$ and $\boldsymbol{\rho_2}(k)$ are 4×1 state-dependent parameter vectors for inputs u_1 and u_2,

respectively. Parameters $a_i\{\chi_1(k)\}, i = 1,2,\ b_j\{\chi_1(k)\}, j = 0,1$ and $\bar{b}_j\{\chi_2(k)\}, j = 0,1$ are assumed to be functions of one of the variables in non-minimal state vectors $\chi_1^T(k) = [\mathbf{z}_1^T\ \mathbf{U}^T(k)]$ and $\chi_2^T(k) = [\mathbf{z}_2^T\ \mathbf{U}^T(k)]$ relating to inputs u_1 and u_2, respectively. Here $\mathbf{U}(k) = [U_1(k)\, U_2(k)\ \ldots\ U_r(k)]^T$ is a $r \times 1$ vector of other variables that may affect the relationship between the two primary variables, but are not variables that appear in $\mathbf{z}_1(k)$ or $\mathbf{z}_2(k)$.

3.2.2.2 First order State-Dependent Parameter model form

The multi input, single output discrete-time form of a first order SDP model having two input terms with common denominator can be formulated as

$$y(k) = \mathbf{z}_1^T(k) \cdot \boldsymbol{\rho}_1(k) + \mathbf{z}_2^T(k) \cdot \boldsymbol{\rho}_2(k) + e(k); \qquad e(k) = \mathcal{N}(0, \sigma^2) \tag{3.2.13}$$

where

$$\mathbf{z}_1^T(k) = [-y(k-1)\, u_1(k-\delta)] \tag{3.2.14}$$

$$\boldsymbol{\rho}_1(k) = [a_1\{\chi_1(k)\}\, b_0\{\chi_1(k)\}]^T \tag{3.2.15}$$

and

$$\mathbf{z}_2^T(k) = [-y(k-1)\, u_2(k-\delta)] \tag{3.2.16}$$

$$\boldsymbol{\rho}_2(k) = [a_1\{\chi_1(k)\}\, \bar{b_0}\{\chi_2(k)\}]^T \tag{3.2.17}$$

and $y(k)$ is an output variable, $\mathbf{z}_1^T(k)$ and $\mathbf{z}_2^T(k)$ are 1×2 regression vectors of previous input and output signals for the first and second input u_1 and u_2, respectively, and $\boldsymbol{\rho_1}(k)$ and $\boldsymbol{\rho_2}(k)$ are 2×1 state-dependent parameter vectors for u_1 and u_2 inputs, respectively. Parameters $a_1\{\chi_1(k)\}$, $b_0\{\chi(k)\}, j = 0,1$ and $\bar{b}_j\{\chi(k)\}, j = 0,1$ are assumed to be functions of one of the variables in non-minimal state vectors $\chi_1^T(k) = [\mathbf{z}_1^T\ \mathbf{U}^T(k)]$ and $\chi_2^T(k) = [\mathbf{z}_2^T\ \mathbf{U}^T(k)]$ relating to u_1 and u_2 inputs, respectively. Here $\mathbf{U}(k) = [U_1(k)\, U_2(k)\ \ldots\ U_r(k)]^T$ is a $r \times 1$ vector of other variables that may affect the relationship between the two primary variables, but are not variables that appear in $\mathbf{z}_1(k)$ or $\mathbf{z}_2(k)$.

3.3 Second order State-Dependent Parameter model of an indoor thermal process

Consider the first principle model of an indoor air temperature represented by Equation (2.4.8); internal and solar irradiation heat gains q and q_i are neglected. If the fan speed changes over time and varies the air mass flow rate $m_a(s)$, the respective SDP form of Equation (2.4.8) is formulated as

$$\Big(s^2 + a_1\{m_a(s)\}s + a_2\{m_a(s)\}\Big) \cdot T_r(s) = \Big(b_0\{m_a(s)\}s + b_1\{m_a(s)\}\Big) \cdot T_s(s) + \Big(\bar{b_0}s + \bar{b_1}\Big) \cdot T_a(s) \tag{3.3.1}$$

containing both state-dependent and constant value parameters

$$\begin{aligned}
a_1\{m_a(s)\} &= \frac{(UA)_{int}}{C_r} + \frac{n_v}{3600} + \frac{m_a(s)}{V_r} + \frac{(UA)_{int} + (UA)_{ext}}{C_w} \\
a_2\{m_a(s)\} &= \frac{(UA)_{int} + (UA)_{ext}}{C_w} \cdot \Big[\frac{m_a(s)}{V_r} + \frac{n_v}{3600}\Big] + \frac{(UA)_{int}(UA)_{ext}}{C_w C_r} \\
b_0\{m_a(s)\} &= \frac{m_a(s)}{V_r} \\
b_1\{m_a(s)\} &= \frac{(UA)_{int} + (UA)_{ext}}{C_w} \cdot \frac{m_a(s)}{V_r} \\
\bar{b_0} &= \frac{n_v}{3600} \\
\bar{b_1} &= \frac{(UA)_{int} + (UA)_{ext}}{C_w} \cdot \frac{n_v}{3600} + \frac{(UA)_{int}(UA)_{ext}}{C_w C_r}
\end{aligned}$$

Analysing the state-dependent model parameters of Equation (3.3.1), it appears that $a_2\{m_a(s)\} = b_1\{m_a(s)\} + \bar{b_1}$, whereas $b_0\{m_a(s)\}$ and $\bar{b_0}$ are two out of four elements summing into $a_1\{m_a(s)\}$ and the other two relate to the heat transfer through the walls. Secondly, it has been noted, that a and b parameters are dependent on the air mass flow rate $m_a(s)$ and $\bar{b}$ parameters are not state-dependent. That is expected as $\bar{b}$ parameters are bounded to $T_a(s)$ term, all representing changes in the indoor air temperature due to the temperature of the ambient air surrounding the building through the building structure only. On the contrary, b parameters are bounded to the temperature of the air supplied from the AHU at the air mass flow rate $m_a(s)$. Finally, since a parameters are bounded to the output $T_r(s)$, it is expected that a parameters are state-dependent as changes in the indoor air temperature $T_r(s)$ strongly depend on the rate at which the air is supplied through the ductwork.

Applying relations between $T_d(t)$, $T_r(t)$ and $T_a(t)$ from Equation (2.3.2) and $T_s(t) = T_d(t) + \Delta T(t)$ from Figure 2.6, $T_s(t)$ is reformulated to

$$T_s(t) = \Delta T(t) + T_d(t) = \Delta T(t) + u_d(t) \cdot T_a(t) + T_r(t) - u_d(t) \cdot T_r(t) \tag{3.3.2}$$

and its Laplace transform is

$$T_s(s) = \Delta T(s) + T_d(s) = \Delta T(s) + u_d(s) \cdot T_a(s) + T_r(s) - u_d(s) \cdot T_r(s) \tag{3.3.3}$$

Applying these properties to substitute $T_s(s)$ in Equation (3.3.1), it takes new form

$$\begin{aligned}\Big(s^2 + a_1\{m_a(s)\}s + a_2\{m_a(s)\}\Big) \cdot T_r(s) = \\ \Big(b_0\{m_a(s)\}s + b_1\{m_a(s)\}\Big) \cdot \Big(\Delta T(s) + u_d(s) \cdot T_a(s) + T_r(s) - u_d(s) \cdot T_r(s)\Big) \\ + \Big(\bar{b_0}s + \bar{b_1}\Big) \cdot T_a(s)\end{aligned} \tag{3.3.4}$$

which can be rearranged to

$$\begin{aligned}\Big(s^2 + a_1\{m_a(s)\}s + a_2\{m_a(s)\}\Big) \cdot T_r(s) = \\ + \Big(b_0\{m_a(s)\}s + b_1\{m_a(s)\}\Big) \cdot \Delta T(s) \\ + \Big(b_0\{m_a(s)\}s + b_1\{m_a(s)\}\Big) \cdot u_d(s) T_a(s) \\ + \Big(b_0\{m_a(s)\}s + b_1\{m_a(s)\}\Big) \cdot \Big(T_r(s) - u_d(s) T_r(s)\Big) \\ + \Big(\bar{b_0}s + \bar{b_1}\Big) \cdot T_a(s)\end{aligned} \tag{3.3.5}$$

and then to

$$\begin{aligned}\Big(s^2 + \alpha_1\{m_a(s), u_d(s)\}s + \alpha_2\{m_a(s), u_d(s)\}\Big) \cdot T_r(s) = \\ + \Big(\beta_0\{m_a(s)\}s + \beta_1\{m_a(s)\}\Big) \cdot \Delta T(s) \\ + \Big(\bar{\beta_0}\{m_a(s)\}s + \bar{\beta_1}\{m_a(s)\}\Big) \cdot T_a(s)\end{aligned} \tag{3.3.6}$$

representing a second order model of the system with state-dependent model parameters subjected to the air mass flow rate and the position of damper blades conforming to

$$\begin{aligned}
\alpha_1\{m_a(s), u_d(s)\} &= a_1\{m_a(s)\} - b_0\{m_a(s)\} + b_0\{m_a(s)\}u_d(s) \\
\alpha_2\{m_a(s), u_d(s)\} &= a_2\{m_a(s)\} - b_1\{m_a(s)\} + b_1\{m_a(s)\}u_d(s) \\
\beta_0\{m_a(s)\} &= b_0\{m_a(s)\} \\
\beta_1\{m_a(s)\} &= b_1\{m_a(s)\} \\
\bar{\beta_0}\{m_a(s), u_d(s)\} &= \bar{b_0} + b_0\{m_a(s)\}u_d(s) \\
\bar{\beta_1}\{m_a(s), u_d(s)\} &= \bar{b_1} + b_1\{m_a(s)\}u_d(s)
\end{aligned}$$

Note that even when the air mass flow rate $m_a(s)$ is constant, the model parameters will still vary following the damper blades position control input. Conclusively, the model (3.3.6) is identified as a highly nonlinear system.

3.4 First order State-Dependent Parameter model of an indoor thermal process

Following derivation of the second order SDP model of an indoor air thermal process introduced in Section 3.3, similar methodology can be applied to obtain first order SDP model. This will be referred to as a reduced order model of the system as the first principles model is simplified. Assuming $\frac{\mathrm{d}T_w(t)}{\mathrm{d}t} = 0$, $q(t) = 0$ and $q_i(t) = 0$, the set of Equations (2.4.1) takes the following form

$$C_r \frac{\mathrm{d}T_r(t)}{\mathrm{d}t} = m_a(t)\rho_a c_a \left[T_s(t) - T_r(t)\right] - (UA)_{int}\left[T_r(t) - T_w(t)\right] - \frac{n_v C_r}{3600}\left[T_r(t) - T_a(t)\right] \tag{3.4.1a}$$

$$0 = (UA)_{int}\left[T_r(t) - T_w(t)\right] - (UA)_{ext}\left[T_w(t) - T_a(t)\right] \tag{3.4.1b}$$

This assumption is made to simplify the overall model by eliminating one dynamic state out of two. This approximation is based on a reason that the heat transfer through the walls is so slow that it is close to 0. In other words, assuming rate of the wall temperature nearly 0 over each time step, this can be approximated and treated as a stationary point (or critical point) like $\frac{\mathrm{d}x}{\mathrm{d}y} = 0$, see e.g. (Pender et al., 2012, p. 318). Note that in this case the wall structure, e.g. thickness, weight, does not matter as C_w term is no longer present. Further simulation study will demonstrate how well the reduced order model of an indoor air thermal process can represent the primary first principles-based model.

Rearranging Equation (3.4.1b) with regard to $T_w(t)$, so that

$$T_w(t) = \frac{(UA)_{int}T_r(t) + (UA)_{ext}T_a(t)}{(UA)_{int} + (UA)_{ext}} \tag{3.4.2}$$

and substituting $T_w(t)$ in Equation (3.4.1a) with right-hand side of Equation (3.4.2) leads to a first order differential equation

$$\begin{aligned} C_r\frac{\mathrm{d}T_r(t)}{\mathrm{d}t} =& m_a(t)\rho_a c_a\left[T_s(t) - T_r(t)\right] - (UA)_{int}\left[T_r(t) - \frac{(UA)_{int}T_r(t) + (UA)_{ext}T_a(t)}{(UA)_{int} + (UA)_{ext}}\right] \\ &- \frac{n_v C_r}{3600}\left[T_r(t) - T_a(t)\right] \end{aligned}$$

which after rearrangements is presented as

$$\begin{aligned} C_r\frac{\mathrm{d}T_r(t)}{\mathrm{d}t} =& m_a(t)\rho_a c_a T_s(t) - m_a(t)\rho_a c_a T_r(t) \\ &- (UA)_{int}T_r(t) + \left[\frac{(UA)_{int}^2}{(UA)_{int} + (UA)_{ext}}\right]T_r(t) - \frac{n_v C_r}{3600}T_r(t) \\ &+ \left[\frac{(UA)_{int}(UA)_{ext}}{(UA)_{int} + (UA)_{ext}}\right]T_a(t) + \frac{n_v C_r}{3600}T_a(t) \end{aligned} \tag{3.4.3}$$

Applying Laplace transform to Equation (3.4.3), assuming zero initial conditions, and using C_r dependencies (2.4.4), the reduced order model of an indoor thermal process in s-domain is

$$\big(s + a\{m_a(s)\}\big)T_r(s) = b_1\{m_a(s)\}T_s(s) + b_2 T_a(s) \tag{3.4.4}$$

with a controllable known input $T_s(s)$ and a non-controllable known input $T_a(s)$, where

$$a\{m_a(s)\} = \frac{m_a(s)}{V_r} + \frac{(UA)_{int}}{C_r} - \frac{1}{C_r}\cdot\frac{(UA)_{int}^2}{(UA)_{int} + (UA)_{ext}} + \frac{n_v}{3600} \tag{3.4.5}$$

$$b_1\{m_a(s)\} = \frac{m_a(s)}{V_r} \tag{3.4.6}$$

$$b_2 = \frac{1}{C_r}\cdot\frac{(UA)_{int}(UA)_{ext}}{(UA)_{int} + (UA)_{ext}} + \frac{n_v}{3600} \tag{3.4.7}$$

Note that parameters $a\{m_a(s)\}$ and $b_1\{m_a(s)\}$ are clearly dependent on the air flow rate, while b_2 is constant. That observation is consistent with the parameters of the second order SDP model (3.3.1), where parameters bounding to $T_a(s)$ are also not state-dependent. If there is no air flow supplied, i.e. $m_a(s) = 0$, then $b_1\{m_a(s)\} = 0$. Consequently, the first term on the right-hand side of Equation (3.4.4) is not present and the outdoor air is the only influence on the indoor air temperature, hence

$$(s + b_2)\cdot T_r(s) = b_2 \cdot T_a(s) \tag{3.4.8}$$

Substituting $T_s(s)$ in the indoor air thermal process described by Equation (3.4.4)

with its equivalent from Equation (3.3.3), the indoor air thermal process is rewritten into

$$\big(s + \alpha\{m_a(s), u_d(s)\}\big)T_r(s) = \beta_1\{m_a(s)\}\Delta T(s) + \beta_2\{m_a(s), u_d(s)\}T_a(s) \tag{3.4.9}$$

with the model parameters defined as

$$\begin{aligned}
\alpha\{m_a(s), u_d(s)\} &= a\{m_a(s)\} - b_1\{m_a(s)\} \cdot \big(1 - u_d(s)\big) \\
\beta_1\{m_a(s)\} &= b_1\{m_a(s)\} \\
\beta_2\{m_a(s), u_d(s)\} &= b_1\{m_a(s)\}u_d(s) + b_2
\end{aligned}$$

It has been observed that the thermal process model's complexity increases when a variable air mass flow rate and the position of damper blades are taken into considerations. Note that the polynomial accompanying $\Delta T(s)$ is dependent on the air mass flow rate and not on the position of damper blades, while the polynomials accompanying $T_r(s)$ and $T_a(s)$ are dependent on both the air mass flow rate and the position of damper blades.

To sum up, Equation (3.4.9) with state-dependent parameters $\alpha\{m_a(s), u_d(s)\}$, $\beta_1\{m_a(s)\}$ and $\beta_2\{m_a(s), u_d(s)\}$ can be used to express the indoor air thermal process of a system with variable fan speed and adjustable source of the supply air. Secondly, the relationship provided in Equation (3.4.9) allows to conclude that the indoor air thermal process can be calculated if the outdoor air temperature, AHU heat load, damper position and air mass flow rate are known. Formulation of the right-hand side equation without direct use of the indoor air temperature provides an equation that has no closed loop effect. Such configuration of a closed loop system would occur if the indoor air temperature is an input as well as output of the system, which occurs when the indoor air is recirculated. Finally, the use of $\Delta T(s)$ has an implication that the difference in the air temperature between the air entering and leaving AHU is calculated independently of the source of the air entering AHU.

Special cases of the reduced order model are covered in the subsections below, where the models with variable and constant position of damper blades are considered as well as models with and without heating load $\Delta T(s)$.

3.4.1 Special cases of the reduced order thermal system model

The indoor air thermal process model shown in Figure 2.7 is expanded to the thermal model of the system by referring to the system configuration proposed in Section 2.3. In this system configuration the position of damper blades can be varied, allowing choice

of the supply air source between the recirculated indoor air or fresh air from the outside. Consider two scenarios, $\Delta T(t) = 0$ and variable $\Delta T(t)$, to identify different model characteristics discussed in the following Sections 3.4.1.1 and 3.4.1.2, where two special cases of the SDP system model are formulated.

3.4.1.1 Reduced order open and closed loop system model interpretation with no heat load of Air Handling Unit

Let $\Delta T(s) = 0$ in Equation (3.3.3), so that $T_s(s) = T_d(s) = u_d(s)T_a(s) + T_r(s) - u_d(s)T_r(s)$. Substituting $T_s(s)$ with this equivalent, Equation (3.4.4) is rewritten into

$$\big(s + a\{m_a(s)\}\big)T_r(s) = b_1\{m_a(s)\}\big(u_d(s)T_a(s) + T_r(s) - u_d(s)T_r(s)\big) + b_2T_a(s) \quad (3.4.10)$$

where $u_d(s)$ shall take either 1 or 0 for the open and closed loop system, respectively. This scenario represents situation, where the air entering the AHU, whether fresh or recirculated, passes through the AHU without any change in its temperature. Let's consider Equation (3.4.10) with regard to the position of damper blades and its structure for the open and closed loop systems individually. Thermal process for the open loop system, i.e. $u_d(s) = 1$ and $T_s(s) = T_a(s)$, is expressed as

$$(s + a\{m_a(s)\})T_r(s) = (b_1\{m_a(s)\} + b_2)T_a(s) \quad (3.4.11)$$

In the same manner, the thermal process for the closed loop system, $u_d(s) = 0$ and $T_s(s) = T_r(s)$, is expressed as

$$\big(s + a\{m_a(s)\}\big)T_r(s) = b_1\{m_a(s)\}T_r(s) + b_2T_a(s) \quad (3.4.12)$$

Moving the indoor air temperature $T_r(s)$ term from the right-hand side to the left-hand side, the thermal process takes form of

$$\big(s + a\{m_a(s)\} - b_1\{m_a(s)\}\big)T_r(s) = b_2T_a(s) \quad (3.4.13)$$

Whereas Equation (3.4.10) has been constructed to cater separately for the open and closed loop system cases as presented in Equations (3.4.11) and (3.4.13), respectively, to remove the dependency on $u_d(s)$, the parameters associated with $T_r(s)$ and $T_a(s)$ for the open loop system remain dependent on the air mass flow rate $m_a(s)$. Note also that when no heating and cooling is present, the model of the system has only one input, $T_a(s)$, making the system model SISO.

3.4.1.2 Reduced order open and closed loop system model interpretation with heat load of Air Handling Unit

Let's assume that $\Delta T(s)$ is variable, i.e. the air passing through the AHU can be heated, cooled or passed without any heat treatment. Substituting $T_s(s)$ with its equivalent following Equation (3.3.3), Equation (3.4.4) is rewritten into

$$\big(s + a\{m_a(s)\}\big)T_r(s) = b_1\{m_a(s)\}\big(\Delta T(s) + u_d(s)T_a(s) + T_r(s) - u_d(s)T_r(s)\big) + b_2T_a(s) \tag{3.4.14}$$

The value of $u_d(s)$ shall be 1 and 0 for the open and closed loop system, respectively. Adopting $u_d(s) = 1$ and $T_s(s) = \Delta T(s)+T_a(s)$ in Equation (3.4.14), the thermal process for the open loop system is expressed as

$$(s + a\{m_a(s)\})T_r(s) = b_1\{m_a(s)\}\Delta T(s) + \big(b_1\{m_a(s)\} + b_2\big)T_a(s) \tag{3.4.15}$$

Further, looking at the closed loop system, $u_d(s) = 0$ and $T_s(s) = \Delta T(s) + T_r(s)$, the thermal process is expressed as

$$\big(s + a\{m_a(s)\}\big)T_r(s) = b_1\{m_a(s)\}(\Delta T(s) + T_r(s)) + b_2T_a(s)$$

Moving the indoor air temperature $T_r(s)$ term from the right-hand side to the left-hand side, the thermal process takes form of

$$\big(s + a\{m_a(s)\} - b_1\{m_a(s)\}\big)T_r(s) = b_1\{m_a(s)\}\Delta T(s) + b_2T_a(s) \tag{3.4.16}$$

Both Equations (3.4.15) and (3.4.16) represent MISO system models with the non-controllable known input $T_a(s)$ and controllable input $\Delta T(s)$. As in Section 3.4.1.1, dependency on $u_d(s)$ is removed and parameters associated with $T_r(s)$ as well as $T_a(s)$ for the open loop system remain dependent on the air mass flow rate $m_a(s)$. Since $\Delta T(s)$ is now present in the model, it is expected that the parameters associated with this term are dependent on $m_a(s)$. This would reflect how quick or at what rate the heated or cooled air is distributed across the air-conditioned area.

3.4.1.3 Reduced order model interpretation with heat loads of heating, cooling and fan units

Let's address AHU elements contributing to the air temperature change $\Delta T(s)$ directly. Substituting $\Delta T(s)$ in Equations (3.4.15) and (3.4.16) with the right-hand side of Equation (2.5.1) (neglecting the outdoor air term related to heat transfer through the walls) to consider the heat loads of AHU components separately, the reduced order model of

the thermal system for the open loop scenario is

$$(s + a\{m_a(s)\})T_r(s) = b_1\{m_a(s)\}\big(\Delta T_h(s) + \Delta T_c(s) + \Delta T_f(s)\big) + \big(b_1\{m_a(s)\} + b_2\big)T_a(s) \tag{3.4.17}$$

and for the closed loop scenario is

$$\big(s + a\{m_a(s)\} - b_1\{m_a(s)\}\big)T_r(s) = b_1\{m_a(s)\}\big(\Delta T_h(s) + \Delta T_c(s) + \Delta T_f(s)\big) + b_2T_a(s) \tag{3.4.18}$$

This extends the idea that all temperature changes within the AHU will drive the thermal process model by means of $m_a(s)$-dependent parameter as they all contribute to the overall supply air temperature $T_s(s)$ distributed at the air mass flow rate $m_a(s)$.

3.4.2 Parameters decomposition

The parameter values calculated from first principles with regard to $m_a(s)$ and $u_k(s)$ values are given in Tables 3.1 and 3.2. It is assumed that the first principles scalars are as provided in Table 2.5. The parameters a, b_1, b_2 are from the first order model represented by Equation (3.4.4) and α, β_1, β_2 from first order SDP model represented by Equation (3.4.9).

TABLE 3.1: Parameter calculations from first principles for $u_d = 0$ and assuming $m_a = 18.5\,[\mathrm{m}^3/\mathrm{s}]$ at 100 % of the maximum fan speed. States, on which parameters are dependent have been condensed from $m_a(s)$ and $u_k(s)$ to m_a and u_k, respectively, for the sake of notional simplicity.

m_a [m^3/s]	$\alpha\{m_a, u_k\}$	$\beta_1\{m_a\}$	$\beta_2\{m_a, u_k\}$	$a\{m_a\}$	$b_1\{m_a\}$	b_2
0 (0%)	1.115^{-4}	0	1.115^{-4}	1.115^{-4}	0	1.115^{-4}
11.5 (62%)	2.352^{-4}	6.18^{-5}	1.115^{-4}	1.733^{-4}	6.18^{-5}	1.115^{-4}
13.4 (72.5%)	2.561^{-4}	7.23^{-5}	1.115^{-4}	1.838^{-4}	7.23^{-5}	1.115^{-4}
14.8 (80%)	2.711^{-4}	7.98^{-5}	1.115^{-4}	1.913^{-4}	7.98^{-5}	1.115^{-4}
18.5 (100%)	2.110^{-4}	9.97^{-5}	1.115^{-4}	2.112^{-4}	9.97^{-5}	1.115^{-4}

3.5 Simulation study

3.5.1 System identification of the first order linear model parameters

This aim of this section is to present and discuss results of the system identification and reduced order model parameters estimation. As in simulation study provided in Chapter 2, Equations (2.6.1) and (2.6.2) representing the first principles system model,

TABLE 3.2: Parameter calculations from first principle for $u_d = 1$ and assuming $m_a = 18.5\,[\mathrm{m}^3/\mathrm{s}]$ at 100 % of the maximum fan speed. States, on which parameters are dependent have been condensed from $m_a(s)$ and $u_k(s)$ to m_a and u_k, respectively, for the sake of notional simplicity.

m_a [m^3/s]	$\alpha\{m_a, u_k\}$	$\beta_1\{m_a\}$	$\beta_2\{m_a, u_k\}$	$a\{m_a\}$	$b_1\{m_a\}$	b_2
0 (0%)	1.115^{-4}	0	1.115^{-4}	1.115^{-4}	0	1.115^{-4}
11.5 (62%)	1.733^{-4}	6.18^{-5}	1.733^{-4}	1.733^{-4}	6.18^{-5}	1.115^{-4}
13.4 (72.5%)	1.838^{-4}	7.23^{-5}	1.838^{-4}	1.838^{-4}	7.23^{-5}	1.115^{-4}
14.8 (80%)	1.913^{-4}	7.98^{-5}	1.913^{-4}	1.913^{-4}	7.98^{-5}	1.115^{-4}
18.5 (100%)	2.112^{-4}	9.97^{-5}	2.112^{-4}	2.112^{-4}	9.97^{-5}	1.115^{-4}

used in simulation study in Section 2.6, have been used to generate data for the system identification using LS with setup as described in Section 2.6.1. Results of this study have been divided into three scenarios depending on the supply fan operation and heating and cooling units operation, in which both open and closed damper position situations are considered. First scenario is to study the indoor air temperature track in the absence of operating supply fan unit, hence no air distributed into the conditioned area using ductwork. Second scenario considers supply fan unit active and air distributed through ductwork, but heating and cooling units are disabled. Third scenario combines operating supply fan with heating and cooling units operating at different levels of their maximum capacity. In each scenario the following steps are performed:

1. Load first principles model parameters.
2. Prepare vector representing the outdoor air temperature T_a as a square wave changing between 0 and 10 °C every 3 days.
3. Simulate the indoor air temperature using equations from Section 2.6.1.
4. Perform system identification with first order system model structure using Least Squares method.
5. Gather relevant coefficients and metrics representing identified model.
6. Produce figures to visually represent identified system model.

The following first order model structure has been considered for the system identification:

$$T_r(s) = G_s(s) \cdot T_s(s) + G_a(s) \cdot T_a(s) \tag{3.5.1}$$

where $G_s(s)$ and $G_a(s)$ are the continuous-time functions corresponding to inputs $T_s(s)$ and $T_a(s)$, respectively. For simplicity, it is assumed that the internal heat gains are not

present. Following the system model given in Equation (3.4.4), the functions $G_s(s)$ and $G_a(s)$ have common denominator and are represented as

$$G_s(s) = \frac{b_1\{m_a(s)\}}{s + a\{m_a(s)\}} \tag{3.5.2}$$

and

$$G_a(s) = \frac{b_2}{s + a\{m_a(s)\}} \tag{3.5.3}$$

In case where $m_a(s)$ is constant and the model parameters are not state-dependent, Equations (3.5.1), (3.5.2) and (3.5.3) can be considered as transfer functions; otherwise, they are referred to as pseudo-transfer functions. The first order system model given in Equation (3.5.1) is used to evaluate how precisely the reduced order model can reflect the reference system model represented by the second order white-box model from Equations (2.4.1) and (2.4.8).

The following holds for the results presented in the subsequent subsections. The indoor air temperature generated by the model in the figures showing system identification results is denoted *data* and the indoor air temperature simulated using parameters obtained by system identification method is denoted SID. The error is calculated as $Error = data - SID$. Step response of a system function representing relationship between input $T_a(s)$ and output $T_r(s)$ is denoted $G_a(s)$. Similarly, step response of a system function representing relationship between input $T_s(s)$ and output $T_r(s)$ denoted $G_s(s)$. Note that only scenario involving heating and cooling will have $G_s(s)$ term present; supply fan on its own is assumed not to introduce additional heat gain input to the system.

3.5.1.1 Supply fan disabled scenario

In this scenario the supply fan is not in operation and $m_a(s) = 0$. The indoor air temperature simulation results including model fit and the input outdoor air temperature are presented in Figure 3.1. Step response of the system function $G_a(s)$ is presented in Figure 3.2.

3.5.1.2 Supply fan in operation scenario

In this scenario the operation of the supply fan is introduced to evaluate the system model separately for the open and closed loop system scenario. Consequently, the supply fan passes through the ductwork either fresh outside air or recirculated indoor air at 75% of its maximum speed. There is no heating and cooling present. The simulation results

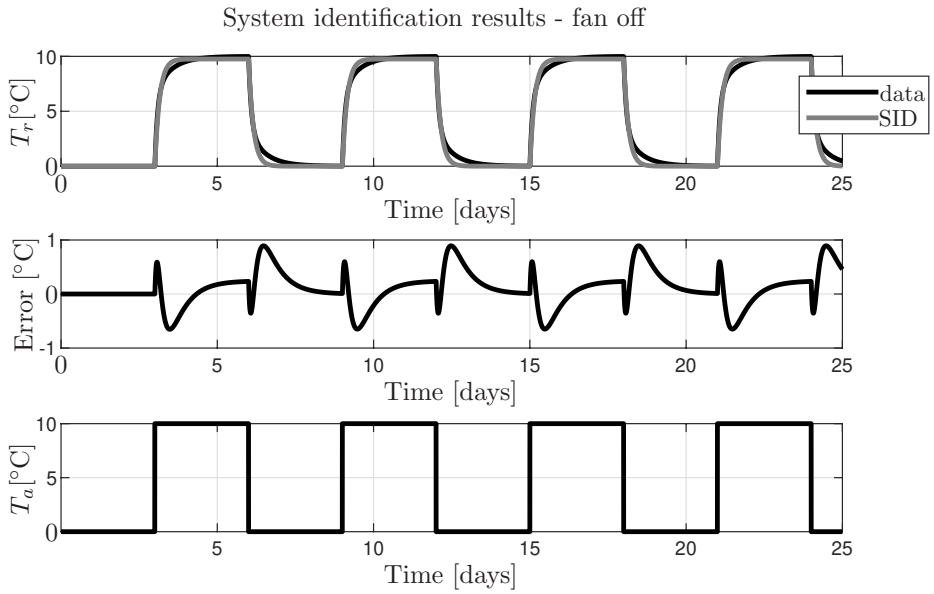

FIGURE 3.1: The indoor air temperature simulation with supply fan disabled scenario (Equation (3.5.1)).

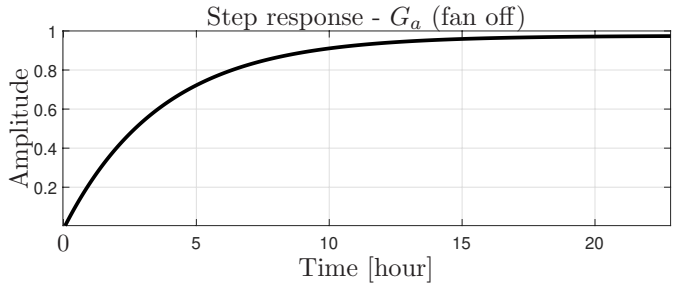

FIGURE 3.2: The outdoor air temperature process (Equation (3.5.3)) step response for supply fan disabled scenario.

of the indoor air temperatures for the open and closed loop systems are presented in Figure 3.3. The indoor air temperature simulation using model parameters from the system identification of the open loop system is presented in Figure 3.4 and in Figure 3.6 for the closed loop system. Step response of the system function G_a for the open loop system is presented in Figure 3.5 and in 3.7 for the closed loop system.

3.5.1.3 Heating and cooling supply scenario

In this scenario the operation of the heating and cooling units is introduced to evaluate the system model with controlled heat gains. Open and closed loop system scenarios are evaluated separately. Consequently, the supply fan passes the air through the ductwork, either fresh outside air or recirculated indoor air, that can be heated or cooled by the heating and cooling units. The simulation results of the indoor air temperatures for the open and closed loop systems are presented in Figures 3.8 and 3.11, respectively. The

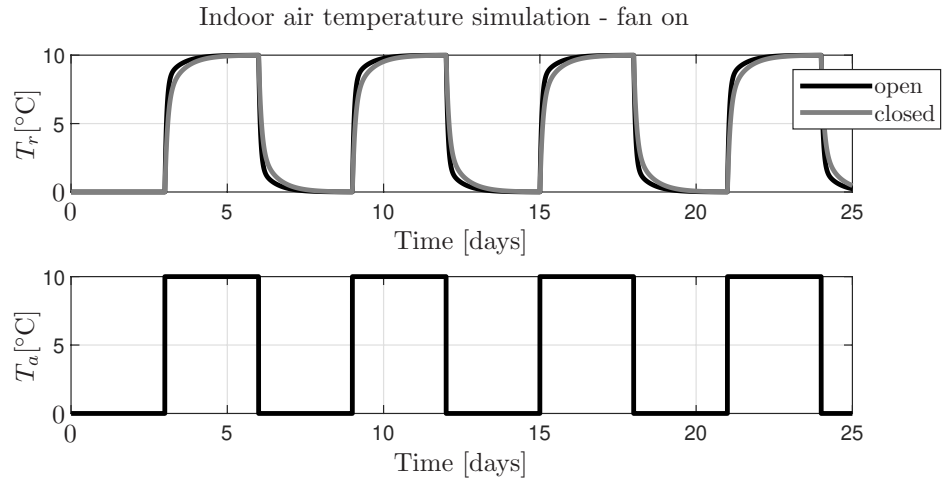

FIGURE 3.3: The indoor air temperature simulation with supply fan operating at 75% of its maximum speed.

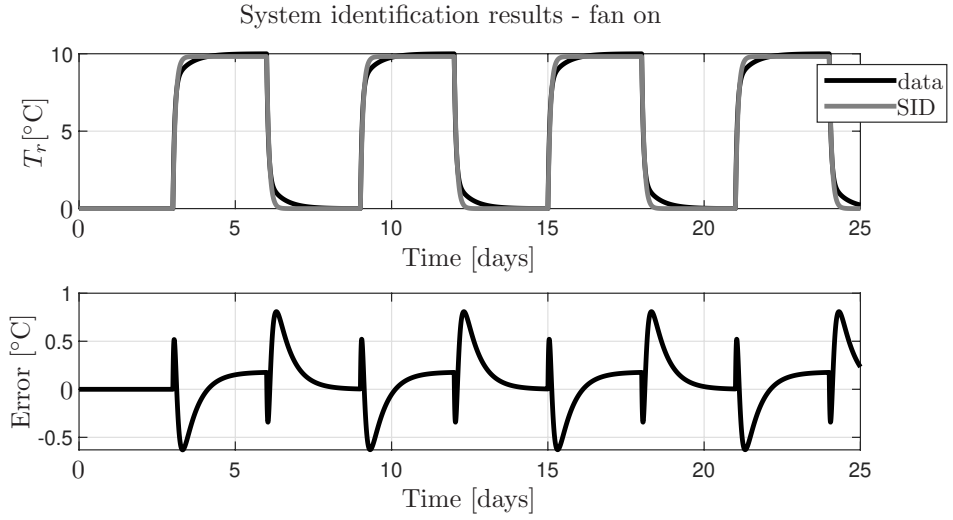

FIGURE 3.4: System identification of the indoor air temperature simulation (Equation (3.5.1)) with supply fan operating at 75% of its maximum speed and damper blades in open position.

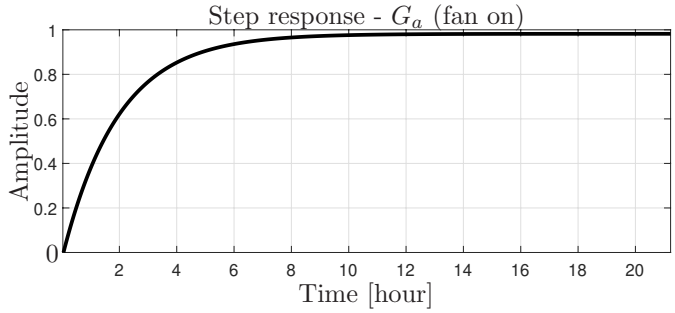

FIGURE 3.5: The outdoor air temperature process (Equation (3.5.3)) step response for supply fan operating at 75% of its maximum speed and damper blades in open position.

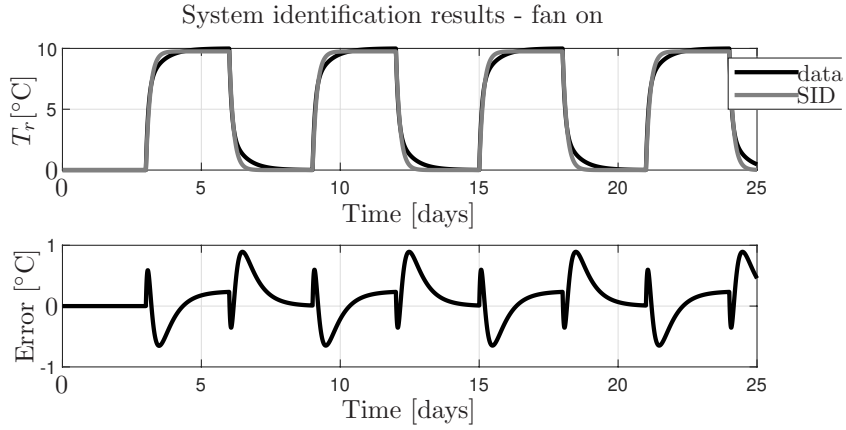

FIGURE 3.6: System identification of the indoor air temperature simulation (Equation (3.5.1)) with supply fan operating at 75% of its maximum speed and damper blades in closed position.

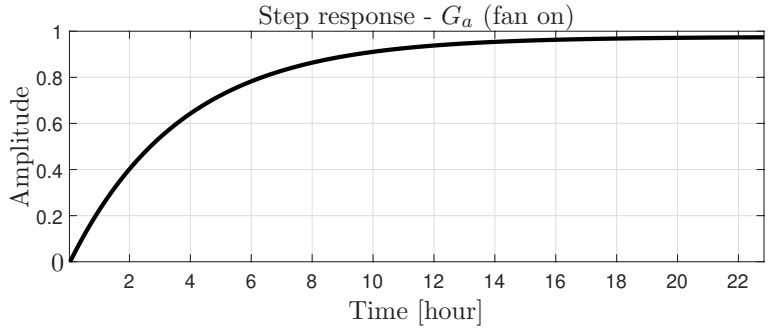

FIGURE 3.7: The outdoor air temperature process (Equation (3.5.3)) step response for supply fan operating at 75% of its maximum speed and damper blades in closed position.

indoor air temperature simulation using model parameters from the system identification of the open loop system is presented in Figure 3.9 and in Figure 3.12 for the closed loop system. Step responses of system functions G_s and G_a for the open loop system are presented in Figure 3.10 and in 3.13 for the closed loop system. It is assumed that the supply fan operates at 75% of its maximum speed.

3.5.1.4 Discussion

Numerical values gathered from system identification for all scenarios and Figures 3.1-3.13 have been summarised in Table 3.3 and 3.4. Additional simulation study has been done for the same setup but with 100% of maximum fan speed with results briefly summarised in Tables 3.5 and 3.6.

Expecting a state-dependent behaviour of the system, it has been demonstrated through simulations, Figures 3.1-3.13, with numerical values presented in Tables 3.3 and 3.5 that the model parameters vary depending on the damper position and the fan speed,

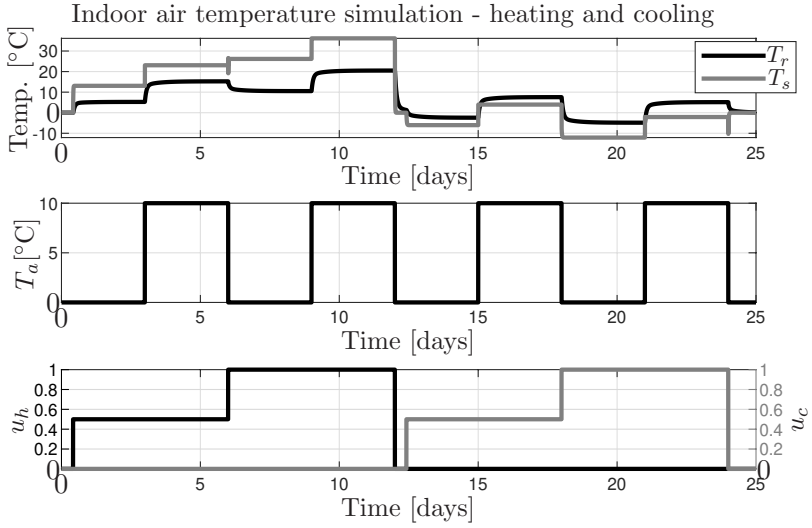

FIGURE 3.8: The indoor air temperature simulation with supply fan operating at 75% of its maximum speed, heating and cooling present and damper blades in open position.

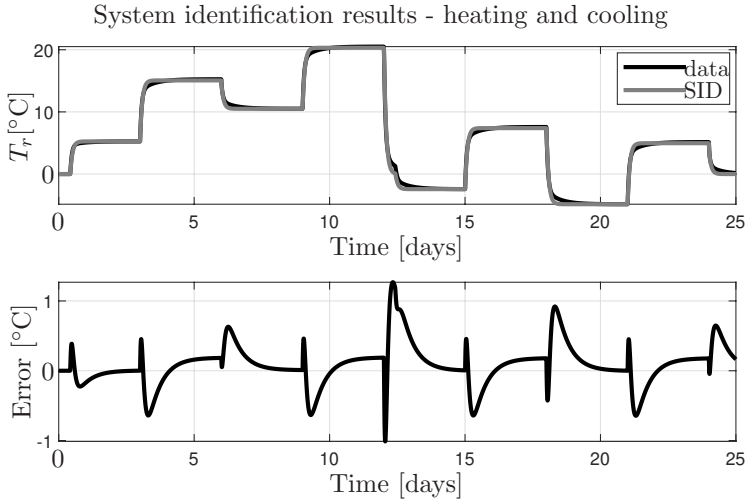

FIGURE 3.9: System identification of the indoor air temperature simulation (Equation (3.5.1)) with supply fan operating at 75% of its maximum speed, heating and cooling present and damper blades in open position.

which translates to the air mass flow rate. This demonstrates that the model parameters of the indoor thermal process are dependent on the position of damper blades and the air flow rate, parameters commonly regulated in a real temperature control system as the manipulated control variables. The process dynamics is changed together with the changing state-dependent parameters; the closed loop process is slower than the open loop and increased $m_a(s)$ makes the process faster. These results are consistent with the simulation study from Chapter 2, where in a similar manner parameters of the second order system model were obtained, see Section 2.6. For this reason, analysis of the characteristics and dynamics of the system based on the results provided will not be repeated here. Simulation results, nonetheless, allow to conclude that one may not be

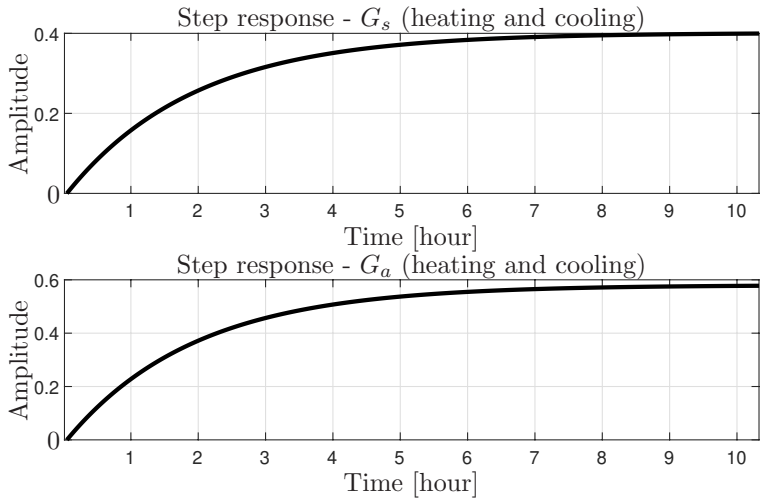

FIGURE 3.10: The supply air temperature (upper plot, Equation (3.5.2)) and the outdoor air temperature process (lower plot, Equation (3.5.3)) step responses for supply fan operating at 75% of its maximum speed and damper blades in open position.

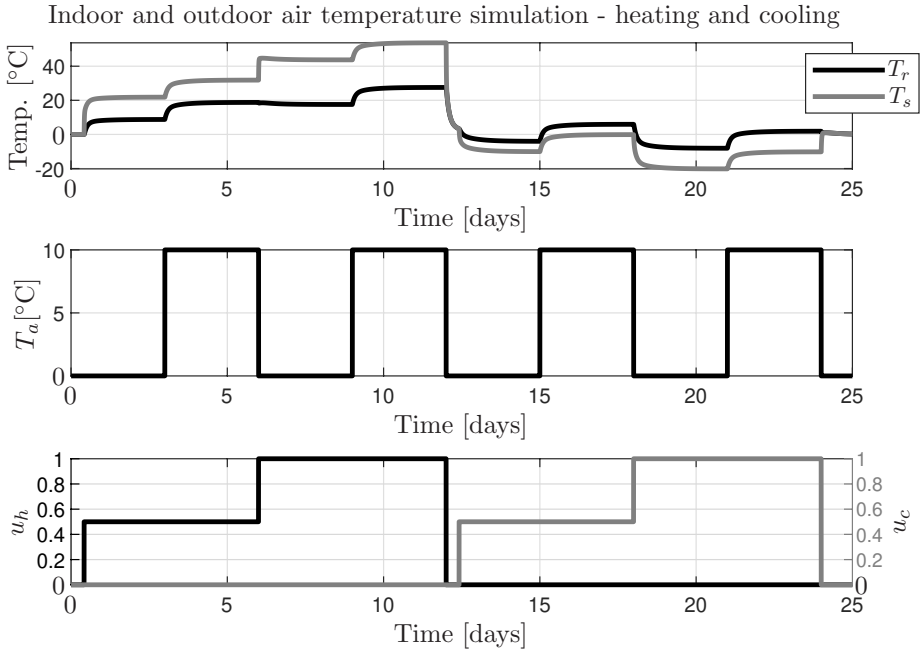

FIGURE 3.11: The indoor air temperature simulation with supply fan operating at 75% of its maximum speed and heating and cooling present. Damper are in closed position.

able to simulate outputs for different fan speeds and positions of damper blades with the same accuracy. If parameters were obtained for a selected fan speed and damper position, which implies certain time constant, rise time, settling time and peak time, then using these parameters to simulate output of the system with different setup may result in discrepancy between simulated and expected output. For this reason, it is concluded that using methods requiring compromise, e.g. linearisation around a working point, may introduce challenges when fan speed or damper positions are changed, whereas the

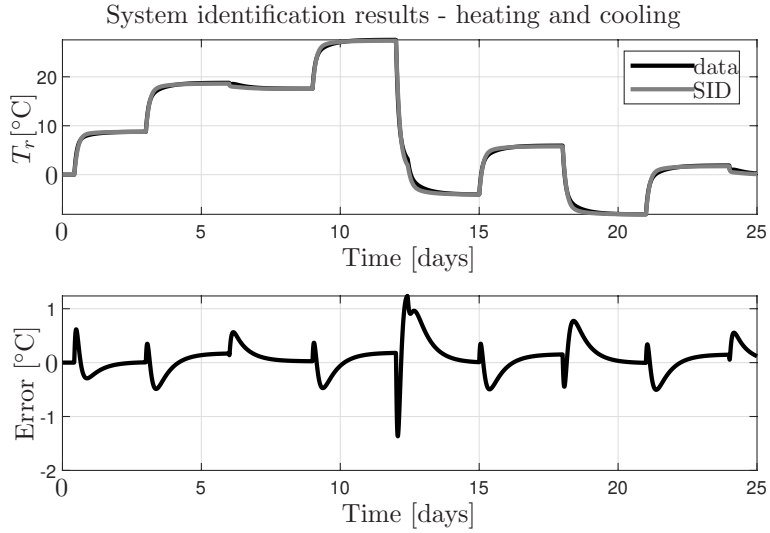

FIGURE 3.12: System identification of the indoor air temperature simulation (Equation (3.5.1)) with supply fan operating at 75% of its maximum speed, heating and cooling present and damper blades in closed position.

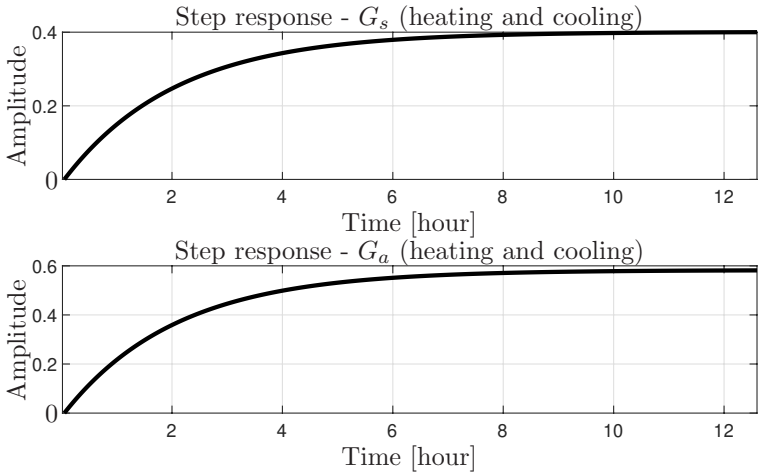

FIGURE 3.13: The supply air temperature (upper plot, Equation (3.5.2)) and the outdoor air temperature process (lower plot, Equation (3.5.3)) step responses for supply fan operating at 75% of its maximum speed and damper blades in closed position.

SDP approach can tackle nonlinearity by adapting parameters to the values according to the system states.

Focusing on the model fit, it has been noticed that the first order model is capable of providing fairly close match to the data generated using second order model of the system with $R_T^2 > 99\%$, IAE between 0.1715 and 0.2441 and MSE 0.0666 and 0.1181. The most critical points causing peaks in discrepancy between *data* and SID trajectories are sharp changes in the system input, i.e. the outdoor air temperature and heating and cooling output; the biggest error has been observed in the heating and cooling scenario, Figures 3.8 and 3.11. This lack of adaption to sharp changes and minimising error is related to

TABLE 3.3: The first order continuous time system model parameters (Equation (3.5.1)) for operating supply fan open and closed position of damper blades and supply fan disabled. Fan operating at 75% of maximum speed for open and closed damper position.

Coefficient	**Heating and cooling**		**Fan on**		**Fan off**
	Open	**Closed**	**Open**	**Closed**	
Time constant [h]	1.9060	2.0383	1.9470	3.6735	3.6735
$G_s(s)$ Gain	0.4013	0.4011	n/a	n/a	n/a
$G_a(s)$ Gain	0.5803	0.5827	0.9821	0.9757	0.9757
b_1	5.849^{-5}	5.466^{-5}	n/a	n/a	n/a
b_2	8.458^{-5}	7.941^{-5}	1.1401^{-4}	7.378^{-5}	7.378^{-5}
a	1.457^{-4}	1.363^{-4}	1.427^{-4}	7.562^{-5}	7.562^{-5}
$G_s(s)$ Rise time [h]	4.15	4.45	n/a	n/a	n/a
$G_s(s)$ Settling time [h]	7.50	8.00	n/a	n/a	n/a
$G_s(s)$ Peak time [h]	11.95	14.95	n/a	n/a	n/a
$G_a(s)$ Rise time [h]	4.15	4.45	4.25	8.10	8.10
$G_a(s)$ Settling time [h]	7.50	8.00	7.65	14.40	14.40
$G_a(s)$ Peak time [h]	11.95	14.95	24.95	26.95	26.95

TABLE 3.4: Measures of the performance criteria for the estimated parameters of a first order model of the system (Equation (3.5.1)) with open and closed position of damper blades. Fan operating at 75% of maximum speed, unless stated differently.

Criteria	**Heating and cooling**		**Fan on**		**Fan off**
	Open	**Closed**	**Open**	**Closed**	
R^2_T [%]	99.8395	99.9293	99.4201	99.4201	99.4201
IAE	0.2066	0.1959	0.1868	0.2441	0.2441
MSE	0.0933	0.0838	0.0771	0.1181	0.1181

reduction of the model order, which prevents model from capturing more sophisticated dynamics. Nonetheless, model fit can be partially improved by using other SID method, e.g. Instrumental Variables (Young, 2011, p. 171), and overcome LS limitations.

3.5.2 Verification of a first order model of the system

This section is to demonstrate how well a first order model can be fitted to represent a second order system when real data is used for simulation.

TABLE 3.5: The first order continuous time system model parameters (Equation (3.5.1)) for operating supply fan open and closed position of damper blades and supply fan disabled. Fan operating at 100% of maximum speed for open and closed damper position.

Criteria	**Heating and cooling**		**Fan on**		**Fan off**
	Open	**Closed**	**Open**	**Closed**	
Time constant [h]	1.6304	1.7501	1.6714	3.6735	3.6735
$G_s(s)$ Gain	0.4718	0.4715	n/a	n/a	n/a
$G_a(s)$ Gain	0.5115	0.5139	0.9836	0.9757	0.9757
b_1	8.037^{-5}	7.484^{-5}	n/a	n/a	n/a
b_2	8.715^{-5}	8.157^{-5}	1.635^{-4}	7.378^{-5}	7.378^{-5}
a	1.704^{-4}	1.587^{-4}	1.662^{-4}	7.562^{-5}	7.562^{-5}
$G_s(s)$ Rise time [h]	3.60	3.85	n/a	n/a	n/a
$G_s(s)$ Settling time [h]	6.40	6.85	n/a	n/a	n/a
$G_s(s)$ Peak time [h]	10.95	11.45	n/a	n/a	n/a
$G_a(s)$ Rise time [h]	3.60	3.85	3.65	8.1	8.1
$G_a(s)$ Settling time [h]	6.40	6.85	6.55	14.4	14.4
$G_a(s)$ Peak time [h]	10.95	11.45	11.95	26.95	26.95

TABLE 3.6: Measures of the performance criteria for the estimated parameters of a first order model of the system (Equation (3.5.1)) with open and closed position of damper blades. Fan operating at 100% of maximum speed, unless stated differently.

Criteria	**Heating and cooling**		**Fan on**		**Fan off**
	Open	**Closed**	**Open**	**Closed**	
R_T^2 [%]	99.8835	99.9567	99.7021	99.4201	99.4201
IAE	0.1923	0.1875	0.1715	0.2441	0.2441
MSE	0.0841	0.0841	0.0666	0.1181	0.1181

3.5.2.1 Reduced order model equations for simulation

Reduced order model represented by the first order differential Equation (3.4.3) has been discretised using the forward Euler method (Atkinson, 2009, p. 4) and implemented in MATLAB for simulation purposes. The implemented discretised equation for the indoor

air temperature is

$$\begin{aligned} T_r(k) = T_r(k-1) &+ \frac{t_s}{V_r} \cdot m_a(k-1) \cdot \big(T_s(k-1) - T_r(k-1)\big) \\ &- \frac{t_s}{C_r} \cdot (UA_{int} - \frac{UA_{int} \cdot UA_{int}}{UA_{int} + UA_{ext}}) \cdot T_r(k-1) \\ &- \frac{t_s \cdot n_v}{3600} \cdot T_r(k-1) + \frac{ts}{C_r} \cdot q(k-1) \\ &+ (\frac{t_s}{C_r} \cdot \frac{UA_{int} \cdot UA_{ext}}{UA_{int} + UA_{ext}}) + ts \cdot \frac{n_v}{3600}) \cdot T_a(k-1) \end{aligned} \tag{3.5.4}$$

where t_s is the sampling interval. Further, Equations (2.6.5) to (2.6.8) for T_s calculation were implemented along Equation (3.5.4) in recursive terms for simulation purposes.

3.5.2.2 First and second order thermal system model simulations

First and second order systems were simulated using Equations (3.5.4) and (2.6.1)-(2.6.2), respectively, and the real data. The models were built representing physical characteristics following Table 2.5. The data was collected by the HVAC system serving pharmaceutical warehouse facility introduced in Chapter 2. The sample count used for this simulation is 2400, 15 min sampling time, collected between 01/05/2016 03:45 and 26/05/2016 03:30. This simulation does not evaluate how well these models can match the recorded indoor air temperature from the data, therefore the recorded indoor air temperature is not displayed. The purpose of this simulation is to demonstrate discrepancies between first and second order model on real data. The output was simulated using the recorded outdoor air temperature T_a, fan speed (reflected in the variable air mass flow rate m_a), heating and cooling outputs as ΔT and damper position, which was closed. It was assumed that $q = 0$. Simulation results are shown in Figure 3.14.

The results presented in Figure 3.14 show that the second order system model presents milder trend, while the first order system model more aggressive one, exceeding upper and lower values of the second order model at the local maximum and minimum values. Note that the error between the first and second order system models will vary depending on the wall model; the second order model will produce different results depending on the wall thickness and material properties, but the first order model is not dependent on these characteristics.

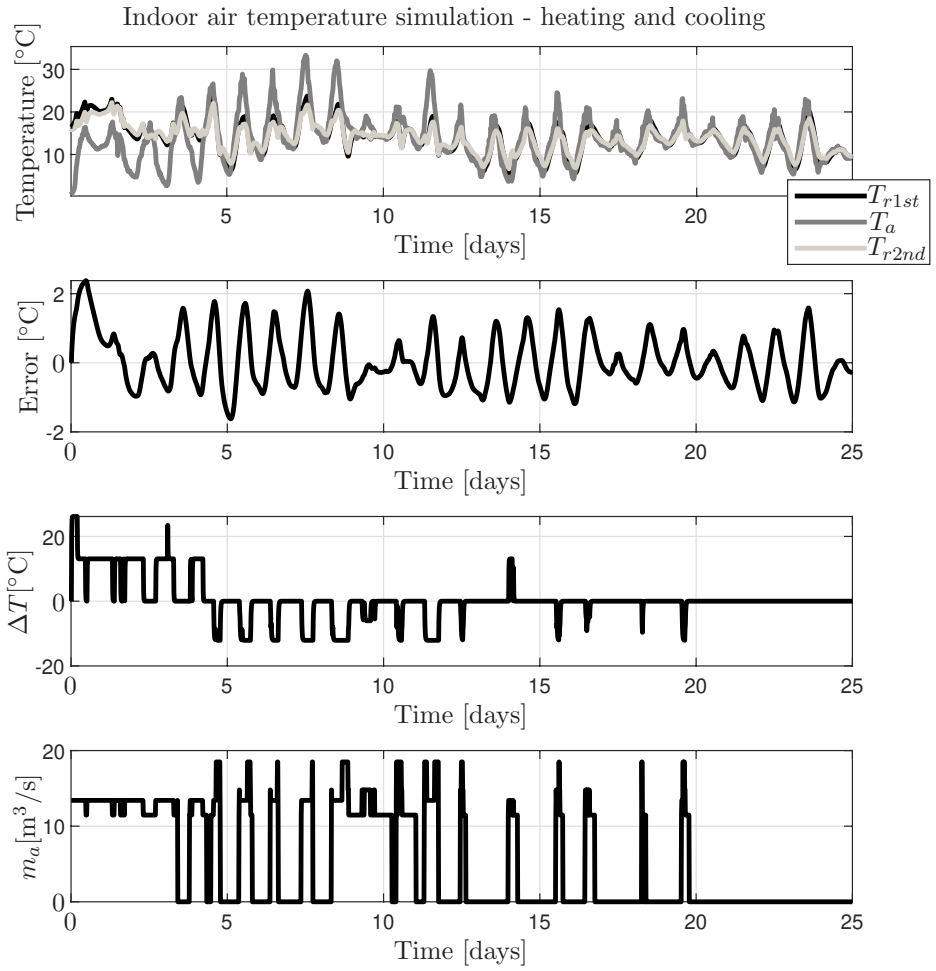

FIGURE 3.14: First (black line) and second (light gray line) order system model simulation (Equations (3.5.4) and (2.6.1)-(2.6.2)). The damper blades are in closed position and the fan speed is variable.

3.5.3 First order linear model and State-Dependent Parameter model parameter estimation using Least Squares method

This section presents the results of the system identification of the data generated using first order system model following model described in Section 3.5.2.1. The data is identified using two models, for the first order linear model expressed by Equation (3.4.4) (or variation (3.4.8) for fan off scenario) and the first order SDP model from Equation(3.4.9).

3.5.3.1 Real data input simulation

Simulation study presented in this section differs from the previous ones in the input data used to generate data for SID; the real data gathered by a local temperature control

unit in the warehouse introduced in Chapter 2 is used. The data has been recorded with 15 min sampling interval during the period of 01/05/2016 03:45-04/05/2016 13:15 (327 samples) for active AHU scenario, where heating goes on and off and supply fan on, and 21/05/2016 20:45-27/05/2016 14:15 for fan off scenario (641 samples). The data used as the inputs include the outdoor air temperature, supply fan speed and operation of the heating and cooling units. Since the recorded data reflects operation of a real HVAC system, the speed at which supply fan operates varies over time. For this reason one cannot extract SDP parameters using simple LS and reverse engineer to obtain m_a for each fan speed; this will be demonstrated in further section. This section aims to analyse results and investigate if the relationships shown and noted in Section 3.4 can also be observed in the estimated parameters. While the recorded data states damper blades closed all the time, this simulation has two scenarios for active AHU, dampers always open and dampers always closed. Consequently, this approach can test only for m_a values as the damper position doesn't change through each simulation, but can still demonstrate the difference in the parameters between the open and closed loop systems.

(1) Fan off scenario The indoor air temperature was simulated using a first order model implemented as in Equation (3.5.4) (see Section 3.5.2.1) using the outdoor air temperature as the only input to the system; the input and output of the model are presented in Figure 3.15, top plot. The system identification results covering the model fit and the error between the expected T_r and the one simulated using estimated parameters are presented in the middle and bottom plots, respectively. Assuming the first order system model with one input as in Equation (3.4.8), the step response for a function corresponding to input T_a is shown in Figure 3.16. Numerical results are presented in Tables 3.7-3.8.

(2) Active Air Handling Unit scenario The indoor air temperature was simulated using a first order model implemented as in Equation (3.5.4) using the outdoor air temperature, fan speed, heating unit operation and the damper position as the inputs to the system as presented in Figure 3.17 for the open loop system and 3.22 for the closed loop system. System identification was performed for two models separately: the first order linear model (3.4.4) with inputs T_s and T_a, and the first order SDP model (3.4.9) with inputs ΔT and T_a. Numerical results are presented in Tables 3.7-3.8.

(2a) Linear model The system identification results covering the model fit and the error between the expected T_r and the one simulated using estimated parameters are presented in Figure 3.18 for the open loop system and Figure 3.23 for the closed loop system. Assuming the first order system model with two inputs as given in Equation

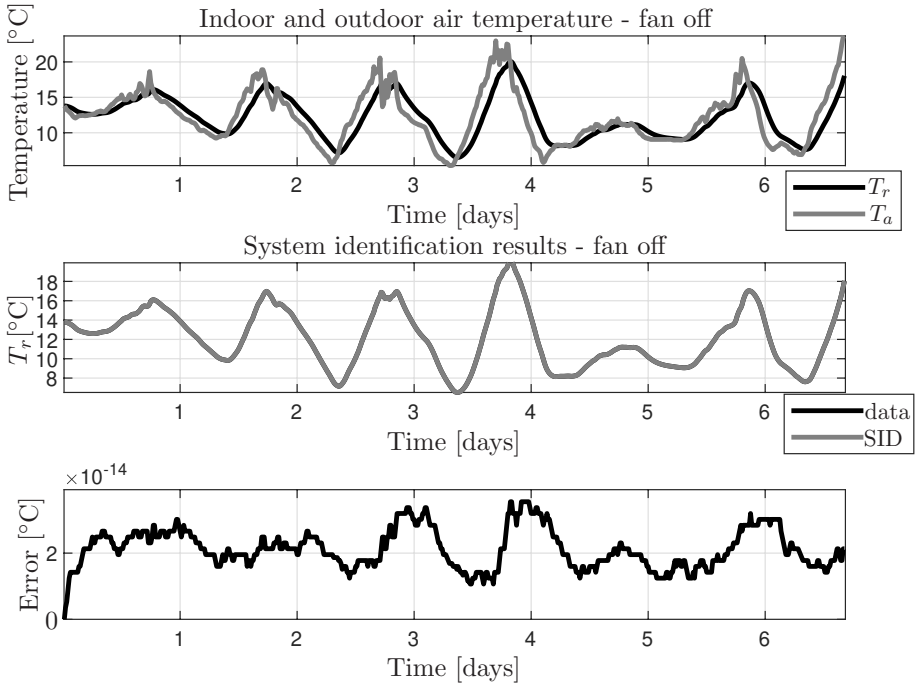

FIGURE 3.15: System identification of the first order model parameters of the indoor air temperature model with single input T_a (Equation (3.4.8)). Simulation of the input data is based on real data. Supply fan is off.

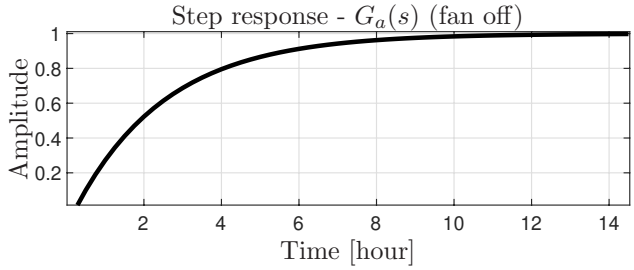

FIGURE 3.16: The outdoor air temperature process step response for first order indoor air temperature model with supply fan off (Equation (3.4.8)).

(3.4.4), the step responses for the function corresponding to inputs T_s and T_a are shown in Figures 3.19 and 3.24 for the open and closed loop system, respectively.

(2b) State-Dependent Parameter model The system identification results covering the model fit and the error between the expected T_r and the one simulated using estimated parameters are presented in Figure 3.20 for the open loop system and Figure 3.25 for the closed loop system. Assuming the first order system model with two inputs as given in Equation (3.4.9), the step responses for the function corresponding to inputs ΔT and T_a are shown in Figures 3.21 and 3.26 for the open and closed loop system, respectively.

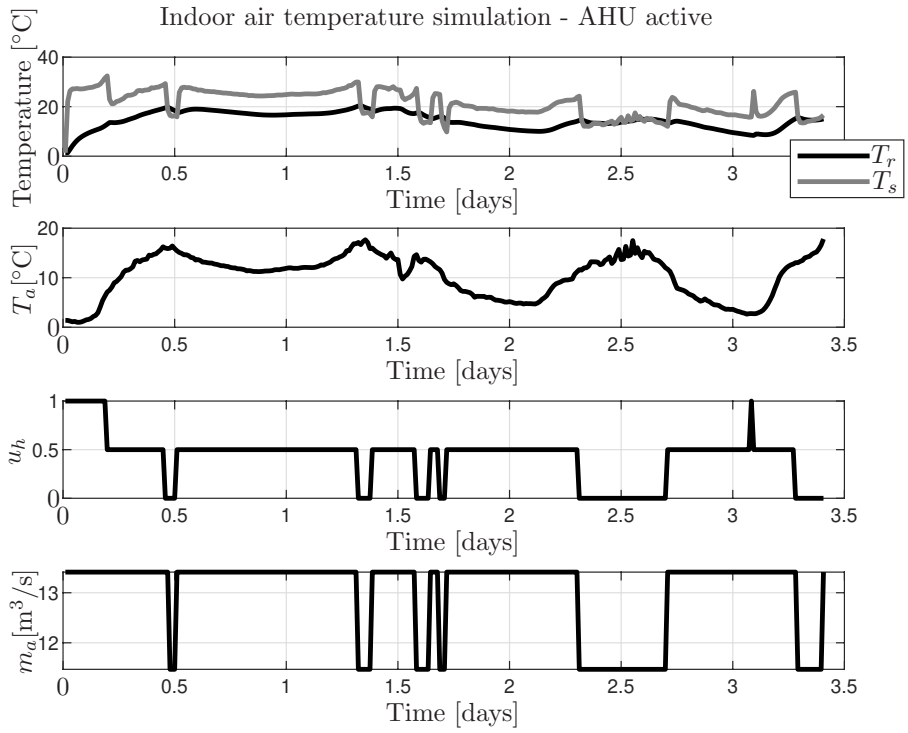

FIGURE 3.17: The indoor air temperature simulation based on real data with variable supply fan speed, damper blades in open position and heating unit active (Equation (3.4.4)).

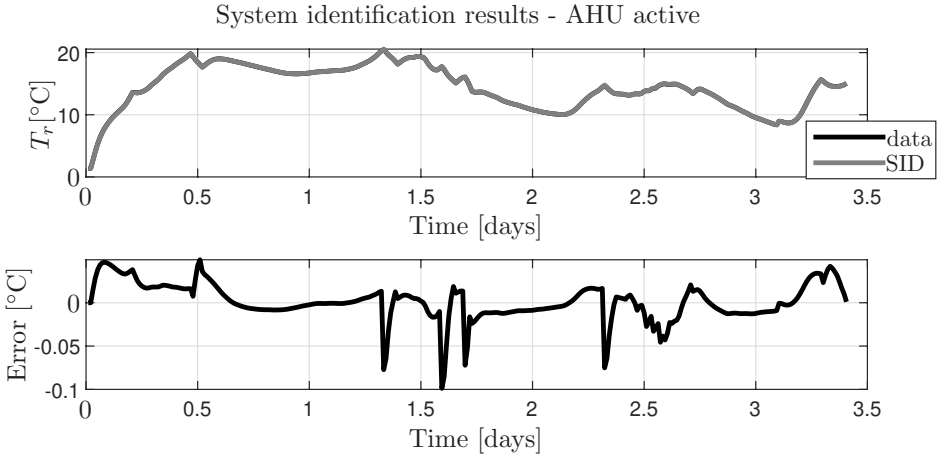

FIGURE 3.18: System identification of the first order parameters of the indoor air temperature model with inputs T_s and T_a (Equation (3.4.4)). Simulation of the input data is based on real data. This scenario has variable supply fan speed, damper blades in open position and heating unit active.

Results analysis and discussion Estimated parameters together with other values describing the model characteristics are introduced in Table 3.7 and performance criteria in Table 3.8.

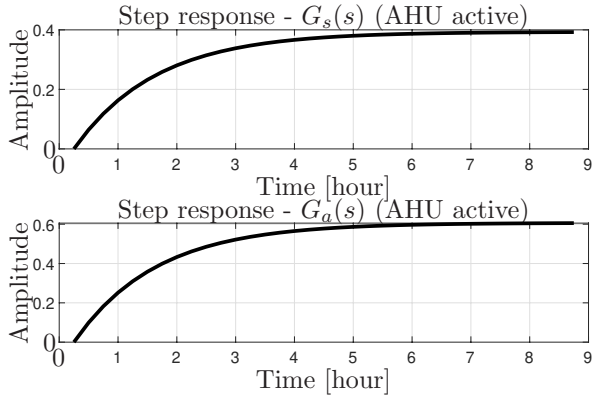

FIGURE 3.19: Step responses for processes corresponding to inputs T_s and T_a, respectively, for scenario with variable supply fan speed, damper blades in open position and heating unit active (Equation (3.4.4)).

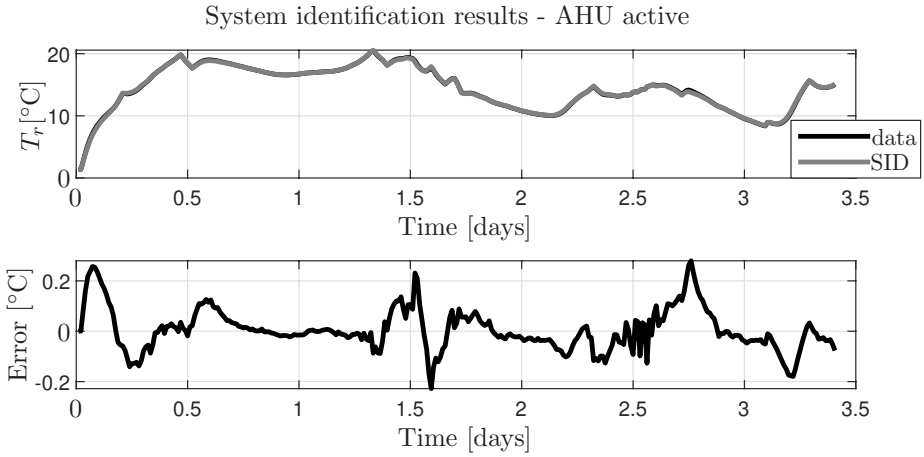

FIGURE 3.20: System identification of the first order parameters of the indoor air temperature model with inputs ΔT and T_a (Equation (3.4.9)). Simulation of the input data is based on real data. This scenario has variable supply fan speed, damper blades in open position and heating unit active.

Fan off scenario The simulation of the indoor air temperature utilising estimated model parameters resulted in a well-fit trajectory with a minimal error of less than $4 \cdot 10^{-14}$, with the biggest discrepancies occurring at the local maximum peaks. The steady state gain of the step response is 1, with time constant being 2.36 h, which is 1.2 h less than the value obtained from SID of the second order system model with the first order model structure. Also, rise time and settling time are 5.25 h and 9.5 h, which is, respectively, approx. 3 and 5 hours lower compared to values in Table 3.3.

Active Air handling Unit scenario Comparing model fit between the linear model and the SDP model, it shows that the estimated SDP model provides slightly worse results than the estimated linear model. It is demonstrated in the error trajectories, which peak just outside of ±0.2 band for the SDP model (see Figure 3.20) and

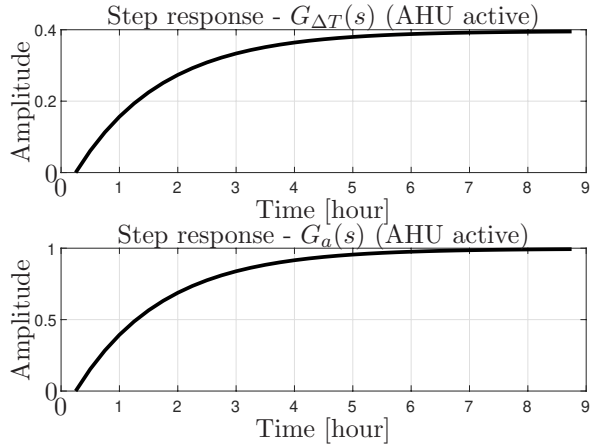

FIGURE 3.21: Step responses for processes corresponding to inputs ΔT and T_a, respectively, for scenario with variable supply fan speed, damper blades in open position and heating unit active (Equation (3.4.9)).

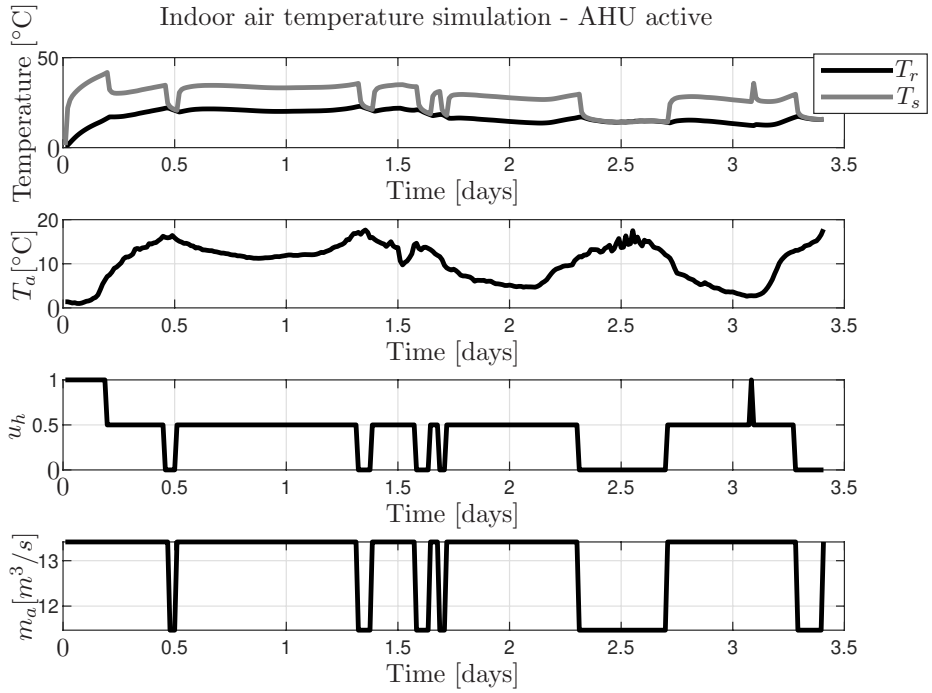

FIGURE 3.22: The indoor air temperature simulation based on real data with variable supply fan speed, damper blades in closed position and heating unit active (Equation (3.4.9)).

remains below ± 0.13 for the linear model. This is reflected in performance criteria, Table 3.8, where it seems that the linear model outperforms the SDP model. On the flip side, the results provided in Table 3.7 show that the linear model didn't differentiate between the open and closed loop system, whereas the SDP model identified the open and closed loop system simulations with distinct time constants, rise times and settling times. Time constants, rise times and settling times for the linear model are similar to those for the open loop SDP model, differing by approximately 0.1, 0.25 and 0.5,

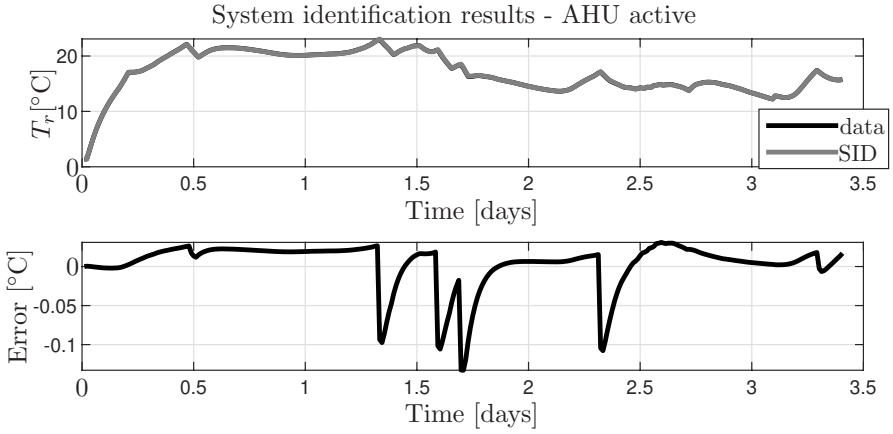

FIGURE 3.23: System identification of the first order parameters of the indoor air temperature model with inputs T_s and T_a (Equation (3.4.9)). Simulation of the input data is based on real data. This scenario has variable supply fan speed, damper blades in closed position and heating unit active.

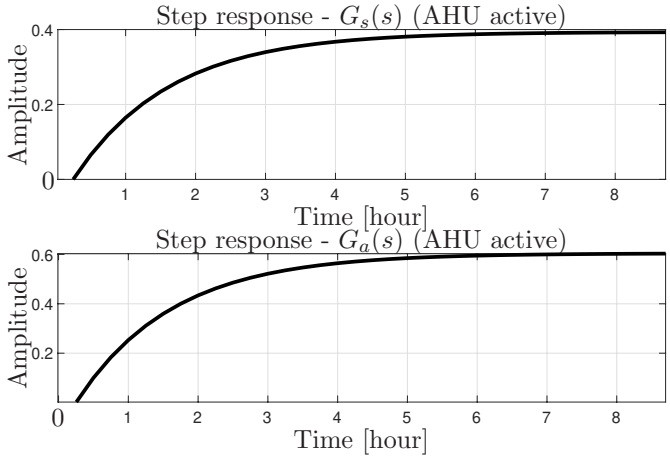

FIGURE 3.24: Step responses for processes corresponding to inputs T_s and T_a, respectively, for scenario with variable supply fan speed, damper blades in closed position and heating unit active (Equation (3.4.9)).

respectively. Introducing a fresh outside air directly instead of recirculating the air is expected to provide faster changes in the system, therefore it is expected that the open loop model has faster dynamics and lower time constant, rise time and settling time than the closed loop system. Compared to results in Table 3.3 and 3.5, where the differences between the open and closed loop model characteristics are much less pronounced, results presented in Table 3.7 seem to reflect expected dynamics more accurately. Note that β_1 and β_2 values for $u_d = 1$ are between β_1 and β_2 values for $m_a = 13.4$ and $m_a = 14.8$ in Table 3.2. These estimated values are as expected as the fan speed in the active AHU scenario varies with m_a taking values either $m_a = 13.4$ or $m_a = 14.8$. As a result, the estimated parameter is an approximated value that is a compromise for both fan speeds. For $u_d = 0$, both β parameters are slightly below the expected values, falling below β

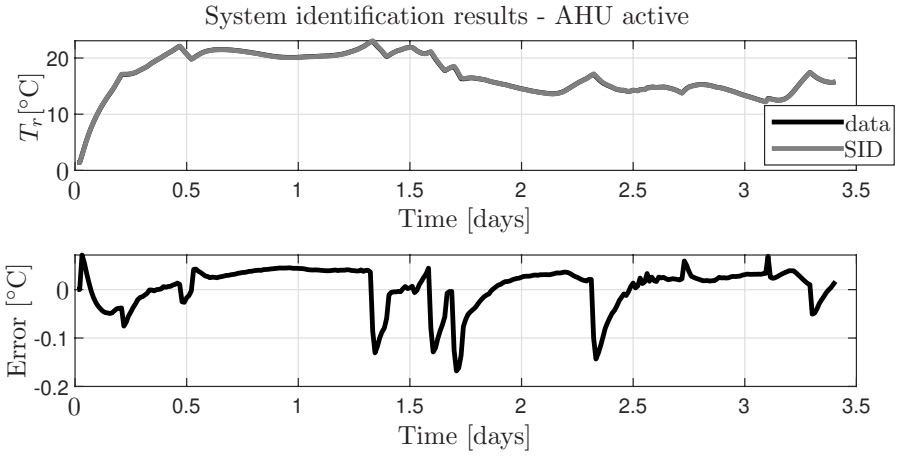

FIGURE 3.25: System identification of the first order parameters of the indoor air temperature model with inputs ΔT and T_a (Equation (3.4.9)). Simulation of the input data is based on real data. This scenario has variable supply fan speed, damper blades in closed position and heating unit active.

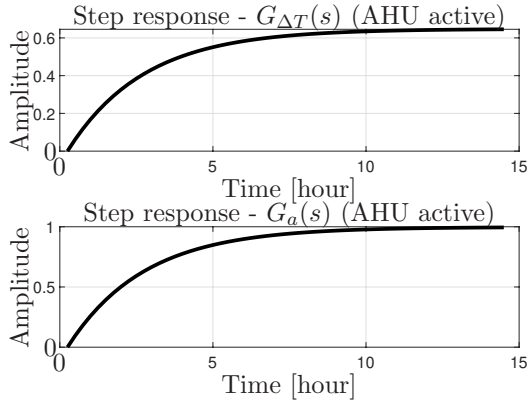

FIGURE 3.26: Step responses for processes corresponding to inputs ΔT and T_a, respectively, for scenario with variable supply fan speed, damper blades in closed position and heating unit active (Equation (3.4.9)).

values at $m_a = 13.4$ from Table 3.1. Parameters a in Table 3.7 lie between a values for 80% and 100% of the maximum fan speed in Tables 3.1 and 3.2, being above the expected fan speed. For α, value for the open loop system in Table 3.7 falls between the expected α values for $m_a = 13.4$ and $m_a = 14.8$ in Table 3.2, representing a valid compromise between fan speed trend of the identified data. The α value for the closed loop system in Table 3.7, however, is far from the expected value from Table 3.1, representing approximately no fan in operation. Overall, most of the model parameters are close to the expected values from Tables 3.1 and 3.2, demonstrating fairly good representation of the system model that was identified.

The results presented in Figures 3.15-3.26 are reflection of the simulation study performed on the real data collected from the existing temperature control system. As far as the operation of the components within AHU can be predicted based on the control

TABLE 3.7: Estimated parameters and numerical values for the first order system model for Equations (3.4.4) and (3.4.9). Parameters were estimated based on input generated from real data.

Coefficient	**AHU active**				**Fan off**
	T_s		ΔT		
	$u_d = 0$	$u_d = 1$	$u_d = 0$	$u_d = 1$	
Time const. [h]	1.38	1.40	2.49	1.49	2.36
Gain $G_s(s)$	0.3936	0.3934	-	-	-
Gain $G_{\Delta T}(s)$	-	-	0.6478	0.3963	-
Gain $G_a(s)$	0.6044	0.6069	0.9977	0.9967	1.0
Total gain	0.9980	1.0003	1.6455	1.3930	1.0
b_1	7.908^{-5}	7.805^{-5}	-	-	-
β_1	-	-	7.199^{-5}	7.372^{-5}	-
b_2	1.214^{-4}	1.204^{-4}	-	-	1.175^{-4}
β_2	-	-	1.109^{-4}	1.854^{-4}	-
a	2.009^{-4}	1.984^{-4}	-	-	1.175^{-4}
α	-	-	1.111^{-4}	1.86^{-4}	-
Rise time [h]	3.0	3.0	5.5	3.25	5.25
Settling time [h]	5.5	5.5	10.0	6.0	9.5

TABLE 3.8: Measures of the performance criteria for the estimated parameters of a first order model of the system with open and closed position of damper blades (Equations (3.4.4) and (3.4.9)). Parameters were estimated based on input generated from real data.

Coefficient	**AHU active**				**Fan off**
	T_s		ΔT		
	$u_d = 0$	$u_d = 1$	$u_d = 0$	$u_d = 1$	
R^2_T [%]	99.9936	99.9964	99.9867	99.9452	100
IAE	0.0198	0.0151	0.0336	0.0596	2.128^{-14}
MSE	8.7345^{-4}	4.4617^{-4}	1.827^{-3}	6.819^{-3}	4.8793^{-28}

logic implemented on the local controller, the rest depends on the outdoor conditions, which are predictable to a degree. Therefore, the operation of the AHU cannot be fully predicted and is correlated with the outdoor conditions. On the opposite side, previous simulation studies involved simple inputs like a square wave of regular frequency to control the whole AHU operation as well as simulation of the outdoor air temperature, which demonstrated results for pure simulation-based unrealistic setup.

Model fit demonstrating some discrepancies visualised as the error in Figures 3.15-3.26 and performance criteria values in Tables 3.7 and 3.8 is fairly optimistic, nevertheless, note that it was SID of the data generated using the first order system model,

being the same order as the SID model structure. The fit could be worse, if the data was generated using a second order system model, but it is expected discrepancy could be far less than comparison between the first and second order model fit simulated using real data shown in Figure 3.14 if appropriate methods would be used, e.g. SID using IV LS to improve the parameter estimation and the SDP model that takes different values depending on the fan speed and position of damper blades.

3.5.3.2 Estimation of the state-dependent parameters

The simulation study presented in this section focuses on a system identification of the model with SDP parameters α, β_1 and β_2, where inputs m_a and u_d are held constant. Doing so enabled finding parameter values for each state. The estimated SDP parameters are shown in Tables 3.9 and 3.10 for $ud = 0$ and $ud = 1$, respectively. The values obtained, as presented in Tables 3.9 and 3.10, can then be compared to the expected values presented in Tables 3.1 and 3.2. The first observation is that the values for the open loop system have been estimated fairly well, while the closed loop values are much less accurate. It is demonstrated by β_2 oscillating somewhere around 1.115^{-4} and decreasing with the fan speed. The biggest discrepancy is in α, where values align with the estimated β_2 and drift away from expected α by decreasing in value, therefore increasing time constant and slowing down the system dynamics. This phenomena can be related to the fact that this type of the closed loop system with positive feedback is more challenging for system identification and parameters estimation, requiring different approach to obtain expected results. the control inputs used to generate the input data for the system identification are presented in Figure 3.27.

The performance criteria for the results presented in Tables 3.9 and 3.10 demonstrate good fit, producing R^2_T >99.93, IAE<0.8 for $u_d = 1$ and IAE< 2.2^{-2} for $u_d = 0$ and MSE< 1.2^{-2} for $u_d = 1$ and MSE< 8.4^{-4} for $u_d = 0$. While the open loop system model parameter estimation underperformes compared to the closed loop system parameter estimation, the parameters estimated reflect more accurately the expected parameters according to calculated state-dependent parameter values provided in Tables 3.1 and 3.2.

Performing similar experiment with the same input as in Figure 3.27, but generating data using the second order system model expressed by Equations (2.6.1)-(2.6.2) to be identified with the first order model structure given by Equation (3.4.9), another set of the estimated parameters has been obtained and presented in Tables 3.11 and 3.12 for the closed and open loop system, respectively. It has been noted, that the time constants are greater as compared to the results related to the first order system identification from

TABLE 3.9: SDP model system identification for $u_d = 0$ and assuming $m_a = 18.5\,[\mathrm{m}^3/\mathrm{s}]$ at 100 % of the maximum fan speed. States, on which parameters are dependent have been condensed from $m_a(s)$ and $u_k(s)$ to m_a and u_k, respectively, for the sake of notional simplicity. Data for system identification have been generated using first order system model.

m_a [m^3/s]	$\alpha\{m_a, u_k\}$	$\beta_1\{m_a\}$	$\beta_2\{m_a, u_k\}$	Time constant [h]
0 (0%)	1.175^{-4}	0	1.175^{-4}	2.36
11.5 (62%)	1.114^{-4}	6.18^{-5}	1.114^{-4}	2.49
13.4 (72.5%)	1.105^{-4}	7.171^{-5}	1.105^{-4}	2.51
14.8 (80%)	1.1^{-4}	7.868^{-5}	1.099^{-4}	2.52
18.5 (100%)	1.084^{-4}	9.693^{-5}	1.084^{-4}	2.56

TABLE 3.10: SDP model system identification for $u_d = 1$ and assuming $m_a = 18.5\,[\mathrm{m}^3/\mathrm{s}]$ at 100 % of the maximum fan speed. States, on which parameters are dependent have been condensed from $m_a(s)$ and $u_k(s)$ to m_a and u_k, respectively, for the sake of notional simplicity. Data for system identification have been generated using first order system model.

m_a [m^3/s]	$\alpha\{m_a, u_k\}$	$\beta_1\{m_a\}$	$\beta_2\{m_a, u_k\}$	Time constant [h]
0 (0%)	1.175^{-4}	0	1.175^{-4}	2.36
11.5 (62%)	1.759^{-4}	6.29^{-5}	1.76^{-4}	1.58
13.4 (72.5%)	1.861^{-4}	7.342^{-5}	1.862^{-4}	1.49
14.8 (80%)	1.935^{-4}	8.097^{-5}	1.936^{-4}	1.44
18.5 (100%)	2.139^{-4}	1.013^{-4}	2.139^{-4}	1.30

Tables 3.9 and 3.10 and demonstrating second order system model to have slower dynamics than the first order system model. This is consistent with the observation from Section 3.5.2.2, where more aggressive behaviour was admitted to the first order system model. Time constants, however, decrease as the fan speed increases in both open and closed loop system model results in Tables 3.11 and 3.12. The dynamics of the closed loop system is slower, as expected, as the indoor air is recirculated. Looking at the time constants for the open loop system, it is noticed that the time constant range related to the fan speed between 0 and 100% is wider in the estimated parameters from the second order system model, Table 3.12, than from the reduced order system model, Table 3.10.

The performance criteria for the results presented in Tables 3.11 and 3.12 demonstrate fair fit, but with loss of accuracy due to model order reduction. The results obtained are $93.3 < \mathrm{R}_T^2 < 98.2$, $0.6 < \mathrm{IAE} < 0.7$, $0.5 < \mathrm{MSE} < 0.68$ for $u_d = 0$ and $97.83 < \mathrm{R}_T^2 < 98.2$, $0.43 < \mathrm{IAE} < 0.61$, $0.26 < \mathrm{MSE} < 0.51$ for $u_d = 1$.

TABLE 3.11: SDP model system identification for $u_d = 0$ and assuming $m_a = 18.5\,[\mathrm{m}^3/\mathrm{s}]$ at 100 % of the maximum fan speed. States, on which parameters are dependent have been condensed from $m_a(s)$ and $u_k(s)$ to m_a and u_k, respectively, for the sake of notional simplicity. Data for system identification have been generated using second order system model.

m_a [m^3/s]	$\alpha\{m_a, u_k\}$	$\beta_1\{m_a\}$	$\beta_2\{m_a, u_k\}$	Time constant [h]
0 (0%)	8.482^{-5}	0	8.296^{-5}	3.28
11.5 (62%)	8.314^{-5}	4.903^{-5}	8.126^{-5}	3.34
13.4 (72.5%)	8.539^{-5}	5.805^{-5}	8.336^{-5}	3.25
14.8 (80%)	8.718^{-5}	6.48^{-5}	8.506^{-5}	3.18
18.5 (100%)	9.195^{-5}	8.362^{-5}	8.962^{-5}	3.02

TABLE 3.12: SDP model system identification for $u_d = 1$ and assuming $m_a = 18.5\,[\mathrm{m}^3/\mathrm{s}]$ at 100 % of the maximum fan speed. States, on which parameters are dependent have been condensed from $m_a(s)$ and $u_k(s)$ to m_a and u_k, respectively, for the sake of notional simplicity. Data for system identification have been generated using second order system model.

m_a [m^3/s]	$\alpha\{m_a, u_k\}$	$\beta_1\{m_a\}$	$\beta_2\{m_a, u_k\}$	Time constant [h]
0 (0%)	8.482^{-5}	0	8.296^{-5}	3.28
11.5 (62%)	1.355^{-4}	5.169^{-5}	1.334^{-4}	2.05
13.4 (72.5%)	1.459^{-4}	6.076^{-5}	1.347^{-4}	1.90
14.8 (80%)	1.537^{-4}	6.742^{-5}	1.514^{-4}	1.81
18.5 (100%)	1.753^{-4}	8.591^{-5}	1.728^{-4}	1.58

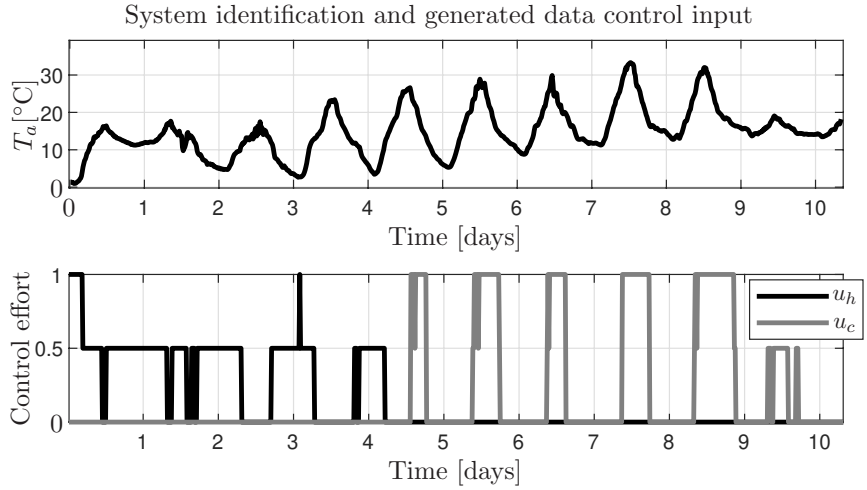

FIGURE 3.27: Variable control inputs used for data generation and system identification based on real data.

3.5.3.3 Parameter extraction from estimated values

Calculation of the first order model parameters a, b_1, b_2 with regard to m_a and u_d from Equation (3.4.4) from the SDP model parameters of Equation (3.4.9) using equations

$$\begin{aligned}\alpha\{m_a(s), u_d(s)\} &= a\{m_a(s)\} - b_1\{m_a(s)\} \cdot \big(1 - u_d(s)\big)\\ \beta_1\{m_a(s)\} &= b_1\{m_a(s)\}\\ \beta_2\{m_a(s), u_d(s)\} &= b_1\{m_a(s)\}u_d(s) + b_2\end{aligned}$$

allows to extract some parameters to calculate the other ones without SID. To demonstrate this, let's consider the estimated parameters of an open loop model as presented in Table 3.10, which will be used to obtain the closed loop model parameters that are more difficult to estimate; there are methods dedicated for system identification in a closed loop system setup proposed by Taylor et al. (2013, p. 253). The values of the parameters a, b_1, b_2 with regard to m_a and u_d calculated from α, β_1 and β_2, presented in Table 3.13, are calculated as follows

$$\begin{aligned}b_1\{m_a(s)\} &= \beta_1\{m_a(s)\}\\ a\{m_a(s)\} &= \alpha\{m_a(s), u_d(s)\} + b_1\{m_a(s)\} \cdot \big(1 - u_d(s)\big)\\ b_2 &= \beta_2\{m_a(s), u_d(s)\} - b_1\{m_a(s)\}u_d(s)\end{aligned}$$

TABLE 3.13: Linear model (Equation (3.4.4)) parameters calculation for $u_d = 1$ from SDP model parameters (Equation (3.4.9)).

m_a [m^3/s]	$a\{m_a(s)\}$	$b_1\{m_a(s)\}$	b_2	Time constant [h]
0 (0%)	1.175^{-4}	0	1.175^{-4}	2.36
11.5 (62%)	1.759^{-4}	6.29^{-5}	1.131^{-4}	1.58
13.4 (72.5%)	1.861^{-4}	7.34^{-5}	1.128^{-4}	1.49
14.8 (80%)	1.935^{-4}	8.10^{-5}	1.126^{-4}	1.44
18.5 (100%)	2.139^{-4}	1.013^{-4}	1.126^{-4}	1.30

The calculated values of the parameters a, b_1 and b_2 can then be used to calculate the closed loop system parameters α, β_1 and β_2, following aforementioned definition. The values obtained for parameters α, β_1 and β_2 representing a closed loop system calculated from parameters a, b_1 and b_2 presented in Table 3.13 are presented in Table 3.14. Note that parameter b_2 in Table 3.13 should keep the same value, regardless of the fan speed. The fact that it varies shows that the estimated model was not able to fully capture the dynamics and has some flaws.

TABLE 3.14: SDP model parameters (Equation (3.4.9)) calculation for $u_d = 0$ from linear model (Equation (3.4.4)) parameters.

m_a [m^3/s]	$\alpha\{m_a, u_k\}$	$\beta_1\{m_a\}$	$\beta_2\{m_a, u_k\}$	Time constant [h]
0 (0%)	1.175^{-4}	0	1.175^{-4}	2.36
11.5 (62%)	1.130^{-4}	6.29^{-5}	1.131^{-4}	2.46
13.4 (72.5%)	1.127^{-4}	7.34^{-5}	1.128^{-4}	2.46
14.8 (80%)	1.125^{-4}	8.10^{-5}	1.126^{-4}	2.47
18.5 (100%)	1.126^{-4}	1.013^{-4}	1.126^{-4}	2.47

The results presented in Table 3.14 differ in some respect from those obtained directly shown in Table 3.9. Firstly, time constant when the supply fan is on is greater than when fan is off and the value is approximately the same for the simulated fan speed, with negligible differences of around 1 minute; this reflects the differences in α values. All of the parameters for the fan speed greater than 0 have slightly higher values than their respective parameters in Table 3.9.

Following the same approach, conversions for parameters obtained from second order model SID have been made using values from Table 3.12 as a starting point. The results are provided in Tables 3.15 and 3.16, presenting linear model parameters calculated from the SDP model parameters and vice versa, respectively.

TABLE 3.15: Linear model (Equation (3.4.4)) parameters calculation for $u_d = 1$ from SDP model (Equation (3.4.9)) parameters.

m_a [m^3/s]	$a\{m_a(s)\}$	$b_1\{m_a(s)\}$	b_2	Time constant [h]
0 (0%)	8.482^{-5}	0	8.296^{-5}	3.27
11.5 (62%)	1.355^{-4}	5.17^{-5}	8.17^{-5}	2.05
13.4 (72.5%)	1.459^{-4}	6.08^{-5}	7.39^{-5}	1.90
14.8 (80%)	1.537^{-4}	6.74^{-5}	8.40^{-5}	1.81
18.5 (100%)	1.753^{-4}	8.59^{-5}	8.69^{-5}	1.58

The calculated values of parameters a, b_1 and b_2 can then be used to calculate the closed loop system model parameters α, β_1 and β_2 following the aforementioned definition. The values obtained for parameters α, β_1 and β_2 representing the closed loop system calculated from parameters a, b_1 and b_2 presented in Table 3.15 are presented in Table 3.16. Note that the parameter b_2 in Table 3.15 should keep the same value regardless of the fan speed. The fact that it varies shows that the estimated model was not able to fully capture the dynamics and has some flaws.

TABLE 3.16: SDP model (Equation (3.4.9)) parameters calculation for $u_d = 0$ from linear model (Equation (3.4.4)) parameters.

m_a [m^3/s]	$\alpha\{m_a, u_k\}$	$\beta_1\{m_a\}$	$\beta_2\{m_a, u_k\}$	Time constant [h]
0 (0%)	8.482^{-5}	0	8.296^{-5}	3.27
11.5 (62%)	8.381^{-5}	5.169^{-5}	8.171^{-5}	3.31
13.4 (72.5%)	8.514^{-5}	6.076^{-5}	7.394^{-5}	3.26
14.8 (80%)	8.628^{-5}	6.742^{-5}	8.398^{-5}	3.22
18.5 (100%)	8.939^{-5}	8.591^{-5}	8.689^{-5}	3.11

Considering values in Table 3.16 in light of the values obtained directly presented in Table 3.11, they are not exactly the same, but close enough to provide similar time constant (9 minutes as the biggest discrepancy) and dynamics, looking at β parameters. The values for the fan off scenario provides the most consistent result. Notably, the more significant discrepancies are related to the fact that a first order model was used to identify data generated using a second order model.

3.5.4 State-Dependent Parameter model demonstration

A set of equations incorporating full SDP model structure recalculating the model parameters at every time step with respect to m_a and u_d has been implemented in MATLAB. The state-dependent model parameters are calculated in the following way at each time step:

1. Reduced order model parameters a, b_1 and b_2 of a linear model are calculated based on first principles following Equation (3.4.4) at each time step using the most recent m_a value.

2. Calculated parameters a, b_1 and b_2 are transformed from continuous-time domain into discrete-time domain assuming ZOH.

3. Discrete-time parameters a, b_1 and b_2 are used to calculate discrete-time parameters α, β_1 and β_2 of the SDP model structure formulated in Equation (3.4.9) using the most recent u_d value.

4. Parameters α, β_1 and β_2 are used to simulate the indoor air temperature T_r for the current time step.

The results of the simulation are presented in Figure 3.28. The system inputs T_a, m_a, heating and cooling were taken from the data recorded and presented in the

previous section. The damper position input has been created manually as in the data the damper is closed throughout all samples recorded. The damper position switches between open and closed every two days.

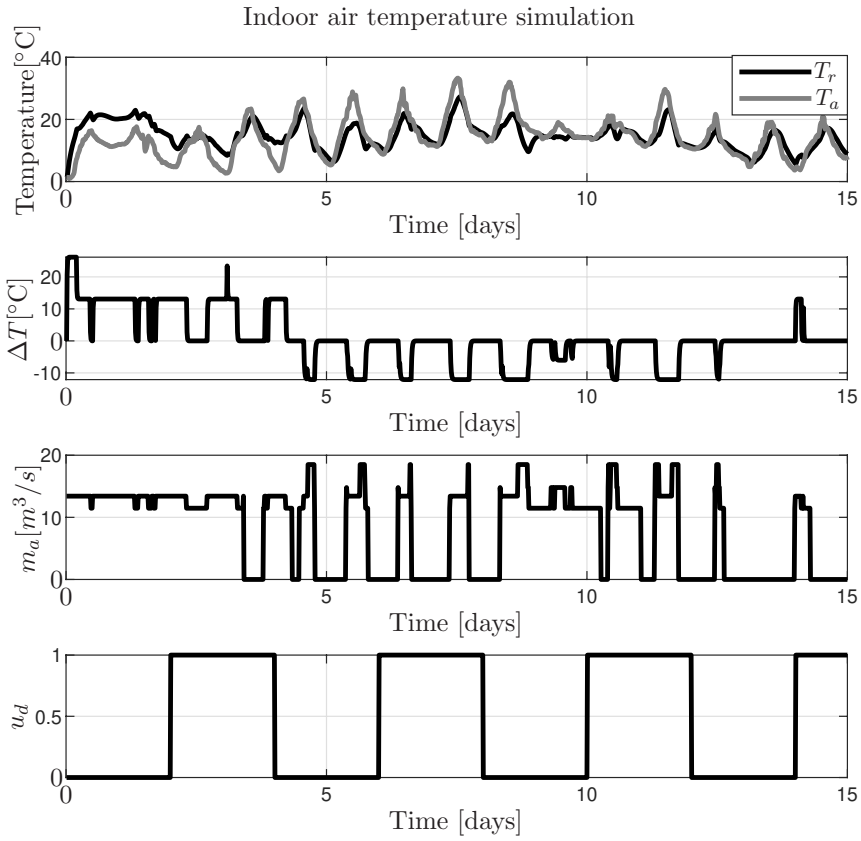

FIGURE 3.28: SDP model simulation with variable fan speed and damper position. State-dependent model parameters are calculated at every time step according to the most recent m_a and u_d values.

There are few observations consistent with the statements and characteristics presented in the previous part on this chapter and Chapter 2. Firstly, the system behaviour changes depending on the position of the damper blades. Comparing the indoor air temperature T_r in days 1-2 ($u_d = 0$) with days 3-4 ($u_d = 1$), where heating is present most of the time ($\Delta T > 0$), the indoor air temperature takes higher values compared to the outdoor air temperature when the damper is closed and the air is recirculated. On the contrary, T_r for days 3-4 when the damper position is open does not deviate that much from T_a as fresh air heated up is introduced to the building. Secondly, the damper position does not make a difference to the indoor air temperature if the supply fan speed is not in operation and $m_a = 0$. Thirdly, if the supply fan is off, the indoor air temperature simply follows the outdoor air temperature with some delay. Finally, if there is no heating and cooling ($\Delta T = 0$), but the supply fan is on ($m_a > 0$) and the damper blades are in open position, the indoor air is affected more by the outdoor air,

bringing its values closer to T_a faster than with the fan off. Since the observations are consistent with the expect behaviour, the model is considered adequate to represent the indoor air thermal behaviour of the studied system and suitable for control application studies.

Demonstration of the fan speed and the air mass flow rate contribution to the system dynamics is shown in Figure 3.29, where a simple scenario was simulated using sine wave as T_a and m_a, which is varied as a square wave with rising steps.

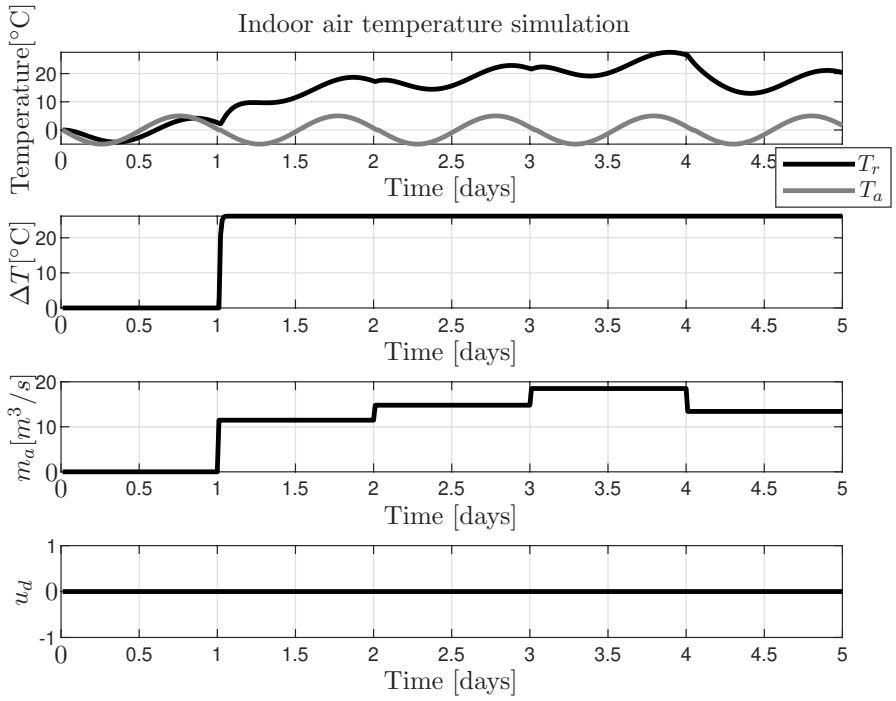

FIGURE 3.29: SDP model simulation with variable fan speed, $u_d = 0$ and heating present when fan is in operation. State-dependent model parameters are calculated at every time step according to the most recent m_a and u_d values.

Note the changes in the fan speed causing different levels of the indoor air temperature obtained. This demonstrates that greater amount of a hot air warms up the indoor air faster even if the same heating output is the same.

3.6 Conclusions

This chapter has introduced the SDP model structure for the indoor air thermal process, having correlated the thermal response and dynamic behaviour of the system with changes of the position of damper blades and the supply air flow rate. It is believed that the results are meaningful for the temperature control systems employing model-based predictive methods, where the model of the indoor air temperature is a necessity.

The flexibility of the SDP model benefits from its ability to adapt the model parameters, hence improve the model of the thermal process, based on the manipulated control inputs influencing the indoor thermal dynamics. These inputs are often a part of a temperature control system, especially when energy efficiency is emphasised during the design phase of the control system.

As an important contribution, the reduced order system model has been formulated in Section 3.4 representing the second order system model based on first principles from Chapter 2. This concept compromises some accuracy due to order reduction. The simulation study revealed that it is the lower time constant that shows predominant discrepancy between the first and second order system models. It was noted, however, that the model is able to represent the studied system well enough to be used for control provided the model is well tuned and the parameters are estimated correctly.

Study of the indoor air temperature model provided an interesting insight into the model structure and dependencies within. It has been noted that it is enough to estimate either open or closed loop system model parameters to simulate the system. A state-dependent structure involving damper position allows to convert between the open and closed loop model parameters. Another unique aspect of the indoor air temperature model are the inputs. In particular, an indoor air temperature input, known and non-controllable signal, could be perceived as a disturbance. With a damper blades control in mind, however, the amount of the fresh air can be regulated as a part of an energy efficient control scheme. In other words, the impact of the outdoor conditions is partially controllable through the position of the damper blades. The simulation study is also provided to demonstrate how the values representing the air mass flow rate and damper position affect the model parameters, behaviour and output. It has been concluded, that the SDP model provides more accurate results than the linear model with constant parameters.

The approach taken in this chapter concentrates on a well-formulated SDP model updating parameters at every time step to simulate the indoor air temperature and for control application. This model, incorporating heating, cooling, supply fan operation, damper blades position and disturbances (additional heat gains), is a core of the energy efficient control strategy to be used in conjunction with the MPC technique presented in Chapter 5 and a contribution of this chapter. It is also used to develop SDP-PIP controller for heating and cooling control proposed in Chapter 4 implemented as a part of the MPC strategy.

Chapter 4

Proportional-Integral-Plus control approach for state-dependent indoor air temperature models

4.1 Introduction

In control systems engineering terms, control is used to influence the dynamic behaviour of the system, to achieve the desired behaviour within a dynamic environment or its elements (Taylor et al., 2013). In this thesis it is the thermal process that is subject to control, i.e. the indoor air temperature. The indoor conditions in this instance are influenced by means of heating and cooling in order to maintain the desired air temperature within the building. For this purpose, Underwood (1999) proposed the application of Proportional-Integral-Derivative (PID), adaptive and intelligent techniques. The classical PID controller is still found the most common control method used in heating, ventilation and air conditioning (HVAC) systems. As the good HVAC control with PID controller requires appropriate choice of parameters, the problem of tuning and selecting parameters for PID controllers is a subject of continuous development (e.g., Lim et al., 2009; Wang et al., 1998). Nowadays, its application is often supported by other techniques, e.g. by combining with the neural networks (Delnero, 2000) or developing adaptive PI controller (Bai & Zhang, 2007). With a range of different control approaches, a method chosen for the indoor air temperature control in this thesis is a Proportional-Integral-Plus (PIP) controller deriving from a state variable feedback (SVF) pole assignment approach for linear discrete-time systems proposed by Peter Young and others in 1987 (Young et al., 1987). PIP is a digital controller that thrives on a growth within electronics industry and development of a modern computer

with the computational power and complexity of algorithms it offers. Being digital, it relies on the discrete-time samples of the input variables and uses online algorithm to update the control input variables at each time step. On the contrary, widely applied and commonly used even nowadays PID (Proportional-Integral-Derivative) controller originates from classical control sustaining, traditionally, continuous-time operation, in which PIP controller's roots are embedded. PIP controller demands good *a priori* discrete time modelling of the controlled process, which usually implies adequate assumptions regarding the model structure and sampling interval as well as obtaining representative model parameters using system identification and parameter estimation methods. In return, PIP is a convenient solution for control systems imposing constraints on the input or output that makes use of Non-minimal State Space (NMSS) model. This method allows calculating of the output based only on the known, variables, i.e. the past and present samples of the input and output. It is also not so difficult to implement, robust, adaptive and can be interpreted in a variety of terms, including feedback and forward path control filters, resembling those used in classical designs. It can also work with state-dependent model forms, such as SDP introduced in Chapter 3. Fundamentally, it inherits from both classical and modern control systems architectures. Nevertheless, a considerable advantage of the PIP method is the tuning process, which can be rather tedious for PID and is performed offline, while pole placement allows for optimal design and stability (Taylor et al., 2013).

4.1.1 Literature review

One of the earliest work on structural and predictive aspects of PIP control is by Taylor et al. (1996) who establishes the conditions for the full equivalence between PIP, Generalised Predictive Controller (GPC), and minimal Linear Quadratic (LQ) designs, demonstrating the advantages of the NMSS-based PIP approach. Formulation of a PIP controller that accommodates constraints in both the input and output variables is proposed by McCabe et al. (2000). This approach relies on the feedback loop, where constraints are transferred to the reference signal; an appropriate reference input filter (RIF) is employed to prevent overshoot to maintain the integrity of the feedback loop and ensure stability of the system. Ziemian & Burnham (2002) report on the advantages of extending the existing linear philosophy of PIP control to a bilinear case, covering quasilinearisation, design methods and tuning of the bilinear PIP controller.

While some uses of the PIP controller were already covered in Chapter 3, where examples cited show SDP model as a part of the PIP controller, see Section 3.1.1.1, the list is by no means extensive. It is worth noting, however, that PIP controllers tend to be based on a state-dependent model structure. Example of use of the PIP controller with

a first order system similar to the reduced order model used in this thesis is covered by Young et al. (1987), where it is applied to control a temperature in a glasshouse. Due to its heritage, PIP design reduces to a conventional Proportional-Integral (PI) controller when a first order system model is considered, but in contrast to the PI controller used normally in a glasshouse, the PIP implementation is a true digital design (as oppose to a digitalised continuous-time PI system). Selection of the PIP method to control the temperature in a glasshouse allowed to increase sampling time from PI's 1 min to 10 min. The results presented shown that when compared, the conventional PI system shows itself sluggish and oscillatory in its response to both set-point changes and disturbances, while PIP system response is rapid and critically damped due to pole assignment design, reducing oscillations and providing better set-point tracking (Young et al., 1987). Further, Taylor et al. (2011b) propose design and implementation of a gain-scheduled PIP controller to control a ventilation rate in mechanically ventilated agricultural buildings. This approach is taken to mitigate the difficulties of the fan system control caused by the pressure disturbances across the fan and wind disturbances from outside the building. Another application of the PIP controller relying on the SDP model is used to control a highly nonlinear and time-varying pH neutralisation process proposed by Ogun et al. (2017). This SDP-PIP controller is compared to a digital PI controller, where the optimal SDP-PIP controller outperforms PI both in set point and disturbance changes. In a recent research summarised by Zakeri & Moeinkhah (2019) the PIP controller is proposed in a novel approach as an adaptive optimal proportional-integral-plus (AOPIP), used to control the beam-like ionic polymer-metal composite (IPMC) actuators. The paper states that compared to a digital PID controller and other opened-loop techniques applied to the same systems, the superiority of the AOPIP control method was obvious, in terms of tracking error, the level of controller output, and smoothness of the tracking desired signals, manifested in both simulation studies and real-time experimental tests.

Observing examples of the PIP controller applications, it is clear that this approach is utilised and developed, however, not to such extent as PID or other methods. Despite the fact that no demand for PIP use in the HVAC control systems has been noticed in the literature, the variety of other applications justify the approach proposed in this chapter to be investigated.

4.1.2 Chapter overview

This chapter introduces the PIP controller and its derived form for an indoor air temperature application. Section 4.2 provides a brief introduction to NMSS form, servomechanism, being the core of the PIP, pole placement and then narrows these general patterns

into a first order system model forms. Section 4.3 expands the first order model into a form suitable for an indoor air temperature control. Then, Section 4.4 is there to propose an SDP-PIP controller for an indoor air temperature control following the SDP model introduced in Chapter 3. This special SDP-PIP form sets the main contribution of this chapter and will be used as a heart of the model predictive controller proposed in Chapter 5. Subsequently, simulation study is provided in Section 4.5, demonstrating operation of the SDP-PIP controller. Finally, the whole chapter is summarised in Section 4.6.

4.2 Proportional-Integral-Plus control

This section introduces a NMSS model used in a PIP controller as well as the control law under which the PIP controller operates.

4.2.1 Non-minimal state space model representation

Consider a discrete-time SISO transfer function model in general form defined as

$$y(k) = \frac{B(z^{-1})}{A(z^{-1})}u(k) = \frac{b_1 z^{-1} + \ldots + b_m z^{-m}}{1 + a_1 z^{-1} + \ldots + a_n z^{-n}}u(k) \tag{4.2.1}$$

where z^{-1} is a backward-shift operator. As the model (4.2.1) is deterministic, it is possible to formulate NMSS equations (Taylor et al., 2013) representing it as

$$\begin{aligned} \boldsymbol{x}(k) &= \boldsymbol{F}\boldsymbol{x}(k-1) + \boldsymbol{g}u(k-1) + \boldsymbol{d}y_d(k) \\ y(k) &= \boldsymbol{h}\boldsymbol{x}(k) \end{aligned} \tag{4.2.2}$$

with $\boldsymbol{x}(k)$ being the state vector of dimension $n + m$, consisting of present and past samples of the output variable $y(k)$, the past values of the input variable $u(k)$ (control action) and the *integral of error* state $z(k)$ introduced to ensure Type 1 servomechanism performance and accommodate the reference input error sum automatically in the feedback loop (McCabe et al., 2000). The *integral of error* state $z(k)$ is defined as

$$z(k) = z(k-1) + (y_d(k) - y(k)) \tag{4.2.3}$$

where $y_d(k)$ is the command input, or, alternatively, with a discrete-time integrator $\frac{1}{1-z^{-1}}$ as

$$z(k) = \frac{1}{1 - z^{-1}}\left(y_d(k) - y(k)\right) \tag{4.2.4}$$

Therefore, the state vector $\boldsymbol{x}(k)$ is $(n+m)\times 1$ and consists of

$$\boldsymbol{x}(k) = \begin{bmatrix} y(k) & y(k-1) & \dots & y(k-n+1) & u(k-1) & u(k-2) & \dots & u(k-m+1) & z(k) \end{bmatrix}^T$$

The associated matrix and vectors are defined as the state transition matrix $\boldsymbol{F}$ with dimensions $(n+m)\times(n+m)$, the $(n+m)\times 1$ input vector $\boldsymbol{g}$, the $1\times(n+m)$ command input vector $\boldsymbol{d}$ and the $1\times(n+m)$ output vector $\boldsymbol{h}$ in the following forms

$$\boldsymbol{F} = \begin{bmatrix} -a_1 & -a_2 & \cdots & -a_{n-1} & -a_n & b_2 & b_3 & \cdots & b_{m-1} & b_m & 0 \\ 1 & 0 & \cdots & 0 & 0 & 0 & 0 & \cdots & 0 & 0 & 0 \\ 0 & 1 & \cdots & 0 & 0 & 0 & 0 & \cdots & 0 & 0 & 0 \\ \vdots & \vdots & \ddots & \vdots & \vdots & \vdots & \vdots & \ddots & \vdots & \vdots & \vdots \\ 0 & 0 & \cdots & 1 & 0 & 0 & 0 & \cdots & 0 & 0 & 0 \\ 0 & 0 & \cdots & 0 & 0 & 0 & 0 & \cdots & 0 & 0 & 0 \\ 0 & 0 & \cdots & 0 & 0 & 1 & 0 & \cdots & 0 & 0 & 0 \\ 0 & 0 & \cdots & 0 & 0 & 0 & 1 & \cdots & 0 & 0 & 0 \\ \vdots & \vdots & \ddots & \vdots & \vdots & \vdots & \vdots & \ddots & \vdots & \vdots & \vdots \\ 0 & 0 & \cdots & 0 & 0 & 0 & 0 & \cdots & 1 & 0 & 0 \\ a_1 & a_2 & \cdots & a_{n-1} & a_n & -b_2 & -b_3 & \cdots & -b_{m-1} & -b_m & 1 \end{bmatrix}$$

$$\boldsymbol{g} = \begin{bmatrix} b_1 & 0 & 0 \dots 0 & 1 & 0 & 0 \dots 0 & -b_1 \end{bmatrix}^T$$

$$\boldsymbol{d} = \begin{bmatrix} 0 & 0 & 0 \dots 0 & 0 & 0 & 0 \dots 0 & 1 \end{bmatrix}$$

$$\boldsymbol{h} = \begin{bmatrix} 1 & 0 \dots 0 & 0 & 0 & 0 \dots 0 & 0 & 0 \end{bmatrix}$$

4.2.2 State Variable Feedback and Proportional-Integral-Plus control

The SVF control law associated with the NMSS model (Taylor et al., 2013) formulated in Equation (4.2.2) can be written as

$$u(k) = -\boldsymbol{k}^T \boldsymbol{x}(k) \tag{4.2.5}$$

where $\boldsymbol{k}$ is the $n+m$-dimensional SVF vector consisting of control gains

$$\boldsymbol{k}^T = \begin{bmatrix} f_0 & f_1 & \dots & f_{n-1} & g_1 & \dots & g_{m-1} & -k_I \end{bmatrix}$$

The feedback control gains are selected by the designer to achieve desired closed loop characteristics. Block diagram representation of the controller (4.2.5), depicted in Figure

4.1 is refereed to as the NMSS servomechanism controller or the *Proportional-Integral-Plus (PIP) control law*. The corresponding filter polynomials are defined as

$$F(z^{-1}) = f_0 + f_1 z^{-1} + \ldots + f_{n-1} z^{-(n-1)}$$
$$G(z^{-1}) = 1 + g_1 z^{-1} + \ldots + g_{m-1} z^{-(m-1)}$$

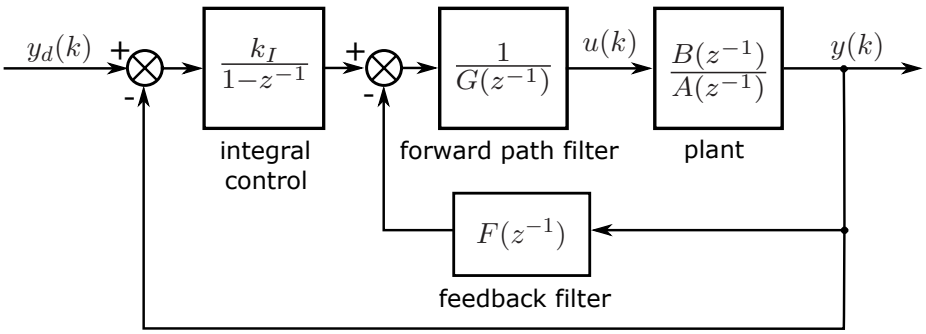

FIGURE 4.1: Standard form of PIP controller - servomechanism control system. (Taylor et al., 2013)

4.2.3 Pole assignment control tuning

Consider a system model given by the discrete-time transfer function expressed by Equation (4.2.1) and the corresponding control law in Equation (4.2.5) defined in Section 4.2.2. The control law for the input $u(k)$ can be rewritten into

$$u(k) = \frac{1}{G(z^{-1})}\Big[- F(z^{-1})y(k) + \frac{k_I}{1 - z^{-1}}(y_d(k) - y(k))\Big] \tag{4.2.7}$$

A polynomial describing the desired characteristics is given as

$$D(z^{-1}) = 1 + d_1 z^{-1} + d_2 z^{-2} + \ \ldots \ + d_{n+m} z^{n+m} = 1 + \sum_{i=1}^{n+m} d_i z^i \tag{4.2.8}$$

where d_i are the desired coefficients of the model. Knowing from the block diagram in Figure 4.1 that for the closed loop model the output can be expressed as

$$y(k) = \frac{k_I B(z^{-1})}{\big(1 - z^{-1}\big)\Big[G(z^{-1})A(z^{-1}) + F(z^{-1})B(z^{-1})\Big] + k_I B(z^{-1})} y_d(k) \tag{4.2.9}$$

the following relationship can be formulated:

$$\big(1 - z^{-1}\big)\Big[G(z^{-1})A(z^{-1}) + F(z^{-1})B(z^{-1})\Big] + k_I B(z^{-1}) = D(z^{-1}) \tag{4.2.10}$$

Once the system reaches steady-state there is no difference between the current and past sample, therefore $y(k) = y(k-1)$ and $(1 - z^{-1})y(k) = 0$. It also occurs in steady-state that the output signal equals the reference signal and $y_d(k) - y(k) = 0$. Therefore, the desired closed loop transfer function having unity steady-state gain and demanded denominator $D(z^{-1})$ is

$$y(k) = \frac{1 + \sum_{i=1}^{n} d_i}{D(z^{-1})} y_d(k) \tag{4.2.11}$$

Knowing that in steady-state $z \to 1$ ($s \to 0$ for a continuous-time domain model), this substitution causes the polynomial $D(z^{-1})$ to become a sum of coefficients as

$$D(z^{-1} = 1) = 1 + d_1 + d_2 + \ \ldots \ + d_{n+m} = 1 + \sum_{i=1}^{n+m} d_i \tag{4.2.12}$$

This relation is valid only for static set-points or for a case when a transfer function system model has only one b_i parameter (Zajíc, 2014). The method described is taken from PI tuning technique and is also known as pole placement. More extensive information and derivation for pole assignment is discussed by Taylor et al. (2013, p. 101), Åström & Wittenmark (2008, p. 92) and Bobál et al. (2005, p. 149).

4.2.4 Non-minimal State Space design and Proportional-Integral-Plus controller for a first order system model

Assuming a first order model of a SISO system defined as

$$y(k) = -a_1 y(k-1) + b_1 u(k-1) \tag{4.2.13}$$

or as a transfer function

$$y(k) = \frac{b_1 z^{-1}}{1 + a_1 z^{-1}} u(k) \tag{4.2.14}$$

the corresponding NMSS form representing Equation (4.2.13) is

$$\begin{aligned} \boldsymbol{x}(k) &= \boldsymbol{F}\boldsymbol{x}(k-1) + \boldsymbol{g}u(k-1) + \boldsymbol{d}y_d(k) \\ y(k) &= \boldsymbol{h}\boldsymbol{x}(k) \end{aligned} \tag{4.2.15}$$

with

$$\boldsymbol{x}(k) = [y(k) \quad z(k)]^T \tag{4.2.16}$$

and the *integral of error* state

$$z(k) = z(k-1) + (y_d(k) - y(k)) \tag{4.2.17}$$

expanded for the first order SISO system model as

$$z(k) = z(k-1) + y_d(k) + a_1 y(k-1) - b_1 u(k-1) \tag{4.2.18}$$

The NMSS model of the first order system model is defined by the state and observation equations (Taylor et al., 2013), respectively, as

$$\begin{aligned} \boldsymbol{x}(k) &= \begin{bmatrix} y(k) \\ z(k) \end{bmatrix} = \begin{bmatrix} -a_1 & 0 \\ a_1 & 1 \end{bmatrix} \begin{bmatrix} y(k-1) \\ z(k-1) \end{bmatrix} + \begin{bmatrix} b_1 \\ -b_1 \end{bmatrix} u(k-1) + \begin{bmatrix} 0 \\ 1 \end{bmatrix} y_d(k) \\ y(k) &= \begin{bmatrix} 1 & 0 \end{bmatrix} \boldsymbol{x}(k) \end{aligned} \tag{4.2.19}$$

Using the same SVF control law as defined by Equation (4.2.5), the control gain vector $\boldsymbol{k}^T$ is

$$\boldsymbol{k}^T = \begin{bmatrix} f_0 & -k_I \end{bmatrix} \tag{4.2.20}$$

and the polynomials $F(z^{-1})$ and $G(z^{-1})$ of PIP controller are defined as

$$F(z^{-1}) = f_0 \tag{4.2.21a}$$

$$G(z^{-1}) = 1 \tag{4.2.21b}$$

As for SVF, the control action $u(k)$ can also be represented as

$$u(k) = -\begin{bmatrix} f_0 & -k_I \end{bmatrix} \begin{bmatrix} y(k) \\ z(k) \end{bmatrix} = -f_0 y(k) + k_I z(k) \tag{4.2.22}$$

and, substituting $z(k)$ with its equivalent from the right-hand side of Equation (4.2.4), $u(k)$ is defined as

$$u(k) = -f_0 y(k) + \frac{k_I}{1 - z^{-1}} (y_d(k) - y(k)) \tag{4.2.23}$$

Note that this first order system model is equivalent to PI controller, where f_0 represents the proportional term and k_I the integral term. The difference between classical PI design and the presented approach using SVF controller is that instead of manual tuning, numerical values of the control gains are determined from pole assignment. To maintain consistency with a classic PI controller, the sign associated with k_I is negative. As a result, the integral control appears in the forward path of the negative feedback control system, see Figure 4.1. Finally, as required for Type 1 servomechanism performance, the steady-state gain of the closed loop system is unity (Taylor et al., 2013).

4.2.4.1 Pole assignment control tuning of a first order system

Design of the controller using pole assignment method relying on denominators comparison (briefly introduced in Section 4.2.3) for a first order system model can be obtained from the characteristic equations according to (4.2.10) equating as

$$\left(1 - z^{-1}\right)\left[(1 + a_1 z^{-1}) + f_0 b_1 z^{-1}\right] + k_I b_1 z^{-1} = 1 + d_1 z^{-1} + d_2 z^{-2} \tag{4.2.24}$$

Performing possible multiplications, this is unwrapped into

$$1 + a_1 z^{-1} + f_0 b_1 z^{-1} - z^{-1} - a_1 z^{-2} - f_0 b_1 z^{-2} - k_I b_1 z^{-1} = 1 + d_1 z^{-1} + d_2 z^{-2} \tag{4.2.25}$$

Next, elements of the same z^{-i} order can be equated as

$$\begin{aligned} z^0: &\quad 1 = 1 \\ z^{-1}: &\quad a_1 z^{-1} + f_0 b_1 z^{-1} - z^{-1} - k_I b_1 z^{-1} = d_1 z^{-1} \\ z^{-2}: &\quad - a_1 z^{-2} - f_0 b_1 z^{-2} = d_2 z^{-2} \end{aligned}$$

Dividing sides by z^{-i}, the equations are now

$$\begin{aligned} z^0: &\quad 1 = 1 \\ z^{-1}: &\quad - 1 + a_1 + f_0 b_1 - k_I b_1 = d_1 \\ z^{-2}: &\quad - a_1 - f_0 b_1 = d_2 \end{aligned}$$

Since a_i and b_i parameters are known, as well as d_i as chosen by the user, the above equations can be rearranged by separating f_i and b_i from d_i and a_i into

$$\begin{aligned} z^0: &\quad 1 = 1 \\ z^{-1}: &\quad f_0 b_1 - k_I b_1 = d_1 - (-1 + a_1) \\ z^{-2}: &\quad - f_0 b_1 = d_2 - (0 - a_1) \end{aligned}$$

Respective equations for z^{-1} and z^{-2} can be rewritten into

$$\begin{bmatrix} b_1 & b_1 \\ -b_1 & 0 \end{bmatrix} \begin{bmatrix} f_0 \\ -k_I \end{bmatrix} = \begin{bmatrix} d_1 - (-1 + a_1) \\ d_2 - (0 - a_1) \end{bmatrix} \tag{4.2.26}$$

Then, rearranging it to keep the matrix with unknown f_0 and k_I on the left hand-side of the equation as

$$\begin{bmatrix} f_0 \\ -k_I \end{bmatrix} = \begin{bmatrix} d_1 - (-1 + a_1) \\ d_2 - (0 - a_1) \end{bmatrix} \begin{bmatrix} b_1 & b_1 \\ -b_1 & 0 \end{bmatrix}^{-1} \tag{4.2.27}$$

allows to obtain the desired parameters f_0 and k_I.

4.3 Control design of Proportional-Integral-Plus controller for an indoor air temperature control

The model allowing to simulate the indoor conditions introduced in Chapters 2 and 3 as a MISO system will be used to design a SVF controller suited for this purpose. Having two inputs present in the model, only one of them is controllable, i.e. control input related to the supply air as T_s or ΔT, while the other input, the outdoor air temperature, is a known uncontrollable input. The structure formulated in this section will focus on designing a PIP controller deploying a two-input one-output NMSS model.

The PIP controller proposed in this section is used to determine the control signals sent to the AHU commanding heating and cooling units, following the specific environment requirements described in Section 4.3.1.

4.3.1 Indoor air temperature requirements

An indoor air temperature controller relevant to the system introduced in Chapter 2, where AHU contains heating and cooling unit, requires two set-points, one for heating and one for cooling, separated by a dead-band. General presentation of such requirements with exemplary set-points is depicted in Figure 4.2. It is expected that the heating unit is controlled in such a way that the indoor air temperature remains above the heating set-point r_h and similarly, the cooling unit is controlled in such a way that the indoor air temperature remains below the cooling set-point r_c. In an overall picture, the controller ensures that the indoor air temperature remains within the dead-band as often as possible; no heating and cooling takes place when the indoor air temperature is within the dead-band. It is important, in such configuration, that the two components, heating controller and cooling controller, don't act against each other and compensate each other. One of the solutions for that is having two controllers constrained by the inequalities around the set-points. For example, heating controller would have heating set-point, where heating can be triggered only if the indoor air temperature is below the set-point $T_r < r_h$ and cannot be applied otherwise. In the same manner, the cooling unit would operate only if the indoor air temperature is in exceed of the cooling set-point $T_r > r_c$, providing no cooling output if the indoor air temperature is lower than the cooling set-point. Alternatively, there could be one controller with a single variable set-point, switching between the dead-band borders, and depending on the sign of the calculated control input, the command would go either to the cooling unit ($\Delta T < 0$) or to the heating unit ($\Delta T > 0$), however, inequality constraint on the set-point is required as well.

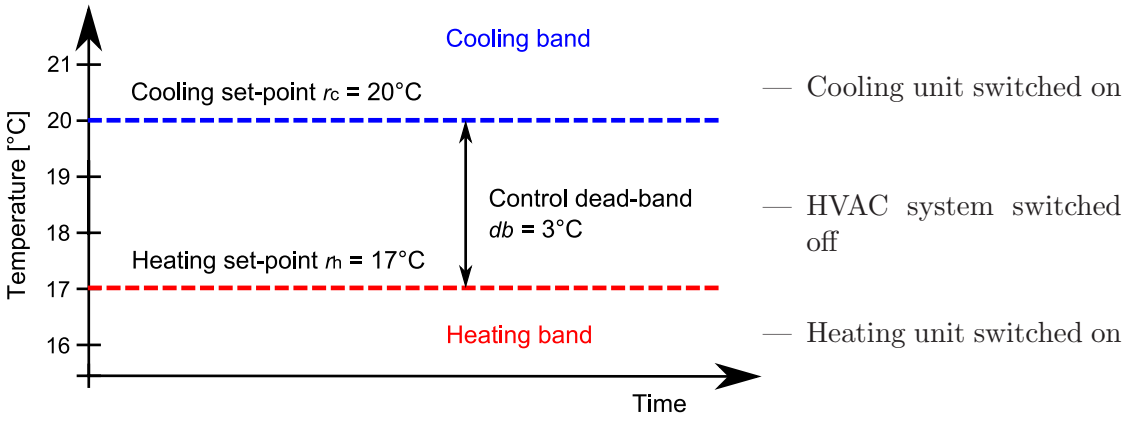

FIGURE 4.2: Environmental requirements of the indoor space for dual temperature set-point controller. The controller manages the indoor air temperature by operating one component for heating control and another one for cooling control.

4.3.2 Non-minimal State Space model of an indoor air temperature model

Consider a first order discrete-time model with two inputs and one output defined as

$$y(k) = -a_1 y(k-1) + b_1 u_1(k-1) + b_2 u_2(k-1) \tag{4.3.1}$$

or in a transfer function form as

$$y(k) = \frac{b_1 z^{-1}}{1 + a_1 z^{-1}} u_1(k) + \frac{b_2 z^{-1}}{1 + a_1 z^{-1}} u_2(k) \tag{4.3.2}$$

Modifying the model expressed by Equation (4.3.1) to represent the reduced model (3.4.4) of the indoor thermal process, the MISO system is defined as

$$T_r(k) = -a_1 T_r(k-1) + b_1 T_s(k-1) + b_2 T_a(k-1) \tag{4.3.3}$$

with transfer function defined as

$$T_r(k) = \frac{b_1 z^{-1}}{1 + a_1 z^{-1}} T_s(k) + \frac{b_2 z^{-1}}{1 + a_1 z^{-1}} T_a(k) \tag{4.3.4}$$

Here a general model concept is considered, the input $u_1(k)$ can be either $T_s(k)$, as in Equation (3.4.4), or $\Delta T(k)$, as in model (3.4.9), as the model structure remains the same. Note, however, that the parameters may take different values and are not state-dependent. The corresponding NMSS form representing model given by Equation (4.3.1) is

$$\begin{aligned} \boldsymbol{x}(k) &= \boldsymbol{F}\boldsymbol{x}(k-1) + \boldsymbol{g_1} u_1(k-1) + \boldsymbol{g_2} u_2(k-1) + \boldsymbol{d} y_d(k) \\ y(k) &= \boldsymbol{h}\boldsymbol{x}(k) \end{aligned} \tag{4.3.5}$$

with

$$\boldsymbol{x}(k) = [y(k) \quad z(k)]^T \tag{4.3.6}$$

and the *integral of error* state

$$z(k) = z(k-1) + (y_d(k) - y(k)) = z(k-1) + y_d(k) + a_1 y(k-1) - b_1 u_1(k-1) - b_2 u_2(k-1) \tag{4.3.7}$$

expanded for the first order MISO system model with two inputs as

$$z(k) = z(k-1) + y_d(k) + a_1 y(k-1) - b_1 u_1(k-1) - b_2 u_2(k-1) \tag{4.3.8}$$

The associated matrix and vectors are defined as the state transition matrix $\boldsymbol{F}$, input vector $\boldsymbol{g}$, command input vector $\boldsymbol{d}$ and output vector $\boldsymbol{h}$ in the following forms

$$\boldsymbol{F} = \begin{bmatrix} -a_1 & 0 \\ a_1 & 1 \end{bmatrix}$$

$$\boldsymbol{g_1} = [b_1 \quad -b_1]^T$$

$$\boldsymbol{g_2} = [b_2 \quad -b_2]^T$$

$$\boldsymbol{d} = [0 \quad 1]$$

$$\boldsymbol{h} = [1 \quad 0]$$

The resulting NMSS model is defined as

$$\begin{aligned} \boldsymbol{x}(k) &= \begin{bmatrix} y(k) \\ z(k) \end{bmatrix} = \begin{bmatrix} -a_1 & 0 \\ a_1 & 1 \end{bmatrix} \begin{bmatrix} y(k-1) \\ z(k-1) \end{bmatrix} + \begin{bmatrix} b_1 \\ -b_1 \end{bmatrix} u_1(k-1) + \begin{bmatrix} b_2 \\ -b_2 \end{bmatrix} u_2(k-1) + \begin{bmatrix} 0 \\ 1 \end{bmatrix} y_d(k) \\ y(k) &= \begin{bmatrix} 1 & 0 \end{bmatrix} \boldsymbol{x}(k) \end{aligned} \tag{4.3.9}$$

4.3.3 State Variable Feedback control law

Following the SVF control law formulated in Equation (4.2.5), the control actions for the input $u_1(k)$ is

$$u_1(k) = -\boldsymbol{k}^T \boldsymbol{x}(k) \tag{4.3.10}$$

and there is no control law formulated for the second input $u_2(k)$ as it is assumed to be the outdoor air temperature T_a, which is known, but not controllable input. The control gain vector for the input $u_1(k)$ is

$$\boldsymbol{k}^T = \begin{bmatrix} f_0 & -k_I \end{bmatrix} \tag{4.3.11}$$

and the polynomials $F(z^{-1})$ and $G(z^{-1})$ of the PIP controller are defined as

$$F(z^{-1}) = f_0$$
$$G(z^{-1}) = 1$$

The control action $u_1(k)$ can also be represented as

$$u_1(k) = -\begin{bmatrix} f_0 & -k_I \end{bmatrix} \begin{bmatrix} y(k) \\ z(k) \end{bmatrix} = -f_0 y(k) + k_I z(k) \tag{4.3.13}$$

and, substituting $z(k)$ with its equivalent from the right-hand side of Equation (4.2.3), $u_1(k)$ is defined as

$$u_1(k) = -f_0 y(k) + \frac{k_I}{1 - z^{-1}}(y_d(k) - y(k)) \tag{4.3.14}$$

4.3.3.1 Proportional-Integral-Plus controller for the indoor air temperature control

Tailoring variables name in Equation (4.3.13) to the indoor thermal process, the control action takes the following form

$$T_s(k) = -\begin{bmatrix} f_0 & -k_I \end{bmatrix} \begin{bmatrix} y(k) \\ z(k) \end{bmatrix} = -f_0 T_r(k) + k_I z(k) \tag{4.3.15}$$

where $\Delta T(k)$ can be used in place of $T_s(k)$ as appropriate. It is assumed that the output $y(k) = T_r(k)$. The reference signal $y_d(k)$ will become in this instance a set-point, either for cooling, r_c or heating, r_h. The equations employing SVF for the indoor air temperature control are proposed as

$$\Delta T_c(k) = \Delta T(k-1) - \begin{bmatrix} f_0 & -k_I \end{bmatrix} \cdot \begin{bmatrix} y(k) - y(k-1) \\ r_c - y(k) \end{bmatrix} \tag{4.3.16a}$$

$$\Delta T_h(k) = \Delta T(k-1) - \begin{bmatrix} f_0 & -k_I \end{bmatrix} \cdot \begin{bmatrix} y(k) - y(k-1) \\ r_h - y(k) \end{bmatrix} \tag{4.3.16b}$$

for heating unit and cooling unit, respectively. Further, applying constraints on the cooling and heating capacity within the AHU and holding a dead-band between set-points r_c and r_h ensures that no heating or cooling takes place when the indoor air temperature is within the dead-band. Consequently,

$$\Delta T_{min} \leq \Delta T_c(k) < 0$$

and

$$0 < \Delta T_h(k) \leq \Delta T_{max}$$

where ΔT_{min} denotes the maximum cooling output, i.e. the heat that cooling unit is able to withdraw from the air passing through the AHU, and ΔT_{max} the maximum heating output, i.e. the heat that heating unit is able to add to the air passing through the AHU. A zero in above constraints means that the unit is switched off and does not contribute to the AHU operation.

4.4 State-dependent Proportional-Integral-Plus controller

The PIP method is capable of controlling the state-dependent models (Taylor et al., 2013). Consider the following SDP-NMSS representation of a SISO SDP model following the general form as introduced in Chapter 3, Section 3.2.1, employing SVF as introduced in Section 4.2.2 formulated as

$$\begin{aligned} \boldsymbol{x}(k) &= \boldsymbol{F}\{\chi(k)\}\boldsymbol{x}(k-1) + \boldsymbol{g}\{\chi(k)\}u(k-1) + \boldsymbol{d}y_d(k) \\ y(k) &= \boldsymbol{h}\boldsymbol{x}(k) \end{aligned} \tag{4.4.1}$$

The state variable feedback defining the control law for SDP-PIP is therefore

$$u(k) = -\boldsymbol{k}^T\{\chi(k)\}\boldsymbol{x}(k) \tag{4.4.2}$$

where the control gains vector now is state-dependent and defined as

$$\boldsymbol{k}^T\{\chi(k)\} = \begin{bmatrix} f_0\{\chi(k)\} & \dots & f_{n-1}\{\chi(k)\} & g_1\{\chi(k)\} & \dots & g_{m-1}\{\chi(k)\} & -k_I\{\chi(k)\} \end{bmatrix} \tag{4.4.3}$$

Note that the $(n+m) \times (n+m)$ matrix $\boldsymbol{F}\{\chi(k)\}$, the $(n+m) \times 1$ vectors $\boldsymbol{g}\{\chi(k)\}$, $\boldsymbol{k}\{\chi(k)\}$, polynomials $F(z^{-1})\{\chi(k)\}$ and $G(z^{-1})\{\chi(k)\}$ as well as $a_i\{\chi(k)\}$ and $b_i\{\chi(k)\}$ parameters are now state-dependent.

Pole placement for State-Dependent Parameter-Proportional-Integral-Plus There are three approaches for determining the control gains proposed by Taylor et al. (2013). First, scheduled LQ design, which assumes solving LQ control problem online at each sampling instant and assumes point-wise controllability. Second, scheduled pole assignment, relying on solving a standard linear pole assignment problem at each sampling interval as briefly described in Section 4.2.3. Third, stabilising pole assignment for all-pole SDP models, developed in response to limitations of a scheduled pole assignment to cater for SDP-NMSS model. The SDP-PIP controller utilised in this thesis employs the

second method, recalculating the poles at each time step according to the polynomial $D(z^{-1})$, following the user's design and choice of d_i coefficients.

4.4.1 State-Dependent Parameter-Proportional-Integral-Plus for a first order system

Consider the first order SDP SISO model provided in Equation (3.2.1). The NMSS representation of this model is

$$\begin{aligned}\boldsymbol{x}(k) &= \begin{bmatrix} y(k) \\ z(k) \end{bmatrix} = \begin{bmatrix} -a_1\{\chi(k)\} & 0 \\ a_1\{\chi(k)\} & 1 \end{bmatrix} \begin{bmatrix} y(k-1) \\ z(k-1) \end{bmatrix} + \begin{bmatrix} b_1\{\chi(k)\} \\ -b_1\{\chi(k)\} \end{bmatrix} u(k-1) + \begin{bmatrix} 0 \\ 1 \end{bmatrix} y_d(k) \\ y(k) &= \begin{bmatrix} 1 & 0 \end{bmatrix} \boldsymbol{x}(k) \end{aligned} \tag{4.4.4}$$

The *integral of error* state is therefore

$$z(k) = z(k-1) + (y_d(k) - y(k)) = z(k-1) + y_d(k) + a_1\{\chi(k)\}y(k-1) - b_1\{\chi(k)\}u(k-1) \tag{4.4.5}$$

The control gain vector $\boldsymbol{k}^T$ of SVF control law for SDP SISO model is then

$$\boldsymbol{k}^T = \begin{bmatrix} f_0\{\chi(k)\} & -k_I\{\chi(k)\} \end{bmatrix} \tag{4.4.6}$$

as the polynomials $F(z^{-1})$ and $G(z^{-1})$ of PIP controller are defined as

$$\begin{aligned} F(z^{-1}) &= f_0\{\chi(k)\} \\ G(z^{-1}) &= 1 \end{aligned}$$

Accordingly, the control action $u(k)$ is represented as

$$u(k) = -\begin{bmatrix} f_0\{\chi(k)\} & -k_I\{\chi(k)\} \end{bmatrix} \begin{bmatrix} y(k) \\ z(k) \end{bmatrix} = -f_0\{\chi(k)\}y(k) + k_I\{\chi(k)\}z(k) \tag{4.4.8}$$

and, substituting $z(k)$ with its equivalent from the right-hand side of Equation (4.2.4), $u(k)$ is defined as

$$u(k) = -f_0\{\chi(k)\}y(k) + \frac{k_I\{\chi(k)\}}{1 - z^{-1}}(y_d(k) - y(k)) \tag{4.4.9}$$

which provides basis of SDP-PIP in regard to a SISO system model.

4.4.1.1 State-Dependent Parameter-Proportional-Integral-Plus for the indoor air temperature control

Following the introduction of PIP controller and the complementary NMSS model for the indoor air temperature control in Section 4.3, this section aims to establish SDP-PIP design for the indoor air temperature control of a system with two inputs and one output, as described in Section 4.3.

Firstly, the control action related to the supplied air control input takes the following form:

$$T_s(k) = -\begin{bmatrix} f_0\{\chi(k)\} & -k_I\{\chi(k)\} \end{bmatrix} \begin{bmatrix} y(k) \\ z(k) \end{bmatrix} = -f_0\{\chi(k)\}T_r(k) + k_I\{\chi(k)\}z(k) \quad (4.4.10)$$

where $\Delta T(k)$ can be used in place of $T_s(k)$ as appropriate, following two approaches introduced in Chapter 3. It is also assumed that the output $y(k) = T_r(k)$ and that the reference signal $y_d(k)$ will become a set-point, either for cooling, r_c or heating, r_h. The equations employing SVF for the indoor air temperature control following the SDP-PIP methodology are proposed as

$$\Delta T_c(k) = \Delta T(k-1) - \begin{bmatrix} f_0\{\chi(k)\} & -k_I\{\chi(k)\} \end{bmatrix} \cdot \begin{bmatrix} y(k) - y(k-1) \\ r_c - y(k) \end{bmatrix} \quad (4.4.11a)$$

$$\Delta T_h(k) = \Delta T(k-1) - \begin{bmatrix} f_0\{\chi(k)\} & -k_I\{\chi(k)\} \end{bmatrix} \cdot \begin{bmatrix} y(k) - y(k-1) \\ r_h - y(k) \end{bmatrix} \quad (4.4.11b)$$

for heating unit and cooling unit, respectively. Note that f_0 and k_I are now state-dependent and will be reevaluated at each time step. The constraints on heating and cooling within the AHU remain as stated in Section 4.3.

The overall SDP-NMSS model for the indoor air temperature control with variable fan speed and position of damper blades is

$$\begin{aligned} \boldsymbol{x}(k) = \begin{bmatrix} y(k) \\ z(k) \end{bmatrix} &= \begin{bmatrix} -a_1\{\chi(k)\} & 0 \\ a_1\{\chi(k)\} & 1 \end{bmatrix} \begin{bmatrix} y(k-1) \\ z(k-1) \end{bmatrix} \\ &+ \begin{bmatrix} b_1\{\chi(k)\} \\ -b_1\{\chi(k)\} \end{bmatrix} u_1(k-1) + \begin{bmatrix} b_2\{\chi(k)\} \\ -b_2\{\chi(k)\} \end{bmatrix} u_2(k-1) + \begin{bmatrix} 0 \\ 1 \end{bmatrix} y_d(k) \\ y(k) &= \begin{bmatrix} 1 & 0 \end{bmatrix} \boldsymbol{x}(k) \end{aligned} \quad (4.4.12)$$

where the input $u_1(k)$ is related to the air supplied, i.e. $T_s(k)$ for (3.4.4) model or $\Delta T(k)$ for (3.4.9) model, $u_2(k)$ is the known and uncontrollable input attributed to the outdoor air temperature $T_a(k)$ and the output is the indoor air temperature $T_r(k)$. The

corresponding *integral of error* state is

$$\begin{aligned} z(k) &= z(k-1) + (y_d(k) - y(k)) = z(k-1) + y_d(k) \\ &\quad + a_1\{\chi(k)\}y(k-1) - b_1\{\chi(k)\}u_1(k-1) - b_2\{\chi(k)\}u_2(k-1) \end{aligned} \tag{4.4.13}$$

The model represented by Equation (4.4.12) can be implemented in MATLAB along with equations for the cooling and heating demand (4.4.11) and related constraints, where the heating and cooling temperature demands sum up into $\Delta T(k)$ as in Equation (2.5.1). Using pole assignment method briefly described in Section 4.2.3 at each time step of the simulation will allow to calculate the most recent values of $f_0\{\chi(k)\}$ and $k_I\{\chi(k)\}$.

4.5 Simulation study

A demonstration of the SDP-PIP controller operation is presented in this simulation study consisting of two parts. In the first part the outdoor air temperature input vector is considered to be a sine wave to illustrate the control response when the outdoor conditions are predictable and the main day-night temperature cycle is preserved. The second part makes use of real data, mimicking the controller operation under real conditions. Each part contains two scenarios to account for unlimited and limited heating and cooling unit capacities. The study will also test different SDP-PIP designs with selected pole assignment preferences.

The simulation study presented in this section relies on the SDP-PIP design proposed in Section 4.4.1.1 for the indoor temperature control and relies on the model structure in Equation (3.4.9) where two inputs are present, ΔT and T_a. The parameters a, b_1 and b_2 of the model (4.4.12) correspond to α, β_1 and β_2, respectively, where the values are calculated from first principles as specified for model (3.4.9). The first principles coefficients are calculated based on the values presented in Table 2.5. The model parameters were converted from a continuous-time domain to discrete-time domain using the ZOH method.

4.5.1 Pole placement

Design of the SDP-PIP controller is demonstrated though simulations for three different pole assignment probations, i.e. rapid response (dead-beat, (Åström & Wittenmark, 2008, p. 143)), moderately fast response and slow response. The poles and corresponding d_i coefficients are presented in Table 4.1. Note that the poles consist only of real part, imaginary part equals 0.

TABLE 4.1: Desired closed loop locations of pole assignment for SDP-PIP.

Poles	d_1	d_2
0	0	0
0.5	-1.0	0.25
0.9	-1.8	0.81

Note that this controller has no restrictions on the control action values and changes (other than heating and cooling capacities), which can be inefficient, especially in rapidly changing cases such as dead-beat. Additional algorithms need to be implemented to regulate control action increment and other adequate preferences to optimise the controller.

4.5.2 First principles State-Dependent Parameter-Proportional-Integral-Plus simulation with sine wave input

This part is focused on an overall demonstration of the SDP-PIP controller using simple generated data with various damper position scenarios and the air mass flow rate. The simulation was performed for no restrictions on the heating and cooling capacity scenario and with restrictions imposed.

4.5.2.1 Unrestricted heating and cooling

The results are dived into two sections. The first one demonstrates the different outputs based on the pole choice and keeps the damper position and the air mass flow rate constant. The second part allows for variable damper position and the air mass flow rate while simulating the indoor air temperature series.

Constant u_d and m_a The simulation results of the SDP-PIP controller with constant supply air flow and damper position are shown in Figures 4.4 to 4.8 containing a pair of the open and closed loop system simulations for each of the poles as per Table 4.1.

Performance assessment by means of heating and cooling actions together with the number of samples that were out of the dead-band are presented in Tables 4.2 and 4.3 for closed and open loop systems, respectively. The signal $y_{out}(k)$ indicates the location of $T_r(k)$ expressed in Equation (4.5.1). The total number of samples for a 3-days simulation

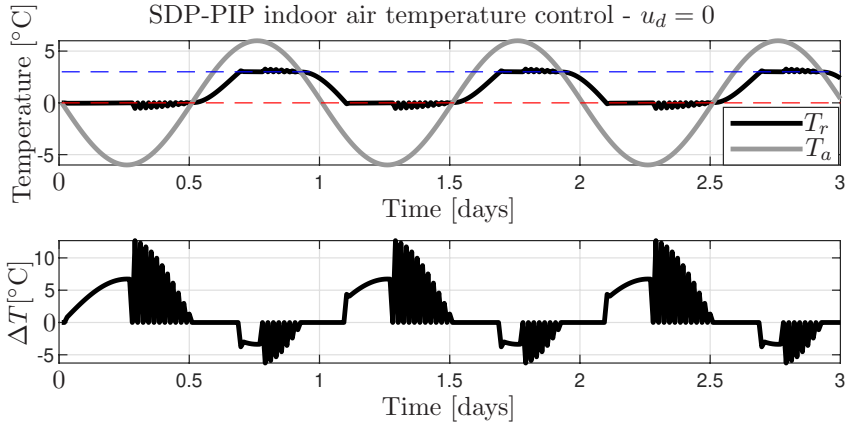

FIGURE 4.3: SDP-PIP indoor air temperature control with poles at 0. The set-points $r_c = 3°\text{C}$ and $r_h = 0°\text{C}$ are marked with dash line. The damper position $u_d = 0$ and the air mass flow rate $m_a = 18.5\,\text{m}^3/\text{s}$.

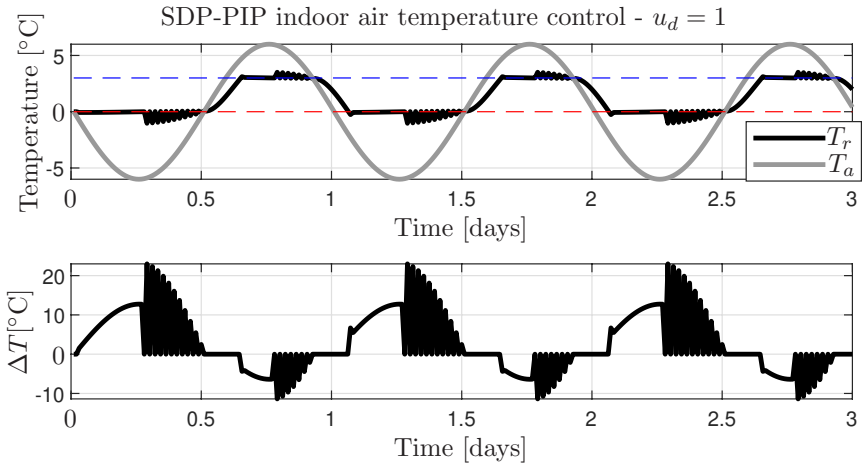

FIGURE 4.4: SDP-PIP indoor air temperature control with poles at 0. The set-points $r_c = 3°\text{C}$ and $r_h = 0°\text{C}$ are marked with dash line. The damper position $u_d = 1$ and the air mass flow rate $m_a = 18.5\,\text{m}^3/\text{s}$.

with 15 min sampling time is $N = 288$.

$$y_{out}(k) = \begin{cases} 1, & T_r(k) > r_c(k) \\ 0, & r_h(k) \leq T_r(k) \leq r_c(k) \\ 1, & T_r(k) < r_c(k) \end{cases} \tag{4.5.1}$$

There are few observations that have been made based on the Figures 4.4 to 4.8. Firstly, the system dynamics and the AHU operation are affected by the design of the PIP controller and the choice of poles. Secondly, as a consequence, there is a trade-off between the fast response (dead-beat), accompanied by a lot of chattering (Figures 4.3 and 4.4), and the slow response, where chattering is minimised, but the indoor air temperature requirements are not met (Figures 4.7 and 4.8). Therefore, the SDP-PIP

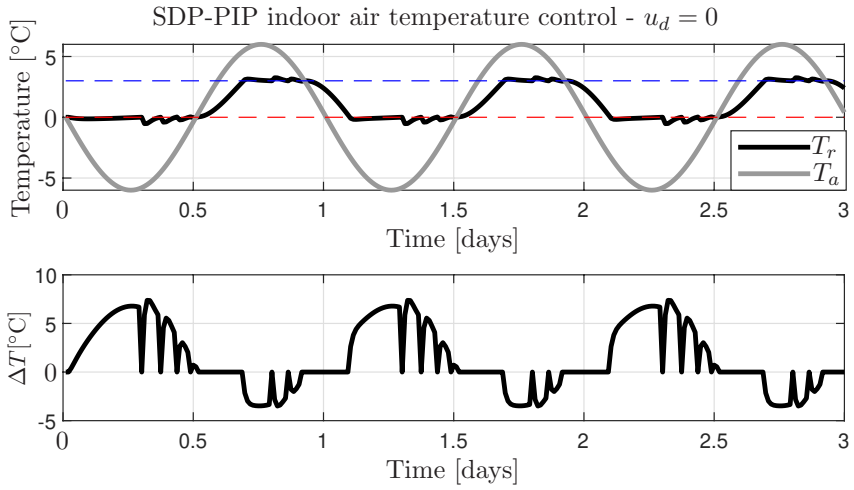

FIGURE 4.5: SDP-PIP indoor air temperature control with poles at 0.5. The set-points $r_c = 3°\text{C}$ and $r_h = 0°\text{C}$ are marked with dash line. The damper position $u_d = 0$ and the air mass flow rate $m_a = 18.5\,\text{m}^3/\text{s}$.

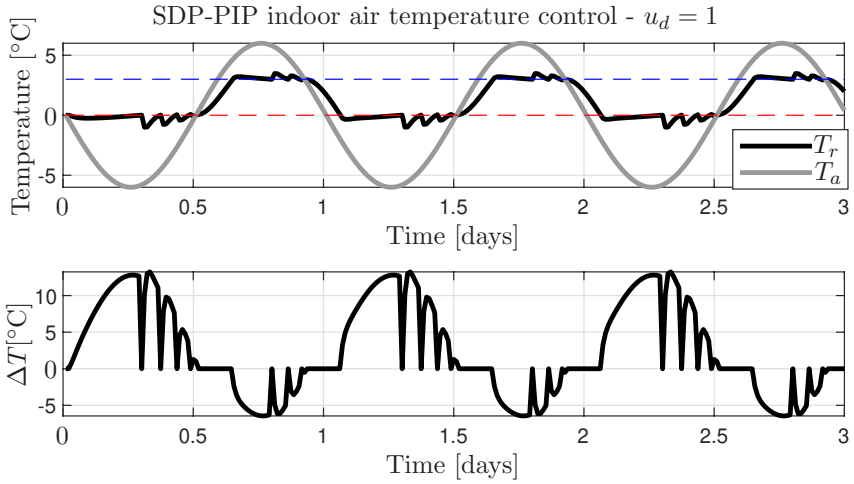

FIGURE 4.6: SDP-PIP indoor air temperature control with poles at 0.5. The set-points $r_c = 3°\text{C}$ and $r_h = 0°\text{C}$ are marked with dash line. The damper position $u_d = 1$ and the air mass flow rate $m_a = 18.5\,\text{m}^3/\text{s}$.

controller requires tuning specific for the system and preferred response type. Then, it has been noted that regardless of the pole placement the dynamic responses remain different for the open and closed loop systems, showing that the SDP-PIP controller does not compensate for it and that the SDP model given by Equation (3.4.9) relying on the damper position and the air mass flow rate is valid. Finally, the aforementioned observations are consistent with analysis of Tables 4.2 and 4.3, i.e. slower response consumer less energy over time, but the indoor air temperature criteria are not met as thoroughly as for poles related to faster response. It is reflected in Figures 4.3 to 4.8 in the fact that the maximum (minimum) values achieved by ΔT are higher (lower) for faster response while slow dynamic system oscillates tighter around 0.

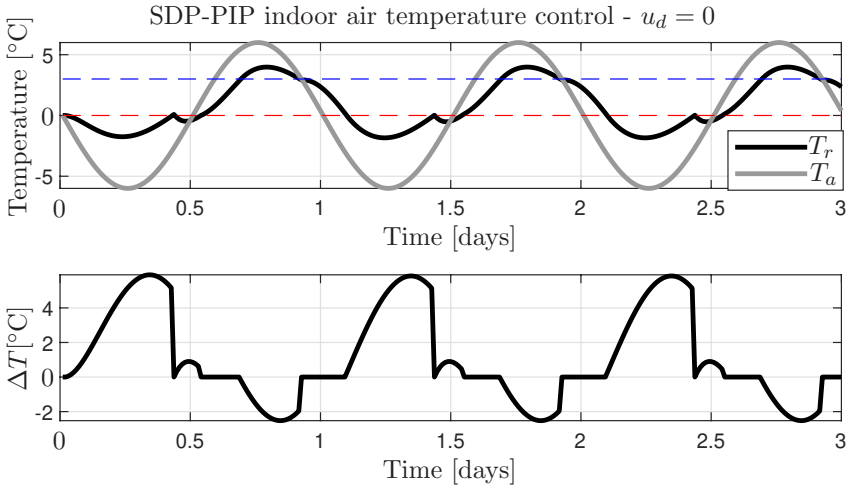

FIGURE 4.7: SDP-PIP indoor air temperature control with poles at 0.9. The set-points $r_c = 3°\text{C}$ and $r_h = 0°\text{C}$ are marked with dash line. The damper position $u_d = 0$ and the air mass flow rate $m_a = 18.5\,\text{m}^3/\text{s}$.

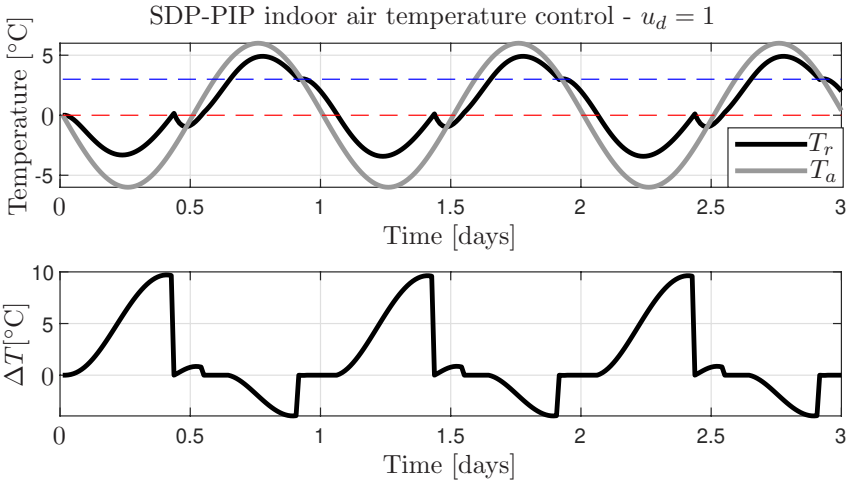

FIGURE 4.8: SDP-PIP indoor air temperature control with poles at 0.9. The set-points $r_c = 3°\text{C}$ and $r_h = 0°\text{C}$ are marked with dash line. The damper position $u_d = 1$ and the air mass flow rate $m_a = 18.5\,\text{m}^3/\text{s}$.

TABLE 4.2: SDP-PIP controller performance assessment for the closed loop system $u_d = 0$. The air mass flow rate is $m_a = 18.5\,\text{m}^3/\text{s}$, heating and cooling unconstrained.

Poles	$\sum_{k=1}^{N} \Delta T_h(k)$	$\sum_{k=1}^{N} \Delta T_c(k)$	$\sum_{k=1}^{N} (\Delta T_h(k) + \lvert\Delta T_c(k)\rvert)$	$\sum_{k=1}^{N} y_{out(k)}$
0	574.15	-167.15	741.30	138
0.5	569.15	-164.19	733.34	174
0.9	438.92	-125.43	564.35	200

Variable u_d and m_a The simulation results of the SDP-PIP controller with variable supply air flow and damper position are shown in Figures 4.9-4.10 containing a pair of

TABLE 4.3: SDP-PIP controller performance assessment for the open loop system $u_d = 1$. The air mass flow rate $m_a = 18.5\,\mathrm{m}^3/\mathrm{s}$, heating and cooling unconstrained.

Poles	$\sum_{k=1}^{N} \Delta T_h(k)$	$\sum_{k=1}^{N} \Delta T_c(k)$	$\sum_{k=1}^{N} (\Delta T_h(k) + \lvert\Delta T_c(k)\rvert)$	$\sum_{k=1}^{N} y_{out(k)}$
0	1100.1	-359.2	1459.3	156
0.5	1080.2	-350.6	1430.8	195
0.9	604.18	-172.02	776.20	222

the open and closed loop system simulations for the dead-beat and 0.5 poles as per Table 4.1.

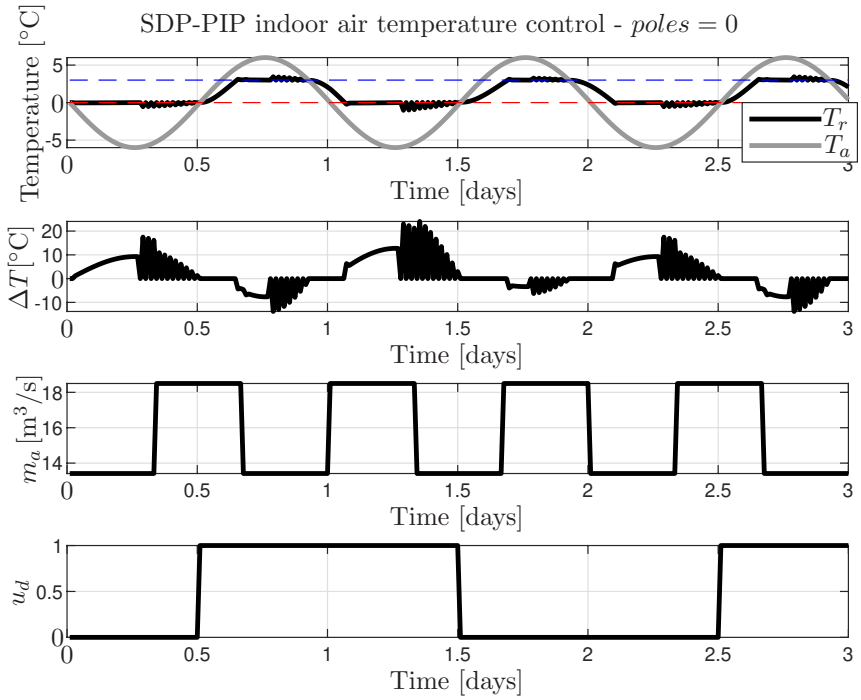

FIGURE 4.9: SDP-PIP indoor air temperature control with poles at 0. The set-points $r_c = 3°\mathrm{C}$ and $r_h = 0°\mathrm{C}$ are marked with dash line. The damper position and the air mass flow rate are variable.

TABLE 4.4: SDP-PIP controller performance assessment of a system with variable damper position u_d and the air mass flow rate is m_a, heating and cooling unconstrained.

Poles	$\sum_{k=1}^{N} \Delta T_h(k)$	$\sum_{k=1}^{N} \Delta T_c(k)$	$\sum_{k=1}^{N} (\Delta T_h(k) + \lvert\Delta T_c(k)\rvert)$	$\sum_{k=1}^{N} y_{out(k)}$
0	878.52	-341.15	1219.7	149
0.5	866.84	-334.29	1201.1	185

The simulation outputs presented in Figures 4.9 and 4.10 demonstrate the state-dependent nature of the model exposed in the distinct amplitudes of ΔT when the

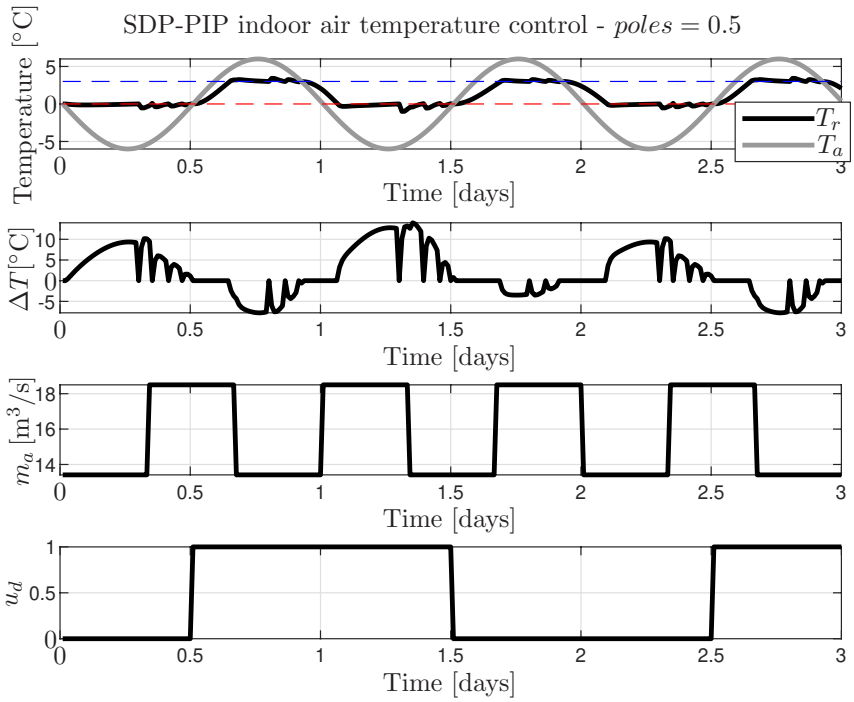

FIGURE 4.10: SDP-PIP indoor air temperature control with poles at 0.5. The set-points $r_c = 3°\text{C}$ and $r_h = 0°\text{C}$ are marked with dash line. The damper position and the air mass flow rate are variable.

air is supplied at different rate. Notably, similar trend is observed with regard to the position of damper blades, where more heating and cooling is needed when the indoor air is not recirculated. The observations are consistent for both tested pole placements. Assessing the performance of the SDP-PIP controller based on the results in Table 4.4, it is visible that faster response yields more control action, i.e. higher demand for heating and cooling ensuring that the time spent outside the dead-band will be minimised; this observation is also consistent with those for constant air mass flow rate and damper position results presented in Tables 4.2 and 4.3.

4.5.2.2 Heating and cooling constraints

The results are divided into two sections. The first one demonstrates the different outputs based on the pole choice and keeps the damper position and the air mass flow rate constant. The second part allows for variable damper position and the air mass flow rate while simulating the indoor air temperature series. There are constraints on the heating and cooling units $0 \leq \Delta T_h \leq 10$ and $-5 \leq \Delta T_c \leq 0$.

Constant u_d and m_a The simulation results of the SDP-PIP controller with constant supply air flow and damper position are shown in Figures 4.11-4.13 containing a pair of

the open and closed loop system simulations for each of the poles as per Table 4.1.

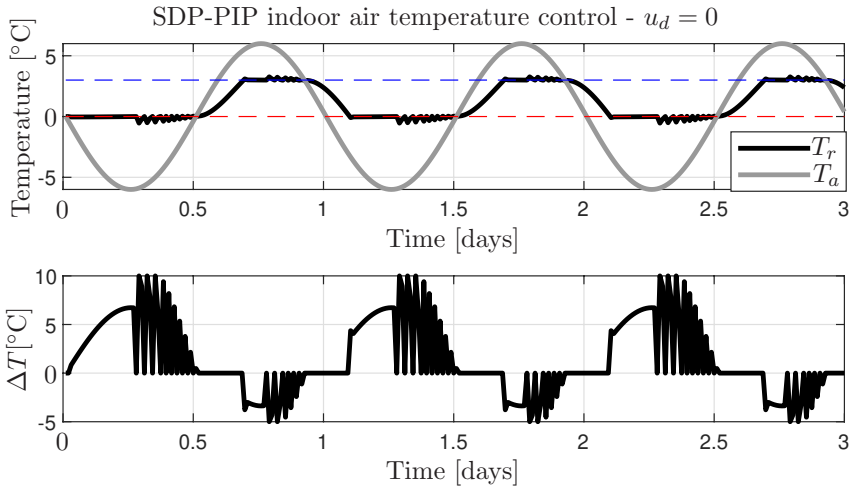

FIGURE 4.11: SDP-PIP indoor air temperature control with poles at 0. The set-points $r_c = 3°\text{C}$ and $r_h = 0°\text{C}$ are marked with dash line. The damper position $u_d = 0$ and the air mass flow rate $m_a = 18.5\,\text{m}^3/\text{s}$.

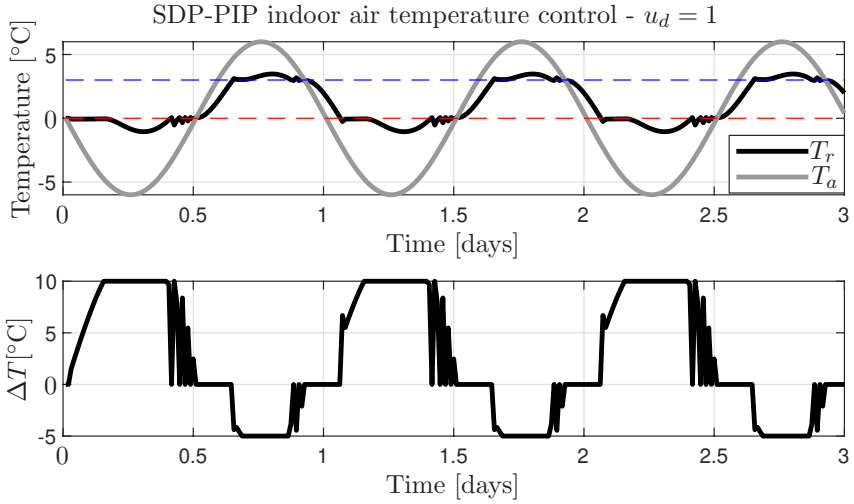

FIGURE 4.12: SDP-PIP indoor air temperature control with poles at 0. The set-points $r_c = 3°\text{C}$ and $r_h = 0°\text{C}$ are marked with dash line. The damper position $u_d = 1$ and the air mass flow rate $m_a = 18.5\,\text{m}^3/\text{s}$.

Figures showing results of simulations for the closed loop system with poles at 0.5 and the open and closed loop systems with poles at 0.9 have been omitted and are not displayed. The reason for that is ΔT does not reach constraints, therefore the output is exactly the same as for the unconstrained scenario with the respective Figures 4.5, 4.7 and 4.8.

Performance assessment by means of heating and cooling actions together with the number of samples that were out of the dead-band are presented in Tables 4.5 and 4.6 for the closed and open loop systems, respectively.

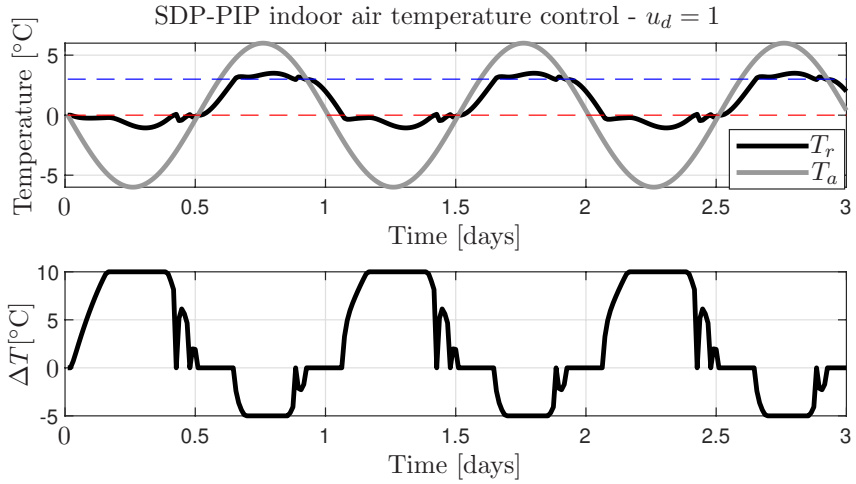

FIGURE 4.13: SDP-PIP indoor air temperature control with poles at 0.5. The set-points $r_c = 3°\text{C}$ and $r_h = 0°\text{C}$ are marked with dash line. The damper position $u_d = 1$ and the air mass flow rate $m_a = 18.5\,\text{m}^3/\text{s}$.

TABLE 4.5: SDP-PIP controller performance assessment for the closed loop system $u_d = 0$. The air mass flow rate is $m_a = 18.5\,\text{m}^3/\text{s}$, heating and cooling unconstrained.

Poles	$\sum_{k=1}^{N} \Delta T_h(k)$	$\sum_{k=1}^{N} \Delta T_c(k)$	$\sum_{k=1}^{N} (\Delta T_h(k) + \lvert\Delta T_c(k)\rvert)$	$\sum_{k=1}^{N} y_{out(k)}$
0	575.19	-167.47	742.66	147
0.5	569.15	-164.19	733.34	174
0.9	438.92	-125.43	564.35	200

TABLE 4.6: SDP-PIP controller performance assessment for the open loop system $u_d = 1$. The air mass flow rate $m_a = 18.5\,\text{m}^3/\text{s}$, heating and cooling unconstrained.

Poles	$\sum_{k=1}^{N} \Delta T_h(k)$	$\sum_{k=1}^{N} \Delta T_c(k)$	$\sum_{k=1}^{N} (\Delta T_h(k) + \lvert\Delta T_c(k)\rvert)$	$\sum_{k=1}^{N} y_{out(k)}$
0	1039.7	-340.6	1380.3	192
0.5	1018.3	-330.6	1348.9	201
0.9	604.18	-172.02	776.20	222

While the observations are common with those made for unconstrained scenario, the additional note concerns the result of heating and cooling restrictions. As a matter of fact, ΔT does not exceed 10 and does not decrease below -5, therefore the overall effort made by the heating and cooling units is slightly lower. It acts in similar way as if the poles were located closer to a boundary of the unity circle, therefore it takes more time to satisfy the indoor air temperature requirements.

Variable u_d and m_a The simulation results of the SDP-PIP controller with variable supply air flow and damper position are shown in Figure 4.14 to 4.15 containing a pair of the open and closed loop system simulations for the dead-beat and 0.5 poles as per Table 4.1.

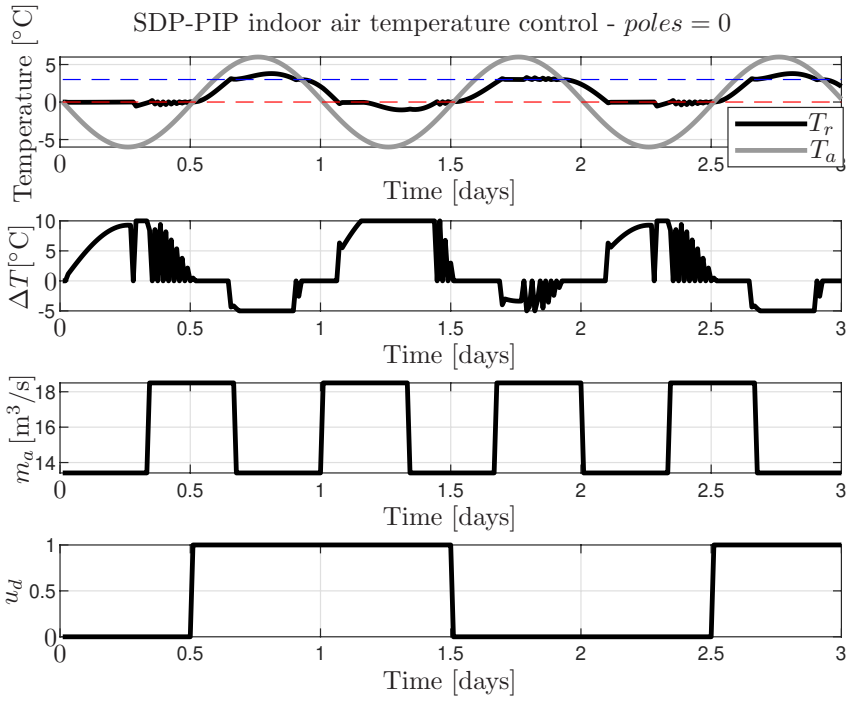

FIGURE 4.14: SDP-PIP indoor air temperature control with poles at 0. The set-points $r_c = 3°C$ and $r_h = 0°C$ are marked with dash line. The damper position and the air mass flow rate are variable.

TABLE 4.7: SDP-PIP controller performance assessment of a system with variable damper position u_d and the air mass flow rate is m_a, heating and cooling unconstrained.

Poles	$\sum_{k=1}^{N} \Delta T_h(k)$	$\sum_{k=1}^{N} \Delta T_c(k)$	$\sum_{k=1}^{N} (\Delta T_h(k) + \lvert\Delta T_c(k)\rvert)$	$\sum_{k=1}^{N} y_{out(k)}$
0	854.92	-297.46	1152.4	176
0.5	839.79	-290.66	1130.5	191

The results of the simulation employing the SDP-PIP controller with constraints on heating and cooling shown in Figures 4.14 and 4.15 and including Table 4.7 demonstrate likewise trends as the previously analysed scenarios in Section 4.5.2. Therefore, it is deemed, based on the tested scenarios, that the SDP-PIP controller designed for the indoor air temperature control fits the purpose in general terms.

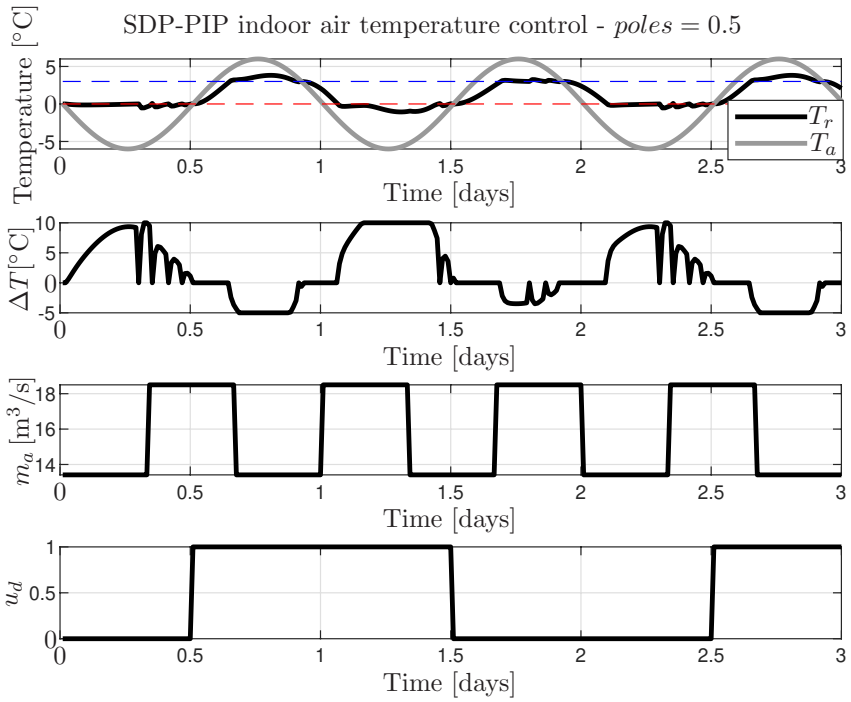

FIGURE 4.15: SDP-PIP indoor air temperature control with poles at 0.5. The set-points $r_c = 3$°C and $r_h = 0$°C are marked with dash line. The damper position and the air mass flow rate are variable.

4.5.3 First principles SDP-PIP simulation with real data

This part is focused on an overall demonstration of the SDP-PIP controller, using real data for the outdoor air temperature and varying the damper position and the air mass flow rate using square wave. Simulation was performed on a scenario with restrictions imposed on the heating and cooling units reflecting their approximate real respective sizes, i.e. 24°C and -10°C. The results of the simulation for poles at 0 and 0.5 are presented in Figures 4.16 and 4.17, respectively. The controller performance is assessed as in Section 4.5.2 using calculations of $\Delta T_h(k), \Delta T_c(k)$ and $y_{out}(k)$ and results are provided in Table 4.8.

TABLE 4.8: SDP-PIP controller performance assessment of a system with real data input for the outdoor air temperature and variable square wave input for damper position u_d and the air mass flow rate is m_a.

Poles	$\sum_{k=1}^{N} \Delta T_h(k)$	$\sum_{k=1}^{N} \Delta T_c(k)$	$\sum_{k=1}^{N} (\Delta T_h(k) + \lvert\Delta T_c(k)\rvert)$	$\sum_{k=1}^{N} y_{out(k)}$
0	5935.3	-944.0	6879.3	508
0.5	5870.7	-916.7	6787.3	596

The results presented in Figures 4.16 and 4.17 demonstrate an outcome of the simulation for the SDP-PIP controller with the dead-beat design and a moderately fast

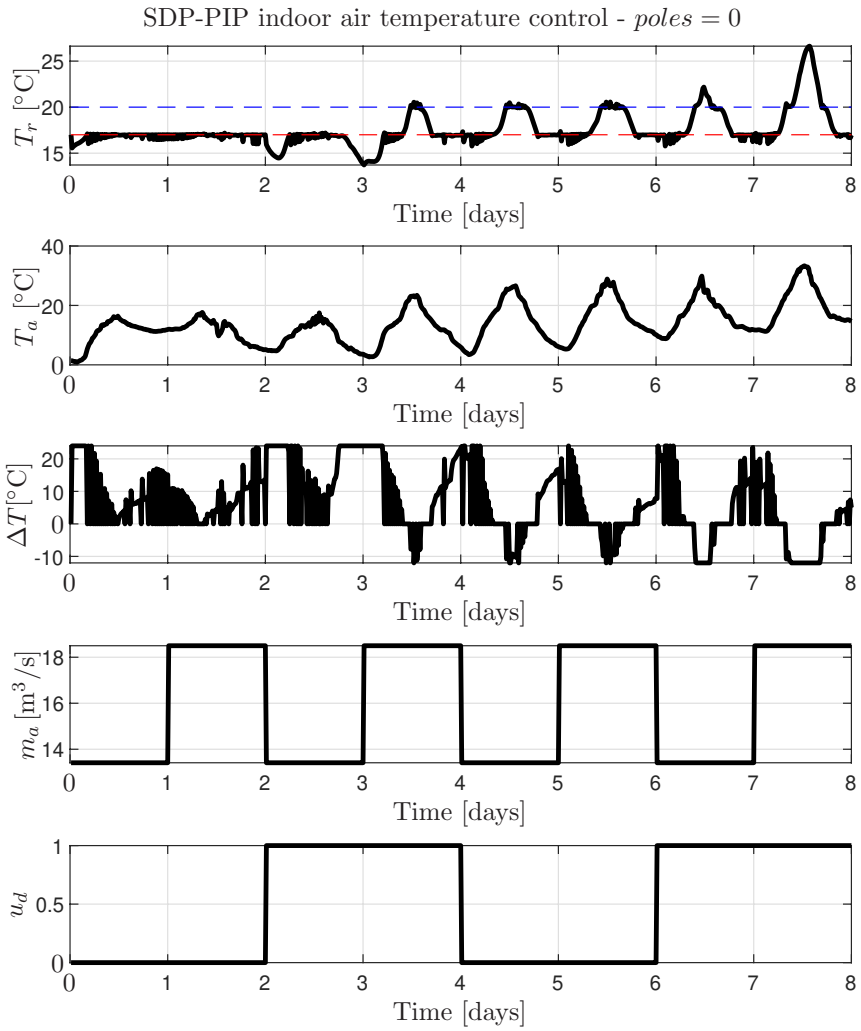

FIGURE 4.16: SDP-PIP indoor air temperature control with poles at 0. The set-points $r_c = 20°\text{C}$ and $r_h = 17°\text{C}$ are marked with dash line. The damper position and the air mass flow rate are variable.

dynamics. To mimic the behaviour of the real system, real data-based outdoor air temperature is used, the system input recorded by the HVAC system serving pharmaceutical warehouse located in Midlands introduced in Chapter 2. Also, the operation of the heating and cooling loads generated by the model was restricted to the values representing the real HVAC components of the aforementioned pharmaceutical warehouse, specifically sized for the purpose. While the indoor air thermal process dynamics is faster than the real system as the model is based on a simple first principles approach with limited knowledge about the inputs, the simulation represents well the phenomena observed by the author of this thesis when analysing the real data records. In particular, it illustrates the problem of constraints on heating and cooling due to physical capabilities of these units, resulting in an inability of the indoor air temperature requirements to be met.

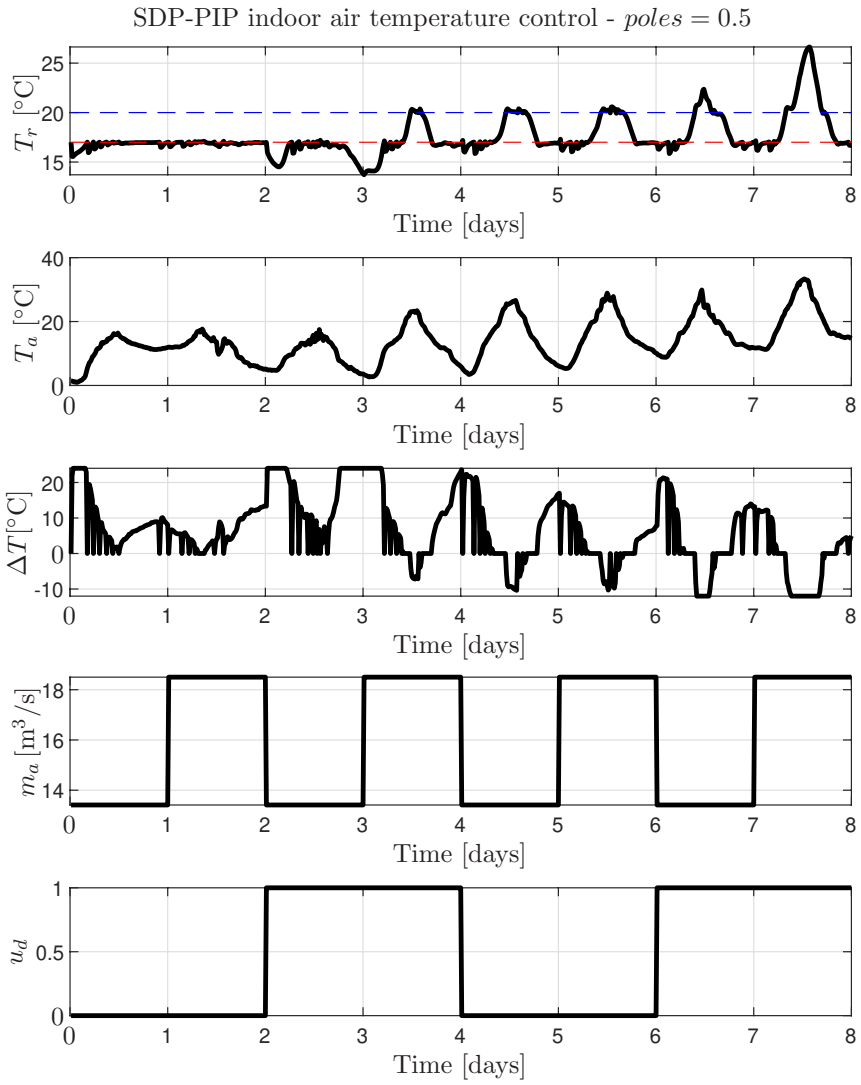

FIGURE 4.17: SDP-PIP indoor air temperature control with poles at 0.5. The set-points $r_c = 20°\text{C}$ and $r_h = 17°\text{C}$ are marked with dash line. The damper position and the air mass flow rate are variable.

While the heating and cooling units are designed to meet the indoor air temperature requirements under certain assumptions regarding the outdoor conditions, the sizing covers *majority* of the weather conditions predicted to happen throughout the year. The AHU may underperform if the outdoor temperature is higher than the maximum or lower than the minimum stated in the design document for Midlands, UK, e.g. during exceptionally hot summer days or rare harsh winter conditions. The heating and cooling units cannot be design to cover all exceptional weather conditions as it makes the design not optimal for regular conditions. Therefore, it is concluded that the SDP-PIP controller is suitable for applications where simple matching of the output to the set-point is required and is enough. However, more advanced techniques such as predictive may exhibit improved results, i.e. less time spent out of the dead-band and less energy spent on heating and

cooling. Also, some improvement might be achieved while using the PIP controller if a variable set-point is employed. Such set-point value could be calculated using e.g. Kalman Filter (Young, 2011, p. 71) to forecast the outdoor conditions, which allows to estimate the appropriate set-point favouring flexible dead-band and pre-cooling or pre-heating methods. Adaptive set-point adjustment strategy was proposed by Oswiecinska (2014) as a part of energy efficient HVAC control scheme, where gain scheduling technique was used to extend the time of the indoor air temperature remaining within the dead-band.

4.6 Conclusions

This chapter has considered the general form of the PIP controller together with the SISO NMSS model structure, the first order SISO NMSS model and the PIP controller and their respective SDP-PIP interpretations. The main contribution of this chapter is the discrete-time SDP-PIP controller formulated specifically for the indoor air temperature control following the models and assumptions provided in Chapters 2 and 3. This special approach dealing with two-input model, out of which only one is fully controllable, provides a method to determine the heating and cooling unit control actions used by the HVAC system to meet the demanded environmental conditions within the building and will be employed within the MPC design proposed in the following chapter.

The simulation study demonstrated the operation of the SDP-PIP controller subjected to basic input signals such as a sine wave and constant values and then using more complicated inputs or real data. This allowed to observe the system output under various conditions and evaluate its use for the intended indoor air temperature control. It has also shown that there is a need to tune the PIP controller, compromising fast response to achieve the designated output in short time and the control action with its increment values between samples. This translates into efficiency concerns and may imply constraints on the actual control systems. Note that badly tuned controller may not be able to meet the requirements and match the designed output value as poles are getting closer to 1. On the other hand, well-tuned controller will not be able to achieve the designed output if the constraints on the input hinder the control actions. On the final note, SDP-PIP is a controller suitable for applications, where set-point tracking is required, constant or variable, which makes it good candidate for wide range of control applications in industries.

Chapter 5

Model Predictive Control for energy efficient indoor air temperature control

5.1 Introduction

Model Predictive Control (MPC) is an advanced control method for multi-variable systems with constraints. Being mature and well-established in the industry, it is widely used in automotive, power systems, process industries, thermal systems, finance, healthcare, embedded systems. MPC is not a single technique, but a set of different methodologies, and uses a system model to predict the future responses at the current time step based on a given prediction horizon, computes a trajectory of optimal control action by minimising a predefined cost function, apply only the first value of the control action and repeat the calculation for the next time step. Its wide use is attributed to the benefits MPC offers which include online (event-based) optimisation, utilising future information, anticipation of future events, and dealing with many inputs and outputs constraints over a finite prediction horizon. A recognised advantage is that if the future evolution of the reference is known beforehand, the system can react before the change has effectively been made, thus avoiding the effects of delay in the process response. Additionally, MPC can be used with various model structures, e.g. linear, nonlinear, hybrid, state-space, stochastic, mixed-integer. Recommended reading on MPC concepts include works by Åström & Wittenmark (2008); Camacho & Bordons (1999); Wang (2009); Bemporad (2020), which have been also consulted during the research process and writing up of this chapter. A summary on the MPC concept can be found in a paper published in Encyclopedia of Systems and Control (Grüne, 2015), covering the

most important aspects of history, general form, stability, feasibility and performance analysis. Since the MPC is widely recognised and used method, there are existing solution offering Model predictive Control, such as MathWorks' Model Predictive Control Toolbox for MATLAB providing functions, an app and Simulink model for simulating the model predictive controllers (MathWorks, n.d.d). This toolbox, however, was not used for the purpose of research described in this thesis due to associated costs and custom needs of the project.

5.1.1 Basic Model Predictive Control concept

There are three components involved in the MPC approach, each of them can be defined in various ways and use different algorithms. These components are:

- **Prediction model** is the fundamental part. Good models for MPC should be descriptive enough to capture the most significant dynamics of the system and simple enough for solving optimisation problem. Often there is a trade off between these two criteria, therefore the design of MPC should be approached with these considerations.
- **Objective function** (or cost function) is the function that is minimised using the control action sequence in optimisation algorithm. Depending on the control objective, the cost function has weighting matrices that can be tuned according to the required control effort. For example, the control action can be penalised more to reduce transient or less to improve response speed.
- **Control law** is an algorithm (or functions) that determines the control action to be taken. These control laws are often expressed as a function of the states. An observer is usually included for state estimation in the case not all states are accessible.

Ultimately, MPC is used to find the most optimal control sequence over a future horizon of defined number of steps while avoiding deviations of the output from reference trajectory. A model of the process is used to predict the future evolution of the process to optimise the control signal. At each time step, measurements/data is collected to recalculate and update the current state. This knowledge is used to solve optimisation problem with respect to selected one of more control actions or parameters minimising an objective function. Once optimal control sequence is identified, the first optimal control action is applied, while the remaining items from control sequence are discarded. The idea of how MPC works can be compared to playing chess. Each player first analyses the situation on the board, then predicts possible scenarios together with accompanying

moves. Finally, player chooses to follow one of the predicted scenarios and performs single move using one piece. Another daily example representing MPC concept is driving a car or following a sat-nav. Driver (or sat-nav) constantly evaluates situation on the road to choose best possible action, e.g. follow originally intended route or divert to avoid traffic bottle necks.

Another illustrative example of a car driver demonstrates difference between classic industrial standard Proportional-Integral-Derivative (PID) controller and MPC, see Table 5.1. A driver that is able to control the vehicle, but cannot see through the windscreen, is denied of information lying ahead; the decisions need to be taken based on views from the mirrors only. Secondly, control over the vehicle using PID controller analogy is limited to the fixed gains, the driver for MPC would have a knowledge of the vehicle response to the pedal inputs, which represents model-based approach. Finally, PID controller is normally a SISO system, hence each controlled element would need separate operator or driver, while MPC manages multiple inputs and outputs using one controller, like the driver having control over all vehicle. Note that is example focuses on main features to help understanding of MPC concept and its advtanages over PID.

Table 5.1: Car driver analogy representing main differences between PID controller and MPC.

PID controller	**Model predictive controller**
Cannot 'look ahead' (only looking in the mirrors)	Can make use of future information (road ahead)
Fixed gains	Knowledge of the vehicle response to pedal inputs
Single input, single output (SISO). A controller needed for each actuator.	Multiple input, multiple output (MIMO). One controller manages all actuators.

5.1.2 Chapter overview

This chapter presents the Genetic Algorithm Model Predictive Control (GA MPC) approach developed for the indoor air temperature control to minimise the energy consumption and is the main contribution of this chapter. The method is based on a ventilation through opening the damper blades and forcing the fresh air from the outside in. The idea of ventilation and free cooling is introduced in Section 5.2. The description of the MPC algorithm developed specifically for this project is provided in Section 5.3, whereas more details on each of the components and the GA MPC algorithm are given in Section 5.4. The simulation study in Section 5.5 demonstrates the operation of the algorithm and its ability to find the optimal solution. The final conclusions are provided in Section 5.6.

5.2 Ventilation and free cooling

To understand the use of the damper position control to minimise the operating costs and energy consumption of the heating, ventilation and air conditioning (HVAC) system, it is crucial to introduce the fundamental role of ventilation in the indoor conditions maintenance. Ventilation using outdoor air is generally used to ensure the indoor air quality does not fall below the safety standard for breathing and odour control, and in the same time is a part of the energy efficient strategies. The purposes of ventilation are provided in Table 5.2.

TABLE 5.2: Purposes of ventilation. (Chartered Institution of Building Services Engineers, 2005)

Purpose	**Explanation**
To provide sufficient 'background' ventilation for occupants in terms of air quality for breathing and odour control	Typical rates need to be increased where smoking is permitted or additional sources of pollution are present. Most pollutants originate from sources other than people but in such cases general ventilation has been shown to be much less effective than treating the problems at source: e.g. by specification, cleanliness and local extraction.
To provide natural cooling during the occupied period	Care must be taken to avoid excessive air change rates that may cause draughts or disturb documents. Higher rates may be practicable in spaces occupied transitionally, such as atria. The balance point above which mechanical cooling will provide a more effective solution should be considered.
To provide natural cooling outside the normal occupied period	Night cooling or 'night purging' can remove heat built-up in a structure and its contents, and provide some pre-cooling for the following day. Practical limitations will exist in terms of acceptable secure openable areas in the case of natural ventilation and on duct size and fan energy consumption for ducted mechanical systems.
To exhaust heat and/or pollutants from localised sources or areas	Examples are kitchens, toilets, vending areas and equipment rooms. This enables adjacent areas to be more comfortable with less conditioning of the air. Such systems often need to operate for longer hours than those serving the main spaces, therefore independent extract systems are preferred.
To act as a carrier mechanism for mechanical cooling and/or humidity control	This can be either via an all-air system, in which the air is treated centrally, or via air/water or unitary systems in which the air is recirculated and treated locally.
To prevent condensation within the building fabric **(34)**	Adequate ventilation for condensation control exceeds the minimum rate of fresh air necessary for health and comfort. There is a specific need to address the ventilation of areas where moisture generating activities occur.
To enable the efficient operation of processes	Needs are entirely dependent on the process. Ventilation may be required to ensure safe combustion or to ensure that machinery is maintained within a suitable temperature range, e.g. lift motor rooms.

Additionally, to achieve an acceptable energy efficiency in the indoor air temperature control with regards to air management, it is important to appreciate the diversity

of ventilation strategies, as identified by Chartered Institution of Building Services Engineers (2005):

- **Natural ventilation** Natural ventilation relies on moving air through a building under the natural forces of wind and buoyancy. Wind driven ventilation is realised by cross flow or single or double-sided opening. Buoyancy driven ventilation is reliant on stacks, wind towers, atria rooflights, conservatories, or by façade itself. While this ventilation type is applicable to many types of buildings, industrial buildings might be an exception due to size or specific dimensions.
- **Mechanical ventilation** Mechanical ventilation requires fan power to cause the movement of air through a building; filtration and heating of the air may also take place. Common distribution techniques involve flood, ceiling or wall supply. This ventilation typically builds upon balance between supplying and extracting, which can include both mechanical and natural supply or extract.
- **Comfort cooling** Comfort cooling makes use of the mechanical cooling to maintain control over the maximum air temperature achieved in the indoor space. The supplied air can be incidentally dehumidified during the cooling process.
- **Air conditioning** Term commonly used with or instead of comfort cooling is air conditioning, which means full control over the humidity within the conditioned space as well as temperature control. A more refined variation of air conditioning is close control, which demands more specific or tight temperature and humidity control requirements.
- **Mixed mode system** Mixed mode may be defined as the combination of natural and mechanical ventilation and/or cooling systems. Sub-classes of this ventilation type are contingency designs, allowing for selective additional mechanical ventilation or cooling systems when needed on top of being a naturally ventilated building, such as complementary systems, where natural and mechanical systems are destined for integrated operation, and zoned systems, allowing for different strategies occurring in different parts of the building.

Note that each ventilation purpose or strategy may require a different air supply rate in order to achieve most effective results. For deeper insight on this matter, reader is encouraged to consult (Chartered Institution of Building Services Engineers, 2005) where the subject is comprehensively covered. Since the research presented in this thesis focuses mostly on energy efficient control strategies using mechanical cooling and mechanical ventilation, matters out of this scope will not be discussed.

5.2.1 Free cooling and night cooling

Free cooling is a commonly used term referring to using outside air ventilation without mechanical cooling as a means of cooling a building. While this strategy can support the reduction of the energy use, there are few fundamental limitations present. The first limitation lies in the outdoor air temperature. The energy used to transport the air can be greater than the delivered cooling energy. At worst, the work involved in moving the air (both supply and recirculated) will raise its temperature, resulting in warming of the building. Secondly, without the use of mechanical cooling, the outside air is generally higher than the inside temperature at the times when cooling is most necessary. This can partly be remedied by using overnight cooling, when outdoor air temperatures are lower, however, this is less energy efficient than daytime cooling, and the benefits of natural as opposed to mechanical night cooling would need to be considered. In terms of the night cooling methodology (or night purge), this is a cooling ventilation method used to remove heat built-up within a building and pre-cool the indoor space for the following day (Chartered Institution of Building Services Engineers, 2005). This type of ventilation would typically occur during unoccupied hours. Night cooling could be achieved using natural cooling or supply fan assisted air distribution. Nevertheless, night cooling is often used to limit a temperature rise. The air cools the fabric of the building and the stored cooling is then available the next day to offset heat gains. For this reason, night cooling provides best results with a thermally heavyweight building constructions. The thermal capacity of buildings may be increased (commonly by exposing soffits) to increase the amount of cooling that may be stored. The cooling would also be stored in the items, e.g. furniture, products, machinery, within the building, contributing as a thermal storage mass.

5.3 Model Predictive Control approach for an indoor air temperature control

The indoor air temperature model introduced in Chapter 2 and then expanded to State-dependent Parameter (SDP) form in Chapter 3 is a nonlinear, multi-variable process with state-dependent parameters. Once the energy and/or cost efficiency are identified, adapting MPC for an indoor environment conditions management is straightforward considering the numerous benefits of MPC. In this thesis, energy efficient operation is achieved by minimising heating/cooling operation, heat load shifting and making use of the outdoor. It is carried out through manipulation of the damper blades to switch between fresh and recirculated air intake, free cooling and mechanical ventilation,

variable set-point and pre-heating or pre-cooling. The main components of MPC for the indoor air temperature control problem presented in this thesis are:

- **Model for control** The SDP model of the indoor air temperature has two inputs (ΔT, T_a) and one output (T_r), where the model parameters change with respect to the fan speed, which changes the air mass flow rate m_a, and the position of damper blades u_d. This model is used to predict the indoor air temperature over time in MPC, based on which the control actions are taken.
- **Heating and cooling control method** The Proportional-Integral-Plus (PIP) controller is implemented to evaluate the demand for heating and cooling and decide on the control action ΔT for the SDP model.
- **Cost function** The aim of this function is to minimise the energy consumption or running costs of the heating and cooling. The original function consist of weighted sum of control actions ΔT and penalty for the time spent outside of the dead-band. A variation adds cost per energy unit and provides more valuable results if the cost per unit varies during the day. Note that none of the inputs (ΔT, T_a) is MPC-controlled by means of optimising these control actions, however ΔT depends on the position of damper blades and generates the actual energy cost.
- **Optimisation algorithm** Genetic Algorithm is used to find the optimal position of damper blades. This approach was selected as not many available optimisation methods were found that would meet all of the criteria during development of MPC. The solver is required to handle: integer problem, constraints on input and output and multivariable function.

The advantage of using MPC to solve this energy efficiency control problem lay in its versatility. The MPC design proposed in this chapter does not follow the standard MPC formulation presented in books such as (Camacho & Bordons, 1999) and (Wang, 2009), but rather creates bespoke control method while preserving all of MPC components and general structure. This application-specific solution is the main contribution of this chapter. The details on each of the components are discussed in Section 5.4. The method proposed is fully customised to the application and for this reason the conventional form of the MPC is not introduced in the thesis.

Consider the basic structure of Model Predictive Control shown in Figure 5.1. To demonstrate its operation, an example of a controller optimising an objective function using control sequence of damper position to maintain the indoor air temperature is shown in Figure 5.3. The controller minimises the cost function J over the prediction horizon h_p and makes use of the first output element. This corresponds to the operation

of *Optimisation* block and its output used by the system model in *Model* block. The objective of the function is to minimise the distances between the dead-band boundaries and the predicted output, which is the room temperature. This could be referred to the summation node of *Reference Trajectory* and *Predicted Outputs* resulting in *Future Errors*. In other words, *Future Errors* are a part of the objective function. As a result, the controller produces the vector of predicted room temperature values, *Predicted Outputs*, and the corresponding dampers positions, which is the *Future Inputs*. In principle, the predicted room temperature vector, *Predicted Outputs*, is based on the damper position vector, *Future Inputs*. The prediction horizon h_p is equal to the length of the weather forecast vector T_a. For the future calculations, only the first elements are applied, meaning the room temperature $T_r(k)$, *Past Output*, and its corresponding damper position. This can also be considered as the controller having an insight into the future and takes decision concerning the nearest output only. This procedure is repeated with every new space temperature data sample, hence this type of control is also known as receding horizon control.

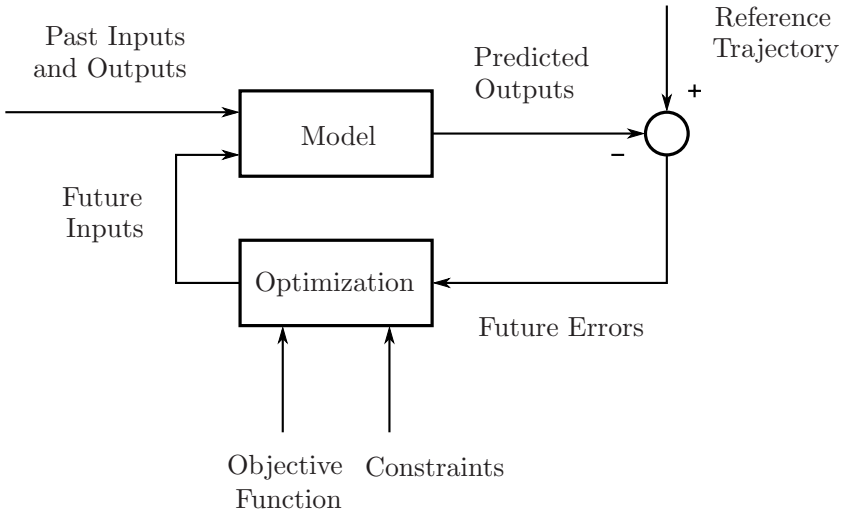

FIGURE 5.1: Basic structure of MPC. (Camacho & Bordons, 1999)

A block diagram in Figure 5.2 shows the designed GA MPC structure incorporating SDP model of the indoor air temperature and PIP controller calculating the heating and cooling demand. The MPC module has a number of inputs required for its operation. T_a is the outdoor air temperature reading fed from the plant, which in real application would be the current outdoor temperature sensor reading, r_h and r_c are the heating and cooling set-points, respectively, $T_{a\,[\,]}$ is a vector of the future outdoor air temperature values (sourced from weather forecast in real application for example), $T_{r\,[\,]}$ is a vector of the future simulated indoor air temperature values, u_d is a damper blades control input, u_h is a heating unit control input, u_c is a cooling unit control input, $u_{d\,[\,]}$ is a vector of the proposed damper blades control input and T_r is the indoor air temperature.

The length of vectors $T_{a\,[]}$, $T_{r\,[]}$ and $u_{d\,[]}$ equals to the control horizon h_p. GA feeds a vector of damper blades positions to the SDP-PIP module and uses it to obtain data needed to calculate ΔT control action employed in the cost J; see the optimisation problem formulated in Section 5.4.3. Once GA converges to the solution and vector $u_{d\,[]}$ resulting in the lowest J is known, the first element of $u_{d\,[]}$ is passed to the SDP-PIP module to calculate the heating and cooling control inputs, which are then fed to the AHU control system.

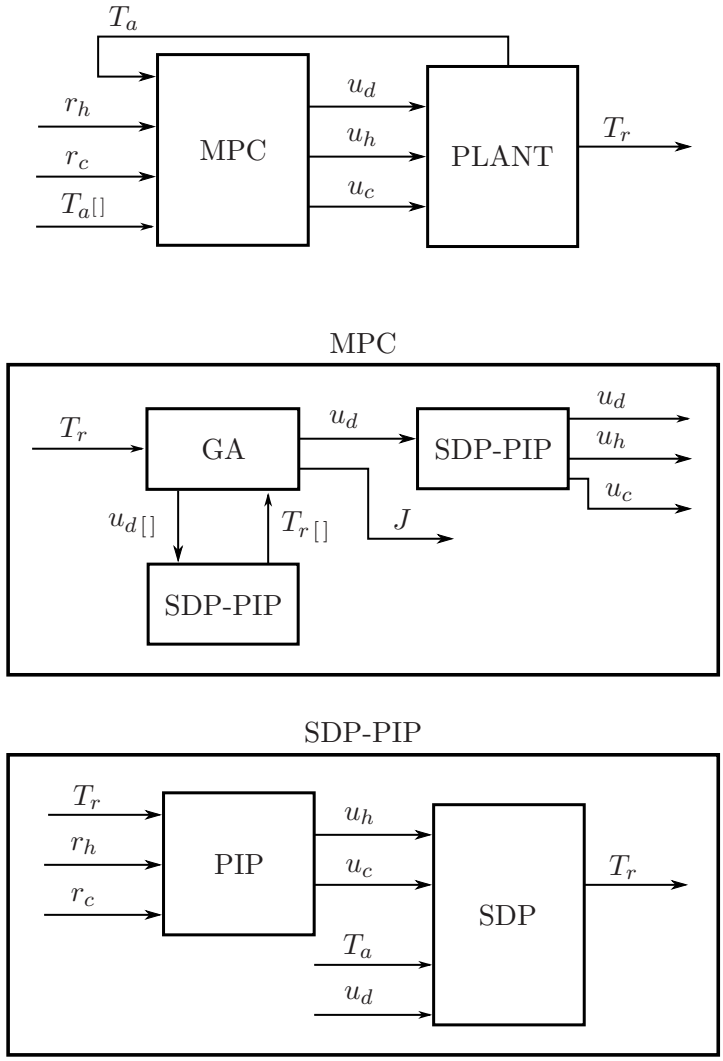

FIGURE 5.2: Model Predictive Control block diagram for energy efficient HVAC system operation using Genetic Algorithm to find the optimal damper position.

5.4 Design of the Model Predictive Controller

Section 5.3 introduced the main components forming the MPC controller to optimise the efficiency of the HVAC system. Each of these components is defined in more details in Sections 5.4.1-5.4.5.

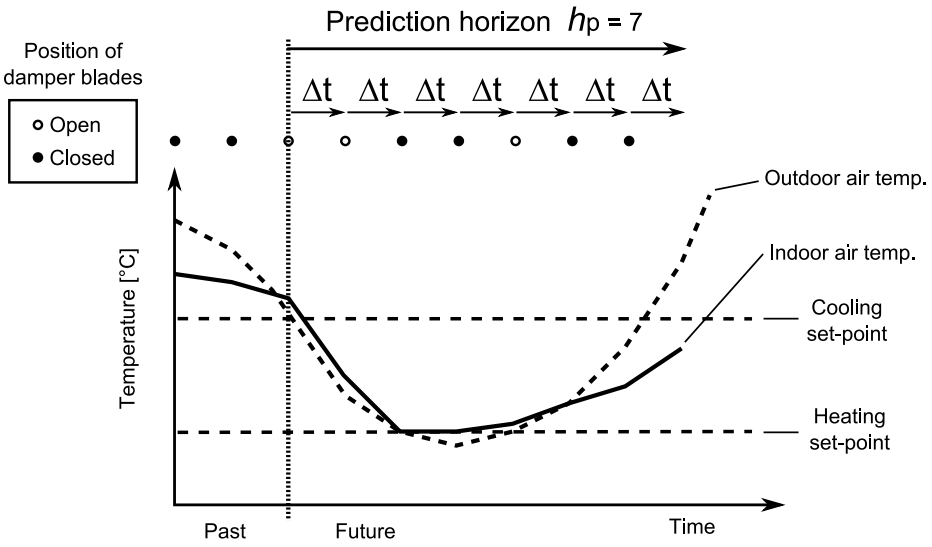

FIGURE 5.3: Indoor air temperature control using MPC: the consecutive positions of damper blades over prediction horizon h_p form the control sequence. Δt denotes the time interval between consecutive samples. (Oswiecinska, 2014)

5.4.1 Model for control formulation

The model structure employed within the MPC controller for simulation of the indoor air temperature over the prediction horizon and used as a part of the SDP-PIP controller has been previously introduced in Chapter 3 and utilised in Chapter 4 to demonstrate the SDP-PIP controller operation. To summarise, the reduced order MISO SDP model for the indoor air temperature control follows Equation (3.4.9) and in NMSS form (see Equations (4.4.12)) is formulated as

$$\begin{aligned}\boldsymbol{x}(k) &= \begin{bmatrix} T_r(k) \\ z(k) \end{bmatrix} = \begin{bmatrix} -\alpha\{m_a(k), u_d(k)\} & 0 \\ \alpha\{m_a(k), u_d(k)\} & 1 \end{bmatrix} \begin{bmatrix} T_r(k-1) \\ z(k-1) \end{bmatrix} \\ &+ \begin{bmatrix} \beta_1\{m_a(k)\} \\ -\beta_1\{m_a(k)\} \end{bmatrix} \Delta T(k-1) + \begin{bmatrix} \beta_2\{m_a(k), u_d(k)\} \\ -\beta_2\{m_a(k), u_d(k)\} \end{bmatrix} T_a(k-1) + \begin{bmatrix} 0 \\ 1 \end{bmatrix} y_d(k) \\ T_r(k) &= \begin{bmatrix} 1 & 0 \end{bmatrix} \boldsymbol{x}(k) \end{aligned} \tag{5.4.1}$$

where the state-dependent model parameters are recalculated at each time step as defined for the model in Equation (3.4.9). For implementation, the model is simplified and reduced to extract the output $T_r(k)$ directly as

$$T_r(k) = \begin{bmatrix} -T_r(k-1) & \Delta T(k-1) & T_a(k-1) \end{bmatrix} \cdot \begin{bmatrix} \alpha\{m_a(k), u_d(k)\} \\ \beta_1\{m_a(k)\} \\ \beta_2\{m_a(k), u_d(k)\} \end{bmatrix} \tag{5.4.2}$$

5.4.2 State-Dependent Parameter-Proportional-Integral-Plus controller

The heating and cooling demand is determined by the PIP controller utilising the following control law from Equation (4.4.11):

$$\Delta T_c(k) = \Delta T(k-1) - \begin{bmatrix} f_0\{\chi(k)\} & -k_I\{\chi(k)\} \end{bmatrix} \cdot \begin{bmatrix} T_r(k) - T_r(k-1) \\ r_c - T_r(k) \end{bmatrix} \tag{5.4.3a}$$

$$\Delta T_h(k) = \Delta T(k-1) - \begin{bmatrix} f_0\{\chi(k)\} & -k_I\{\chi(k)\} \end{bmatrix} \cdot \begin{bmatrix} T_r(k) - T_r(k-1) \\ r_h - T_r(k) \end{bmatrix} \tag{5.4.3b}$$

with constraints heating and cooling as $0 \leq \Delta T_h \leq \Delta T_{max}$ and $\Delta T_{min} \leq \Delta T_c \leq 0$, where ΔT_{max} and ΔT_{min} represent the maximum outputs of the heating and cooling unit, respectively. Whenever the indoor air temperature is within the dead-band, no heating and cooling can be requested. The elements of the SVF control gains vector are calculated at each time step as follows:

1. Following pole assignment method for the first order model in Section 4.2.4.1, initialise matrices $\boldsymbol{S}$ and $\boldsymbol{b}$ as

$$\boldsymbol{S} = \begin{bmatrix} \beta_1(k-1) & \beta_1(k-1) \\ -\beta 1(k-1) & 0 \end{bmatrix} \boldsymbol{b} = \begin{bmatrix} d_1 - (\alpha(k-1) - 1) \\ d_2 - (0 - \alpha(k-1)) \end{bmatrix}$$

2. Obtain the control gains vector $\boldsymbol{k}^T$ from

$$\boldsymbol{S} \cdot \boldsymbol{k}^T = \boldsymbol{b}$$

3. Extract control gains from $\boldsymbol{k}^T$

$$f_0 = \boldsymbol{k}(1)$$
$$k_I = \boldsymbol{k}(2)$$

5.4.3 Optimisation problem formulation

The research proposed in the thesis aims to develop energy efficient control approach for the indoor thermal process. The optimisation problem is formulated as

$$\begin{aligned} \min_{u_d \in [0,1]} \quad & J = \sum_{i=1}^{h_p} |\Delta T(i)| + w_{out} \cdot r_{out} \\ \text{subject to} \quad & r_h \leq T_r(i) \leq r_c,\ i = 1, \ldots, h_p. \end{aligned} \tag{5.4.4}$$

where

- J is the objective function to be minimised over the h_p-variable vector ΔT,
- r_{out} is the number of T_r samples recorded outside of the dead-band,
- w_{out} is the weight corresponding to r_{out} element,
- $r_h \leq T_r(i) \leq r_c$ are the inequality constraints defining the required indoor air temperature boundaries,

and i represent the current time instance. The cost function consists of two elements: a sum of heating and cooling loads applied over prediction horizon, which represents the energy integrator, and weighted number of instances while the indoor air temperature did not meet the criteria defined by the inequality constraints. Note that these criteria are soft constraints as the indoor air temperature does go out of the dead-band triggering heating or cooling action, depending on the outdoor conditions. However, it is desired that the indoor air temperature remains within the dead-band, yet it is not always possible without activating heating and cooling units within the AHU. Penalising time spent out of the dead-band through r_{out} is motivated by the fact, that there is a thermal mass that includes all items within the building and the building fabric itself. The longer the indoor air temperature requirements are not met, the more time for the goods and fabric to absorb the heat (or have it removed for $T_r < r_h$) and store it. This is undesirable as it prolongs the time for the indoor air temperature to be brought within the dead-band limits. The building thermal storage mass utilisation for the heating and cooling benefits is summarised by Smarter Homes (n.d.), which explains how to use material properties to absorb more heat or prevent it. To avoid penalising time spent out of the dead-band and generate the cost exclusively based on the heating and cooling units loads, the weight can be set to zero $w_t = 0$. Finally, the overall cost J in normalised to unify the cost value regardless of the sampling interval chosen using the following equation

$$J = \frac{J}{sph}, \quad sph = \frac{60}{t_s/60} \tag{5.4.5}$$

where sph denotes the number of samples per hour subjected to the sampling interval t_s. Following this formula allows obtain the cost values that are comparable even if simulations were performed at different sampling intervals. Additional measure is focused on evaluating the temperature changes only and in normalised form is

$$S_{\Delta T} = \sum_{i=1}^{h_p} |\Delta T(i)|/sph \tag{5.4.6}$$

The variations of the cost function could account for the energy consumption based on energy cost per unit, e.g. if the energy is cheaper at night time. It could refer only to heating and cooling unit running costs, but could also cover supply fan unit, where the cost increases together with fan speed. Alternatively, it could also include penalty on rate of change between consecutive control actions on heating, cooling, fan speed or damper position.

5.4.4 Solver

The optimisation problem defined in Section 5.4.3 is solved using Genetic Algorithm belonging to the larger class of evolutionary algorithms (EA) (Goldberg, 1989; Janiak & Lichtenstein, 2011). The choice of this the nature-inspired method is motivated by the capabilities of GA to find solutions to various difficult problems with constraints in a metaheuristic manner, outperforming classical methods. As a method that relies on natural selection and additional methods, such as mutation and crossover, this solver can provide the best optimal solution beyond local minimum and maximum solutions. To achieve the best results, it is necessary to configure GA by tuning the parameters defining its performance and operation. The most important parameters configurable by the user in the GA method provided within MATLAB toolbox (MathWorks, n.d.a) contents are:

- Population size - specifies the amount of members within a population per each generation.
- Generations - specifies the number of iterations before the algorithm will stop.
- Elite size - defines how many members of a population with the best score is preserved for the next generation in an unchanged form. The default value is 0.05, however, for integer problems it is recommended to choose bigger value to improve algorithm performance.
- Crossover fraction - defines how the composition of a member is exchanged. The higher the crossover fraction, the lower the mutation rate, therefore for integer problems it is recommended to use values above 0.8 (default).
- Initial population - specifies the members of the initial population, which otherwise are randomly created.
- Variables - specifies the number of variables per each member. In this project it is assumed that by default the number of variables is equal to control horizon $h_c = h_p$, i.e. the number of samples over which the indoor air temperature is forecasted.

- Constraints on input and output - allows to specify upper and lower limit on the input and output. For the input u_d the limits are 0 and 1, and for the output the limits are defined by the heating and cooling set-points.

Note that not all of the default parameters for the GA can be changed, if an integer problem is to be solved as the basic algorithm is modified; see (MathWorks, n.d.c) for using the GA to solve mixed integer problems. The significant difference is that the creation, crossover and mutation functions enforce variables to be integers. Also, the genetic algorithm attempts to minimise a penalty function, not the fitness function; the penalty function includes a term for infeasibility. Note also that the number of variables, or the prediction horizon, is strictly dependent on the future outdoor air temperature information, i.e. h_p is limited to the last point in time at which the forecasted outdoor air temperature is known. Finally, the tuning of the GA parameters and settings requires some insight into scenario for which the problem is solved. For example, using GA to solve a simple problems will lead to convergence of the optimal solution in much less iterations, i.e. require lesser number of generations for a stopping criteria than a more complicated problem. The selected GA setup is a compromise than performing better in certain scenarios and performing lesser for others. Finally, regardless of the initial setup, the fundamental operation of GA lies on random process, therefore the results may not be repeatable from run to run.

5.4.5 Algorithm for simulation

The MPC algorithm for simulation using MATLAB for the implementation and operation of the proposed method is presented in Figure 5.4. The algorithm operates in the following manner:

1. **LOAD Control setup, GA setup** The following parameters are initialised:
   - Control setup: poles for the PIP controller D, heating and cooling set-points r_h and r_c, respectively, prediction horizon h_p and control horizon h_c.
   - GA setup: population size, number of generations, elite size, crossover fraction, objective function, number of variables (equal to control horizon) and input constraints (damper position between 0 and 1).
2. **LOAD Model inputs** Initialisation of the outdoor air temperature vector T_a (last, current and future samples), the indoor air temperature T_r (last and current sample), the damper position u_d (last, current and future samples) and the heating load within the AHU ΔT (previous sample).

3. **LOAD Initial population** By default, initialisation of the initial population member is random. Initialising some of the members with u_d vector containing only zeros for closed damper position helps to encourage faster convergence toward optimal solution. Similarly, further iterations might also be initialised with the last most optimal u_d vector shifted by one sample to improve performance and the end results of the GA.

4. **RUN GA to find optimal damper position** Genetic algorithm is run to find the vector of damper blades position that is related to the lowest cost J.

5. **RETURN Vector u_d for the best J** The optimal damper blades position vector is returned.

6. **SAVE $u_d(1)$ as current damper position** The damper position corresponding to the current time interval is extracted and applied as the control input to the mixing box within AHU.

7. **SIMULATE T_r using SDP-PIP** The indoor air temperature is simulated using the SDP model to obtain the output T_r for the next time step $k+1$. It represents shifting taking measurements of the indoor air temperature one sample later. PIP controller is used to calculate the control input for heating and cooling units.

8. **REPEAT for next time step?** To repeat search for the next optimal damper position for the next sample, i.e. after select time interval t_s, practising receding horizon technique, follow YES. To finish operation of the MPC algorithm, follow NO.

9. **PASS Latest inputs and output** Recent simulated (recorded) values of the system inputs and output obtained in step 7 are passed to initialise another iteration of the MPC algorithm run.

The subalgorithm covering GA operation in step 4 expanded in block **Run GA** consists of the following steps:

1. **LOAD Vector u_d from population** Initialise vector u_d with a member of a population.

2. **SIMULATE T_r using SDP-PIP** The indoor air temperature is simulated using SDP model to forecast the output T_r over h_p samples using provided u_d vector.

3. **RETURN Vector T_r, vector ΔT** The indoor air temperature values and the heating and cooling unit loads are extracted and passed into cost function.

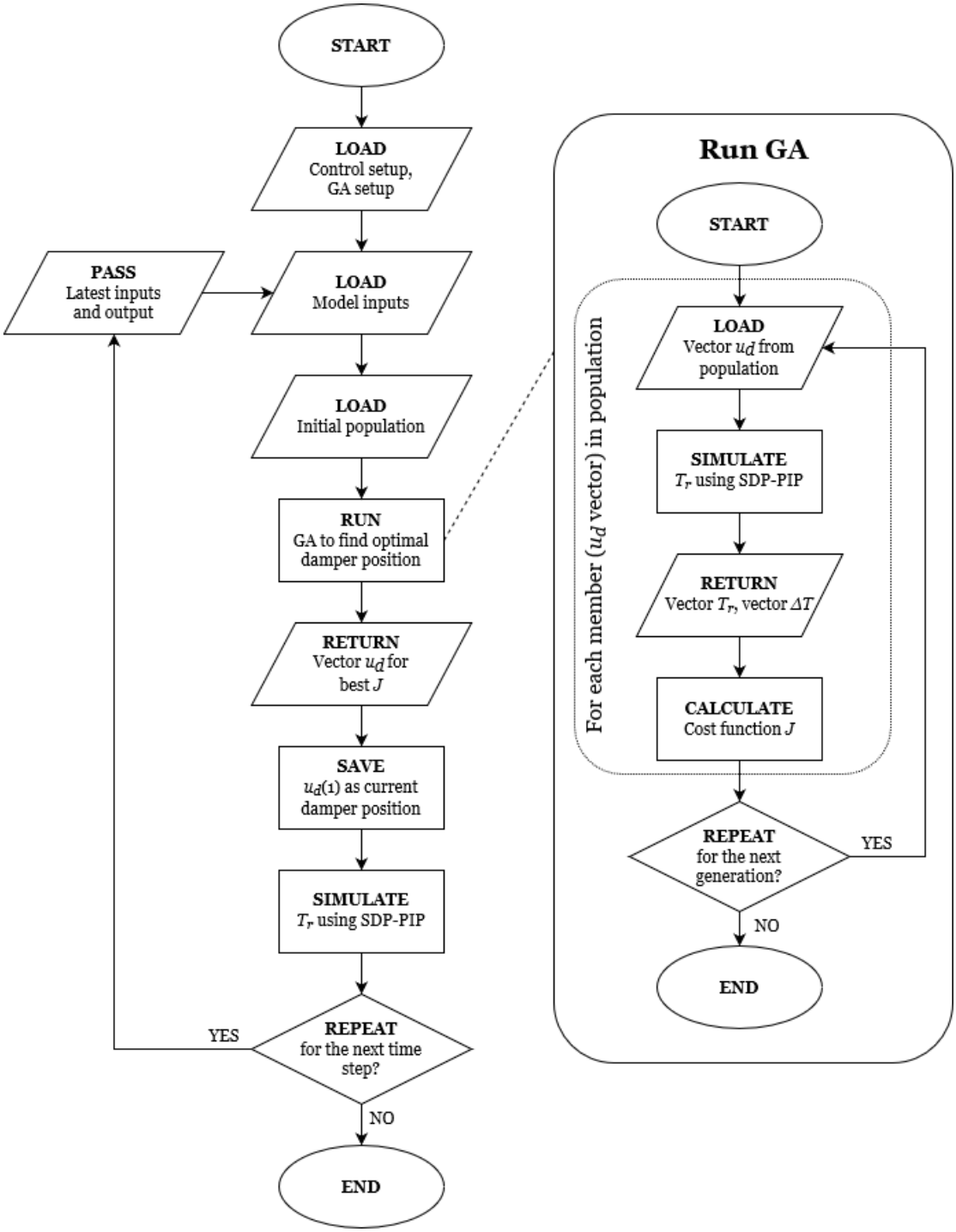

FIGURE 5.4: MPC algorithm flowchart.

4. **CALCULATE Cost function *J*** The overall cost J over prediction horizon is calculated based on the indoor air temperature provided together with heating and cooling units load. The set-point values for heating and cooling are used to evaluate the time spent outside of the dead-band.

5. **REPEAT for the next generation?** To repeat the cycle for the next generation,

provided the stopping criteria is not met, follow YES. To stop the algorithm, follow NO.

Steps 1-4 are repeated for each member within the population, until cost function has been evaluated for all of the members. The default operation of the GA algorithm as implemented in MATLAB (MathWorks, n.d.b) is summarised in the following steps:

1. The algorithm begins by creating a random initial population.
2. The algorithm then creates a sequence of new populations. At each step, the algorithm uses the individuals in the current generation to create the next population. To create the new population, the algorithm performs the following steps:
   (a) Scores each member of the current population by computing its fitness value. These values are called the raw fitness scores.
   (b) Scales the raw fitness scores to convert them into a more usable range of values. These scaled values are called expectation values.
   (c) Selects members, called parents, based on their expectation.
   (d) Some of the individuals in the current population that have lower fitness are chosen as *elite*. These elite individuals are passed to the next population.
   (e) Produces children from the parents. Children are produced either by making random changes to a single parent-*mutation*-or by combining the vector entries of a pair of parents-*crossover*.
   (f) Replaces the current population with the children to form the next generation.
3. The algorithm stops when one of the stopping criteria is met.

5.5 Simulation study

5.5.1 First principles Genetic Algorithm Model Predictive Control simulation with sine wave input

Demonstration of the MPC algorithm on a simple scenario with sine wave T_a input is presented in this section, where a single run of the MPC is performed and the results present the forecasted scenario. The following settings are used: $t_s = 15\,\text{min}$, control horizon is 1 day and $h_p = h_c$, $w_{out} = 0.25$, population size 120, number of generations 50, elite size 10% of population size, crossover fraction 0.9 and 20% of the population is initialised with vectors $u_d(i) = 0 \; \forall \; i = 1, \ldots h_p$. The results are presented in Figure

5.5, where the outcome of a single MPC run provided the values of $\Delta T(i)$ from the PIP controller with a dead-beat setup and $u_d(i)$ values are determined by the GA. The control dead-band is defined by the heating and cooling set-points $r_h = 18°\text{C}$ and $r_c = 21°\text{C}$. The fan speed has been set manually to operate at 75% of the maximum capacity at all times for simplification. In real application, however, the fan speed typically depends on the heating and cooling demand or as set by the user.

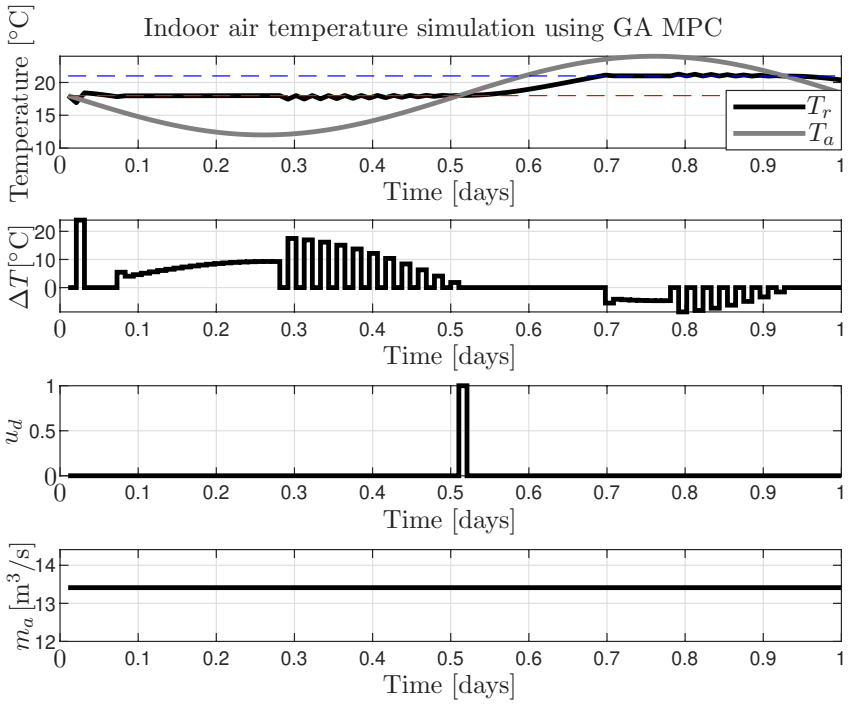

FIGURE 5.5: MPC prediction of the indoor air temperature for $h_p = 1\,\text{day}$. The poles of the PIP controller are at 0. The set-points $r_c = 21°\text{C}$ and $r_h = 18°\text{C}$ are marked with dash line. The air mass flow rate is set to $m_a = 13.41\,\text{m}^3/\text{s}$, which is 75% of the maximum fan speed.

GA is able to converge to the best optimal solution (or the best score close to the best optimal solution), which is demonstrated in the position of damper blades being closed almost all the time; the best solution in the case considered would be to keep the dampers closed over all prediction length. The cost function for the prediction presented in Figure 5.5 is $J = 95.8766$ and the normalised sum of heating and cooling is $S_{\Delta T} = 92.9391$. Note that there is one sample, where the damper blades are in open position. It has been observed that in majority of the situations, where single spikes $u_d(k+i) = 1$, $i \in [1, h_p]$ the damper position does not influence the dynamics enough to generate (noticeable) changes in the cost function. This could happen when the indoor air temperature is within the dead-band and the air mass flow rate is low or 0, for example. Secondly, if the MPC algorithm is run at regular time intervals, the damper position vector will be recalculated every time and only first value is applied, rejecting the rest, minimising the chances of spikes being applied by the HVAC control system. To

mitigate unnecessary spikes and improve the results, additional smoothering algorithm can be implemented. Such algorithm at a basic level would penalise changes in u_d. Alternatively, it would have to smooth spikes in u_d and recalculate the cost function J to make sure that the cost didn't increase; otherwise, spikes would remain untouched. For comparison, the same scenario, but with dampers closed through all simulation has $J = 95.8782$ and $S_{\Delta T} = 92.9407$. While these are values are slightly higher than for the results for Figure 5.5 scenario, the difference is negligible.

Observing the indoor air temperature in Figure 5.5 and the inputs, it can be seen that if the heating set-point was decreased temporary around 0.4-0.5 day, it would take more time for the indoor air temperature to reach and exceed the cooling set-point. The additional delay could also be caused by opening the damper blades around this period and close once the outdoor air temperature matches the indoor air. Adaptive set-point strategy proposed by Oswiecinska (2014) temporary compromises the default indoor conditions within agreed boundaries, but can lower the energy consumption in the long-term.

Another simulation was performed using the settings, but with poles at 0.2. The results are presented in Figure 5.6.

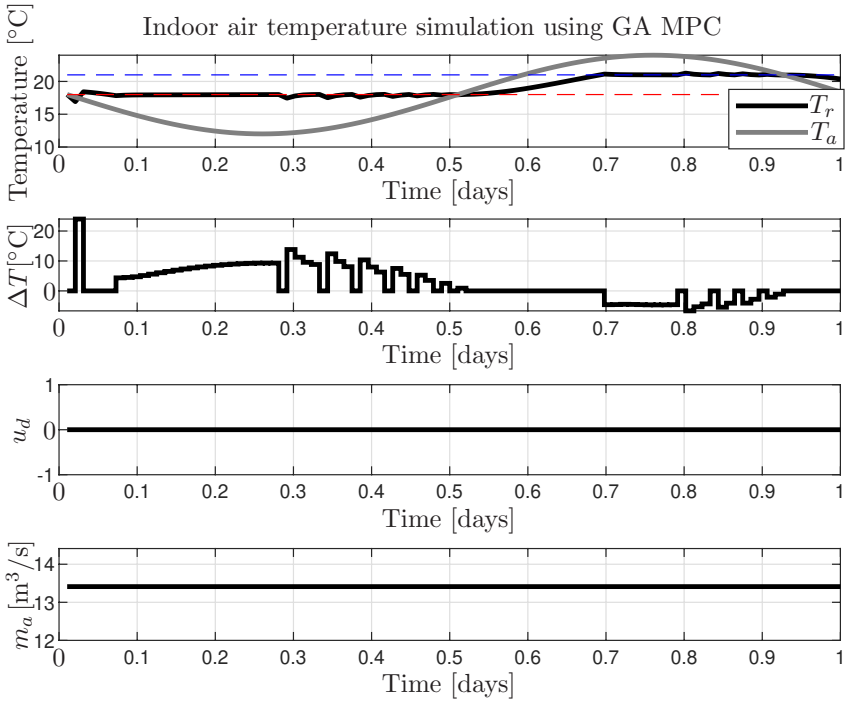

FIGURE 5.6: MPC prediction of the indoor air temperature for $h_p = 1$ day. The poles of the PIP controller are at 0.2. The set-points $r_c = 21°$C and $r_h = 18°$C are marked with dash line. The air mass flow rate is set to $m_a = 13.41\,\mathrm{m}^3/\mathrm{s}$, which is 75% of the maximum fan speed.

The cost function for the prediction presented in Figure 5.6 is $J = 96.5457$ and $S_{\Delta T} = 93.1082$. Note that the cost J is higher than for the dead-beat controller, however, the difference is less than 1%. Similarly, the overall heating and cooling load is lower, hence more energy is consumed. This relates directly to the PIP controller design and pole assignment described in Section 4.2.3 and corresponding observations gathered in Section 4.5.

To demonstrate briefly the importance of the number of generations, consider the results presented in Figure 5.7, where the number of generations was set to 20. The function for the prediction presented in Figure 5.6 is $J = 95.8766$ and $S_{\Delta T} = 92.9391$. While these values are not that much different than in previous demonstrations in Figures 5.5 and 5.6, it is observed that there is a higher tendency to obtain spikes in the u_d vector. This phenomena has its roots in the way the GA works, especially crossover function: initial population consists mostly of randomly created members, taking values either 0 or 1 for the member's variables. As the number of iterations goes up, the random spikes are less likely to be carried over to the next generations, therefore increasing chances for smoother and more optimal solution.

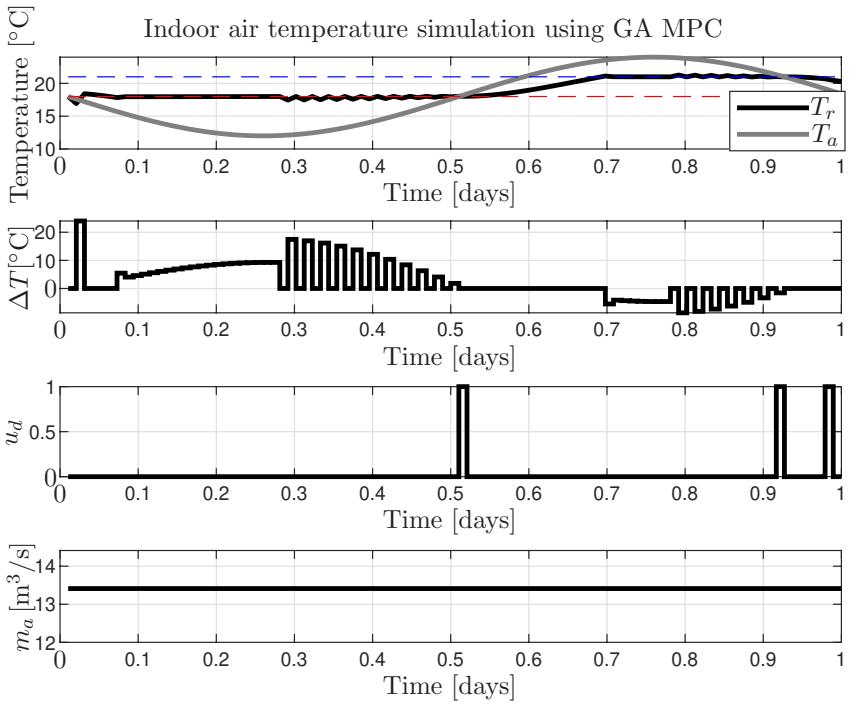

FIGURE 5.7: MPC prediction of the indoor air temperature for $h_p = 1$ day. The poles of the PIP controller are at 0. The set-points $r_c = 21$°C and $r_h = 18$°C are marked with dash line. The air mass flow rate is set to $m_a = 13.41\,\mathrm{m}^3/\mathrm{s}$, which is 75% of the maximum fan speed.

5.5.1.1 Model Predictive Control simulation

Simulations of the MPC operation over a period of one day has been performed to simulate the real operation of the MPC controller. On the contrary to simulation study from Section 5.5.1, where the results provided are a forecast of the inputs and outputs for a single MPC run, this section demonstrates the control actions taken as recalculated and proposed by the MPC algorithm at each time step as detailed in the flowchart diagram in Figure 5.4. The following settings are used: $t_s = 15\,\text{min}$, control horizon is 1 day and $h_p = h_c = 96$ samples, $w_{out} = 0.25$, population size 120, number of generations 50, elite size 10% of population size, crossover fraction 0.9 and 20% of the population is initialised with vectors $u_d(i) = 0 \; \forall \; i = 1, \ldots h_p$. The results of four consecutive simulations run with the same initial settings are presented in Figures 5.8-5.11. At each time step the values of $\Delta T(i)$ are determined by the PIP controller with dead-beat setup and $u_d(i)$ values are determined by the GA. The control dead-band is defined by the heating and cooling set-points $r_h = 18°\text{C}$ and $r_c = 21°\text{C}$. The fan speed has been set manually to operate at 75% of the maximum capacity at all times.

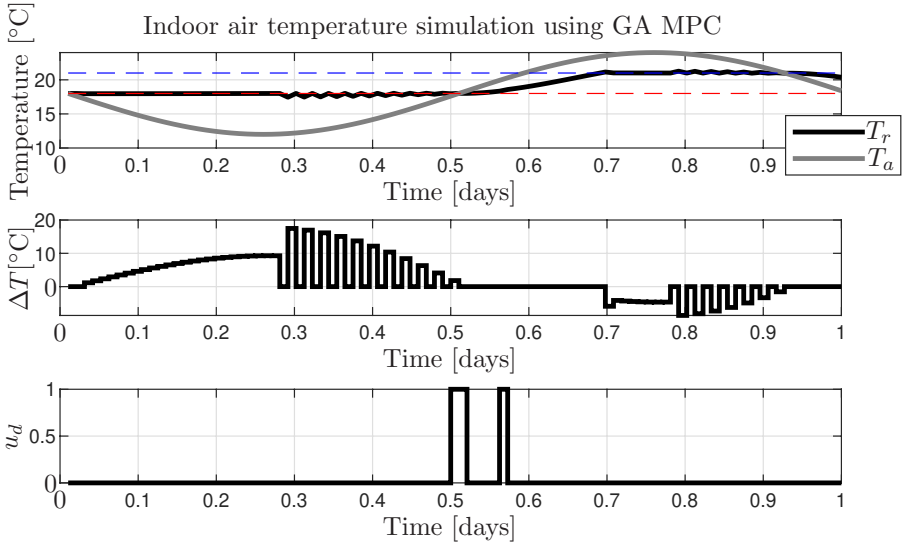

FIGURE 5.8: MPC prediction of the indoor air temperature for $h_p = 1\,\text{day}$ over 1 day of simulation. The poles of the PIP controller are at 0. The set-points $r_c = 21°\text{C}$ and $r_h = 18°\text{C}$ are marked with dash line. The air mass flow rate is set to $m_a = 13.41\,\text{m}^3/\text{s}$, which is 75% of the maximum fan speed.

Analysing the results presented in Figures 5.8-5.11 and the summary of the performance measures for each of the four simulations provided in Table 5.3, it has been observed that the outcomes of the simulation are very similar in values of the control inputs and the cost J. The values of performance measures in each column of Table 5.3 do not differ more than 0.4 from each other. Therefore, it is concluded that the GA MPC is able to provide consistent results despite the stochastic characteristics of the GA. Considering the values from Table 5.3 and comparing to the results provided in

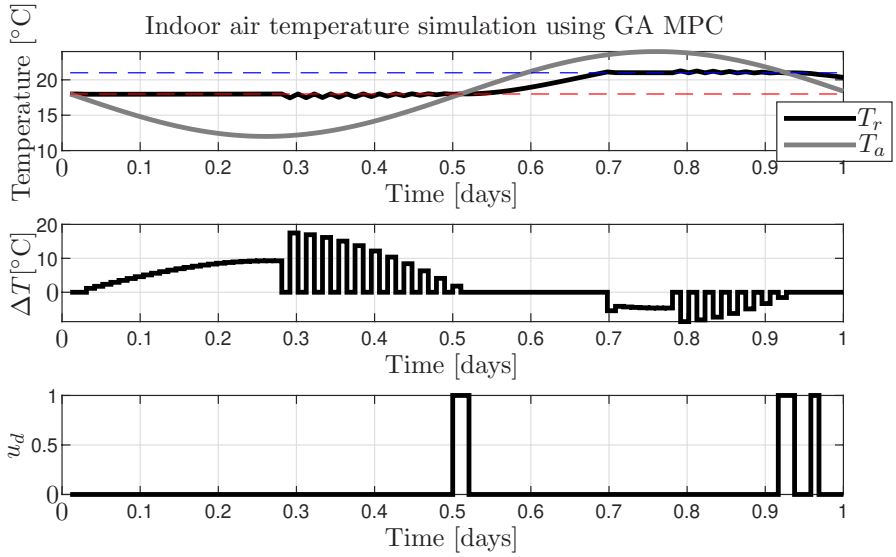

FIGURE 5.9: MPC prediction of the indoor air temperature for $h_p = 1$ day over 1 day of simulation. The poles of the PIP controller are at 0. The set-points $r_c = 21°\text{C}$ and $r_h = 18°\text{C}$ are marked with dash line. The air mass flow rate is set to $m_a = 13.41\,\text{m}^3/\text{s}$, which is 75% of the maximum fan speed.

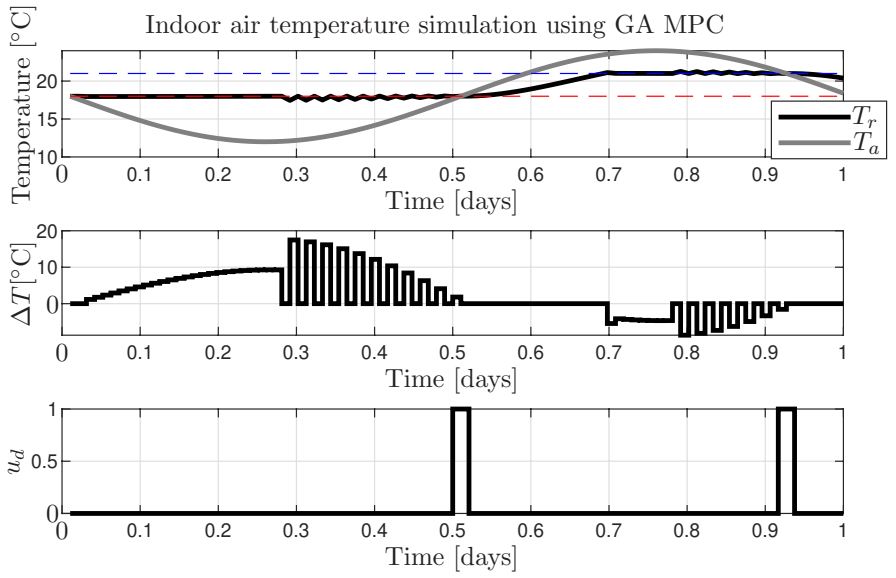

FIGURE 5.10: MPC prediction of the indoor air temperature for $h_p = 1$ day over 1 day of simulation. The poles of the PIP controller are at 0. The set-points $r_c = 21°\text{C}$ and $r_h = 18°\text{C}$ are marked with dash line. The air mass flow rate is set to $m_a = 13.41\,\text{m}^3/\text{s}$, which is 75% of the maximum fan speed.

Section 5.5.1, which were higher by not more than 6, it is concluded that the GA MPC operates correctly and is able to find the optimal solution. It is achieved by means of minimising the heating and cooling loads and the time spent outside of the dead-band. It is worth noting that the results of the simulations 2 and 3 (Figures 5.9 and 5.10) performed exactly in the same way from the cost point of view. The simulation 2, however, differs from the simulation 3 by the damper blades position set to open for one time interval more. Since during this particular time interval the indoor was safely within

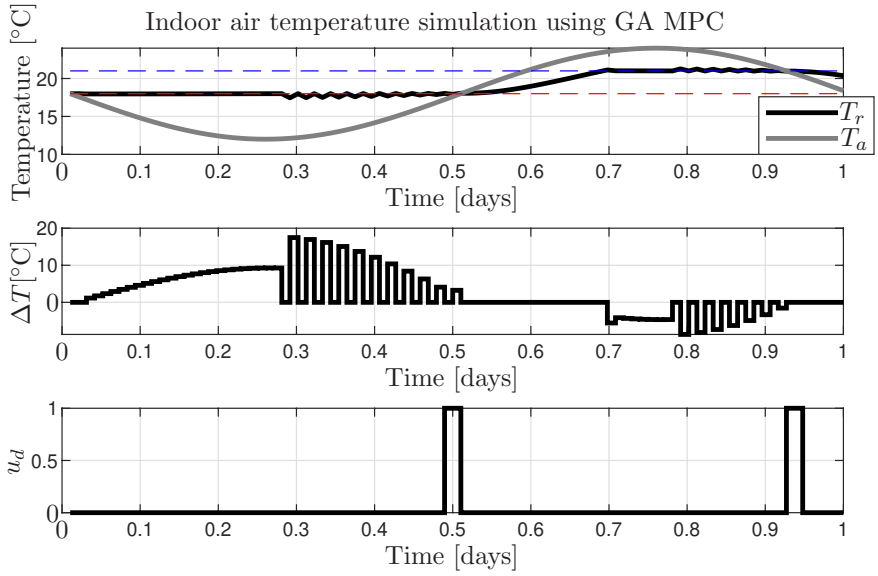

FIGURE 5.11: MPC prediction of the indoor air temperature for $h_p = 1$ day over 1 day of simulation. The poles of the PIP controller are at 0. The set-points $r_c = 21°\text{C}$ and $r_h = 18°\text{C}$ are marked with dash line. The air mass flow rate is set to $m_a = 13.41\,\text{m}^3/\text{s}$, which is 75% of the maximum fan speed.

the dead-band, it did not trigger changes in the temperature of the air supplied.

TABLE 5.3: The performance measures for the GA MPC simulation for four scenarios with identical setup.

Simulation	**Figure**	J	$S_{\Delta T}$
1	5.8	91.7181	88.5931
2	5.9	91.6053	88.4803
3	5.10	91.6053	88.4803
4	5.11	91.9945	88.8695

5.5.2 First principles simulation with real data - 1 day prediction

Demonstration of the MPC algorithm on a real data-based scenario for the input T_a is presented in this section, where a single run of the MPC is performed and the results present the forecasted scenario. The simulation setup is the same as for study with sine wave input from Section 5.5.1. The outdoor air temperature data was collected by the control system for the warehouse located in Midlands, UK, and belongs to the same set that was used in the previous chapters. The results are presented in Figures 5.12, where the outcome of a single MPC run provided the values of $\Delta T(i)$ from the PIP controller with a dead-beat setup and $u_d(i)$ values are determined by the GA.

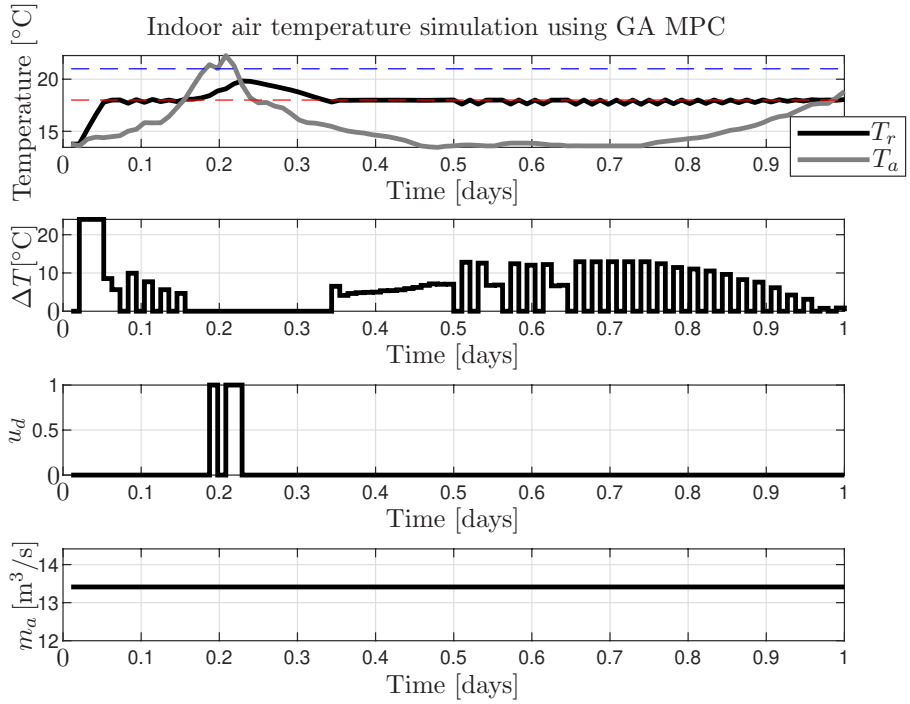

FIGURE 5.12: MPC prediction of the indoor air temperature for $h_p = 1$ day for spring scenario. The poles of the PIP controller are at 0. The set-points $r_c = 21°\text{C}$ and $r_h = 18°\text{C}$ are marked with dash line. The air mass flow rate is set to $m_a = 13.41\,\text{m}^3/\text{s}$, which is 75% of the maximum fan speed.

The results corresponding to Figure 5.12 are $J = 113.2686$ and $S_{\Delta T} = 110.0811$. For comparison, the simulation with the same outdoor air input as in Figure 5.12, but results for the damper blades in a closed position scenario over the prediction horizon are $J = 113.9906$ and $S_{\Delta T} = 110.7406$. Note that in standard control approach the dampers would remain closed during this period. While these results are not much different from each other (the discrepancy is less than 1), it demonstrates again that the GA is able to find optimal solution with a lower cost if there are cooling or heating capabilities in the outdoor air utilisation.

5.5.3 First principles recursive simulation with real data over 1 day

Simulations of the MPC operation over a period of one day has been performed to simulate the real operation of the MPC controller. On the contrary to simulation study from Section 5.5.2, where the results provided are a forecast of the inputs and outputs for a single MPC run, this section demonstrates the control actions taken as recalculated and proposed by the MPC algorithm at each time step as detailed in the flowchart diagram in Figure 5.4. Performing a simulation over a period of one day allows to observe the GA MPC controller operation as a snapshot of its performance. The following settings are used: $t_s = 15\,\text{min}$, control horizon is 1 day and $h_p = h_c = 96$ samples,

$w_{out} = 0.25$, population size 120, number of generations 50, elite size 10% of population size, crossover fraction 0.9 and 20% of the population is initialised with vectors $u_d(i) = 0 \; \forall \; i = 1, \ldots h_p$. The results of four consecutive simulations run with the same initial settings are presented in Figures 5.13-5.14. At each time step the values of $\Delta T(i)$ are determined by the PIP controller with dead-beat setup and $u_d(i)$ values are determined by the GA. The control dead-band is defined by the heating and cooling set-points $r_h = 18°\text{C}$ and $r_c = 21°\text{C}$. The fan speed has been set manually to operate at 75% of the maximum capacity at all times.

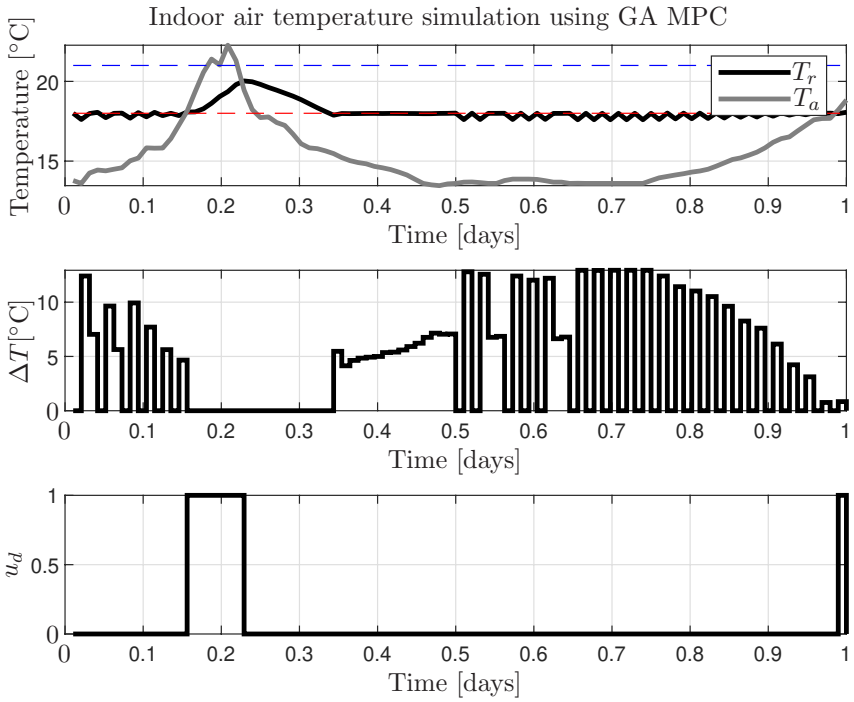

FIGURE 5.13: MPC prediction of the indoor air temperature for $h_p = 1$ day over 1 day of simulation. The poles of the PIP controller are at 0. The set-points $r_c = 21°\text{C}$ and $r_h = 18°\text{C}$ are marked with dash line. The air mass flow rate is set to $m_a = 13.41\,\text{m}^3/\text{s}$, which is 75% of the maximum fan speed.

The summary of the performance measures for each of the four consecutive simulations presented in Figures 5.13-5.15 are provided in Table 5.4. The results obtained demonstrate expected performance, where the control actions proposed and applied by the algorithm lower the cost, therefore improve the energy efficiency of the HVAC system. Comparing the results from Table 5.4 with the cost for scenario with damper blades in closed position, it can be observed that there is a benefit in this particular scenario to variate the damper blades position. The results obtained demonstrate that the GA MPC is able perform the HVAC system control in an energy efficient manner. While more studies is needed to confirm how well it can perform, the initial assumption regarding its capabilities of finding cost-optimal control actions as the default operation is confirmed.

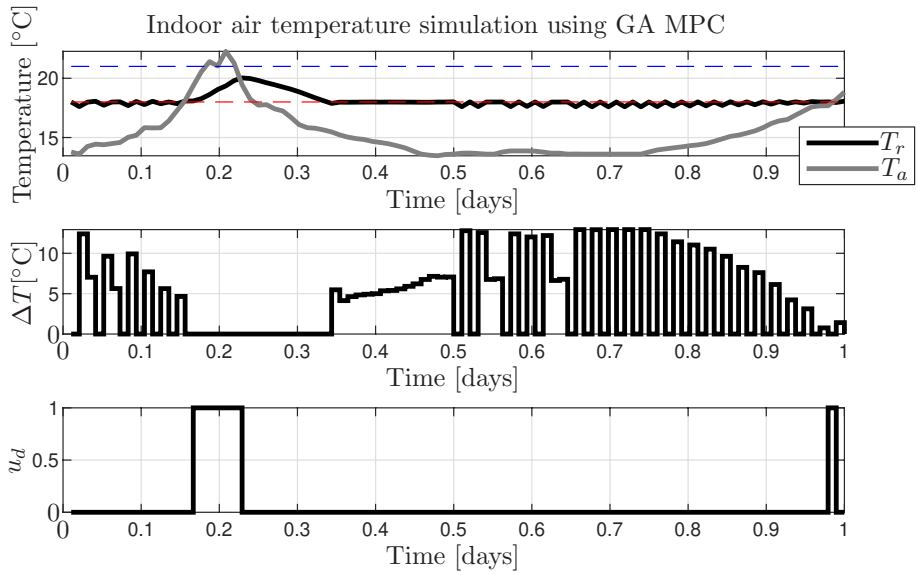

FIGURE 5.14: MPC prediction of the indoor air temperature for $h_p = 1$ day over 1 day of simulation. The poles of the PIP controller are at 0. The set-points $r_c = 21°C$ and $r_h = 18°C$ are marked with dash line. The air mass flow rate is set to $m_a = 13.41\,\mathrm{m}^3/\mathrm{s}$, which is 75% of the maximum fan speed.

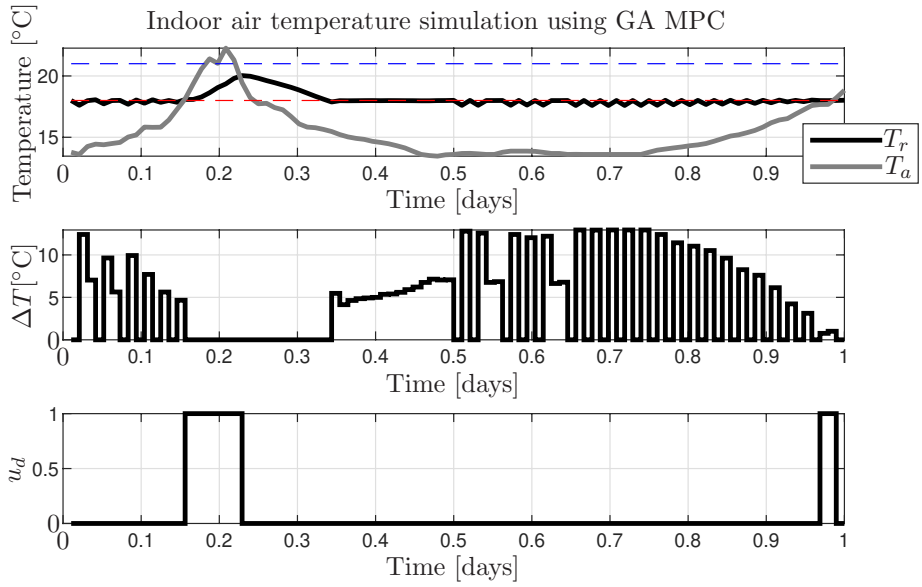

FIGURE 5.15: MPC prediction of the indoor air temperature for $h_p = 1$ day over 1 day of simulation. The poles of the PIP controller are at 0. The set-points $r_c = 21°C$ and $r_h = 18°C$ are marked with dash line. The air mass flow rate is set to $m_a = 13.41\,\mathrm{m}^3/\mathrm{s}$, which is 75% of the maximum fan speed.

5.5.4 First principles recursive simulation with real data over 3 days

By extending the simulation time to three days it is possible to observe the GA MPC controller operation throughout the whole day-to-day cycle over three consecutive days. Therefore, a set of simulations of the MPC operation over a period of three days has been performed to simulate the real operation of the MPC controller. The control actions

TABLE 5.4: The performance measures for the GA MPC simulation for four scenarios with identical setup.

Simulation	**Figure**	J	$S_{\Delta T}$
1	5.13	100.0204	96.9579
2	5.13	100.0204	96.9579
3	5.14	100.1655	97.103
4	5.15	100.0622	96.9997

taken are recalculated and proposed by the MPC algorithm at each time step as detailed in the flowchart diagram in Figure 5.4. The following settings are used: $t_s = 15\,\text{min}$, control horizon is 1 day and $h_p = h_c = 96$ samples, $w_{out} = 0.25$, population size 120, number of generations 50, elite size 10% of population size, crossover fraction 0.9 and 20% of the population is initialised with vectors $u_d(i) = 0\ \forall\ i = 1, \ldots h_p$. The results of three simulations are presented in Figures 5.16, 5.18 and 5.20 with the respective closed damper position simulations in Figures 5.17, 5.19 and 5.21. At each time step the values of $\Delta T(i)$ are determined by the PIP controller with dead-beat setup and $u_d(i)$ values are determined by the GA. The control dead-band is defined by the heating and cooling set-points provided under each figure. The fan speed has been set manually to operate at 75% of the maximum capacity at all times. The other parameters were set as follows: air infiltration $n_v = 0.15$ for Figures 5.16 and Figures 5.17, then $n_v = 0.25$, heat gain $q = 0.26$ for Figures 5.18 and Figures 5.19 and $n_v = 0.25$, $q = 0.26$, poles at 0.3 for Figures 5.20 and Figures 5.21. The heat gain has been added to imitate the internal heat gains generated in the building as well as heat stored in the goods and furniture.

The results in Figures 5.16-5.21 and Table 5.5 show that the MPC is capable of finding a set of damper positions so that the overall heating and cooling running costs are minimised.

TABLE 5.5: The performance measures for the GA MPC simulation for three different weather scenarios.

Simulation	**Figure**	J	$S_{\Delta T}$
1	5.16	99.3871	93.0121
2 (1 with $u_d = 0$)	5.17	100.2936	93.8561
3	5.18	136.7932	132.3557
4 (3 with $u_d = 0$)	5.19	173.1806	165.9306
5	5.20	23.9807	21.7932
6 (5 with $u_d = 0$)	5.21	34.9314	31.8689

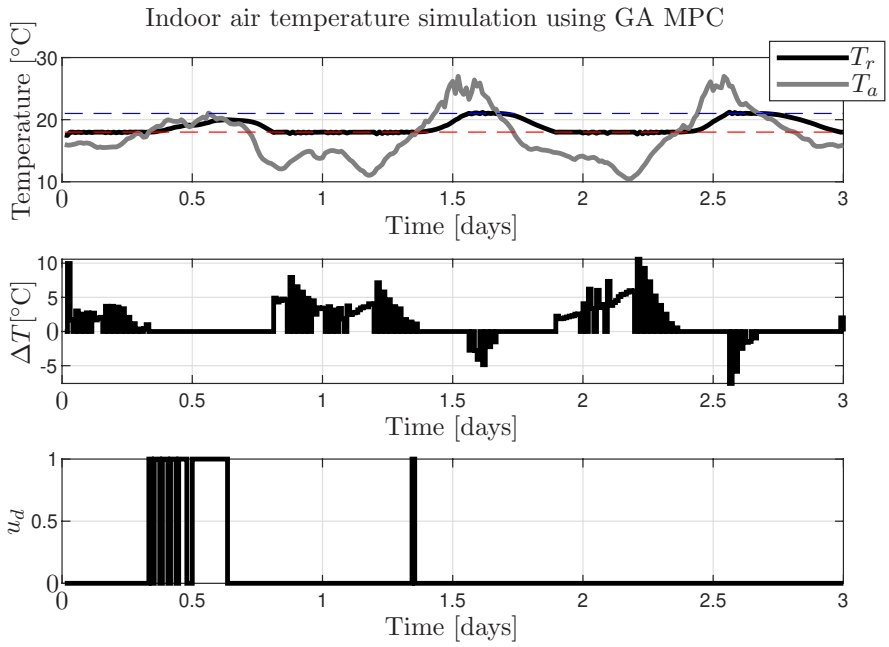

FIGURE 5.16: MPC prediction of the indoor air temperature for $h_p = 1$ day over 3 day of simulation. The poles of the PIP controller are at 0. The set-points $r_c = 21°C$ and $r_h = 18°C$ are marked with dash line. The air mass flow rate is set to $m_a = 13.41\,\mathrm{m}^3/\mathrm{s}$, which is 75% of the maximum fan speed.

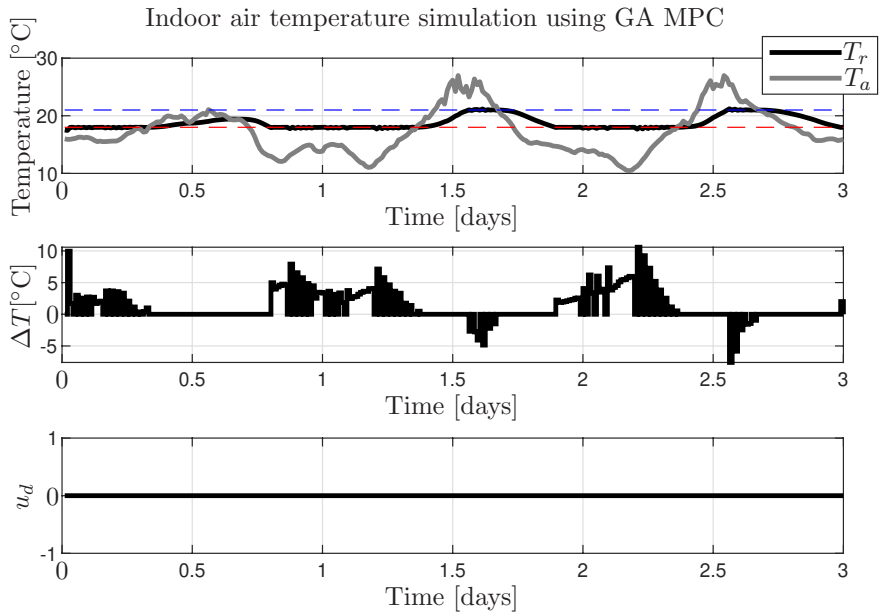

FIGURE 5.17: MPC prediction of the indoor air temperature for $h_p = 1$ day over 3 day of simulation. The poles of the PIP controller are at 0. The set-points $r_c = 21°C$ and $r_h = 18°C$ are marked with dash line. The air mass flow rate is set to $m_a = 13.41\,\mathrm{m}^3/\mathrm{s}$, which is 75% of the maximum fan speed.

In Figure 5.16, the damper is open most of the time between 0.4-0.6 day, allowing in the warmer air from the outside. This is desirable as later the temperature goes down to almost 10°C and heating is required. Then, the damper is closed (apart from one

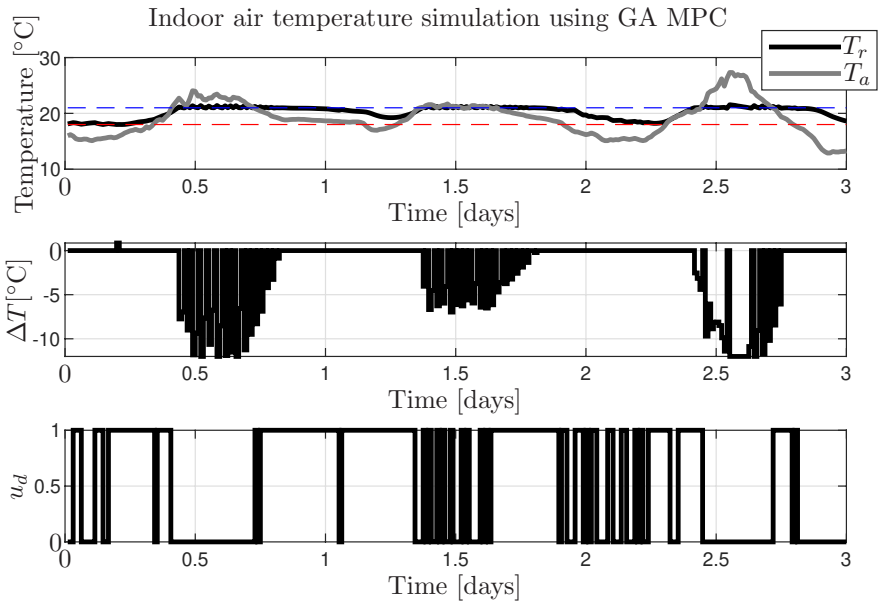

FIGURE 5.18: MPC prediction of the indoor air temperature for $h_p = 1$ day over 3 day of simulation. The poles of the PIP controller are at 0. The set-points $r_c = 21°\text{C}$ and $r_h = 18°\text{C}$ are marked with dash line. The air mass flow rate is set to $m_a = 13.41\,\text{m}^3/\text{s}$, which is 75% of the maximum fan speed.

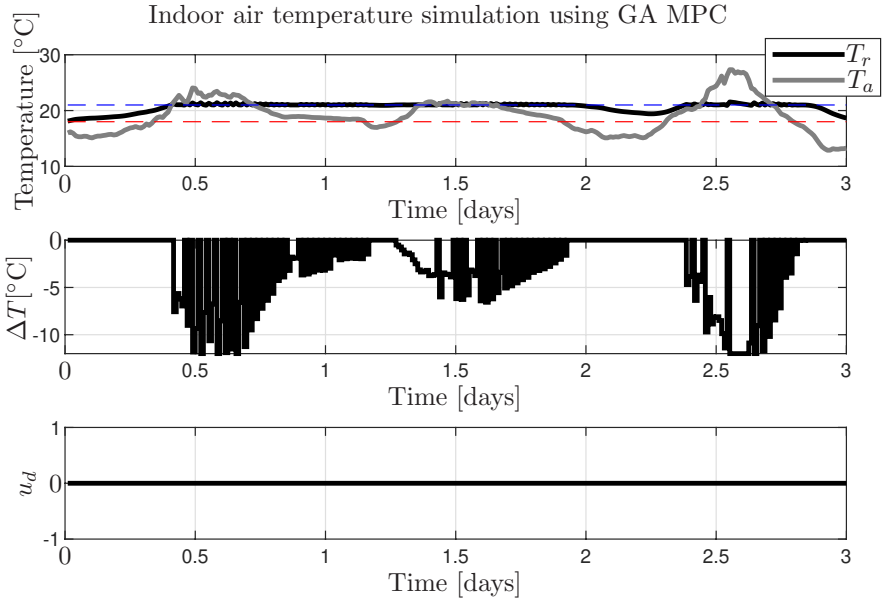

FIGURE 5.19: MPC prediction of the indoor air temperature for $h_p = 1$ day over 3 day of simulation. The poles of the PIP controller are at 0. The set-points $r_c = 21°\text{C}$ and $r_h = 18°\text{C}$ are marked with dash line. The air mass flow rate is set to $m_a = 13.41\,\text{m}^3/\text{s}$, which is 75% of the maximum fan speed.

sample where the indoor air temperature is around heating set-point), as the next peak around 1.5 day causes indoor air temperature rise over the cooling set-point, triggering cooling. In further part of the simulation the damper is closed as there is no benefit in introducing the fresh outside air. The minimum and maximum temperature values

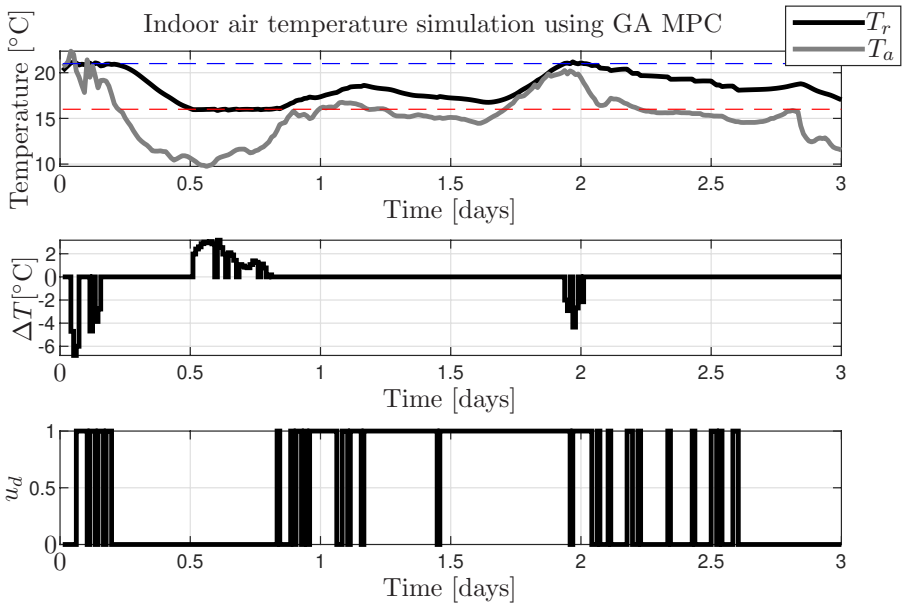

FIGURE 5.20: MPC prediction of the indoor air temperature for $h_p = 1$ day over 3 day of simulation. The poles of the PIP controller are at 0.3. The set-points $r_c = 21°C$ and $r_h = 16°C$ are marked with dash line. The air mass flow rate is set to $m_a = 13.41\,m^3/s$, which is 75% of the maximum fan speed.

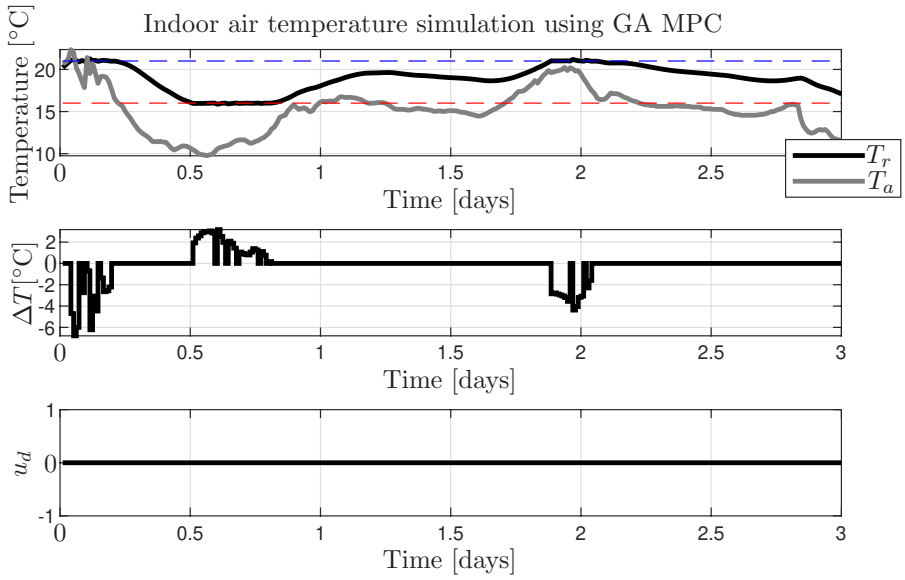

FIGURE 5.21: MPC prediction of the indoor air temperature for $h_p = 1$ day over 3 day of simulation. The poles of the PIP controller are at 0.3. The set-points $r_c = 21°C$ and $r_h = 16°C$ are marked with dash line. The air mass flow rate is set to $m_a = 13.41\,m^3/s$, which is 75% of the maximum fan speed.

relating to natural day-night cycle are too distant (approx. 17°C difference), therefore the indoor air temperature is driven out of the defined dead-band of 3°C. Considering ΔT in Figure 5.17, where damper is kept closed, it can be noticed that the heating is introduced slightly earlier compared to Figure 5.16 around 0.75-0.8 day, increasing the

cost J by 0.9, which is 0.9%. Although this might look insignificant, the small savings achieved by simply opening or closing the damper can accumulate over time, providing more compelling decrease in energy consumption of the temperature control system.

The outdoor air temperature in Figure 5.18 varies significantly less compared to Figure 5.16 with amplitude of around 10°C over the first 2 days and rising up to around 16°C during the third day. Having internal heat gains $q(t) = 0.26$ at each time instance, it is noted that the indoor air temperature doesn't drop below the heating set-point between 0-0.45 day (apart from one sample around 0.22) even though the outdoor air temperature is lower than the indoor and the dampers are open most of the time. The damper is set to open to pre-cool the space with the ambient air and then closed at peak times, around 0.5 and 2.5 day, when the $T_a > T_r$ and mechanical cooling is required to satisfy the indoor climate requirements. This scenario allows for greater energy savings, yielding cost J and $S_{\Delta T}$ lowered by over 20% compared to closed damper position simulation from Figure 5.19, where more cooling is required. Part of these savings could be achieved with control system utilising night purge and free cooling already offered by the industry. The issue with these solutions, however, is that they rely rather on current and past data and are used for cooling only. The risk of using the strategy offered by the industry is that sometimes unnecessary pre-cooling using outdoor air can occur. This happens typically in spring time when days are warm, but nights are still cold. As the controller is not aware of the potential future data, e.g. night temperature drop, pre-cooling in these circumstances decreases the efficiency of the system and adding costs of further heating in the night time. Employing the GA MPC allows to avoid undesired ventilation that would result in higher demand for cooling or heating, applying only the most recent control action based on the predicted data.

The results presented in Figure 5.20 shows another outdoor air temperature scenario and the model used for simulation includes internal heat gains $q(t) = 0.26$ at each time instance. To slow down the PIP controller and remove dead-beat behaviour, the poles are set to 0.3. The heating set-point has also been decreased by 2°C to $r_h = 16$°C, extending dead-band to 5°C. This change allows the simulated indoor air temperature to remain within the dead-band over larger number of time instances. As a consequence, the cost is only $J = 34.93$ when the damper is closed as in Figure 5.21. This cost can be further decreased by over 30% when GA MPC is used, achieving $J = 23.98$ with variable damper position for ventilation. As in this scenario the outdoor air temperature is not as favourable for night purge and free cooling, the GA MPC boosts the energy efficiency of the control system leading to less energy spent on cooling.

5.5.5 First principles recursive simulation with real data over 7 day

The last set of simulations is intended to demonstrate GA MPC operation over a long period of time, 7 days, with real data outdoor air temperature data representing three seasons: spring/autumn, summer and winter. The data for simulation was chosen to illustrate essential tendencies of the season and estimate potential of the energy savings. Note that this is a 7 day snapshot representing 13 weeks long season, therefore the results are rather symbolic and the actual savings will depend on the weather conditions, which can vary significantly. While it would be ideal to perform the simulations with at least 2 or 3 weeks length, a period of 7 days was chosen due to the time required for simulation.

Simulations of the MPC operation over a period of 7 days have been performed to simulate the real operation of the MPC controller. The control actions taken are recalculated and proposed by the MPC algorithm at each time step as detailed in the flowchart diagram in Figure 5.4. The following settings are used: $t_s = 15\,\text{min}$, control horizon is 1 day and $h_p = h_c = 96$ samples, $w_{out} = 0.25$, population size 120, number of generations 50, elite size 10% of population size, crossover fraction 0.9 and 20% of the population is initialised with vectors $u_d(i) = 0\ \forall\ i = 1, \ldots h_p$. The results are presented in Figures 5.22, 5.24 and 5.26 with the respective closed damper position simulations in Figures 5.23, 5.25 and 5.26. At each time step the values of $\Delta T(i)$ are determined by the PIP controller with dead-beat setup and $u_d(i)$ values are determined by the GA. The control dead-band is defined by the heating and cooling set-points at $r_h = 17°\text{C}$ and $r_c = 22°\text{C}$, respectively. The fan speed has been set manually to operate at 75% of the maximum capacity at all times. The other parameters were set as follows: air infiltration $n_v = 0.25$, heat gain $q = 0.26$ and poles at 0.3 for all simulations. The heat gain has been added to imitate the internal heat gains generated in the building as well as heat stored in the goods and furniture.

The results in Figures 5.22-5.26 and Table 5.6 show that the MPC is capable of finding a set of damper positions so that the overall heating and cooling running costs are minimised.

The results shown in Figures 5.22 and 5.23 illustrate an indoor air temperature simulation under weather conditions that occurs in spring and autumn season. The outdoor air temperature in this scenario varies over day 2 and 3 with amplitude over 20°C and oscillates around the heating set-point for the next 3 days with amplitude around 12°C. There is a lot of damper position chattering in Figure 5.22, but the energy savings achieved using GA MPC are negligible. This scenario represents less favourable situation with large changes between the minimum and maximum outdoor air temperatures causing the need for both heating and cooling and the outdoor air temperature

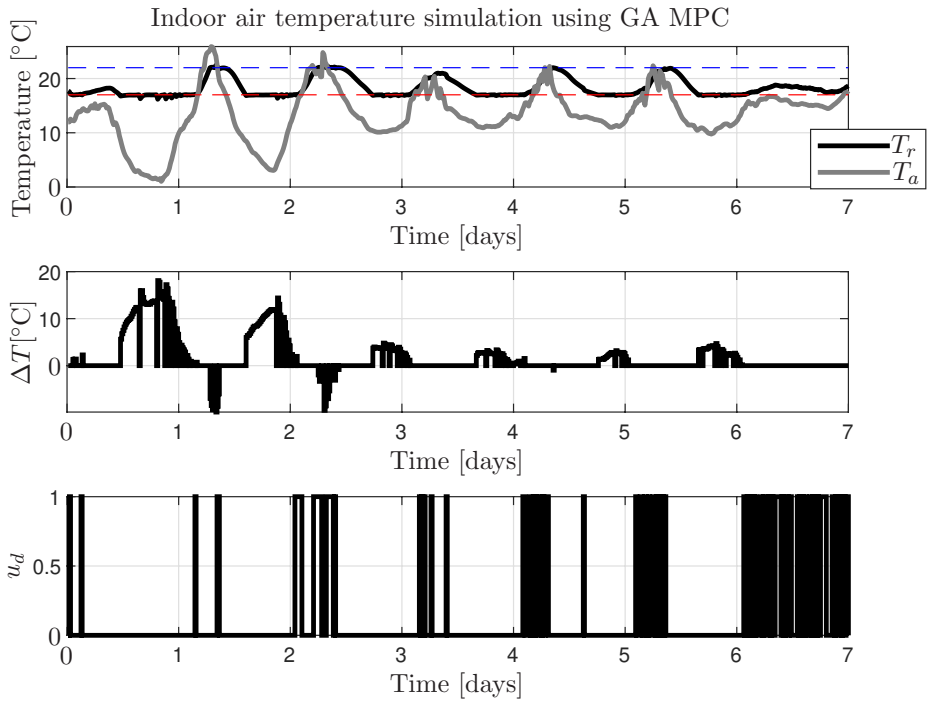

FIGURE 5.22: Spring scenario. MPC prediction of the indoor air temperature for $h_p = 1$ day over 7 day of simulation. The poles of the PIP controller are at 0.3. The set-points $r_c = 22°\text{C}$ and $r_h = 17°\text{C}$ are marked with dash line. The air mass flow rate is set to $m_a = 13.41\,\text{m}^3/\text{s}$, which is 75% of the maximum fan speed.

TABLE 5.6: The performance measures for the GA MPC simulation for three scenarios representing spring/autumn, summer and winter outdoor temperature with identical setup.

Simulation	**Figure**	J	$S_{\Delta T}$
Spring	5.22	348.6384	334.3259
Spring ($u_d = 0$)	5.23	349.965	335.7775
Summer	5.24	388.0365	376.349
Summer ($u_d = 0$)	5.25	421.6933	407.1933
Winter	5.26	1592.699	1555.5115
Winter ($u_d = 0$)	5.26	1592.699	1555.5115

varying between the upper set-point and 10°C, which forces the indoor air temperature to drop below the heating set-point. The energy consumption in this scenario is caused mainly by heating. Although the chosen spring/autumn scenario shows savings of less than 1%, it is possible to achieve higher amount of energy saved whenever the outdoor conditions permit as in Figure 5.20 for example. The spring and autumn seasons are most likely to allow for both heating and cooling of the indoor space using the outdoor air.

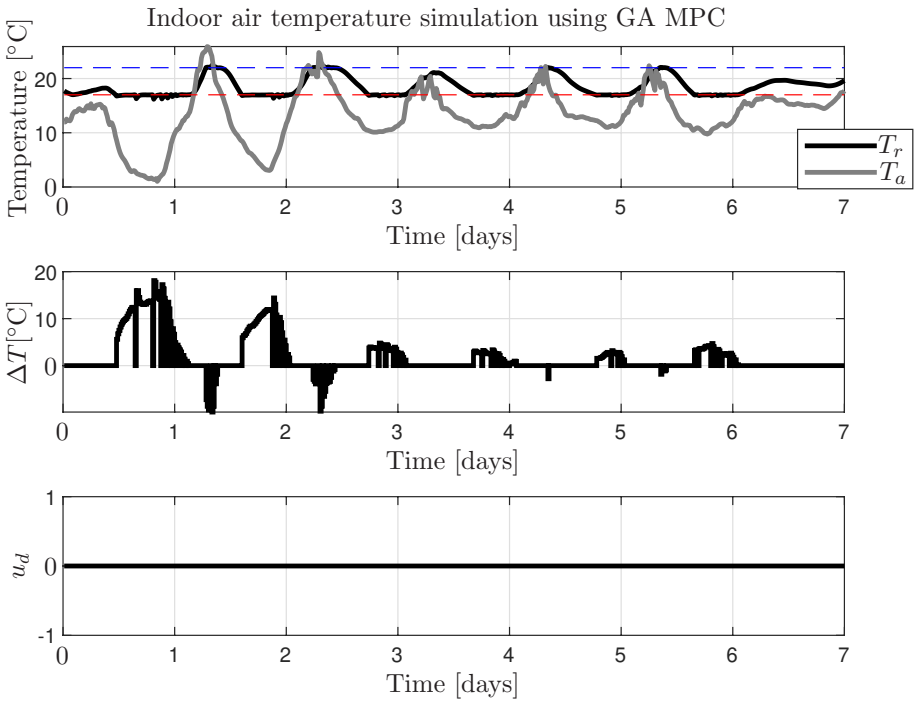

FIGURE 5.23: Spring scenario. MPC prediction of the indoor air temperature for $h_p = 1$ day over 7 day of simulation. The poles of the PIP controller are at 0.3. The set-points $r_c = 22°\text{C}$ and $r_h = 17°\text{C}$ are marked with dash line. The air mass flow rate is set to $m_a = 13.41\,\text{m}^3/\text{s}$, which is 75% of the maximum fan speed.

Analysing summer scenario, the use of damper position control allowed to decrease the energy consumption by 8% for results presented in Figure 5.24 compared to Figure 5.25. This season presents the largest opportunities for saving energy and minimising the cost of maintaining the indoor air temperature within the required limits. This is primarily accomplished through free cooling, relying on warm days and cooler nights, where the outdoor air temperature does not drop below 12-14°C.

The typical winter season in UK presents minimal chances for energy savings that come from damper position manipulation as the outdoor air temperature is low and does not allow for free heating. For this reason the damper positions selected by GA MPC for scenario in Figure 5.26 are closed, recirculating the warm indoor air.

5.5.6 Discussion

The results presented in Section 5.5 are prepared to represent the relationships and behaviours observed in a real system and in simulations presented in this thesis. While the data gathered allows to conclude that advanced control methods can increase the efficiency of the indoor temperature control system, it is important to understand the correlations and dependencies between states and processes. Therefore, it is recognised

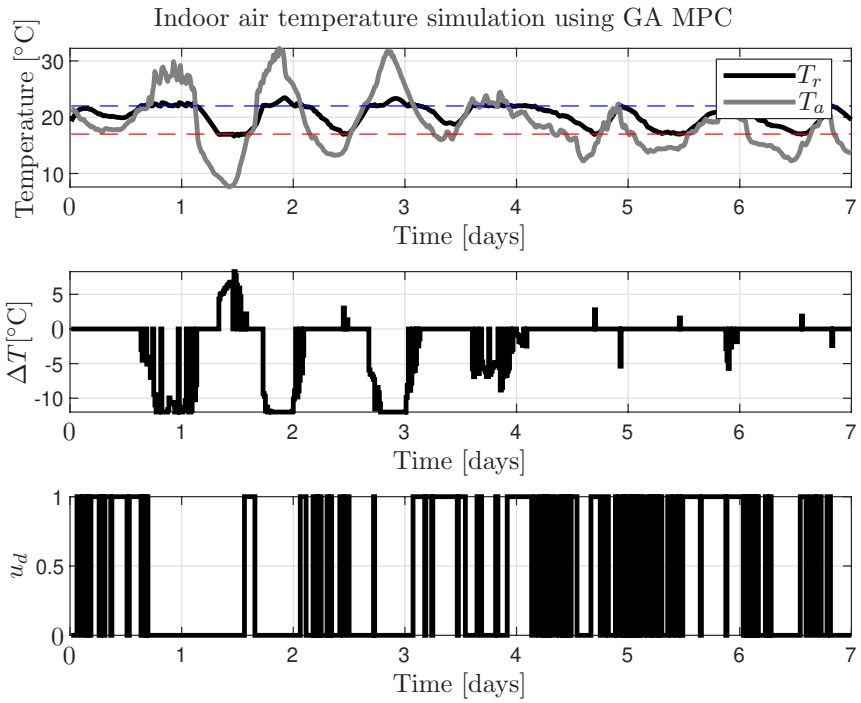

FIGURE 5.24: Summer scenario. MPC prediction of the indoor air temperature for $h_p = 1$ day over 7 day of simulation. The poles of the PIP controller are at 0.3. The set-points $r_c = 22°\text{C}$ and $r_h = 17°\text{C}$ are marked with dash line. The air mass flow rate is set to $m_a = 13.41\,\text{m}^3/\text{s}$, which is 75% of the maximum fan speed.

that the issue of energy efficient indoor temperature control depends on the outdoor conditions, the dead-band and the indoor air temperature in the following manner:

- **Outdoor conditions** The milder the outdoor conditions, the more potential for energy savings. If the outdoor conditions vary a lot, spikes can be observed or the difference between the maximum and minimum temperature throughout the day-night cycle is more significant, less energy savings can be achieved. The outdoor conditions are a critical part contributing to the energy efficiency of the system through damper position control using proposed MPC method. Unfavourable outdoor air temperature, solar irradiation or wind speed may reduce the energy savings to 0, forcing heating and cooling to be used for indoor climate control. Typical examples of such scenarios for UK climate are hot sunny days, warm summer nights, spring time with warm sunny days and cold nights and autumn-winter season with the outdoor air temperature remaining below the heating set-point.

- **Dead-band** Increasing the upper limit, i.e. cooling set-point, and decreasing the lower limit, i.e. the heating set-point allows to maximise the space between the set-points. By doing so, it is possible to delay the moment of heating or cooling

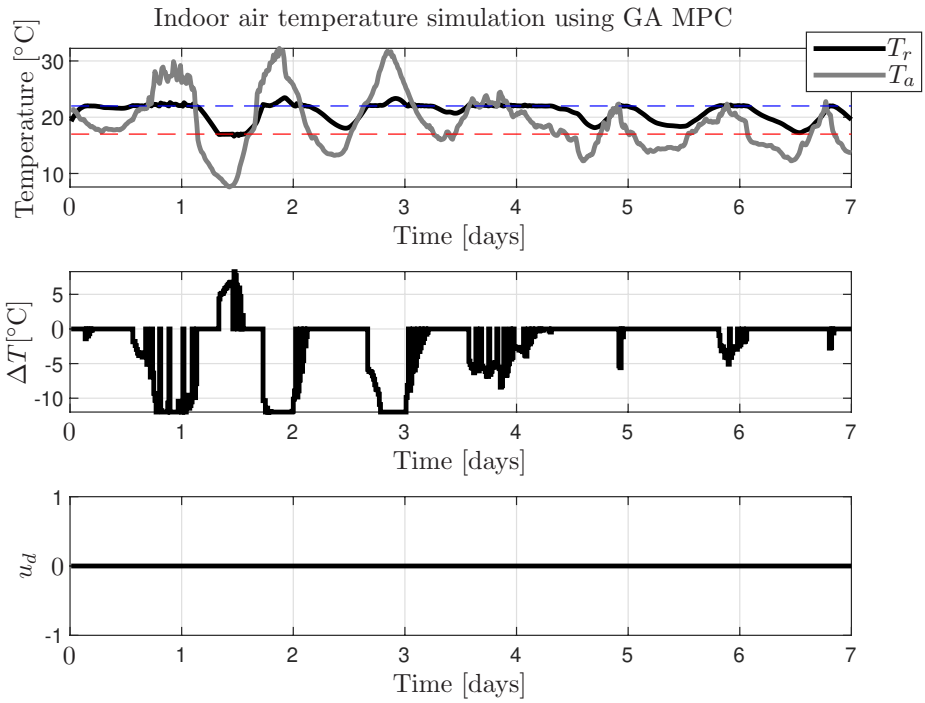

FIGURE 5.25: Summer scenario. MPC prediction of the indoor air temperature for $h_p = 1$ day over 7 day of simulation. The poles of the PIP controller are at 0.3. The set-points $r_c = 22°\text{C}$ and $r_h = 17°\text{C}$ are marked with dash line. The air mass flow rate is set to $m_a = 13.41\,\text{m}^3/\text{s}$, which is 75% of the maximum fan speed.

unit activation and reduce their use. Therefore, expanding the dead-band within safe limits increases the energy efficiency of the HVAC system.

- **Indoor air temperature** The heating and cooling are triggered by the indoor air temperature located outside of the dead-band. If the indoor air temperature remains between the upper and lower limits, no energy should be consumed on heating and cooling. While the indoor air temperature being within the dead-band results in no need for heating and cooling, it is beneficial to look beyond this simple measure. The location of the indoor air temperature relative to the upper and lower limit matters and is used to improve the energy efficiency of the HVAC system. The desired indoor air temperature location within the dead-band is determined mainly by the current and future outdoor conditions. For example, if it is expected that it will be cold outside, the optimal current indoor temperature would be as close as possible to the upper limit, i.e. the furthest point within the dead-band from the heating set-point. This will result in prolonging the moment when the activation of the heating unit is required to meet the indoor air temperature requirement. On the contrary, if the outdoor air temperature oscillates within or around the dead-band, the indoor air temperature location within the dead-band is less important as the indoor conditions requirements will

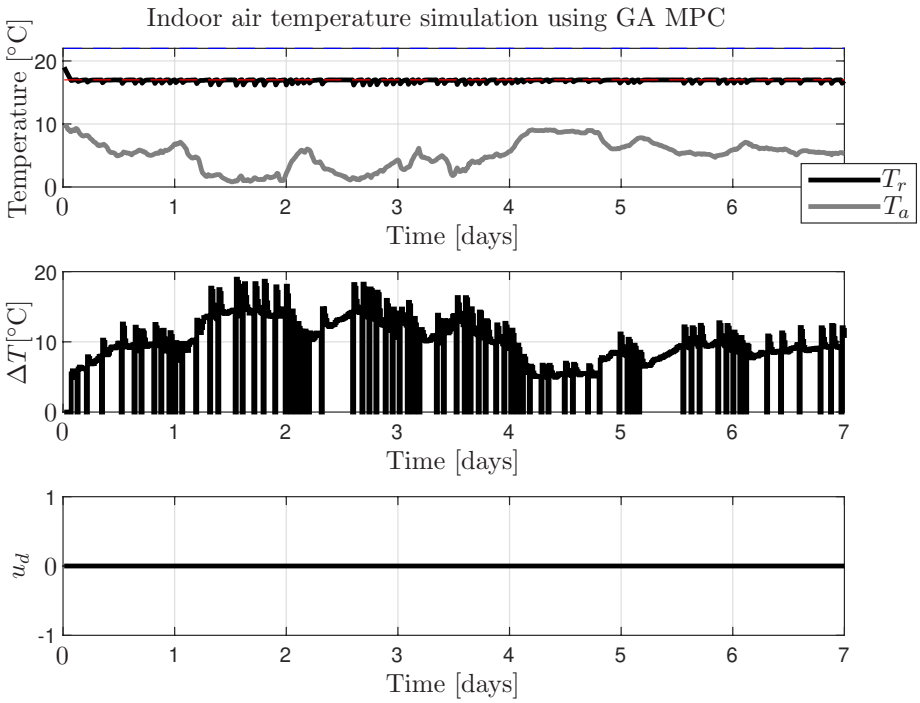

FIGURE 5.26: Winter scenario. MPC prediction of the indoor air temperature for $h_p = 1$ day over 7 day of simulation. The poles of the PIP controller are at 0.3. The set-points $r_c = 22°\text{C}$ and $r_h = 17°\text{C}$ are marked with dash line. The air mass flow rate is set to $m_a = 13.41\,\text{m}^3/\text{s}$, which is 75% of the maximum fan speed.

be met most of the time due to mild outdoor conditions, similar to the required indoor conditions.

5.6 Conclusions

In this chapter a novel approach to the HVAC energy consumption optimisation was proposed. The method relies on the predictions of the indoor conditions using the weather forecast and the PIP controller model used as a part of the MPC. The solver for the optimisation problem is GA, which finds the optimal position of damper blades, therefore can benefit from the outdoor air heating or cooling capabilities, as weather permits. The results obtained show that while the GA MPC optimises the energy, it performs best when it is run at each time step rather than performing one simulation over prediction horizon and apply these actions over time. While the GA MPC relying only on the damper position manipulation is able achieve savings in the energy consumed by the HVAC system, an additional decrease of the energy consumption would be achieved when other methods would be implemented simultaneously. For example, adaptive set-point technique can prolong the time of the indoor air temperature remaining within

the dead-band by temporary expanding or moving the dead-band in a safe, controlled manner. It also allows to pre-cool or pre-heat the space.

The GA used as a solver for the energy optimisation problem is computationally intensive. This is not a problem for the large space building applications, where the sampling interval is much bigger than the computational time, however, could present challenges in smaller applications with more frequent sampling rate. The smaller application would require separate tuning of the GA as the optimal prediction and control horizons and other GA-specific parameters might vary from the studied large space building. A proposed method to alleviate the computational intensity is to set restrictions on how often the position of damper blades can change. This can be achieved through setting a condition that the damper blades must remain at least 2 (or other number) sampling intervals in selected position. Alternatively, the number of variables for optimisation can be reduced by finding one position of damper blades per period of time. In this case the damper blades could move, for instance, only every 30 min, which would reduce the number of variables by half if the sampling interval is 15 min.

Chapter 6

Conclusions

6.1 Conclusions

Motivated by the economical and environmental aspects of the heating ventilation and air conditioning (HVAC) systems utilisation, this thesis proposed a novel approach to the indoor air temperature control with focus on the large open space buildings. These structures are characterised by slow dynamics and nonlinear behaviour associated with the building structure itself, thermal mass stored in storage units, goods and machinery, air stratification, internal heat gains generated by the staff and operating machinery, additional heat gains and losses on every wall and roof from the solar irradiation and high speed winds and disturbance introduced by opening the large doors such as for HGVs when no vehicle is parked on the warehouse entry. Additional challenges are introduced by the HVAC system operation, where the control strategy together with the components within the Air Handling Unit (AHU) also demonstrate nonlinear characteristics. The solution in this thesis was designed to provide energy efficient operation of the HVAC system serving open space buildings such as the studied warehouse located in Midlands, UK, where the aforementioned challenges have been observed. This building represents typical HVAC setup for the large space buildings indoor air temperature control with heating and cooling capabilities. It has been achieved through development of the indoor air temperature model and the controller to ensure the indoor air requirements are satisfied. The existing methods have been used and combined together into a unique control approach for the indoor air temperature management.

Reflecting on the outcomes and progress achieved during the run of the project, some important findings were observed during the model investigation leading to State-dependent Parameter (SDP) structure. Additionally, preliminary tests of the proposed

Genetic Algorithm Model Predictive Control (GA MPC) approach exposed valuable insight into the potential savings and provided a basis for future research following the improved energy efficiency of the simulated HVAC system. While there could be done more in terms of model development to include more disturbances such as solar irradiation, wind speed and variable internal heat gain, the presented nonlinear model encourages future attempts and continuation of the indoor air temperature model improvement and expansion. The research aim was addressed by various studies and development activities along the objectives provided in Chapter 1 and provided valid contributions to the body knowledge. Although the preliminary results provided are satisfactory, the research constitutes future studies to direct further work starting with a thorough comparison of the GA MPC approach against other control methods, enhancement of the optimisation algorithm, model accuracy increase and evaluation of the proposed method on a real HVAC system, confirming the energy efficiency potential and help to identify more areas in which the method could be improved. In light of that, the following sections summarise the research presented in this thesis and the last section identifies the scope of the future studies on this topic.

6.1.1 Indoor air temperature modelling

The indoor air temperature model detailed in Chapter 2 is developed from first principles and the energy balance. Modelling of this complex process requires a number of assumptions and simplifications, leading to a lower order model. As a key component of a model-based approach, the model provides accuracy suitable for control and simulation applications. The indoor air temperature control system by default represents a closed-loop system, where the indoor air is recirculated. This structure has a positive feedback loop as the indoor air is passed again into the indoor space. Estimation of the model parameters from data collected in this configuration is more challenging as the fraction of the system output is also an input. Using the outdoor air in place of the recirculation by setting the damper blades to open position removed the loop and the parameter estimation becomes straightforward. This method is widely used as a ventilation technique to improve the air quality and energy efficiency of the HVAC system. Consequently, the study performed on the system properties for the open and closed loop scenarios revealed a relationship between the model parameters and the position of damper blades. The State-dependent Parameter (SDP) approach has been proposed in Chapter 3 for its ability to accommodate the model to the changes in states, which are the control signals and variables representing the current settings and operation of the temperature control system. Using SDP model structure to capture the indoor air temperature process enabled to account for nonlinearity related to the damper position

within the model. It is worth noting that in the closed loop scenario the outdoor air temperature signal is a disturbance, whereas in the open loop scenario it becomes a controllable (to a degree) system input. While the value of the outdoor air temperature input to the model does not change, the model parameters are changed through the position of damper blades, adjusting the amount of the outdoor air introduced into the building. Moreover, it is possible to obtain the closed loop system model parameters from the open loop model if the position of damper blades is known and vice versa, which can be used to obtain the other set of parameters without additional parameter estimation. The SDP model also accounts for the air mass flow rate at which the supply air is distributed across the building, which typically varies throughout the day depending on the heating, cooling and ventilation needs and the implemented control strategy. The air mass flow rate from first principles has an influence on the model parameters, therefore contributes to the nonlinear dynamics of the system.

In Chapter 3 the indoor air temperature model is reduced to first order system model from first principles' second order system representation, which is able to represented the studied system with satisfying accuracy for control application. The former model having the supply air temperature and the outdoor air temperature as the inputs is also rearranged to achieve the state-dependent structure responding to the position of damper blades providing smooth online conversion between open and closed loop models. The derived SDP model has two inputs: the temperature change occurring in the AHU caused by heating or cooling and the outdoor air temperature. Only the first input is directly and fully controllable, while the outdoor air temperature is provided and its influence is partially controlled through the damper blades position. The results of the comparative study demonstrated improved accuracy of the SDP model, outperforming the linear model with constant parameters representing linearisation around the working point. The SDP model of the indoor air temperature is used to develop Non-minimal State Space (NMSS) model structure for the Proportional-Integral-Plus (PIP) controller introduced in Chapter 4 and as a part of the Model Predictive Control (MPC) strategy in Chapter 5 to optimise the HVAC system energy consumption.

6.1.2 Control of the indoor air temperature

Predictive control approach has been chosen as a method to improve the energy efficiency of the HVAC system through the damper position control. The control strategy is extended by including future inputs and outputs into control algorithm supplementary to the past and present inputs and outputs. Switching the damper blades position to recirculate the indoor air or use the fresh air from the outside allows to minimise (or maximise) the outdoor air temperature impact on the indoor space as required,

influencing the dynamics of the indoor thermal process. The optimal damper position is found using Genetic Algorithm (GA). The use of forecasting methods allows to react in advance to the upcoming events, providing an advantage over traditional approach considering only past and present signals. By doing so, it is possible to take preparatory actions and work toward more efficient energy consumption without compromising the indoor air conditions. The results obtained through simulation study using the Genetic Algorithm Model Predictive Control (GA MPC) demonstrate that the use of weather forecast contributes to improve energy efficiency in the indoor air temperature control, offering around 8% of energy savings in summer and 1-3% percent in spring/autumn.

6.2 Further work

The project presented in this thesis has a potential for further research in both modelling and control approach aspects. While the list covers analysed topics, it is by no means extensive as the research is a continuous process. There is always a room for improvement within any research area, worth exploring to advance existing techniques and develop new solutions. The attempt to develop a reliable and more energy efficient control systems for the indoor air temperature control presented in this thesis is a response to the industry and economy needs. Further work and improvement of the proposed method can support the growing demand for acting upon environmental challenges and provide more energy and cost efficient solutions within the indoor climate control sector. The identified directions for the improvements and investigations are:

- **Comprehensive comparative study** evaluating proposed control strategies and selected solutions available on the market could be performed to understand energy and cost efficiency aspects of each. The evaluation would include a variety of weather conditions scenarios, building models and the HVAC system setups, demonstrating the control strategy performance through the most representative experiments analysis. This study could also be extended by detailed model comparison evaluating different model structures, e.g. bilinear, and first and second system order models. Another avenue worth exploring would be a comparative study of MPC (combining SDP-PIP and GA) against other controllers. The proposed controller types are a multivariable controller (with the damper position and heating/cooling as the two control inputs), PID or a linear PIP controller.
- **Model improvement** The following elements could be included and utilised in the model:

  - Inclusion of the disturbances in the model by considering the solar irradiation and the wind speed in the model could improve model accuracy significantly. This is especially true during sunny or windy days, where the outdoor air temperature readings collected by the sensor placed in a shaded, wind-free location are not representative enough to account for the occurring weather conditions. While weather conditions could be fetched from the external source and included in the model, additional improvement in real applications would come from installing a weather station local to the building to gather the most accurate data. In the same manner, including the thermal mass of the goods stored in the building, the changes in heat load generated by the machinery and people operating in the building and the heat losses related to the natural ventilation through the open doors and windows would also contribute to the model accuracy improvement.
  - **Inclusion of the delays in the model** could account for the fact that the dynamics of the indoor thermal process is slow, therefore the changes in the outdoor air do not happen immediately.
  - **Inclusion of the AHU components sub-models** could account more accurately for the heating, cooling and supply fan unit components and their nonlinear characteristics. While doing so is not crucial as the offset term can be included in the model to account for it, separating them into separate submodels will increase the model fidelity as well as complexity.

- **Distributed modelling** approach can be used to improve the model accuracy and provide deeper insight into the thermal process. This could be especially important for large open space buildings, where the air stratification is observed. This can be measured with use of several temperature sensors as the air temperature readings from the sensor located closer to the floor are typically lower than the readings from the sensor located closer to the ceiling or the roof. Understanding of the air temperature distribution from 3D model could expose design gaps and help developing more reliable and energy efficient control systems.

- **Adaptive model** algorithm with ability to self-tune and correct the model parameters over time. This technique will find use when the initial model of the building is implemented based on the initial assumptions. The data collected by the controller can then be used to adjust the model parameters, converging toward more accurate results, improving control and energy efficiency of the HVAC system. Further, the same method can be continuously or periodically used to account for the seasonal changes in the outdoor conditions that affect the system differently.

- **Weather forecasting** algorithm could be developed to serve in two ways. First, the weather forecast data could be fetched from external source and adapted to represent more accurately the weather conditions expected in the particular location of the building, in which the indoor air temperature is controlled. In the same manner as the adaptive model algorithm, this technique would improve over time the model predicting the outdoor conditions, learning from the data collected by the controller. Second, the weather forecasting algorithm would predict the weather conditions based on the past data, without relying on the external weather forecast.

- **Genetic Algorithm tuning** performed in a more comprehensive manner would allow to ensure the optimal setup of the GA is used as a part of the GA MPC strategy for the indoor air temperature control. It is proposed to investigate the following parameters: the prediction and control horizons, the number of generations, the population size, the elite size, the initial population members definition and, if possible, improve crossover and mutation functions. Note that different weather conditions and indoor temperature requirements might require different setup, therefore careful parameter selection should be supported by various experiments on diverse scenarios. Additional considerations would account for the computational power and capabilities of the actual controller and the required response time, which can be a limitation in the real applications.

- **Another optimisation methods** would be worth considering to ensure that the utilised optimisation algorithm is the most efficient in terms of time, cost, results and integration with the the MPC and the overall control system. Ideally, the optimisation algorithm should be able to solve integer problems with constraints on input and output and choose control action values from a set. Currently Artificial Intelligence is widely explored in various applications, but it can be computationally intensive.

- **PIP control law** could be improved by designing the controller through pole placement. This approach requires knowledge of the system dynamics and the indoor air temperature requirements. The poles can be chosen by the designer to optimise the energy consumption while complying with the indoor conditions specification.

- **SDP-PIP controllability and stability** were not given much attention in this thesis, therefore it is suggested to investigate SDP-PIP controller in respect of these issues. This is motivated by using the same model for simulation and control. It is suggested that the SDP-PIP is first applied to the ideal model and confirm the expect controllability and stability and this will support testing the robustness

of the approach. SDP-PIP controllability and stability should be tested in both SDP-PIP alone presented in Chapter 4 and as a part of MPC in Chapter 5.

- **Implementation of the control approach to the real system** is a natural progression in a system development process. It is proposed to perform the tests in stages at various levels of integration with the real system. This would include reviewing the control strategy and the model after each phase through validation and verification. As a result, the final solution should be reliable indoor air temperature control system that satisfies the design requirements in an energy efficient manner.

References

Atam, E., & Helsen, L. (2016). Control-oriented thermal modeling of multizone buildings: Methods and issues: Intelligent control of a building system. *IEEE Control Systems*, *36*(3), 86–111.

Atkinson, K. E. (2009). *Numerical solution of ordinary differential equations*. Interscience tracts in pure and applied mathematics.

Bai, J., & Zhang, X. (2007). A new adaptive PI controller and its application in HVAC systems. *Energy Conversion and Management*, *Volume 48*, pp. 1043—-1054.

Bell Jr., A. A. (2000). *HVAC Equations, Data, and Rules of Thumb*. McGraw-Hill.

Bemporad, A. (2020). Model predictive control. Accessed: 2020-03-08.
URL `http://cse.lab.imtlucca.it/~bemporad/mpc_course.html`

Bidar, B., Sadeghi, J., Shahraki, F., & Khalilipour, M. M. (2017). Data-driven soft sensor approach for online quality prediction using state dependent parameter models. *Chemometrics and Intelligent Laboratory Systems*, *162*, 130–141.

Bobál, V., Böhm, J., Fessl, J., & Macháček (2005). *Digital Self-Tuning Controllers: Algorithms, Implementation and Applications*. London: Springer-Verlag.

Camacho, E. F., & Bordons, C. (1999). *Model Predictive Control*. London: Springer-Verlag.

Carbon Brief (2014). Two degrees: The history of climate change's speed limit.
URL `https://www.carbonbrief.org/two-degrees-the-history-of-climate-changes-speed-limit`

Çengel, Y. A., & Boles, M. A. (2006). *Thermodynamics: An Engineering Approach*. Boston, MA: McGraw-Hill College, 5th ed.

Chartered Institution of Building Services Engineers (2005). *Heating, ventilation, air conditioning and refrigeration : CIBSE guide B.*. CIBSE guide ; B. London: CIBSE.

Chen, C.-W., & Chang, Y.-C. (2016). Support vector regression and genetic algorithm for hvac optimal operation. *Mathematical problems in engineering*, *2016*, 1–10.

Cross, P., & Ma, X. (2013). State dependent parameter model-based condition monitoring for wind turbines. *Proceedings of the 10th International Conference on Condition Monitoring and Machinery Failure Prevention Technologies (CM 2013 & MFPT 2013)*.

Delnero, C. C. (2000). *Neural Networks and PI Control using Steady State Prediction Applied to a Heating Coil*. Master's thesis, Colorado State University.

Demirezen, G., Fung, A. S., & Deprez, M. (2020). Development and optimization of artificial neural network algorithms for the prediction of building specific local temperature for hvac control. *International journal of energy research*, *44*(11), 8513–8531.

Exadaktylos, V. (2007). *Model Predictive Control Structures in the Non-Minimal State Space*. PhD thesis, Lancaster University, UK.

Faizollahzadeh Ardabili, S., Mahmoudi, A., & Mesri Gundoshmian, T. (2016). Modeling and simulation controlling system of hvac using fuzzy and predictive (radial basis function, rbf) controllers. *Journal of Building Engineering*, *6*, 301–308.

Fink, L. (2020). Larry Fink's Letter to CEOs.
URL `https://www.blackrock.com/corporate/investor-relations/larry-fink-ceo-letter`

Fitzpatrick, M. (2013). The Global Carbon Budget and Why the Warsaw Climate Talks Matter.
URL `https://blog.ucsusa.org/melanie-fitzpatrick/the-global-carbon-budget-and-why-the-warsaw-climate-talks-matter-303`

Foucquier, A., Robert, S., Suard, F., Stéphan, L., & Jay, A. (2013). State of the art in building modelling and energy performances prediction: A review. *Renewable & sustainable energy reviews*, *23*, 272–288.

Future Earth (2015). The Great Acceleration.
URL `https://futureearth.org/2015/01/16/the-great-acceleration/`

Goldberg, D. E. (1989). *Genetic Algorithms in Search, Optimization and Machine Learning*. USA: Addison-Wesley Longman Publishing Co., Inc., 1st ed.

Goodfellow, H. D., & Tahti, E. (Eds.) (2001). *Industrial ventilation design guidebook*. San Diego, Calif.: Academic Press.

GOV.UK (n.d.). Implementing the Sustainable Development Goals.
URL `https://www.gov.uk/government/publications/implementing-the-sustainable-development-goals/implementing-the-sustainable-development-goals--2`

Grüne, L. (2015). Nominal model-predictive control. In *Encyclopedia of Systems and Control*.

Harish, V. S. K. V., & Kumar, A. (2016a). Modeling and simulation of a simple building energy system. In *International Conference on Microelectronics, Computing and Communication, MicroCom 2016*.

Harish, V. S. K. V., & Kumar, A. (2016b). A review on modeling and simulation of building energy systems. *Renewable and Sustainable Energy Reviews*, *Volume 56*, pp. 1272–1292.

Hitzemann, U. (2013). *Extensions in Non-Minimal State-Space and State-Dependent Parameter Model Based Control with Application to a DC-DC Boost Converter*. PhD thesis, Coventry University, UK.

Hoberock, L. L., & Kohr, R. H. (1966). An experimental determination of differential equations to describe simple nonlinear systems. In *Joint Automatic Control Conference, Washington, Seattle*, vol. 4, (pp. 616—623).

Homod, R. Z. (2013). Review on the HVAC system modeling types and the shortcomings of their application. *Journal of Energy*, *Volume 2013*.

Jackiewicz, Z. (2009). *General linear methods for ordinary differential equations*. Hoboken, N.Y.: Wiley.

Janiak, A., & Lichtenstein, M. (2011). *Advanced algorithms in combinatorial optimization*. Wroclaw: PRINTPAP.

Jet Environmental Systems (n.d.). jet environmental - a market-leading supplier of hvac systems.
URL `https://www.jetenvironmental.com/`

Kampelis, N., Sifakis, N., Kolokotsa, D., Gobakis, K., Kalaitzakis, K., Isidori, D., & Cristalli, C. (2019). Hvac optimization genetic algorithm for industrial near-zero-energy building demand response. *Energies (Basel)*, *12*(11), 2177.

Kusuda, T. (1976). *NBSLD, The Computer Program For Heating and Cooling Loads in Buildings*. Building Science Series 69, National Bureau of Standards. Washington, DC: US Dep. of Commerce.

Larkowski, T., & Burnham, K. J. (2011). *System Identification, Parameter Estimation and Filtering*. Wroclaw: PRINTPAP.

Larsen, S. F., Filippín, C., & Lesino, G. (2009). Thermal behavior of building walls in summer: Comparison of available analytical methods and experimental results for a case study. *Building Simulation*, *2*(1), 3–18.

Li, L., & Lu, Z. (2013). Regional importance effect analysis of the input variables on failure probability and its state dependent parameter estimation. *66*(10), 2075–2091.

Lim, D., Ramussen, B. P., & Swaroop, D. (2009). Selecting PID control gains for nonlinear HVAC& R systems. *HVAC& R Research*, *Volume 15, Issue 6*, pp. 991—-1019.

Ljung, L., & Glad, T. (1994). *Modeling Of Dynamic Systems*. Englewood Cliffs, New Jersey 07632: P T R Prentice Hall.

Maganga, O. (2015). *Advanced Control and Optimisation of DC-DC Converters with Application to Low Carbon Technologies*. Coventry University.

MathWorks (n.d.a). Find minimum of function using genetic algorithm.
URL `https://uk.mathworks.com/help/gads/ga.html`

MathWorks (n.d.b). How the genetic algorithm works.
URL `https://uk.mathworks.com/help/gads/how-the-genetic-algorithm-works.html`

MathWorks (n.d.c). Mixed integer ga optimization.
URL `https://uk.mathworks.com/help/gads/mixed-integer-optimization.html`

MathWorks (n.d.d). Model predictive control toolbox.
URL `https://uk.mathworks.com/products/mpc.html`

Mayer, B., Killian, M., & Kozek, M. (2017). Hierarchical model predictive control for sustainable building automation. *Sustainability (Basel, Switzerland)*, *9*(2), 264.

McCabe, A. P., Taylor, C. J., Chotai, A., & Young, P. C. (2000). Proportional-integral-plus control of feedback-dependent systems with input and output constraints. *Proceedings of the UKACC International Conference on control 2000. University of Cambridge*.

Mendel, J. M. (1969). A priori and a posteriori identification of time varying parameters. *Proceedings, 2nd IEEE Conference on System Sciences*, *4*, 616–623.

Mendel, J. M., & Fu, K. S. (1970). *Adaptive Learning and Pattern Recognition Systems*. New York: Academic Press.

Montgomery, R., & McDowall, R. (2008). *Fundamentals of HVAC Control Systems: A Course Reader*. Burlington, MA: Elsevier Science.

Moon, J., Lee, J.-H., & Kim, S. (2014). Evaluation of artificial neural network-based temperature control for optimum operation of building envelopes. *Energies (Basel)*, *7*(11), 7245–7265.

Narasimhan, T. N. (1999). Fourier's heat conduction equation: History, influence and connections. *Reviews of Geophysics*, *Volume 37, Issue 1*, pp. 151—-172.

Nise, N. S. (2011). *Control Systems Engineering*. Jefferson City, USA: Wiley, 6th ed.

Ogun, O. A., Festus, M. U., & Inyang, I. J. (2017). Optimal PIP control of a pH neutralization process based on state-dependent parameter model. *IFAC-PapersOnLine*, *50*(2), 37 – 42. Control Conference Africa CCA 2017.
URL `http://www.sciencedirect.com/science/article/pii/S2405896317335383`

Oswiecinska, A. (2014). *Energy efficient control strategies for HVAC systems*. Master's thesis, Wroclaw, Poland: Wroclaw University of Technology.

Oswiecinska, A., Hibbs, J., Zajic, I., & Burnham, K. (2015). Towards energy efficient operation of heating, ventilation and air conditioning systems via advanced supervisory control design. *Journal of Physics: Conference Series 659 012030*.

Paris, B., Eynard, J., Grieu, S., Talbert, T., & Polit, M. (2010). Heating control schemes for energy management in buildings. *Energy and buildings*, *42*(10), 1908–1917.

Pender, B., Sadler, D., Shea, J., & Ward, D. (2012). *Cambridge 2 Unit Mathematics Year 11 Enhanced Version*. Port Melbourne, Victoria, Australia: Cambridge University Press, 2nd ed.

Propp, K., Marinescu, M., Auger, D. J., O'Neill, L., Fotouhi, A., Somasundaram, K., Offer, G. J., Minton, G., Longo, S., Wild, M., & Knap, V. (2016). Multi-temperature state-dependent equivalent circuit discharge model for lithium-sulfur batteries. *Journal of Power Sources*, *328*, 289–299.

Ramallo-González, A. P., Eames, M. E., & Coley, D. A. (2013). Lumped parameter models for building thermal modelling: An analytic approach to simplifying complex multi-layered constructionsy. *Energy and Buildings*, *Volume 60*, pp. 174—-184.

Åström, K. J., & Wittenmark, B. (2008). *Adaptive Control*. Dover Publications, 2nd ed.

Sadeghi, J., Tych, W., Chotai, A., & Young, P. C. (2010). Multi-state dependent parameter model identification and estimation for nonlinear dynamic systems. *Electronics Letters*, *46*(18), pp. 1265–1266.

Shaban, E. M., Taylor, C. J., & Chotai, A. (2004). State dependent parameter proportional-integral-plus (SDP-PIP) control of a nonlinear robot digger arm. *5th UKACC International Conference on Control*.

Smarter Homes (n.d.). Using thermal mass for heating and cooling.
URL `https://www.smarterhomes.org.nz/smart-guides/design/thermal-mass-for-heating-and-cooling/`

Stables, M., & Taylor, C. (2006). Non-linear control of ventilation rate using state-dependent parameter models. *Biosystems engineering*, *95*(1), 7–18.

Steffen, W., Broadgate, W., Deutsch, L., Gaffney, O., & Ludwig, C. (2015). The trajectory of the anthropocene: The great acceleration. *The Anthropocene Review*, *2*(1), 81–98.
URL `https://doi.org/10.1177/2053019614564785`

Tate, O., Cheneler, D., & Taylor, C. (2019). A thermal–electrical analogy model of a four–floor building with occupancy estimation for heating system control. *IFAC-PapersOnLine*, *52*(11), 91–96.

Taylor, C. J., Chotai, A., & Burnham, K. (2011a). Controllable forms for stabilising pole assignment design of generalised bilinear systems. *Electronics Letters*, *47(7)*, 437–439.

Taylor, C. J., Leigh, P., Price, L., Young, P. C., Berckmans, D., & Vranken, E. (2011b). Proportional-integral-plus (PIP) control of ventilation rate in agricultural buildings. *Control Engineering Practice*, *12(2)*, 225–233.
URL `https://doi.org/10.1016/S0967-0661(03)00060-1`

Taylor, C. J., Young, P. C., & Chotai, A. (2013). *True Digital Control: Statistical Modelling and Non-Minimal State Space Design*. Wiley.

Taylor, C. J., Young, P. C., Chotai, A., & Dixon, R. (1996). Structural and predictive aspects of proportional-integral-plus (PIP) control. *Proceedings of the UKACC International Conference on control 1996, University of Exeter*, *Volume 2*, pp. 1374–1379.

Touretzky, C. R., & Baldea, M. (2014). Nonlinear model reduction and model predictive control of residential buildings with energy recovery. *Journal of Process Control*, *Volume 24, Issue 6*, pp. 723–739.

Tsitsimpelis, I., & Taylor, C. J. (2014). A 2 dimensional hammerstein model for heating and ventilation control of conceptual thermal zones. (pp. 186–191).

Underwood, C. P. (1999). *HVAC Control Systems: Modelling, analysing and design*. London: E&FN SPON.

United Nations Development Programme (n.d.). Sustainable Development Goals.
URL `https://www.undp.org/content/undp/en/home/sustainable-development-goals.html`

United Nations Sustainable Development (n.d.). About the Sustainable Development Goals.
URL `https://www.un.org/sustainabledevelopment/sustainable-development-goals/`

Valenzuela, P. E., Ebadat, A., Everitt, N., & Parisio, A. (2020). Closed-loop identification for model predictive control of hvac systems: From input design to controller synthesis. *IEEE transactions on control systems technology*, *28*(5), 1681–1695.

Wallace, M., McBride, R., Aumi, S., Mhaskar, P., House, J., & Salsbury, T. (2012). Energy efficient model predictive building temperature control. *Chemical engineering science*, *69*(1), 45–58.

Wang, L. (2009). *Model Predictive Control System Design and Implementation using MATLAB*. London: Springer-Verlag.

Wang, Q., Hang, C., & Zou, W. (1998). Automatic tuning of nonlinear PID controllers for unsymmetrical processes. *Computers chem. Engng*, *Volume 22, Issue 4/5*, pp. 687—-694.

Young, P. C. (1969). Applying parameter estimation to dynamic systems: Part ii - applications. *Control Engineering 16(11)*, (p. 118–124).

Young, P. C. (1981). A second generation adaptive autostabilization system for airborne vehicles. *Automatica*, *17*, 459–470.

Young, P. C. (2002). Data-based mechanistic and top-down modelling. *International Congress on Environmental Modelling and Software*, *86*, 363–374.

Young, P. C. (2011). *Recursive Estimation and Time-Series Analysis: An Introduction for the Student and Practitioner*. Berlin: Springer, 2nd ed.

Young, P. C., Behzadi, M. A., Wang, C. L., & Chotai, A. (1987). Direct digital and adaptive control by input-outputstate variable feedback pole assignment. *International Journal of Control 46(6)*, (pp. 1867–1881).

Young, P. C., McCabe, A. P., & Chotai, A. (2002). State-dependent parameter nonlinear systems: Identification, estimation and control. *IFAC Proceedings Volumes*, *Volume 35, Issue 1*, 441–446.

Youssef, A., Exadaktylos, V., Ozcan, S. E., & Berckmans, D. (2011a). Proportional-integral-plus (pip) control system for individual thermal zones in a small ventilated space. *ASHRAE transactions*, *117*(1), 48.

Youssef, A., Yen, H. H., Özcan, S. E., & Berckmans, D. (2011b). Data-based mechanistic modelling of indoor temperature distributions based on energy input. *Energy and Buildings*, *43*(11), 2965 – 2972.
URL http://www.sciencedirect.com/science/article/pii/S037877881100291X

Zajíc, I. (2013). *Hammerstein-bilinear Approach with Application to Heating Ventilation and Air Conditioning Systems*. PhD thesis, Coventry University, UK.

Zajíc, I. (2014). Lecture notes in self-tuning and adaptive control.

Zakeri, E., & Moeinkhah, H. (2019). Digital control design for an ipmc actuator using adaptive optimal proportional integral plus method: Simulation and experimental study. *Sensors and Actuators A: Physical*, *298*, 111577.
URL http://www.sciencedirect.com/science/article/pii/S0924424719312841

Ziemian, S., & Burnham, K. J. (2002). Design methods and tuning of bilinear proportional-integral-plus controllers. *IFAC Proceedings Volumes*, *35*(1), 373 – 378. 15th IFAC World Congress.
URL http://www.sciencedirect.com/science/article/pii/S1474667015385645